Integrated modeling for stratigraphic development of the Mackenzie Trough and the Eastern Beaufort Shelf, N.W.T., Canada

by

Kim Picard
B.Sc., Université du Québec à Rimouski, 2001

A Thesis Submitted in Partial Fulfillment
of the Requirements for the Degree of

MASTER OF SCIENCE

in the School of Earth and Ocean Sciences

Supervisory Committee

Integrated modeling for stratigraphic development of the Mackenzie Trough and the Eastern Beaufort Shelf, N.W.T., Canada

by

Kim Picard
B.Sc., Université du Québec à Rimouski, 2001

Supervisory Committee

Dr. Philip R. Hill (School of Earth and Ocean Sciences, Geological Survey of Canada)
Co-Supervisor

Dr. Kim Juniper (School of Earth and Ocean Sciences)
Co-Supervisor

Dr. J. Vaughn Barrie (School of Earth and Ocean Sciences, Geological Survey of Canada)
Departmental Member

Dr. Gwyn Lintern (School of Earth and Ocean Sciences, Geological Survey of Canada)
Additional Member

Abstract

Supervisory Committee
Dr. Philip R. Hill (School of Earth and Ocean Sciences, Geological Survey of Canada)
Co-Supervisor
Dr. Kim Juniper (School of Earth and Ocean Sciences)
Co-Supervisor
Dr. J. Vaughn Barrie (School of Earth and Ocean Sciences, Geological Survey of Canada)
Departmental Member
Dr. Gwyn Lintern (School of Earth and Ocean Sciences, Geological Survey of Canada)
Additional Member

Glaciated shelves develop under the influence of a more complex suite of processes than most non-glaciated shelves. Amongst the specific processes are the glacially-influenced sediment supply and the glacial-isostatic adjustment (GIA), which is largely responsible for the complex nature of regional relative sea-levels (RSLs).

This study first characterizes the impact of GIA on the Mackenzie-Beaufort region by presenting a new set of RSL curves derived from a modern gravitationally self-consistent sea level model computing the effects of glacio-hydro isostasy, geoid changes, and true polar wander. The results of the RSL model present cross-shelf variations in the order of 100 m and along-shelf of 30 m during the LGM. The model also suggests a different timing and range to the single RSL curve presently used for this region. Depending on the location, the lowstand is modeled between 14 and 12 ka BP and reached between 85 and 140 m below present sea-level.

These new findings are used in the second part of the study to evaluate the impacts of GIA along with other factors on the Late Quaternary evolution of the Canadian Beaufort Shelf. SedFlux, a process-based stratigraphic simulation model is used. Uncertainties associated with post-LGM conditions create difficulties in establishing good model parameterization. Thus, simulations are first performed on the Mackenzie Trough area, where data availability permits better evaluation and constraint of parameters that are then applied to the more data poor Eastern Beaufort Shelf environment.

The results of the stratigraphic simulations suggest that the ice sheet margin in the Mackenzie-Beaufort region was more extensive than previously assumed. The impact of GIA on the stratigraphy of the Mackenzie Trough is to develop more progradational than retrogradational stratigraphic features. Simulations of the Eastern Beaufort Shelf suggest that a previously dated sample from the Uviluk borehole is not a RSL indicator as previously thought and by taking this into consideration, the borehole stratigraphy can be modeled. Modeling of multiple cycles of glacial/interglacial RSL with glacial outwash deposition supports the interpretation of the Late Quaternary geology suggested by Murton (2009). Finally, glacial outburst floods funnelling through the area would have mostly bypassed the shelf and contributed to its progradation. If flood water were directed to the Mackenzie Trough, the deposits are likely found within the lower wedge.

Table of Contents

List of Tables

List of Figures

Acknowledgments

I would like to first thank Phil Hill for his great mentorship and support, exciting discussions, and great foresight for the timing of research proposal.

Thanks to the team from the University of Colorado and CSDMS: 1) Andy Wickert for the exciting collaboration regarding RSL predictions. 2) Eric Hutton for the time and patience spent teaching and modifying SedFlux to accommodate this study. 3) James Syvitski as the external examiner, but also for being such a great host and offering great discussions on stratigraphy and process theory. 3) Irina Overeem, Albert Kettner and the rest of the CSDMS team who have been so welcoming and helpful.

Thank you to Kim Juniper from UVic, and Gwyn Lintern and Vaughn Barrie from GSC, for providing advice and review as thesis committee members.

Thanks to Ralph Currie, Carmel Lowe and the GSC for supporting their employee into pursuing grad studies and the Program for Energy Research and Development (PERD), Northern Regulatory Research for funding this research.

Finally but not least, Todd for being so supportive and making my life easier so that I could write during the last couple months.

CHAPTER 1- Introduction

Continental margins evolve under the influence of multiple processes acting at various time-scales, such as sea-level and sediment supply fluctuations, thermal and isostatic subsidence, and sediment dispersion. For Arctic continental shelves, processes also include glacial isostatic adjustment (GIA), permafrost development, iceberg scouring and sea ice coverage. With climate change impacts, territorial sovereignty, and resource exploitations at the forefront in Arctic regions, better understanding of the influence of these factors on the evolution of Arctic continental shelves is required. Resource exploration and exploitation of the Eastern Beaufort Shelf and continental slope has become one of the main drivers of research in the Canadian north. In order to assess the potential geohazards to exploration, such as gas hydrates, permafrost, and slope instability (Hill, et al. 1982; Judge et al. 1987; Taylor 1991a & b; Paull et al. 2007) a solid regional geological framework is needed.

The present regional framework for the pre-Late Quaternary stratigraphy of the Beaufort Shelf is relatively well understood (Dixon and Dietrich, 1990). However, detailed interpretation of the Late Quaternary stratigraphy is lacking. It is inferred from sparse field data such as borehole, core samples, and seismic profiles, the quality of which is impaired by the presence of over 600 m of permafrost on the shelf (Taylor 1991a; Blasco et al., 1990; Murton, 2009). In addition, the scarcity of pre-Holocene radiocarbon dated material limits the extent to which the spatio-temporal development of the shelf can be explained. Spatio-temporal variations are required for assessing the timing of events, such as permafrost development or specific geohazards (e.g. pingo-like features (PLF), slope failures, outburst flood pathways) (Hill et al., 1982; Taylor 1991;

Taylor et al. 1993; Taylor, et al. 1996a, b; Dallimore et al. 1996; Burn and Kokelj 2009; Paull et al., 2007; Murton et al., 2010). Well-studied passive margins, including the New Jersey Shelf and the Gulf du Lion, have shown considerable aggradation and progradation during the Late Quaternary period (Overeem et al. 2005; Jouet et al. 2006, Mountain et al., 2009; Jouet et al. 2008). The Beaufort shelf may reasonably be expected to have formed under similar influences. The changes may have been more complex, however, due to the impact of the Laurentide Ice Sheet.

The need to better understand the recent geological framework is therefore the motivation for this research. A lack of detailed information and the improbability of collecting adequate field information in the near future is why stratigraphic modelling was used to meet the objectives. Because of their capability in integrating multiple processes, stratigraphic models have proven to be helpful in understanding influences that different controls have on the a shelf sedimentary record (Hutton et al., 2004; Overeem et al., 2005; Jouet et al., 2008, Hutton and Syvitski., 2008; Overeem and Syvitski, 2010).

In regions where age and data constraints are limited, modeling long periods can be complex as parameterization has many uncertainties. To limit these uncertainties, it was proposed to first model the Mackenzie Trough where already a better dataset and interpretation were available (Moran et al. 1989; Hill 1996; Hill et al. 2001; Schell et al. 2008). This would help in narrowing down the key parameters and their magnitudes that could then be used in modeling the more poorly constrained Eastern Beaufort Shelf. Notwithstanding the fact that the Mackenzie Trough represented a good experimental area, it also has its share of unanswered questions that modeling could help resolve.

The late Quaternary sedimentary record of the Mackenzie Trough is the product of sediment delivered by the modern Mackenzie River drainage system only established during the late Wisconsinan (Duk-Rodkin and Hughes 1994). As the main drainage recipient for the Mackenzie-Beaufort region since the last glacial maximum (LGM), the geological record of the trough is considered to hold important information about potential glacial outburst floods and pulses of freshwater outflow into the Arctic. These events are deemed to have contributed to the onset of the Younger Dryas (Murton et al., 2010; Teller et al., 2002, Tarasov and Peltier, 2004; 2006), but direct evidence has yet to be identified. Existing core records (Schell et al. 2008) and post-glacial stratigraphic interpretation (Hill, 1996) does not provide adequate evidence for these events, but it may only be because of the resolution and extent of the records.

The present interpretation of the late Quaternary sedimentary record of the Mackenzie Trough relies on Hill's (1996) sequence stratigraphic interpretation, which is based on the relative sea level curved produced by Hill et al. (1985, 1993). A drawback of this interpretation is that it is based on a RSL curve loosely constrained between the LGM and the Holocene. Controversies around the glacial extent and the presence of glacial-isostatic adjustment (GIA) have further complicated bounding this part of the RSL curve and thus the stratigraphy of the Mackenzie-Beaufort region (Hill et al. 1993; Hill et al. 2001; Murton 2009; England et al. 2009; Murton et al. 2010). On the other hand, GIA is an important component in defining RSL (Mitrovica and Milne 2003; Steffen and Wu 2011). It is evident that many issues regarding the Eastern Beaufort Shelf or the Mackenzie Trough require better geological evidence and a better stratigraphic

framework to find answers. The overarching objective of the present research was to fill these knowledge gaps.

1.1 Key scientific objectives

1. Understand the potential impact of GIA on the RSL and on the stratigraphic development of the region.
2. Provide a geological framework for the post-LGM Mackenzie Trough sedimentary record.
3. Provide insight into the stratigraphic development of the Eastern Beaufort Shelf
4. Provide a framework to better understand the impacts of glacial outburst flood events throughout the region
5. Contribute to maximizing the effectiveness of future field research aimed at finding evidence to the questions listed above by defining the potential best-fit areas.

1.2 Structure of the thesis

To meet the objectives, SedFlux, a complex 2D and 3D process-based stratigraphic simulation model, was chosen (Syvitski and Hutton, 2001; Hutton and Syvitski, 2008). In addition, the specific objective on the GIA study was met after establishing collaboration with Andy Wickert from the University of Boulder, Colorado, who provided the GIA modeling expertise. The results of the research are presented herein as two stand-alone publications comprising one chapter each and two appendices. The publications summarise the methods used and the main findings; the first one covering a review of the RSL model for the Mackenzie-Beaufort based on new GIA modeling results and the second one covering the stratigraphic objectives, both for the Mackenzie Trough and the Eastern Beaufort Shelf. These two publications are intended to be published in the

Journal of Geophysical Research and Marine Geology respectively. The appendices present additional details of the method that have not been included in the publication as well as the modeling sensitivity tests results.

CHAPTER 2- Implications of glacio-isostatic adjustment on the relative sea-level model of an Arctic shelf: the Canadian Beaufort Shelf

Kim Picard, Andy Wickert, and Philip R. Hill

2.1 Abstract

Glacial isostatic adjustment (GIA) is a process associated with formerly or presently glaciated regions. Around glaciated margins, it contributes to important variations and complex relative sea-level dynamics. Using a modern gravitationally self-consistent sea level model computing the effects of glacio-hydro isostasy, geoid changes, and true polar wander, this study characterises the impact of GIA over an extensive Arctic shelf by presenting a new set of RSL curves for the Canadian Beaufort Shelf. The model results present cross-shelf variations in the order of 100 m during the LGM and along-shelf of 30 m. The model also suggests a much different timing and range than the single RSL curve presently used for this region. Depending on the location, the lowstand is modeled between 14 and 12 ka BP and reached between 85 and 140 m below present sea-level. The model is reconciled with radiocarbon dates from marine and terrestrial samples presented in other studies. Cross-examination of dated raised shorelines support the argument for more extensive limits of the ice sheet. These data also offer ways of strengthening the present RSL model and better defining the geotechnical properties of the area. The model results presented in this study are important as they open new ways of thinking about stratigraphic problems related to the Canadian Beaufort Shelf and other glaciated shelves.

2.2 Introduction

Glacial isostatic adjustment (GIA) is a process associated with formerly or presently glaciated regions. GIA describes the response of the earth to the presence of ice sheets

during glacial cycles. As ice sheets load the lithosphere, the latter bends into the mantle, which flows to other areas and contributes to the formation of a peripheral forebulge. During deglaciation, the unloading of the crust causes isostatic rebound and the return of pre-glacial surface elevations. Due to the viscoelastic properties of the earth's mantle, today's earth is still recovering from the last deglaciation, especially in Arctic regions where ice sheets last melted (Steffen and Wu, 2011; Tsuji et al., 2009). One of the main consequences of GIA is that it regionally influences relative sea-level (RSL).

Sea-level and sediment supply fluctuations dictate the evolution of continental shelves. Studying the evolution of a particular shelf therefore requires knowledge of regional RSL, which for a glaciated shelf also includes its GIA history. A better understanding of continental shelves in the Arctic regions, will inform climate change impacts, territorial sovereignty, and resource exploitations. Resource exploration and exploitation of the Eastern Beaufort Shelf and continental slope has become one of the main drivers of research in the Canadian north. A better understanding of the regional geological framework is required, so that potential geohazards to exploration, such as gas hydrates, permafrost, and slope instability (Hill, et al. 1982; Judge et al. 1987; Taylor 1991; Paull et al. 2007), can be assessed. Because of the strong link established between the stratigraphic development of a shelf and sea-level, a detailed reassessment of the regional RSL curve is necessary for the region.

The Quaternary evolution of the Eastern Beaufort Shelf and the Mackenzie Trough in the Canadian Arctic has been interpreted by geologists using eustatic and relative sea-level (RSL) curves (Hill et al.,1985; 1993; Moran et al. 1989; Blasco and Lewis 1991; Hill et al. 1991; Hill 1996). Geothermal modellers have used these curves to argue that

the development of thick permafrost on the shelf resulted from low sea-level during glacial periods that exposed it for much of the Wisconsinan (Taylor 1991; Taylor et al. 1993; Taylor, et al. 1996a, b; Dallimore et al. 1996; Burn and Kokelj 2009).

The presently used RSL curve (Hill et al 1985; 1993) was reconstructed from radiocarbon ages measured on peat or shell samples that indicated deposition above or below paleo-sea level respectively. Most samples gave ages younger than 8000 radiocarbon yrs BP with only two ages greater than 10,000 radiocarbon years BP. The older portion of the RSL curve was therefore relatively unconstrained and the shape of the curve was derived from morphologic criteria, notably the presence of incised valleys on an older lowstand surface (Hill et al., 1985), which inferred a latest Wisconsinan sea level lowering.

In many parts of North America, studies of RSL history have taken into account GIA using numerical models (Barnhardt et al., 1995; Stea et al., 2001; James et al., 2009). In Fennoscandia, Steffen and Wu (2011) presented a comprehensive review of GIA models and synthesize the research done on the subject. In summary, these authors indicated that even though much improvement can be done, the GIA models explained observations and contributed to a better understanding of the dynamics of RSL in these glaciated regions. Previous studies in the Mackenzie-Beaufort region have not fully included analysis of the effect of GIA on RSL and the present study shows that significant variations, 100 and 30 m are to be expected respectively across- and along-shelf. These results thus suggest that a single RSL curve applied to the whole shelf area is inappropriate.

The objectives of this paper are first to fill this knowledge gap with a new set of relative sea-level (RSL) curves derived from a modern gravitationally self-consistent sea level model (Mitrovica and Milne, 2003; Kendall et al., 2005). This model computes the effects of glacio-hydro isostasy, geoid changes, and true polar wander (Mitrovica and Milne 2003; Kendall et al. 2005). Ice history and a solid Earth rheology inputs (ICE-5G / VM2; Peltier, 2004) are updated from that used in earlier Canadian GIA studies (e.g., Stea et al., 2001). This model, in combination with local RSL data, provides an improved sea level history for the region (see Steffen and Wu, 2011). Secondly, the model outputs are reconciled with published dated material collected in submarine cores (Hill et al., 1985; 1993) and on raised beaches along McClure Strait (England et al., 2009).

2.2.1 Regional setting

The Eastern Beaufort Shelf and the Mackenzie Trough are part of the Canadian Beaufort Shelf, located in the Arctic (Fig. 1). The eastern shelf covers 50 000 km^2 of seafloor, 400 km along-shelf by 100 to 150 km cross-shelf, with a shelf break located around the 80 to 100 m isobath. Two large glacial troughs cut through the eastern shelf, the Mackenzie Trough and the Amundsen Gulf. Both troughs are thought to have been glacially-incised prior to the Early Wisconsinan, and reworked by the Laurentide Ice Sheet (LIS) lobes during the Late Wisconsin (Hill 1996; Dyke et al. 2003; Dyke 2004; Stokes et al. 2009). The Mackenzie Trough, to the west, hosts one of the largest deltas in the world, the Mackenzie River Delta, and is characterized by a low and uniform gradient of 1- 2 m/km, steepening at the shelf break, located 100 km offshore at the 100 m isobath. The smaller Kugmallit and Ikit Troughs incised the Eastern Beaufort Shelf. Hill et al (1985) originally interpreted the incision of these valleys to be the result of sea-level

lowering, but Hill (1996) raised the possibility that the incision could have resulted from an increase in water discharge.

During the Wisconsin Glaciation, the LIS and its Mackenzie and Admunsen Lobes reached their maximum extent during the Late Wisconsinan (Dyke et al., 2002). The maximum extent appears to have been reached and maintained throughout the LGM, i.e. 21 ka BP. Uncertainties about the maximum limits of the LIS remain, especially in the offshore area where little evidence has been found (Fig. 2.1; Rampton, 1988; Blasco et al., 1990; Murton, 2009; Murton et al., 2010). Recent studies in the region however support a

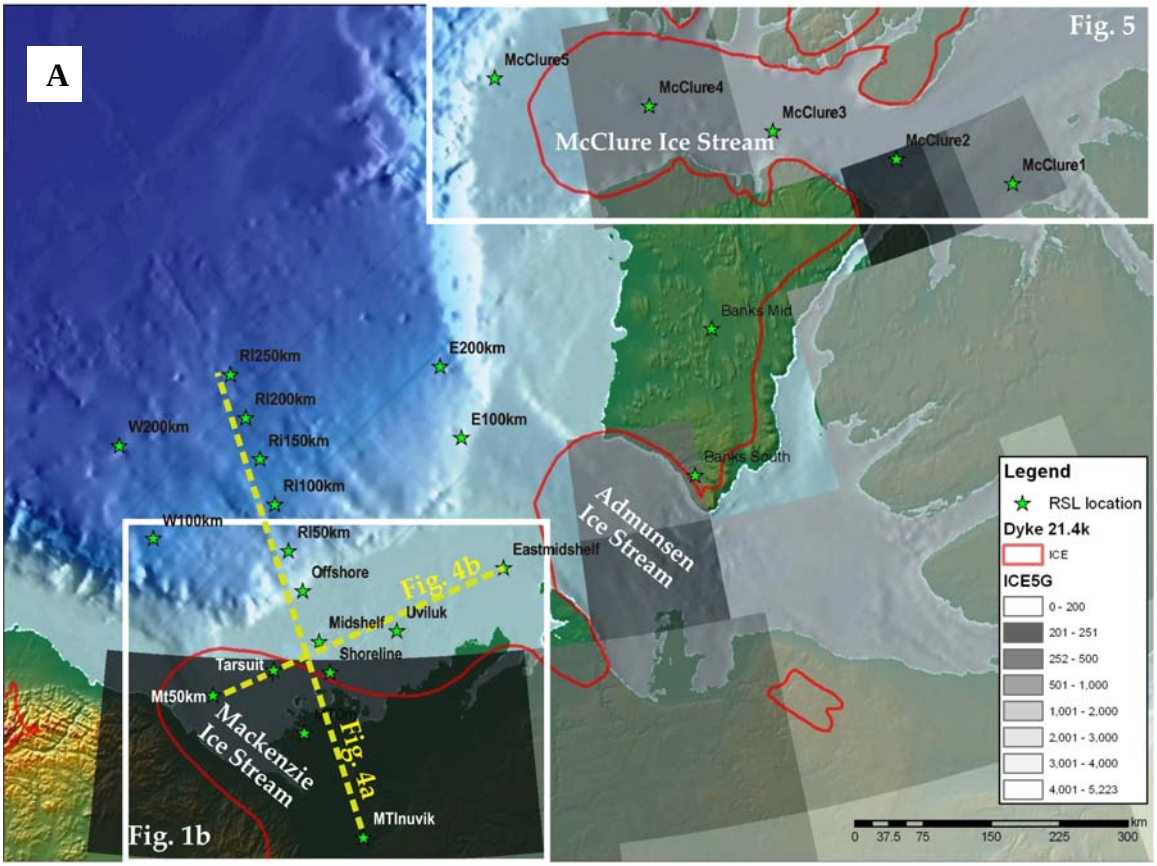

Figure 2.1 A. Map showing the location of the figures, RSL curves, and transects. The map also includes the LGM ice extent as defined by Dyke et al. (2003) and modeled in ICE-5G by Peltier (2004). ICE-5G ice thickness output is presented.

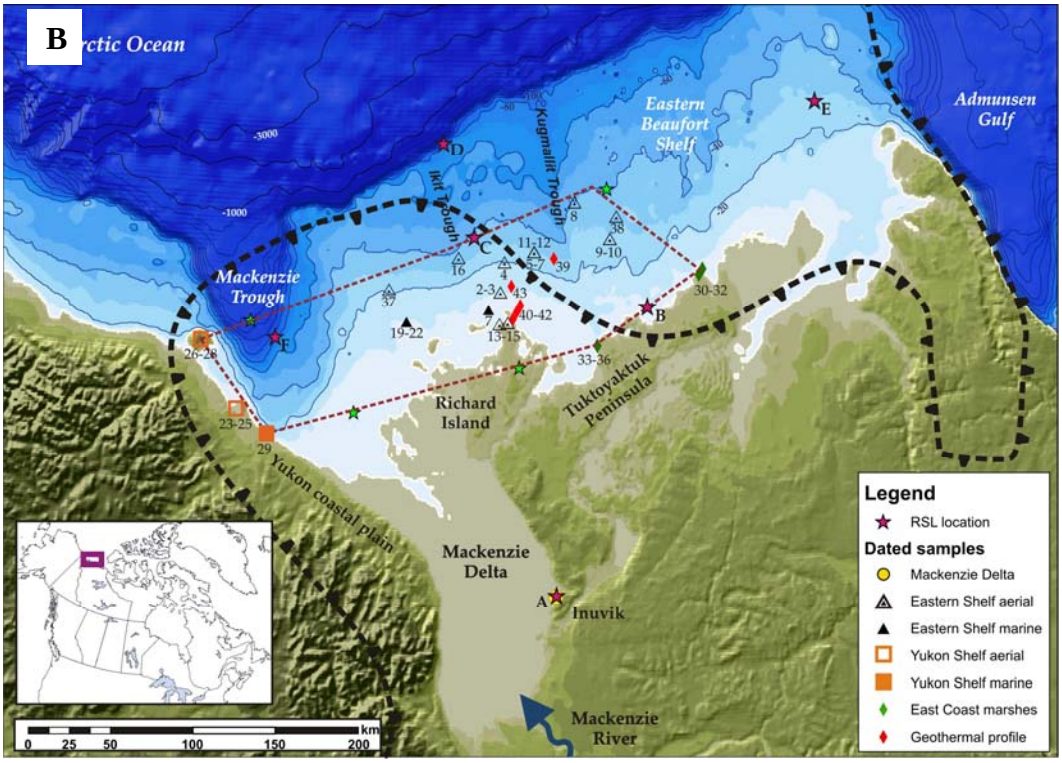

Figure 2.1 B. Location map showing the main features of the Eastern Beaufort Shelf and Mackenzie Trough, including the LGM ice extent of the LIS after Rampton (1988). Dated sample locations are represented based on their sample type (aerial or marine) and numbers following Hill et al. (1993) table. The extent of the sample area is bounded by a red polygon. The star symbols (green and pink) show the location of the RSL modeled curves investigated for this study; the pink stars showing the location of the curves presented in Figure 2.2 and 3.

more substantial extent around the Mackenzie-Beaufort region than previously thought (Stokes et al., 2009; England et al., 2009; Murton, 2009). The deglacial history of the study area shows that the onset of deglaciation did not occur until 16.5 ka BP and that the ice lobes were the last ones to completely retreat, somewhere between 14.4 and 14.1 ka BP (Dyke et al., 2003).

2.3 Methods

2.3.1 Glacio-isostatic adjustment (GIA) and RSL model

Sea level histories for the Mackenzie Delta region are reconstructed using a numerical implementation (Kendall et al., 2005) of a global sea level theory (Mitrovica and Milne, 2003). This global model uses a one-dimensional spherically symmetric profile of mantle viscoelasticity to compute glacio-hydro isostasy. Changing near-surface mass distributions due to the ice and water loads and their isostatic response are used to compute changes in the geoid and the Earth's rotation vector (i.e. true polar wander). The Mitrovica and Milne (2003) and Kendall et al. (2005) sea-level theory and model, in particular, appropriately handle changes in global water mass distributions due to the onlap and offlap of the oceans at coastlines.

Inputs into this model are the global ice sheet reconstruction ICE-5G and its associated VM2 mantle viscosity model (Peltier, 2004). The coupled ICE-5G (VM2) ice-Earth model has been calibrated to fit a number of observations of postglacial sea level. It performs better in some regions than others; this is due to (1) the fact that its 1-D mantle parameters are likely better-fit to cratonal glaciated regions, and (2) that its lower mantle parameterization has been criticized (Davis and Mitrovica, 1996; Davis et al., 2008) for being lower than indicated by other probes of lower mantle viscosity (e.g Hager and Richerds, 1989). The choice of solid Earth model exerts a large control on the positions of the forebulges and the magnitudes of lithospheric displacement (Steffen and Wu 2011), which can be very significant in setting the sea level histories that are contemporaneous with deposition. Kaufmann et al (2000) demonstrated that using a 3D Earth structure instead of spherical symmetry can result in 10-20 m difference in RSL predictions. In particular, the lower effective elastic thickness of the Beaufort lithosphere

(relative to the Canadian Shield) should cause the modeled forebulges to be too far offshore. In spite of these shortcomings and uncertainties, ICE-5G (VM2) has been established as a standard since its initial release, does a good job of approximating global sea level histories, and (due to its symmetry) limits unconstrained solid Earth variables. We therefore use ICE-5G (VM2) as the input to our RSL calculations.

The model runs from the last interglacial to present, outputting a global sea level record from which regional RSL curves can be extracted. RSL curves present significant spatial variability, with the largest magnitude signals being the result of glacial isostatic response. The model does not account for tectonic or compaction-related subsidence in the region. These processes and the associated increase in local ocean loading must be modeled separately.

2.3.2 Relative sea-level curve reconciliation with the RSL model

The resulting RSL curves were compared against the radiocarbon age determinations from Hill et al (1985; 1993; Fig.2.2). All ages were converted to calendar years using the Fairbanks et al. (2005) calibration and marine ages were adjusted by 400 yrs for the marine reservoir effect (Coulthard et al. 2010). In addition, since the sea-level predictions account for the effects of ice and water loading, but not for sediment loading and compaction, the latter two processes were evaluated and added to the original dated sample depths. Estimating sediment loading subsidence is not a straightforward exercise as sedimentation is not uniform in time and space (Hutton and Syvitski 2008). Studies on the Mississippi Delta suggest highly variable rates, i.e. from 1 to 8 mm/yr (Ivins et al. 2007; Hutton and Syvitski 2008; Yuill et al. 2009). To better constrain the loading rates for each sample, an experiment testing water loading effect on the crust was conducted

using Sedflux 2.0 flexural module (Hutton and Syvitski, 2008). The elastic thickness and relaxation time of the lithosphere were set respectively to 100 km and 2.5 ka. A value of between 45 and 65 km for the lithospheric elastic thickness would be more specific to the region (Kirby and Swain 2009), but the larger value was picked to more closely approximate the global parameters used in the RSL model. The water loading values, measured at each sample site, were multiplied by a factor of 1.77 to represent the density difference between loading the crust with water (1000 kg/m^3) versus saturated sediment (2000 kg/m^3). This factor of conversion was calculated following Watts and Ryan (1976):

$$T = d(\rho_m - \rho_w)/ (\rho_m - \rho_s),$$

where T represents the final thickness, d represents the initial sea depth, ρ_m represents the mantle density, ρ_w represents the water density, and ρ_s represents the sediment density. The subsidence values obtained corresponded to 20 to 31% of the sample depth.

Compaction rates for the Beaufort area are difficult to estimate because of the presence of permafrost and interstitial ice. For this reason, compaction related subsidence was not included in the adjusted depths. It is however, important to keep in mind that some samples may have been subjected to compaction, because of their location within an area of thawed or non-frozen ground. In this case, compaction-related subsidence rates of 1–5 mm/yr, as seen for the Mississippi Delta (Yuill et al. 2009; Meckel et al. 2006, 2007; Pizzuto and Schwendt 1997), or as much as 40% of the sediment wedge thickness, as seen in the modeling study made by Reynolds et al. (1991), could be applied.

Finally, thermal subsidence is another mechanism affecting sample depth. Bott (1992) suggests a maximum rate at onset on the order of 50 mm per thousand years, which

means at most 1.5m for the oldest sample (Fig. 2.2, 37). In comparison to sediment loading estimates, this amount is considered negligible and thus, was not included.

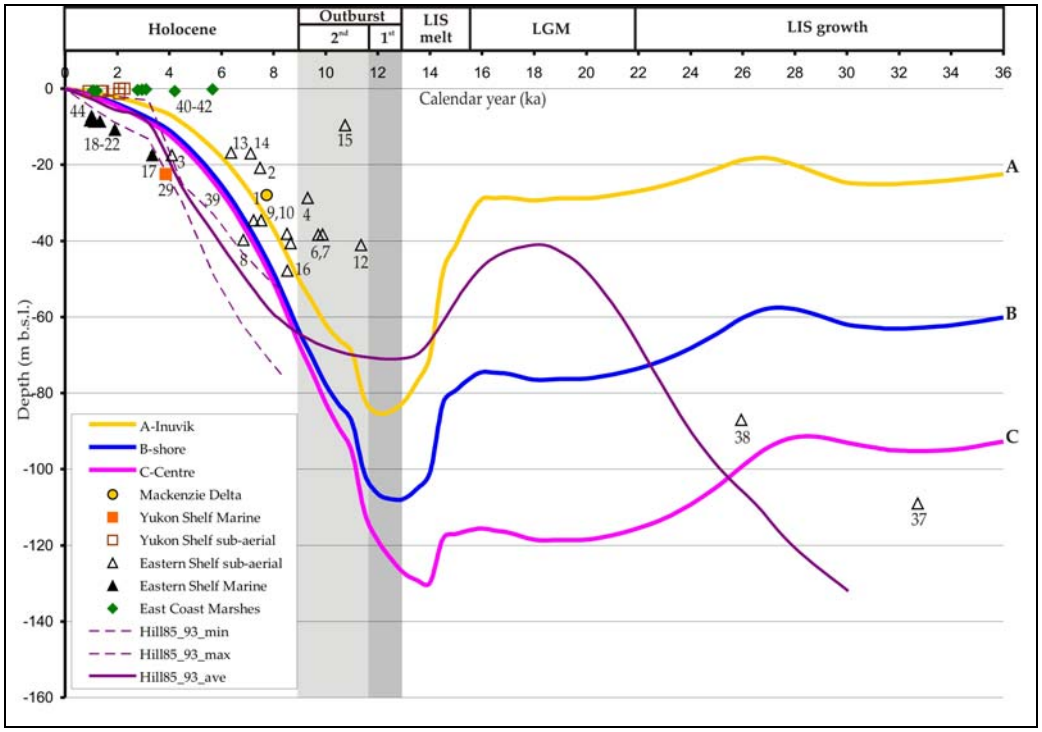

Figure 2.2: Selection of modeled RSL curves representing the variations existing within the radiocarbon dated sample area (Fig. 2.2, red polygon). Hill et al. (1985) curve is displayed with the Holocene section modified according to Hill (1993) and accompanied with its associated error envelope. Available dated samples, converted to calendar ages, from Hill et al. (1985, 1993) with associated cross-referenced sample numbers are plotted. The samples were adjusted for maximum possible sediment loading subsidence. The greyed areas correspond to the 2 outburst periods identified by Murton et al. (2010). LGM: Last Glacial Maximum, LIS: Laurentide Ice Sheet.

2.4 Results

2.4.1 Reconciliation of the modeled curves using dated samples

Figure 2.2 shows three RSL curves extracted from the model. Curves B and C correspond to the extreme cases for the sampled areas on the shelf, and curve A, even though more extreme, is specific to the Mackenzie Delta sample taken at Inuvik (fig. 1a). Curves B and C converge closely and fit the data well after 12 ka BP, when the vast

majority of validation points are available. There are only two exceptions, samples 3 and 8, where the samples should lie above the curves because of their terrestrial peat composition, but fall significantly below. In this case, compaction-related subsidence may be enough to account for the misfit. Sample 3 is the shallowest (below seabed) borehole sample reported by Hill et al (1985) and (although the borehole log is no longer available) was almost certainly located within unfrozen sediments. Therefore, compaction subsidence would likely have affected the elevation of this sample. As for sample 8, in addition to compaction-related subsidence, the date reported by Hill et al. (1985; 1993) represents a single age for a thick sample. This sample is thought to represent the transition from a fluvial-dominated environment to a delta pond environment, similar to the modern Mackenzie Delta ponds. The suggested age span of this sample is from 6200 to 9500 years BP. Since the transition to marine conditions is not clearly defined, the age error envelope for the sample can be expanded and thus support the calculated sea level curve. The RSL curve at Inuvik (A), representative of the subaerial Mackenzie Delta, shows that transgression here occurred earlier than on the shelf, which is supported by the single sample (1) available from this site.

The empirically drawn Holocene curve of Hill et al. (1993), which suggests a later rise in sea-level between 3 and 8 ka BP (Fig. 2.2) than the model, was highly influenced by the sample 3 and 8 data points. Given the uncertainties related to compaction subsidence for these borehole samples and the error margin associated with the RSL model predictions, the difference between the modeled and empirical curves for this age range lies within the margins of error of the data. Prior to 10 ka BP, the RSL curve is constrained by only two dated samples (37 and 38), both of terrestrial origin and older

than 25 ka BP (Fig. 2.2). These samples both located closer to curve C than curve B, lie closely or above the curve once sediment loading subsidence has been taken into consideration, which also suggests reconciliation of the modeled curves with the empirical data (Fig. 2.2).

The much improved physical understanding incorporated into the RSL model suggests that the modeled RSL curves are more reliable than the simplified and smoothed curve proposed by Hill et al (1985). The key feature of the Hill et al. (1985) curve, that of a latest Wisconsinan fall in sea level, is captured by the modeled curves and explained by forebulge migration. However, the suggestion of a very low mid-Wisconsinan RSL by Hill et al. (1985) is refuted and explained by the vertical displacement of the older dated samples (37) by sediment loading subsidence.

2.4.2 Glacial-Isostatic Adjustment (GIA) influence on RSL

The proposed RSL model suggests that sea-level has been strongly controlled by GIA. The influence of GIA is observed regionally across and along-shelf (Fig. 2.3). Curves A, B, C and D presented in Figure 2.3a illustrate the cross-shelf gradient, whereas curves C, E, and F presented in Figure 2.3b show the along-shelf gradient.

Prior to 18 ka BP, the RSL curve extracted for the shelf edge (D, Fig. 2.3b) closely follows the eustatic curve, which reached the lowstand by that point. Cross-shelf RSL variations reach up to 100 m between Inuvik (A) and the shelf edge (D), with high RSL values characterizing the nearshore due to the effects of ice loading under the weight of the Mackenzie lobe. The shape of the shelf edge curve (D) indicates that the isostatic and geoidal effects are still significant 150 km away from the ice margin.

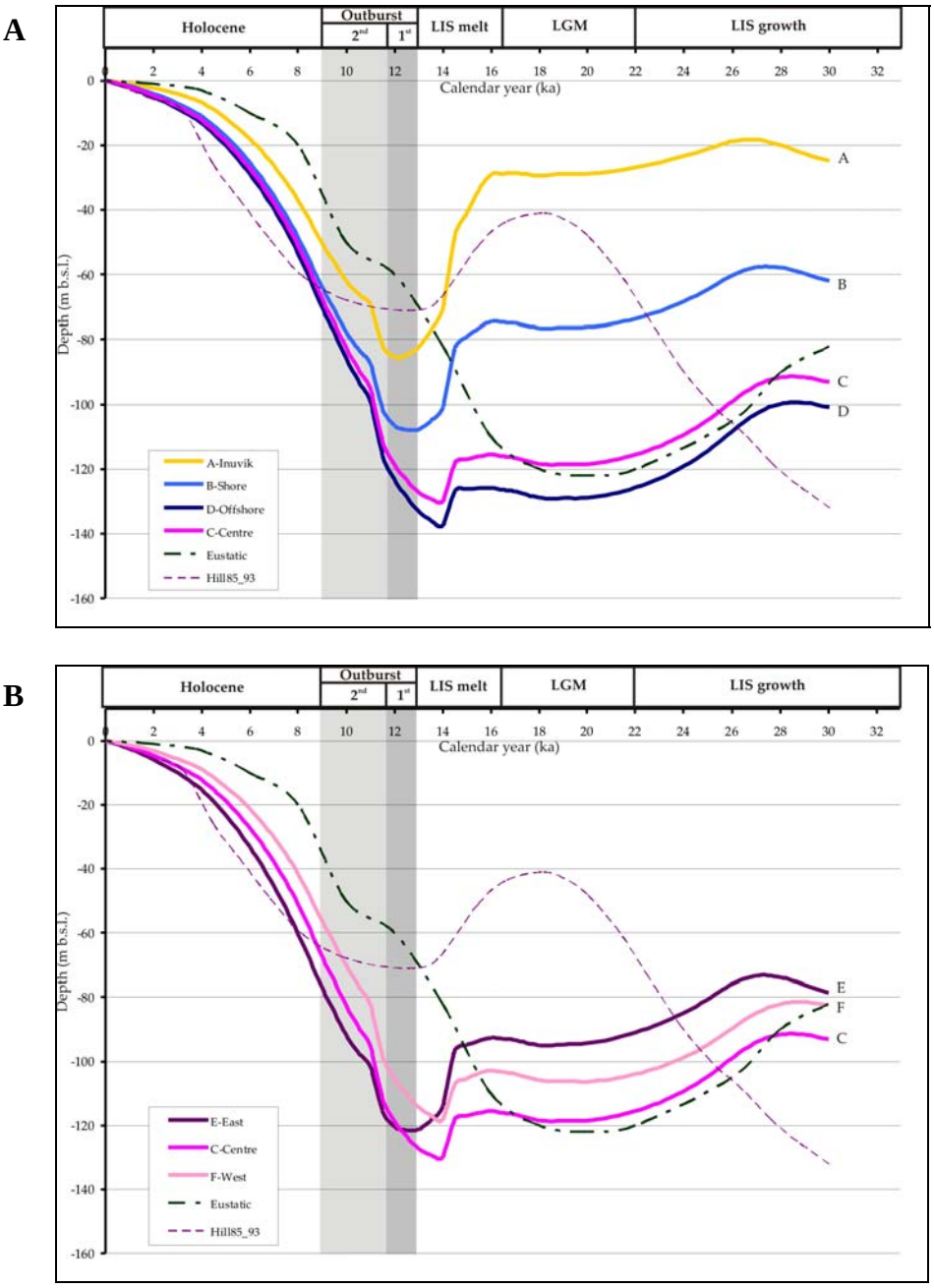

Figure 2.3: A) Model RSL curves showing the variations across-shelf. Curve locations displayed in Figure 2.1. The Waelbroech et al. (2002) eustatic curve and the Hill et al. (1985, 1993) RSL curve are also displayed. B) Model RSL curves showing the variations along-shelf. Curve locations found in Figure 2.1. The Waelbroech et al. (2002) eustatic curve of and Hill et al. (1985, 1993) RSL curve are also displayed.

As the ice sheet starts melting and retreating from the area after 16.5 ka BP (Dyke et al., 2003), the modeled curves diverged from the eustatic curve, lagging several thousand years behind. This lag is in response to the geoid adjustment as well as to a delay in the isostatic rebound due to the mantle visco-elastic properties, also responsible for the forebulge development (see next section). The RSL lowstand is reached between 12 and 14ka BP, well after the onset of deglaciation for the area and the eustatic lowstand. The Inuvik lowstand lags the shelf edge lowstand by 2 ka, probably resulting from a later retreat of the ice sheet, inducing later both isostatic rebound and landward migration of the forebulge. A cross-shelf difference of fifty metres, caused by a lowstand reaching 137 m b.s.l. at the shelf edge (D) and only 85 m b.s.l. at Inuvik (A), is observed during this period. The Holocene transgression is characterized by similar rates of transgression to the eustatic rates, but the RSL curves lag behind the eustatic by 2 to 4 ka. Similarly, convergence amongst the RSL model curves occurs, but not until the Late Holocene in the case of Inuvik. This dynamic is attributed to the final stage of forebulge migration and collapse.

In the Eastern Beaufort Shelf region, substantial cross-shelf variations are also observed. The model shows a 52 m RSL difference between the coastline of Richards Island (curve C) and the shelf break (curve D), and a ~25 m difference at the lowstand (Fig. 2.3a). The timing of lowstand at the shoreline lags behind the shelf edge by 0.5 ka.

Along-shelf variations, though smaller than cross-shelf variations, are considerable (Fig. 2.3b). Three representative sites were selected: E and F at the two opposite extremities of the Eastern Beaufort Shelf and C, at the mid-way point between these extremities and exhibiting the most variability. The largest difference (25 m) occurs

during the LGM between curve E, located at the eastern extremity of the shelf next to the Admunsen Gulf, and C, the mid-way point. During the lowstand, the relationships between the curves change, mainly because curve E is delayed in its transition to transgression. This shuffle causes the majority of the differences between E and F (up to 20 m) to occur during the early part of the Holocene; most likely explained by the dynamics involved in the development and decay of the Mackenzie and the Admunsen ice streams. At 16.5 ka BP, the smaller Mackenzie lobe started its retreat provoking forebulge migration and a change in the geoid, which brought the RSL lowstand (RSL curve F). Located in the footprint of the Mackenzie Lobe, curve C thus behaved similarly. Around 15 ka BP, the Admunsen Ice Stream began to retreat (Dyke et al., 2003; Stokes et al., 2009). Because of its larger mass inducing more isostatic displacement, the area around the Admunsen Ice Stream was subjected to shallower RSL values during the LGM and larger RSL drop during deglaciation. The ensuing Holocene transgression was characterized accordingly by the differential timing in deglaciation of both ice-streams, i.e. with the eastern most location lagging behind the westernmost locations (F, C, then E). Interestingly, the central shelf RSL curve (C) shows the lowest RSL through the LGM and the onset of deglaciation. An explanation for this observation is that the Mackenzie Lobe in the Mackenzie Trough and the Admunsen Lobe in the Admunsen Gulf (Winsborrow 2004; Stokes et al. 2009) depressed the crust at either extremity and thus created a bulge in the central region, approximately 130 km east of the Mackenzie Trough (Fig 4b) and north of Richard Island.

2.4.3 Lithospheric characterisation

To better understand the RSL curves presented above, the RSL model output were subtracted from the eustatic sea level curve (Waelbroech et al., 2002). The resulting curves are thus a combination of (1) glacio-hydro isostatic adjustment, (2) geoid modification by the redistribution of near-surface masses, and (3) changes in the Earth rotation vector, i.e. true polar wander (Fig. 2.4). The Earth rotation signal has a hemispheric wavelength and the gravitational effects vary gradually over a sub-continental scale, meaning that the short-wavelength signals in Figure 2.4 are caused by flexural isostasy. These plots largely depict forebulge migration and collapse that result from the interaction between the ice sheet retreat and the viscoelastic properties of the lithosphere and mantle. In addition, these cross-section plots emphasize that the RSL curve varies depending on its distance to the ice mass (Kaufman et al., 2004)

Figure 2.4 characterises the evolution of the lithospheric displacement using two shelf profiles running perpendicular to each other. Figure 2.4a shows the displacement over the south-north cross-shelf profile, whereas Figure 2.4b presents the deformation of the lithosphere along the east-west profile. The model suggests that the peak of the deformation occurs around 21 ka BP between Inuvik and 400 km offshore (-93 m and + 30.9 m respectively; Fig. 2.4b). At this time, the location where the displacement is null (i.e. sea level equals eustatic) is about 75 km offshore, close to profile C. This suggests that the land south of 75 km offshore is isostatically depressed and the land north of 75 km offshore is uplifted in the forebulge.

Due to the slow growth of the LIS, the assumption is that lithospheric flexure had reached near isostatic equilibrium by 21 ka BP (LGM). Hence, the fully developed peripheral forebulge signal should be reflected in the curve at 21 ka BP (Fig. 2.4a).

According to this curve, the forebulge starts about 80 km offshore and reaches its maximum height of 30m 330 km farther offshore. Assuming symmetrical geometry, the forebulge wavelength should be in the order of 650-700 km. Because of the long-lasting LGM conditions specific to the region, i.e. approximately five thousand years (<21 to 16.5 ka BP), the model shows a stationary forebulge that does not migrate inland or change its general configuration. Between 16.5 and 13.5 ka BP, a large cross-shelf vertical upward shift decreasing northward in magnitude (from 82 m to 39 m between Inuvik and 350 km offshore respectively) is observed on the plots (Fig. 2.4b). During this period, ICE-5G models a massive deglacial event around 14.6 ka BP, which corresponds to a time of rapid global sea level rise (~20 meters in 500 years) known as Meltwater Pulse 1A (Fairbanks 1989). This event would emphasize the massive jump leading to the maximum lithospheric displacement of 73 m, 350 km offshore. As the ice sheet retreats quickly from the region but isostatic rebound takes some time to happen, the temporary mass deficit reduces local RSL (Gomez et al. 2010). The drop in sea level provides a secondary feedback due to seawater self-gravitation because this creates additional mass loss from the region. Referred to as geoidal-eustasy by Fjeldskaar (1991), this effect is observed in Figure 2.3a. Post-16 ka BP, the RSL becomes relatively lower than the eustatic sea level, which induces a lower geoid making everything in the area, including the forebulge, seem higher than today by up to 30 m. These values of geoidal-eustasy incurred during deglaciation fall within the range also estimated for the Fennoscandian ice-sheet (Fjeldskaar, 1991). Therefore, the large vertical displacement calculated in Figure 2.4 results from this effect. Post-12 ka BP, this effect most likely considerably reduced its contribution, leaving the changes in the shape of the curves to express mainly

A

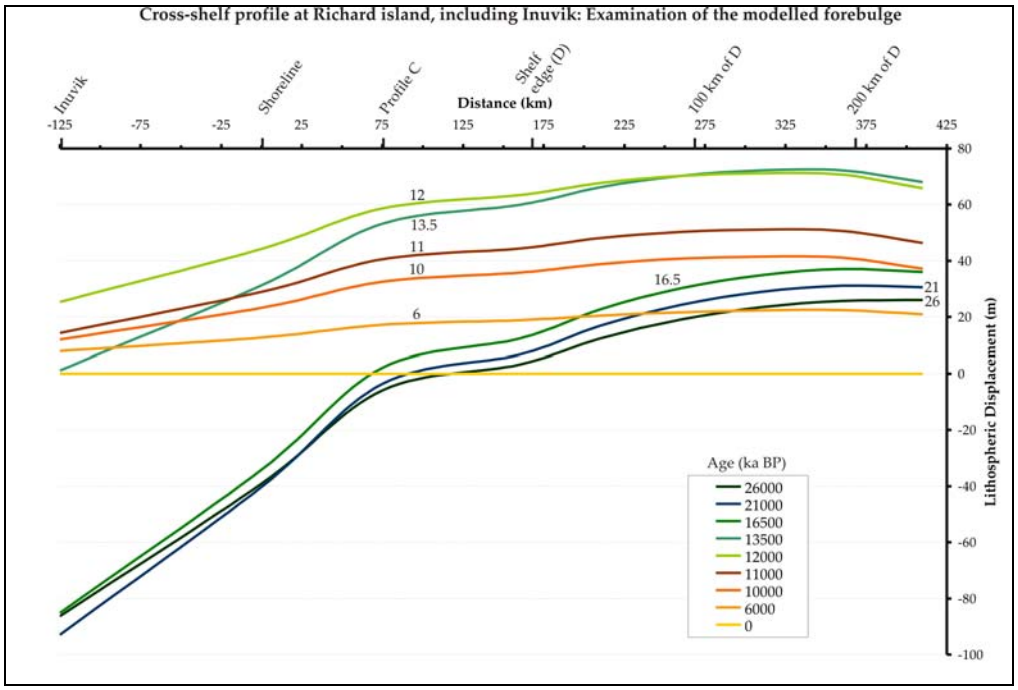

B

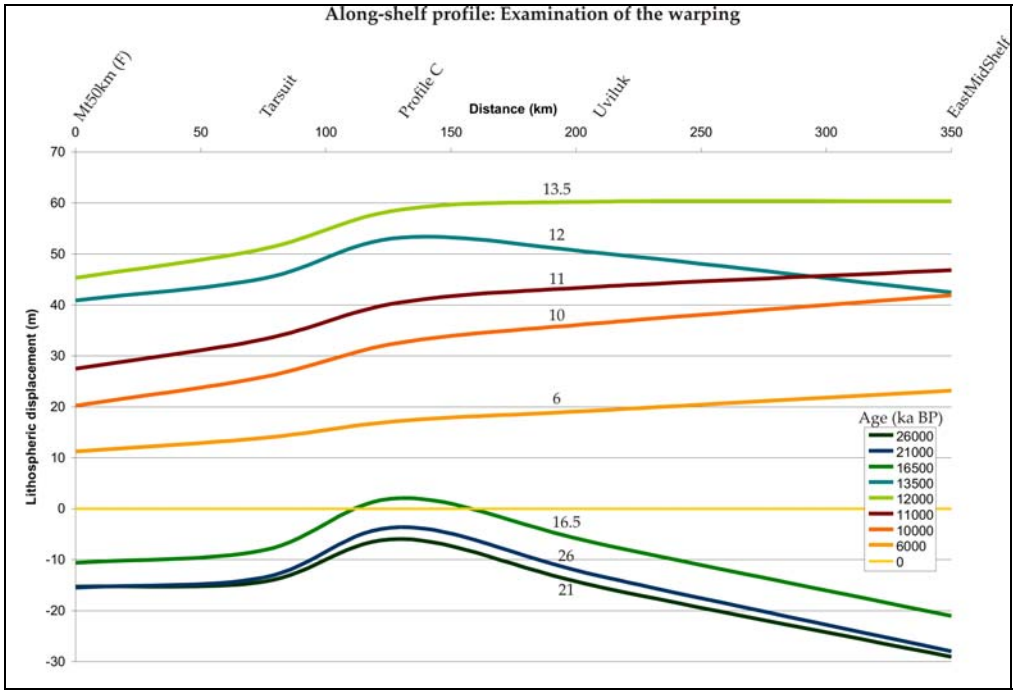

Figure 2.4: A) Examination of the modeled lithospheric displacement along an onshore-offshore profile over Richard Island and the Eastern Beaufort Shelf. Location of transect displayed on figure1. B) Examination of the modeled lithospheric displacement along an east to west profile crossing the Eastern Beaufort Shelf. Location of the transect displayed on Figure 2.1.

a collapse in-place of the forebulge with a possible slight migration southward (Steffen and Wu, 2011).

As mentioned in the previous section, along-shelf variations in RSL are smaller but still significant (20 m during the LGM; Fig. 2.3b). These curves show clearly the upwarp between the Mackenzie and Admunsen ice streams. This mutually-induced relative flexural upwarp between ice streams is at its maximum at the LGM, when the Mackenzie and Eastern Shelf (Admunsen) regions are downwarped by 12 and 25 m, respectively. This mid-shelf bulge is still depressed below eustatic sea level at the LGM, indicating that it is not a forebulge, but rather an area of less flexurally-depressed lithosphere due to its distance from the Mackenzie and Amundsen Ice Streams.

2.5 Discussion

2.5.1 Study comparison and model sensitivity

To strengthen the model results and interpretation presented here, comparisons against other similar studies are made. Stea et al., (2001) ran a similar study for the southeastern region of the LIS. Their model was based on the ice model ICE 3G (Tushingham and Peltier, 1991) and a 150 km thick lithosphere overlying a uniform 10^{21} Pa s linear-viscous mantle. Even though ICE-3G was improved to the later 5G version, their study presents similar results. The difference resides in the interpretation of the results. Stea et al. modeled forebulge has a wavelength of 1200 km with 50 m peak amplitude at 12 ka. The peak was interpreted as the forebulge maximum, but following the reasoning presented here, the magnitude of the peak could also be interpreted as a result of geoidal-eustasy. The forebulge itself would thus be smaller and reach equilibrium sooner. This interpretation is supported by Barnhardt et al. (1995) who revised the previous estimates of forebulge height to about 20-25 m and added an

estimated migration speed of 70 – 110 km/ka. Other recent studies based on field observations of the Fennoscandian forebulge show a remaining forebulge of 20 m in height and 230 km in width (Steffen and Wu, 2011). At its apex, the forebulge height is likely to have reached over 60 m.

Compared to the Stea et al. study, the smaller wavelength and peak amplitude observed in our study reflect the difference in model parameters, particularly the elastic structure of the Earth. As mentioned previously, a smaller lithospheric effective elastic thickness narrows the forebulge, increases its amplitude, and reduces its distance to the ice margin, all of which are observed in this model comparison. For the Mackenzie-Beaufort region, the lithosphere is expected to be even thinner than what was used in our model, i.e. on the order of 45 km (Alvey et al. 2008). This statement suggests that the model results presented herein may show greater variations once more regional earth structure parameters are taken into account. To complement this affirmation, ice sheet extents are also a factor to consider when evaluating the lithospheric response. Since the LGM limits of the LIS over the Beaufort Shelf is assumed and narrow (Fig. 1, Rampton, 1988; Dyke et al., 2003) and recent studies suggest a more extensive ice margin, including England et al. (2009), it is likely that the isostatic effects were even more significant in the Mackenzie-Beaufort region.

2.5.2 Stratigraphic and geomorphic evidence

The RSL model presented here is most informative for the period between 12 and 24 ka BP, due to the lack of dated samples. This period is critical in explaining some of the geomorphic features found on the shelf and the Mackenzie Delta. Hill et al. (1985) originally used the presence of incised valleys on the shelf, between 70 and 80 m water

depth, to suggest a latest Wisconsinan fall in RSL. This interpretation was later revisited by Hill (1996) who proposed the alternative hypothesis that high rates of glacial outflow could have formed such valleys. This hypothesis was supported by Murton et al. (2010), who documented the passage of two outburst floods over Richard Island and the shelf between 13 ka BP and 9.3 ka BP (Teller et al. 2002).

The modeled curves presented herein suggest that RSL did indeed fall rapidly between 12 and 15 ka, leaving most of the shelf emerged (Fig. 2.3). Incision of the valleys therefore likely occurred in this time interval and would have been coincident with increased glacial outwash from the decaying ice sheet. Incision resulting from the 13 ka outburst flood cannot be ruled out, because this would have occurred at near lowstand conditions for most of the shelf. The 9.3 ka outburst flood would have occurred at a time of rapidly rising RSL. However, most of the shelf would still have been subaerially exposed (RSL: -70 to -78 m b.s.l.), permitting further incision, but only to a shorter cross-shelf distance. The modeled RSL curves therefore provide a more robust framework for future stratigraphic analysis.

In the Mackenzie Trough, Hill (1996) described a progradational delta deposited at a maximum 82 m below present sea level. If subsidence caused by overlying sediment is taken into account, this delta was more likely to have been deposited when sea level was higher. Based on the RSL model for this location (Fig. 2.3b, Mackenzie curve), the progradational unit would thus have been deposited sometime after 11.5 ka BP (-80 m), but prior to 9 ka BP (-50 m). Since a sea level still-stand at this time appears unlikely, the most likely interpretation of this progradational unit is an increase in sediment supply. The timing potentially coincides with the second outburst flood (9.3 to 11.8 ka BP)

proposed by Murton et al. (2010), which would have carried a high volume of the available glacially-derived sediments.

England et al. (2009) identified raised shorelines around McClure Strait in the western Canadian Arctic Archipelago supporting evidence of post-LGM isostatic depression (Fig. 2.5). The elevation of the beaches spans between 130 m a.s.l. landward and 28 m a.s.l. seaward with ages ranging between 14 and 12.8 calendar year BP. Figure 2.5a presents the modeled RSL curves along a transect located in McClure Strait. The curves match the data points relatively well considering that ICE-5G does not predict ice over Banks Island (fig. 1a) and that the VM2 earth structure model is likely over-estimating the lithospheric elastic thickness of the area, which is estimated around 50 km (Kirby and Swain, 2009). Therefore, by correcting the ice model and using regional earth structure parameters, the lithospheric displacements would likely be greater (larger depression) and be reflected by larger values of RSL. This effect is assessed in Figure 2.5b, where by vertically translating the initial graph by 60 meters upward, the RSL curves fall within the data points. This amount of displacement can be explained by four factors: 1) 3D Earth structure instead of spherical symmetry, which can result in 10 to 20 m difference (Kaufmann, 2004); 2) the effective elastic thickness (Te), which showed 10 m of additional flexion in a flexural test varying only Te between 100 and 40 km; 3) relaxation time, which is controlled by the mantle viscosity (Jouet et al., 2008); and 4) ice sheet extent. The correlation between the RSL model and field observational data is potentially significant, but to completely evaluate this statement, it will be necessary to make the adjustment to the ice model and find a way to use more regional parameters in the sea level model.

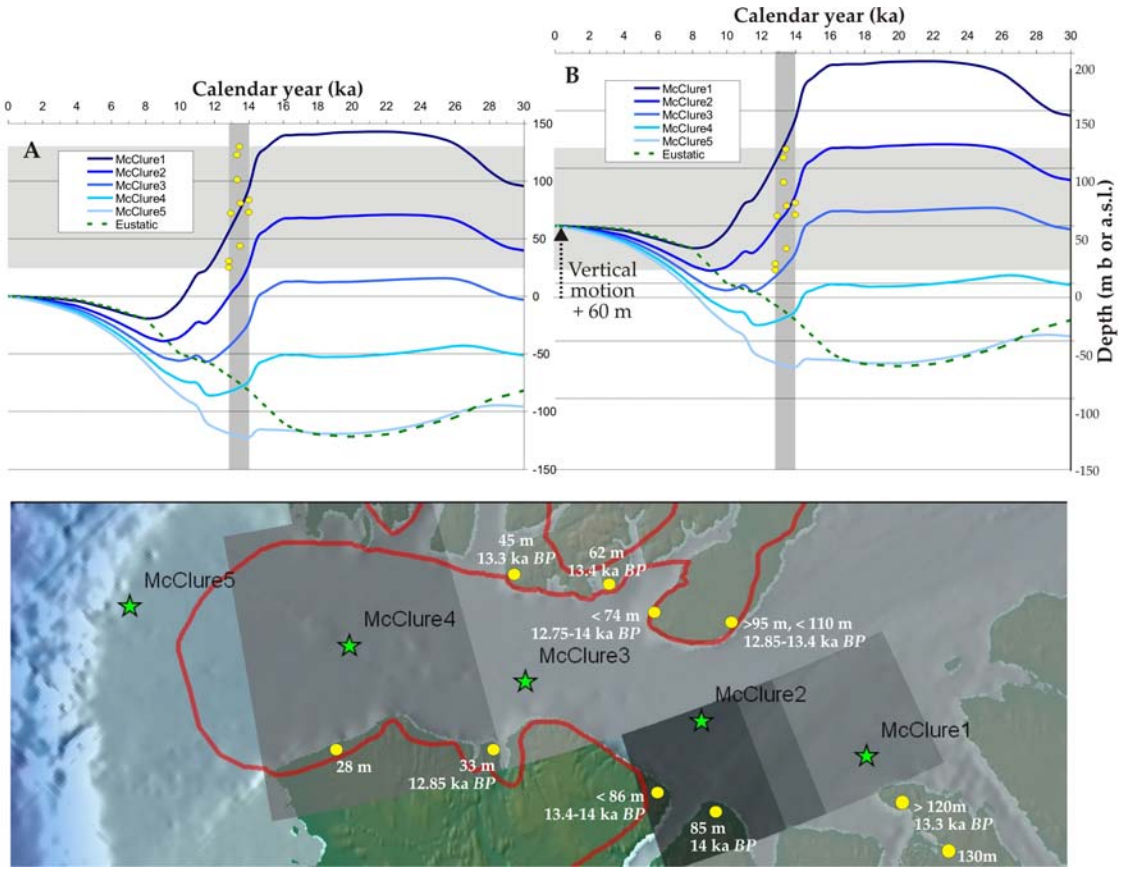

Figure 2.5: Comparison of recent field data observation with the RSL model results in McClure Strait. A) Field observations plotted against RSL model outputs. B) Field observations plotted against RSL model outputs translated up by 60 m. Samples taken from England et al., 2009.

2.6 Conclusion

It may be appropriate to use one single RSL curve in regions that are not influenced by glacial isostatic adjustment, but this is not the case in regions closer to the ice sheets. The previously accepted RSL curve for the Canadian Beaufort Shelf was developed based on widely distributed dated samples. The new RSL model outputs suggest however, that due to the GIA, the RSL varied largely within the sampled area and the timing and magnitude of events differed considerably. Depending on the location, the lowstand was modeled between 14 and 12 ka BP and reached between 85 and 140 m

below present sea-level. These model results are important as they open new ways of thinking about stratigraphic problems related to the Canadian Beaufort Shelf.

Constraining RSL histories in the Arctic has important implications for understanding the stratigraphic evolution of these shelves and the potential geohazards that may impede the economic development of glaciated marine regions. Therefore, future work should evaluate the impacts of using a partially dynamic RSL model in comparison to using a more conventional single RSL curve on the evolution of shelves. This work is presented in chapter 3.

Presently, RSL model outputs are the only reasonable option available to provide regional RSL information for this region. The present study clearly highlighted that RSL in the Beaufort-Mackenzie region may have been quite different than previously thought. As a next step, empirical observations are needed to validate and increase the robustness of the model and the model predictions can be used to target these future sample sites. The new information published about raised beaches around McClure Strait and glacial extent on Banks Island (England et al., 2009) can also be used along with the model to quantify geotechnical parameters for the regions, which in turn will contribute to improving the model and the RSL predictions. Comparing the results of England et al. (2009) study to the model results also indirectly supports claims that ice margins offshore were more extensive than presently assumed.

CHAPTER 3- The influence of glacial-isostatic adjustment on the stratigraphic development of glaciated shelves – an insight into the Canadian Beaufort Shelf

Kim Picard and Philip Hill

3.1 Abstract

Glaciated shelves develop under the influence of a more complex suite of processes than most non-glaciated shelves. Amongst the specific processes are the glacially-influenced sediment supply and the glacial-isostatic adjustment (GIA), which is largely responsible for the complex nature of regional relative sea-levels. This study explores the impact of these complex factors on the Late Quaternary evolution of the Canadian Beaufort Shelf as a case-study using the process-based stratigraphic simulation model, SedFlux.

Uncertainties associated with post-LGM conditions create difficulties in establishing good model parameterization. Thus, simulations are first performed on the Mackenzie Trough area, where data availability provides better views for evaluating and constraining parameters that will be next applied to the shelf environment.

The results specific to the Mackenzie-Beaufort region suggest that the ice sheet margin was more extensive than previously assumed, consequently modifying the regional RSL history. A new geological framework for the Mackenzie Trough, presenting a different timing for the various structures identified in the previous model, is thus provided. Simulations of the Eastern Beaufort Shelf reveal that the stratigraphy found at the Uviluk borehole cannot be constrained using the depositional environment and the age described in the sample. A review of the sample description however, suggests that this dated sample should not be considered a RSL indicator as it has likely been deposited

in a mid-depth (~ 40 m) deltaic environment. The reassessment of the depositional environment thus better correlates with the stratigraphy of the borehole. Glacial outburst floods funnelling through the area would have mostly bypassed the shelf and contributed to its progradation. If flood water were directed to the Mackenzie Trough, the deposits are likely to be found within the lower wedge.

This study also draws many general conclusions applicable to glaciated shelves. Due to GIA, the differential timing of RSL in the cross-shelf direction influences the stratigraphic development of shelves by developing more progradational than retrogradational stratigraphic features. Glacial-interglacial cycle simulations suggest that subaerial deposition of glacial outwash deposits significantly influences the evolution of glaciated shelves. The higher rates of floodplain deposition likely support more shelf aggradation and shoreline regression, which, along with the high glacial sediment supply, result in more progradation of these shelves.

3.2 Introduction

Continental shelves evolve under the influence of multiple processes acting at various time-scales, such as sea-level and sediment supply fluctuations, thermal and isostatic subsidence, sediment dispersion. Understanding the influence of these controls on the sedimentary record has been proven possible using stratigraphic models (Hutton and Syvitski, 2004; Overeem et al., 2005; Jouet et al., 2008, Hutton and Syvitski., 2008; Overeem and Syvitski, 2010). Most stratigraphic models use a single sea-level curve to represent the area. This scenario is generally valid in areas where relative sea-level (RSL) is regionally constant, but it is not the case for regions that have been glaciated and where glacial isostatic adjustment (GIA) has strongly affected the RSL (Kaufmann, 2004;

Steffen and Wu, 2011). Overeem and Syvitski (2010) were the first to investigate how GIA affected the sedimentary record. The authors evaluated this process specifically on fjord environments where rapid uplift occurred soon after the onset of deglaciation. However, the regional impact of GIA on the stratigraphic evolution of a glaciated shelf has yet to be evaluated. As Kaufmann (2004) points out, the lithospheric displacement induced by the evolution of an ice sheet results in a RSL curve that varies depending on its distance from the ice mass. Therefore, following deglaciation, regions located within the ice sheet perimeter as is the case for fjords, would have been uplifted. In contrast, regions located at the periphery of the ice sheet would have been subjected to forebulge formation and thus, following deglaciation would have seen transgression. Relative sea level change on a glaciated margin is therefore likely to be spatially variable and the stratigraphic record correspondingly complex. The main focus of this study is to evaluate the impact of GIA on stratigraphic evolution of a glaciated shelf, using the Canadian Beaufort Shelf as a case-study (Fig. 3.1).

Several other characteristics of the Canadian Beaufort shelf motivate this study. During the Pleistocene, the Beaufort Shelf underwent major fluctuations in sea-level and sediment supply due to the extensive North American Glaciations. At times of low sea-level, the shelf was subaerially exposed to cold air temperatures that resulted in thick permafrost aggradation. Transgressions resulted in the (relatively slow) degradation of the subsea permafrost. The present day shelf is underlain by up to 600 m of still frozen sediment, the distribution and state of which are intimately associated with the RSL changes and resultant stratigraphic evolution.

The geothermal history of the shelf also affects gas hydrate distribution. The freezing temperatures mean that much of the shelf lies within the gas hydrate stability field. Paull et al. (2007) attribute the effect of permafrost degradation and consequent gas hydrate dissociation resulting from marine transgression to the formation of diapiric features, known as Pingo-Like Feature (PLF), on the shelf. Recent multibeam bathymetric data reveal a large numbers of PLFs on the shelf edge (Blasco et al., 2011).

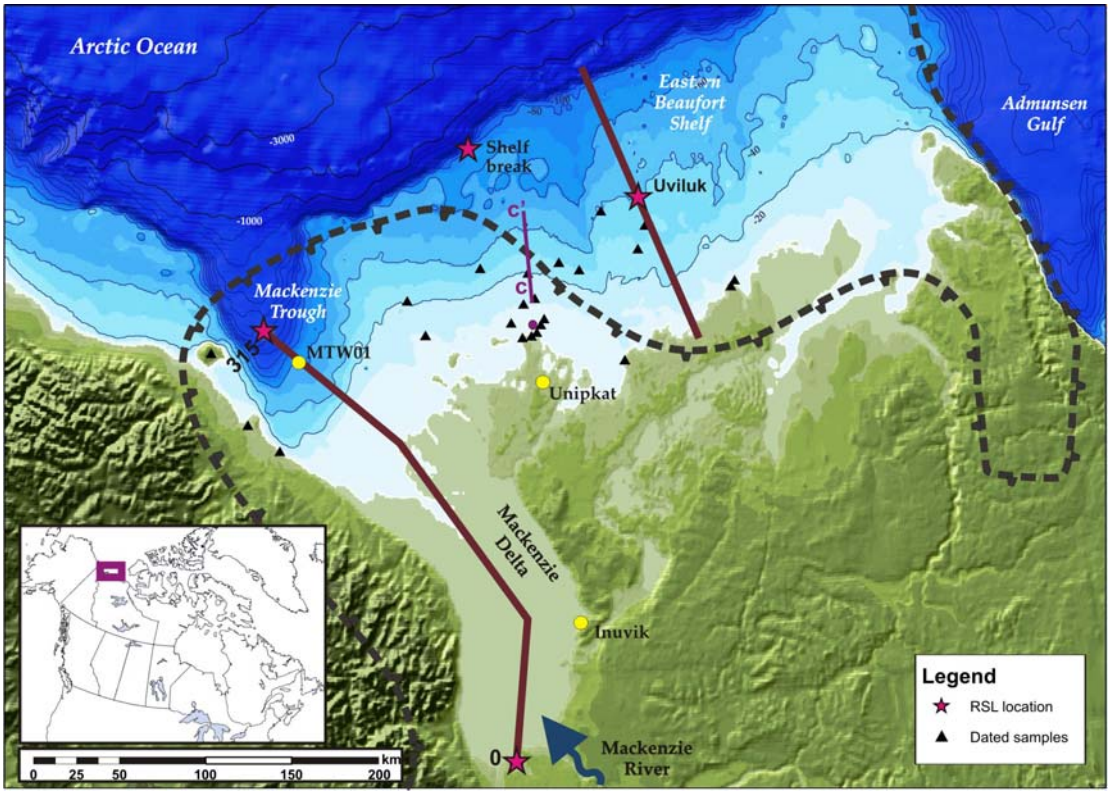

Figure 3.1: Location map of: Hill et al. (1985; 1993) samples (black triangles); RSL curve presented in Figure 3.2 (pink stars); transects used in stratigraphic simulations; limit of LIS at LGM according to Rampton (1988) (doted line); C-C' seismic profile and lithostratigraphic cross-section discussed in figure 3.9.

Knowing that the Beaufort Shelf underwent extensive RSL fluctuations during the Pleistocene, one can expect the geothermal history and stratigraphy of the shelf to be complex. Present geothermal models use a eustatic sea-level curve and a simple layer

cake stratigraphic model. These models do not consider the spatio-temporal variations caused by GIA in the development of a glaciated continental shelf.

Hill et al. (1985; 1993) provided an empirical relative sea-level (RSL) curve for the Mackenzie-Beaufort region using radiocarbon ages measured on peat or shell samples collected over a large marine region, and from which only two sample points help constrain the pre-Holocene portion of the curve. A companion publication, presented in Chapter 2, demonstrates that this regional curve is a generalization of a set of relative sea-level (RSL) curves that can be derived from a modern sea level model (Fig. 3.2; Mitrovica and Milne, 2003; Kendall et al., 2005). This gravitationally self-consistent model computes the effects of glacio-hydro isostasy, geoid changes, and true polar wander using an ice history and a solid Earth rheology (ICE-5G / VM2; Peltier, 2004). The RSL model suggests that significant variations would be expected in both across- and along-shelf directions (Fig. 3.2).

SedFlux (Hutton & Syvitski 2008), a two-dimensional process-based stratigraphic simulation model, coupled with a more complex RSL model, was used to meet the following study objectives:

- Understand the impact of GIA on the stratigraphic development
- Provide a geological framework for the post-LGM Mackenzie Trough sedimentary record.
- Provide insight into the stratigraphic development of the Eastern Beaufort Shelf
- Provide a framework to better understand the impacts of glacial outburst flood events throughout the region

- Contribute to maximizing the effectiveness of future field research aimed at finding evidence to the questions listed above by defining the potential best-fit areas.

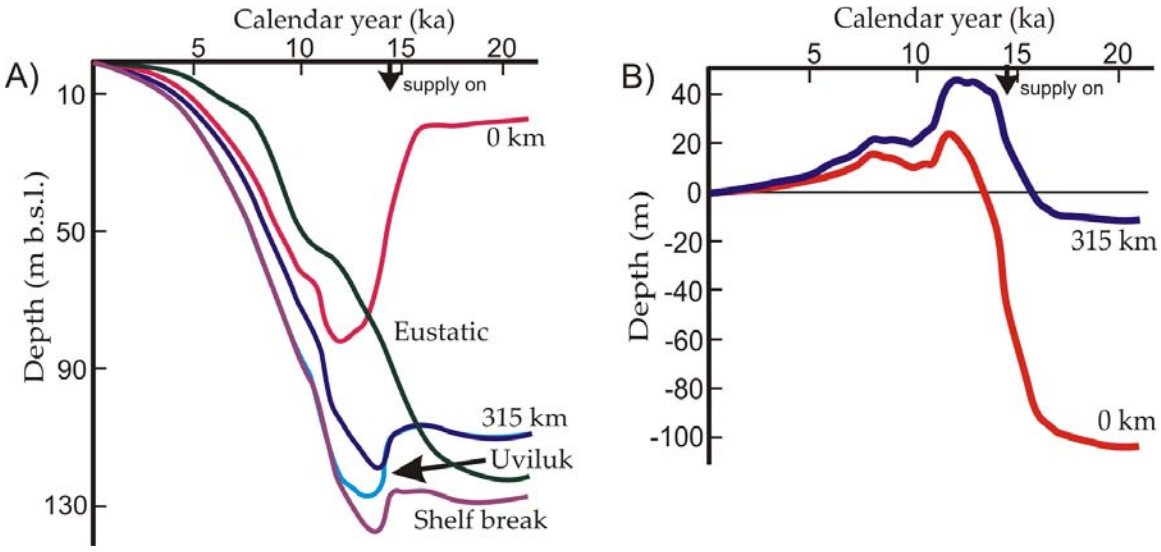

Figure 3.2: A) Relative sea-level (RSL) curves extracted from glacio-hydro-isostatic model for different locations within the study area (refer to pink stars in fig. 1 for locations. B) Lithospheric displacement on the Mackenzie transect calculated by subtracting the RSL from the eustatic curve. The displacement is not a totally true displacement as it includes geoid and true polar wander effects.

3.2.1 Regional setting

The Mackenzie Trough and Eastern Beaufort Shelf (EBS) are part of the Canadian Beaufort Shelf, located in the Arctic (Fig. 3.1). The eastern shelf covers 50 000 km^2 of seafloor, 400 km in length by 100 to 150 km in width, with a shelf break located around the 80 to 100 m isobath. Two large glacial troughs cut through the eastern shelf, the Mackenzie Trough and the Amundsen Gulf, both thought to have been glacially-incised prior to the Early Wisconsinan, and reworked by the Laurentide Ice Sheet (LIS) lobes during the Late Wisconsin (Hill 1996; Dyke et al. 2003; Stokes et al. 2009). The Mackenzie Trough, to the west, hosts one of the largest deltas in the world, the

Mackenzie River Delta, and is represented by a low and uniform gradient of 1- 2 m/km. North of the Mackenzie River Delta, the break in slope is found around the 100 m isobath, a hundred kilometres seaward. Two smaller troughs have been incised the Eastern Beaufort Shelf, Kugmallit and Ikit Troughs. Hill et al (1985) originally interpreted the incision of these valleys to be the result of sea-level lowering, however Hill (1996) raised the possibility that the incision could have resulted from an increase in water discharge. Murton et al. (2010) suggested that two possible glacial outbursts draining Lake Agassiz would have been routed through the Mackenzie-Beaufort region between 13 and 9.3 ka BP. The first event would have happened between 13 and 11.7 ka BP and the second event, between 11.7 and 9.3 ka BP. These events are thoughts to have reshaped the landscape of the Mackenzie-Beaufort region, leaving an extensive eroded surface and thus, a large amount of materials to be deposited offshore (Murton et al., 2010)

During the Wisconsin Glaciation, the LIS and its Mackenzie and Admunsen Lobes reached their maximum extent during the Late Wisconsinan (Dyke et al., 2002). The maximum extent appears to have been reached and maintained throughout the LGM, i.e. 21 ka BP. The location of the maximum ice sheet extent, especially in the offshore area, presents uncertainties as little evidence has yet been found (Rampton, 1988; Blasco et al. 1990; Fig. 3.1). Recent evidence suggesting that Bank Island was overridden by the ice sheet and that McClure Strait ice stream extended farther offshore (England et al., 2009) may however, support a more substantial extent around the Mackenzie-Beaufort region than previously thought. The deglacial history of the study area shows that the onset of

deglaciation did not occur until 17 ka BP and that the ice lobes were the last ones to completely retreat, somewhere between 14.4 and 14.1 ka BP (Dyke et al., 2003).

3.3 General Method

3.3.1 SedFlux stratigraphic simulation model

To model the stratigraphy and evaluate the impact of GIA on the stratigraphy, the two-dimensional process-based stratigraphic simulation model SedFlux was used. SEDFLUX 2.0 basin-fill model runs as a 2D application (Syvitski & Hutton 2001; Hutton & Syvitski 2008). The 2D model simulates lithologic character of basin stratigraphy by parameterising the erosion and deposition of sediments along river beds; the spread of fluvial load into the ocean; the dispersal of suspended sediments via plumes; the dispersal and sorting of sediments based on ocean storms, cross-shore transport due to wave action, failure of margin deposits, as well as transport via turbidity currents and hyperpycnal flows; the change of basin configuration with subsidence and tectonics; and finally, with the compaction and preservation of sediments. In addition, the 3D model deals with river channel avulsion, the 2D diffusion caused by ocean storms and the 2D flexure caused by sediment or ice loading. The model proved to be capable of handling the changing boundary conditions such as bathymetry, sea-level fluctuations and shoreline position. The model reconstructs the temporal stratigraphy for a particular sedimentary environment and outputs sectional sediment properties, synthetic cores and seismic profiles, which can later be compared with field data. Since the model is built with multiple modules, freedom exists to include whichever parameters and processes are feasible. Examples from published papers show the potential and reliability of the model (Syvitski & Hutton 2001; Kubo et al. 2005, Kubo et al. 2006; Hutton & Syvitski 2008; Jouet et al. 2008; Overeem et al. 2005).

SedFlux uses a series of input files containing user-defined parameters serving to activate and control various modules. Specific details on the functionality and the equations behind the modules used by Sedflux are available in the model's original publications (Syvitski and Hutton, 2001; Hutton and Syvitski, 2008). Sensitivity tests were applied to all modules in order to guide the choice of inputs.

Because the Canadian Beaufort Shelf includes two different environments, a formerly glaciated trough occupied by a large modern delta (Mackenzie Trough), and a more typical shallow shelf with modest modern sedimentation (EBS), the study is divided into two sections. The first section uses the Mackenzie Trough (MT) as a test study to set up the Eastern Beaufort Shelf (EBS) study, which is discussed in the second section. The Mackenzie Trough area contains more groundtruth data than the EBS. It is thus possible to better understand the post-glacial conditions that existed at the time and apply the lessons learned to develop a best case scenario for the EBS. The SedFlux modules that contained similar parametization for both study areas are first described here, while the parameters more specific to each area are described in their respective sections.

PROCESS MODULES

Sea-level and subsidence files

Modeled RSL curves were constructed from RSL values depicted every thousand year until 17 ka BP, then every 500 years until present. The curves were extracted every 500 m along the Mackenzie transect. Each curve was then converted to rates of sea-level change by subtracting the older value from the younger value and dividing the result by the amount of years passed. Positive rates meant subsidence or sea-level rise whereas negative values represented uplift or sea-level fall.

Plume

Amongst all the process modules that can be turned on or off, the plume module is essential. The module disperses the suspended load offshore using two different plume processes, hypopycnal and/or hyperpycnal plumes. While hypopycnal plume has to always be activated as it is the main mechanism by which the sediment is transported and deposited offshore, the hyperpycnal plume process is optional. Considering the hyperpycnal plume process increases the model run-time considerably and that the process was not triggered during a sensitivity test, the process was not activated.

Sediment failure, debris flow and turbidity current

These processes have been tested during both eustatic and RSL model simulations, which based on the default settings for each processes, were not triggered. For the same reasons as the hyperpycnal plume module, these processes were kept inactive for all other runs presented.

Bedload dumping

In Sedflux, the bedload dumping module deposits the bed load (first grain-size listed in the sediment file) evenly from the river mouth to a distance set by the user (Table 3. 2). This distance was estimated at 5 km based on the tidal range specific to the region and its associate intertidal plain. Carson et al. (1999) estimated that 34 % of a total sediment flux from the Mackenzie River drainage was retained or trapped in the floodplain, distributed equally between the lakes and their shores, while 66 % made it to the offshore portion of the delta. Considering the small amount of bedload mentioned by the authors, most of the retained sediment must belong to the suspended load. Modelling retention of suspended load is not possible with SedFlux. However, using bedload and the bedload dumping module, it is possible to make reasonable assumptions regarding floodplain deposition. In SedFlux, floodplain deposition is uniform and spread via two possible avenues defined

by two different parameters. These parameters are explained in length here, as other publications do not offer much explanation on the subject.

The first parameter, Ratio of floodplain to bedload rate refers to the ratio of sedimentation rates between the floodplain sedimentation rate (D_f) and the bedload sedimentation rate (D_b). Sedimentation rates are calculated using the following equation:

$D = Q_i/W_d L\rho$ (Syvitski and al. 1988), eq. 1

where Q_i is the load flux (kg/s) in question (Q_b or Q_f), W_d is the width over which the load is distributed, L is the distance from river mouth over which bedload is dumped, and ρ is the uncompacted density of the bedload grains. Once the bedload sedimentation rate is established, the ratio determines the floodplain sedimentation rate. For instance, if the ratio (D_f:D_b) is 2 then $D_f = 2D_b$. Since sedimentation rates are dependant on the length of the profile over which the sediments are deposited, the assumption is that as the floodplain gets narrower mainly because of relative sea-level rise, then the total amount of floodplain deposition is linearly affected ($Q_f=D_f W_d \mathbf{L_f} \rho$). Determining the appropriate ratio was based on Syvitski and Saito (2007) who found that the larger the delta plain, the higher the retention rate in the plain (between 30 and 80%), and thus ratios in the order of 0.6 to 1.5 should be applied. However, a sensitivity test revealed that this parameter did not function as expected and therefore, subaerial deposition for this study relied on the second parameter.

The second parameter, Fraction of bedload retained in the floodplain, allows the user to set a fraction of the bedload to be distributed uniformly over the whole available subaerial plain. The fraction is set between 0 and 1, 1 representing all of the bedload.

Because the load is given as a flux (kg/s), over a constant amount of time, the smaller the floodplain the thicker the sediment layer deposited becomes. This effect is contrary to observations made by Syvitski and Saito (2007). Since the simulations covered mostly a transgressive period and thus a decreasing subaerial plain with time, the amount of bedload should be reduced following the transgression. A sensitivity test was carried out and will be discussed later.

Erosion

Subaerial deposition is subject to erosion processes, assuring that both erosion and deposition occurs along the river bed. The user can choose between two erosion mechanisms: diffusion or slope dependent (Hutton and Syvitski, 2008). For this study, diffusion was used.

Isostasy

The *isostasy* module is used in conjunction with sea-level and sediment supply to evaluate the effects of water and sediment loading (Syvitski and Hutton, 2001; Hutton and Syvitski, 2008). The controlling parameters included in SedFlux are the effective elastic thickness, Young's modulus, and relaxation time. For the Beaufort-Mackenzie region, these values were respectively estimated between 45 and 65 km (Kirby and Swain 2009), $7e^{10}$ Pa, and 2500 yrs (T. James, pers. comm.). For the present study, a new parameter was added to Sedflux. This parameter deactivated water loading, calculating only for sediment loading. This parameter was needed considering that water load, which makes a substantial contribution to the total load, is included in the RSL model used in the sea-level module. Sediment loading tests were carried out to approximate how much loading resulted from specific settings.

3.4 Mackenzie Trough

3.4.1 Quaternary geology of the region

The Mackenzie Trough is thought to have been incised in the early Wisconsinan or prior and filled with more than 200 m of late Pleistocene sediments (Blasco et al., 1990,; Blasco and Lewis, 1991). Post-glacial deposits, mainly deltaic deposits, overlay a thick infill of poorly resolved glacial material capped by a regional reflector. These deposits result mostly from the sediment contribution associated with Mackenzie River drainage system, which was established during the late Wisconsinan. The present interpretation of the Mackenzie Trough development post-LGM relies on Hill's (1996) sequence stratigraphic interpretation (Fig. 3.3), which is based on the Hill et al. (1985, 1993) relative sea-level (RSL) curve. There are two main draw backs to this interpretation. First, it is based on a RSL curve loosely constrained between the LGM and the Holocene and secondly, there are large interpolations between the subaerial delta borehole descriptions and the offshore trough seismic reflections. Details about the lateral variability of the internal structure, from the delta shore face to Inuvik, are missing because seismic reflections are masked by the presence of permafrost.

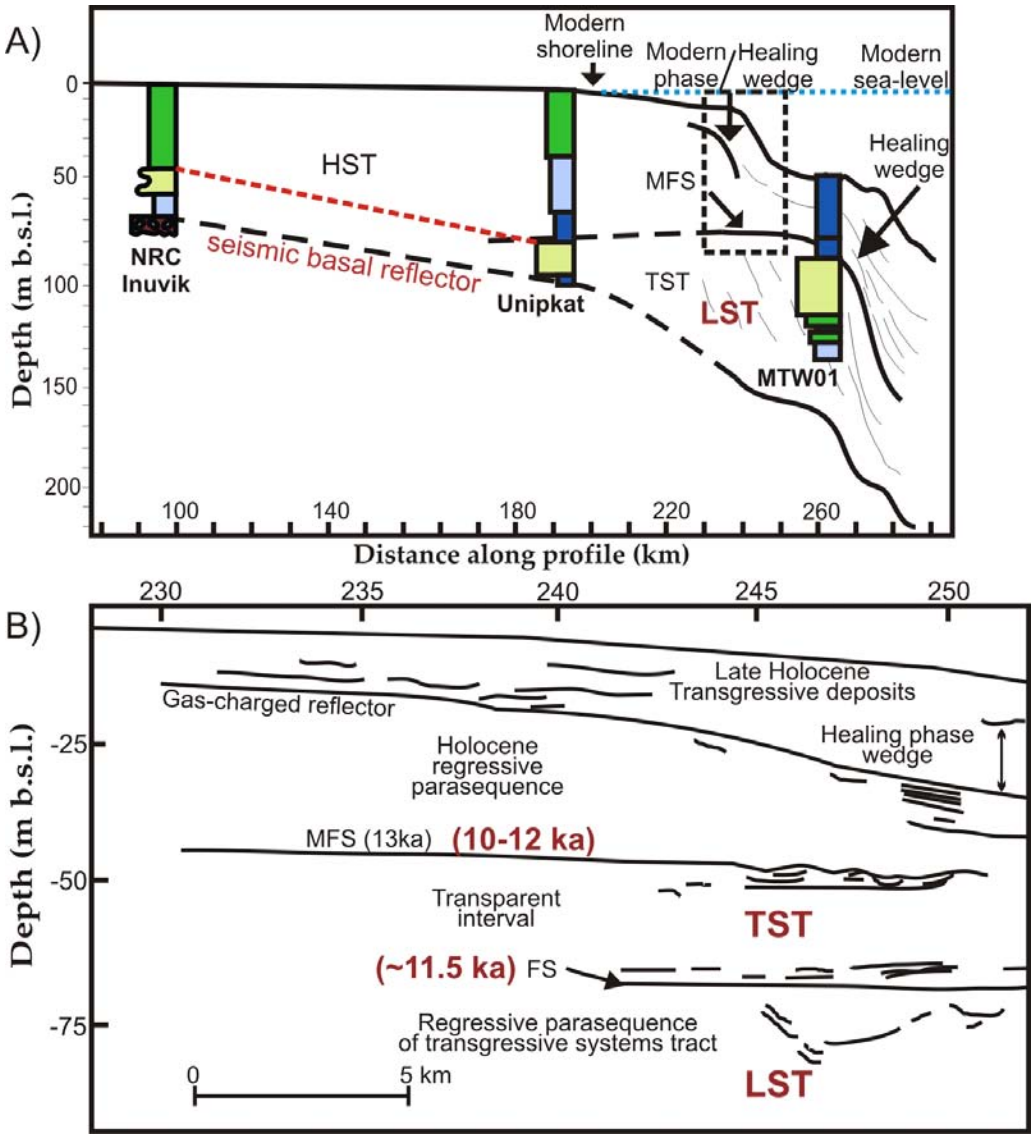

Figure 3.3: Original (black) and newly proposed (red) seismic profile interpretation modified from Hill (1996). A) subaerial and offshore portion of the Mackenzie River Delta B) details of the delta slope. HST: High systems tract; LST: Lowstand systems tract; TST: Transgressive systems tract; FS: Flooding surface; MFS: Maximum flooding surface.

3.4.2 Method

BOUNDARY CONDITIONS

Initial settings

Boundary conditions are set based on a user-defined vertical bathymetric profile (Fig. 3.4) and a constant width (W) over which sediments are deposited (Table 3.1). The width was set to represent the averaged Mackenzie Trough width, i.e. 60 km, based on the

width of the present delta subaerial plain. Because of the 2D model restriction, even though the delta footprint enlarges offshore, the same width was carried out for the offshore portion. The model uses rectangular cells to store the calculated sediment properties. The dimensions of these cells determine the resolution of the model as sediment properties are compiled and averaged over the volume of each cell. The length of the rectangular cell is based on the width value $d_{x,}$ representing the shore-perpendicular width, and $d_{y,}$ representing the depth of the cell (Table 3.1).

Table 3.1: Boundary conditions and sediment file for the Mackenzie Trough base-case simulation

Model resolution	**Base-case scenario (56333) Qs: 124Mt/yr; Qb: 4Mt/yr (Carson et al. 1998)**
INITIATION FILE	
d_x = horizontal grid cell size (m)	400
d_y = vertical grid cell size (m)	0.75
W = basin width	60000
Bathymetry file	corrected for sediment loading
T = Duration of simulation (yr)	21000
d_t = time step	10d
b_0 = river width (m)	2000
h = river depth (m)	8
μ = flow velocity (m/s)	0.7
Number of grain-size	4
SEDIMENT FILE	
D = grain size (μm)	200, 150, 60, 5
ρ_{grain} = grain density (kg/m^3)	2650
$\rho_{saturated}$ = satured density (kg/m^3)	2000, 1955, 1795, 1504
ρ_{grain} = water density (kg/m^3)	1030
λ = removel rate (1/day)	25, 20, 12, 5
c = compaction coefficient (1* 10^{-8})	6.2, 7, 10, 36
φ_0 = minimum void ratio (-)	0.17, 0.15, 0.1, 0.05

The resolution of the model influences the run-time, thus considering the regional scale of the study objectives the simulations were run using relatively coarse resolution. Variability was assumed to be more rapid and important in the vertical (depth) axis than in the longitudinal axis, hence d_x was set between 200 and 400 m and d_y at 0.75 m. The location of the transect was set to cover the entire length of the trough from Point

Separation to the 60 m isobath offshore (Fig. 3.1). Due to the geometry of the trough and the available data, the transect did not follow a straight line, but ran north for 315 kilometres following the mid point across the trough.

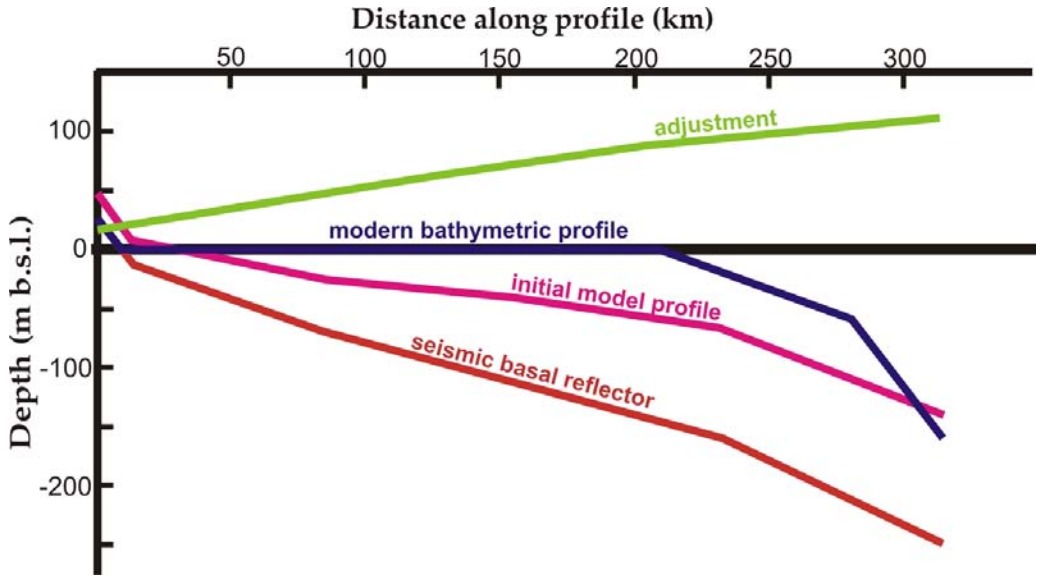

Figure 3.4. Initial model profile before sediment loading adjustment (pink line). Adjustment (green line) made to the seismic basal reflector presented in A (red line), representing the net RSL rise from 21 ka between the start and the end of the transect (Fig. 3.2).

Locations holding important data information, such as NRC Inuvik (80 km), Unipkat (195 km), and MTW01 (265 km) boreholes were extrapolated onto the transect and used to define the initial profile (Fig. 3.4) along with seismic profile interpretations (Fig. 3.3a). Hill et al. (1996) identified a hummocky basal reflector from a seismic profile collected across the offshore Mackenzie Delta (Fig. 3.3a). This reflector, based on its downlapping nature and the unfossiliferous silty clay found in a few samples, was interpreted as a post-LGM flooding surface or its correlative. Considering that the Mackenzie Delta developed post-LGM, this basal reflector was used as a starting point to calculate the initial

bathymetric profile for the model. To cover the subaerial portion of the delta, south of Unipkat borehole, the reflector was projected linearly to the start of the trough at kilometre 10 passing through the depth of bedrock identified in the NRC Inuvik borehole (Johnston and Brown, 1965). It was further extended south by ten kilometres to connect to a point elevated to today's elevation (Fig. 3.4).

In Sedflux, modeling RSL changes can be done using two methods: 1) Sea-level is raised or lowered according to a static bathymetric profile (standard method) or 2) sea-level is held static, but the bathymetric profile becomes dynamic (subsidence method). The first simulation is best used for a simple curve such as the eustatic where a falling sea-level will be simulated using negatively increasing sea-level values. The second simulation however, simulates best a basement uplifting or subsiding differentially based on its position along the profile. For the study presented herein, the integration of the glacio-isostatic RSL model described in Chapter 2 necessitated the use of the second simulation. In this case, RSL was simulated for 21 ka along the 315 km profile (Fig. 3.1). In terms of crustal movement, such RSL estimates are equivalent to having the initial bathymetric profile subsiding over the course of the run between 18 and 110 m depending on the location.

The initial bathymetric profile was then determined by taking the seismic basal reflector and adjusting it for the net sea-level change over the whole time interval (Fig. 3.4). Depending on the sensitivity test, the profile was also adjusted upward to account for the amount of sediment loading measured using the isostatic module. This action was taken so that following a complete run; the modeled basement would end up aligned with the present basal reflector.

River characterization

Sedflux uses a river file to characterize the water discharge, the suspended load concentrations and the bedload flux. Since there is little information available about the discharge and the grain-sizes carried over time by the Mackenzie River system, the assigned values were referenced to the modern observations (Carson et al., 1998; Hill et al., 2001). At present, two main rivers act as primary inputs in the Mackenzie Trough: the Mackenzie and the Peel Rivers. These two rivers combined have a width of about 2.25 km, which split into a complex network of about 57 distributaries running over the delta plain and discharging into the Beaufort Sea. Channel levee heights range between 9 and 1.5 m and current speed varies throughout the year, but averages 0.7 m/s. Because of the 2D approach used in this study, the number of channels or sources to the ocean was not important. Therefore, for modelling purposes, the river was assigned a 2 km width, 8 m depth and the average current value of 0.7 m/s (Table 3.1). The dimensions of the river were not changed over time, but the sediment supply was.

Sediment supply

Hydrological and sedimentological studies of the Mackenzie River and other outlets describing the contribution of sediments to the Mackenzie Delta are not common. Previous studies estimated sediment fluxes ranging between 15 and 150 Mt/yr, but Carson et al. (1998, 1999) provide the most complete and reliable study to date. The authors recorded annual fluctuations between 65 and 225 Mt/yr, but estimated the average annual sediment flux at 128 Mt/yr with a precision of 5% (7 Mt/yr), mainly due to the calculations derived from rating curves. Milliman and Farnsworth (2011) warn scientists to be cautious about sediment load estimates because of the large margin of error created by the different sampling and calculating methods. However, in addition to

their description of uncertainties, the thoroughness followed by Carson et al. throughout their analysis offers confidence in using their estimates.

Suspended load vs bed load

From the total annual flux of 128 Mt/yr estimated by Carson et al., 124 Mt/yr was considered to represent the suspended load and 2-6 % or about 4 Mt/yr the bedload flux. Even though the authors noted from bedform evidence that very little of the bedload moved as bed load and thus should be included in the suspended load, this small fraction was kept as bed load in SedFlux. This decision was made to accommodate other parameters and processes, such as floodplain retention, which required a bedload component in order to be calculated. The bedload is required to be given as a discharge and thus, was set between 130 kg/s (4 Mt/yr or 3%) and 200 kg/s (5% or 6 Mt/yr) depending on the simulations. The suspended load was set to 0.35107 kg/m^3. Both numbers were calculated based on a constant yearly discharge. However, it is recognized that virtually all sediment is supplied to the delta between the months of May and October, with the peak in May, June, and July and with the winter months having negligible contributions (Carson et al., 1999). A sensitivity test was carried out to evaluate the impacts between a yearly averaged delivery and a three month delivery. The results revealed that over the time period considered (21 ka) and based on the resolution of the model, seasonality did not impact the end results.

Grain-sizes

Along with flux estimates to the Mackenzie Delta, Carson et al. (1998) analysed the grain-size distribution for all suspended sediment samples. Most of the load examined belonged to the wash load category, i.e. < 0.125 um and was distributed according to the following percentages: 26 to 34% for clay, 57 to 69% for silt, and 5 to 9% for the sand

particles. Following this *in* situ analysis, the distribution of suspended sediments used in the model was set to a respective ratio of 3:6:1 (Table 3.2). The authors noted from examination of the samples that some of the silt fraction was most likely to include flocculated clay particles. For modelling purposes, it was assumed that flocculated aggregates of clay will behave like single silt particles of the same size and thus, this process did not represent a problem.

Three grain-sizes were chosen to represent the distribution of the suspended load: 150 μm represented the fraction of fine sands, 60 μm to represent the silt fraction, and 5 um for the clay size particles (Table 3.1). Because the Mackenzie Delta is a fine grained delta, the bedload was either assigned a fine sand size of 200 μm or a medium sand size of 300 μm depending on the simulation. In Sedflux, each grain-size is characterized by a suite of properties used in the modelling of various processes. For instance, grain density (quartz: 2650kg/m^3), saturated density, minimum void ratio, and compaction coefficient are used to calculate over time specific processes such as compaction, subsidence, slope failure, etc. Removal rates and diffusion coefficients are used in the calculation of the plume (hyperpycnal or hypopycnal), where the higher the removal rate, the quicker the particle will deposit once it has reached the open water environment. For this study, the specific values for each property were taken from Syvitski and Hutton (2001) and Overeem et al. (2005) and presented in Table 3.1.

Table 3.2: Epoch parameterization for the Mackenzie Trough base-case simulation

	Epoch 1	Epoch 2	Epoch 3	Epoch 4
	21 - 14.3 ka	14.3 - 12 ka	12 - 8 ka	8 - 0 ka
Q = Discharge (m^3/s)	11200	11200	11200	11200
Q_{tot} = total sediment load (X 128Mt/yr)	0	2.5	2	1
Q_s = suspended sediment load (kg/m^3)				
150 μm	0	0.088	0.0702	0.0351
60 μm	0	0.526	0.4208	0.2104
5 μm	0	0.263	0.2104	0.1052
Q_b = bed load (kg/s)				
200 μm	0	500	400	200
L = bedload dumping zone (m)	5000	5000	5000	5000

Epochs

It is apparent for runs starting at the LGM or 21 ka BP, that the sediment supply and grain-size distribution would have fluctuated over time; depending on many factors such as water drainage, the storage capacity of the system and the availability of sediments, the ice proximity, etc. These fluctuations are simulated by using epochs, which are defined as period of time over which the sediment supply and associated characteristics are maintained constant. The modern sediment characteristics and supply described above were used as the reference point for assumptions concerning the epochs. In the base-case and most simulations, four epochs were defined (Table 3.2). Considering that the Mackenzie ice lobe was present in the trough until 14.3 ka BP (ICE5G; (Peltier 2004) and that SedFlux has no means to deal with glacially-derived environments, the first epoch was set from 21 to 14.3 ka BP and delivered no sediment. The second epoch characterized the period following the retreat of the glacial lobe. During this period, it was assumed that large amount of glacial and paraglacial sediments would have been stored and available for re-distribution by the glaciofluvial and glaciomarine systems (Hallet et al. 1996). In addition, glacial outburst floods would have been funnelling through the area and contributing large amounts of sediments. Thus, based on the Murton

et al. youngest outburst flood, the second epoch was set between 14.3 and 12 ka BP and was assigned 2.5 times the modern sediment supply, i.e. 320 Mt/yr. Considering that the duration of the outburst floods were not 2500 years, but most likely occured over a much shorter time period, a separate sensitivity test was carried out, the results of which are presented later. At present, it is difficult to predict how much sediment would have been involved in the outbursts and routed through the Mackenzie Trough or how long this flow would have lasted, but the objective of this sensitivity test was to evaluate the impacts of high discharges over relatively short periods. Two periods of 500 years with sediment output five times the modern sediment supply (640 Mt/yr) were then incorporated amongst the base-case scenario settings. The first pulse spanned between 12.5 and 12 ka BP and the second, between 11.5 and 11 ka BP.

The third epoch spanned between 12 and 8 ka BP and was assumed to represent the waning availability of glacial sediments. This epoch was assigned two times the modern sediment supply (256 Mt/yr). This period acted as a transition period towards the Holocene period (8 ka BP to present), which was set as the fourth epoch and assigned the modern Mackenzie Delta sediment supply (128 Mt/yr). These four epochs were represented in the base-case scenario and evaluated against other time settings.

A present weakness of Sedflux is that the bedload grain size cannot be customized according to the epoch. The sediment parameter file is set so that the first grain-size listed is always the bedload and is followed by the suspended load grain-sizes. For runs spanning over glacial time periods customization of the bedload grain size would be appropriate considering that during time where the ice sheet was in close proximity, the bedload was most likely coarser than the modern day bedload. Considering this model

limitation, the present study does not deal with changing sediment grain-size distribution over the course of a simulation. A sensitivity test was however completed to evaluate the impact of coarser grain-size distribution. The results showed that because coarser grain-size distribution holds a larger average saturated grain density, it reduces the total volume occupied by the sediments. This test thus suggested that if specific periods needed to be represented by coarser grain distribution, then the volume occupied by sediments during these periods would be lessened. This of course does not take into account compaction, which is discussed later in the section.

PROCESS MODULES

Compaction

The decision to activate or not the *compaction* module was based on the permafrost state in the Mackenzie Trough area. Ninety percent of the delta land surface is underlain by permafrost within 3 m of the surface (Nguyen et al. 2009) and the thickness of permafrost is less than 100 m in the subaerial delta due to channel shifting and water bodies (Burn and Kokelj 2009). The offshore region of the Mackenzie Trough however, is known to have little or no permafrost (Judge et al. 1987). An additional uncertainty is that the presence of ice within sediment could significantly expand the total volume of a sediment unit (Dallimore et al. 1996). This effect suggests that permafrost terrain could be subjected to a negative compaction. Therefore, because of the present state of permafrost, its constant evolution since the LGM, and the physical complexity associated with the possible sediment column expansion, the simplest assumption was deactivate the compaction module for all runs.

3.4.3 Results and Discussion

BASE-CASE SCENARIO VS. HILL 1996 INTERPRETATION

Figure 3.5 presents the results of the base-case scenario, which used the RSL model and the parameter inputs described in Table 3.1 and 3.2. This scenario is compared to Hill's (1996) interpretation (Fig. 3.3). The base-case simulation suggests a different timing of events than Hill's interpretation. The results show three progradational wedges separated by flooding surfaces. The early wedge developed from the onset of sediment supply at 14.3 ka BP until around 12 ka BP, where it is capped by a flooding surface. Even though this timing corresponds to the change in sediment supply, this lower wedge was developed due to the RSL fluctuations happening at the time. During this period, progradation was enhanced by the differential movement of the crust between the landward and the seaward portion of the profile (Fig. 3.2). While the seaward part of the profile stopped uplifting, thus giving the transgressive response of the eustatic sea-level control (RSL rising), the landward portion was continually uplifting (slow falling to stable low RSL; inset Fig. 3.5). This resulted in a steepening of the initial profile, creating a period favourable to the development of a progradational wedge. Because this wedge developed mainly during the late falling, stable lowstand and slowly rising sea-level stages, it corresponds to a lowstand systems tract (LST).

In contrast, Hill (1996) assigned the lowest progradational wedge to the transgressive systems tract because its hinge point elevation was well above the assumed lowstand sea level (Fig. 3.3a). Similarly, the bounding surface of the lower wedge was identified as a maximum flooding surface (MFS) (Fig. 3.3a). However, according to the base-case scenario, this bounding surface would correspond to an earlier flooding surface (FS; Fig. 3.5). Nevertheless, Hill (1996) did identify a relatively thick transgressive systems tract

(TST) in high resolution seismic records (Fig. 3.3b) as is apparent in the modeled profile (Fig. 3.5).

The modeled TST is divided into a lower progradational wedge developed between 11.5 and 9.8 ka BP and a retrogradational deposit developed between 9.8 and 7.5 ka BP. The top of the deposit is easily identifiable in the grain-size cross-section by the sharp transition located at 60 metres water depth between the coarser near shore deposits (green) and the finer shelf mud (blue) deposits. The TST is bounded by a maximum flooding surface (MFS). The progradational wedge defining the early part of the TST corresponds to a period where the rates of sea-level rise were more rapid offshore than onshore due to the isostatic displacement of the lithosphere (Fig. 3.2b). This dynamic contributed to maintaining the locus of deposition in place. It appears that the two flooding surfaces, FS and MFS, bounding the TST wedge of the base-case scenario generally correspond to the bounding surfaces of the transparent interval identified by Hill (Fig. 3.3b). Based on the presence of marine sediments identified in Inuvik borehole between 55 and 64 m depth by Johnson and Brown (1965), Hill suggested that the MFS reached as far inshore as this borehole. The model stratigraphy similarly indicates that the MFS extends inland to approximately 140 km from the origin (Fig. 3.5).

Finally, the third and youngest progradational wedge modeled in the base-case scenario formed over the last 7 ka BP as the rates of sea-level rise became similar between the onshore and offshore regions. This wedge corresponds to the Highstand System Tract (HST), as in Hill's interpretation, and represents the modern delta. The delta developed as the rates of sea-level rise slowed down limiting the accommodation space while the sediment supply remained high.

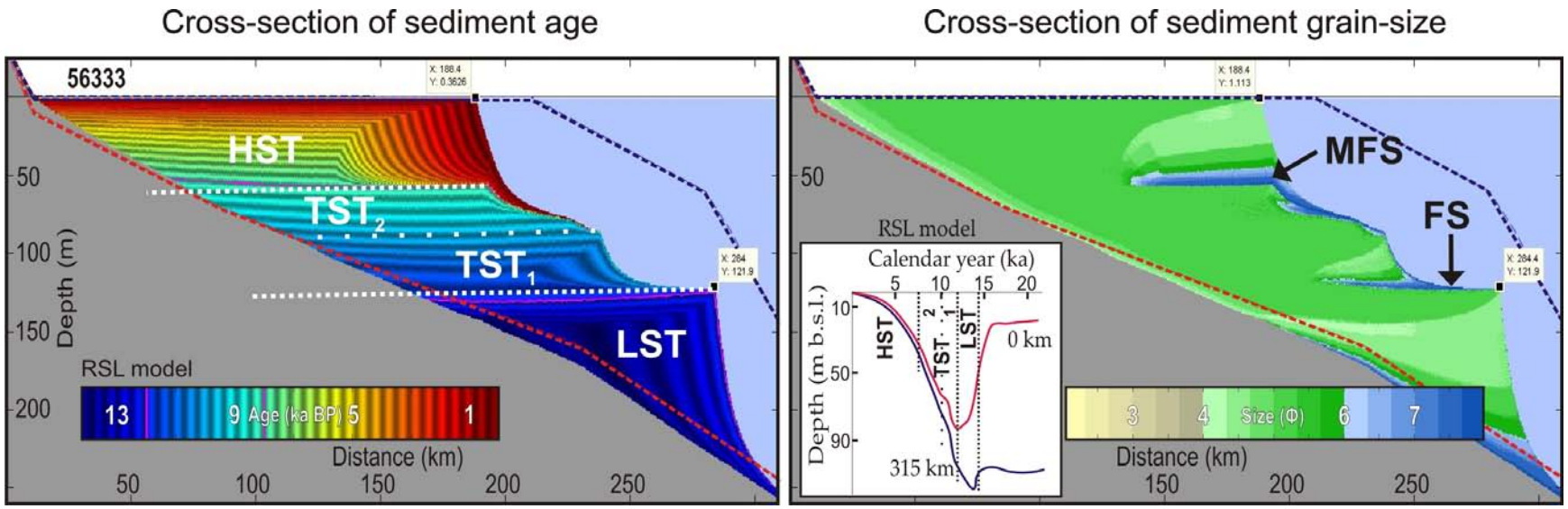

Figure 3.5 Base-case scenario used to compare all other model simulation presented in this paper. The base-case scenario uses RSL model data extracted for the transect running from 0 to 315 km along with the parameters are defined in Tables 3.1 and 3.2. Cross-sections of the sediment age (left); cross-sections of grain-size (right). seismic basal reflector (Fig. 3.3; red dotted line); modern seafloor profile (blue dotted line). LST = Lowstand systems tract, TST = Transgressive systems tract, HST = Highstand systems tract, MFS = Maximum flooding surface, FS= Flooding surface

INFLUENCING FACTORS OFFERING A BETTER STRATIGRAPHIC MATCH

Whereas the base-case scenario approximately matches the stratigraphy documented by Hill (1996), details of the dimensions and depth of the various surfaces do not correlate exactly. Various sensitivity tests can be used to tune the model to a better fit (Fig. 3.6 and 3.7). First, even though the progradational extent of the lower wedge is well approximated, the depth of its deepest hinge line is not. The base-case scenario models the hinge line too deep (120 m) compared to the 82 m reflector depth measured in Hill's interpretation. Amongst the parameters tested, the factors that contribute most to shallowing the top surface depth of the LST wedge were the use of a RSL profile simulating a more extensive ice margin (Fig. 3.6a) and the timing of the sediment supply during the second epoch (Fig. 3.6b).

As shown in Figure 3.6a, the depth of the lower wedge surface is raised when using a RSL profile with more isostatic displacement as it would occur if ice margins were more extensive. In this case, the RSL was characterised by a larger falling stage and shorter lowstand conditions than the standard RSL used in the base-case simulation (Fig. 3.5). This RSL dynamic thus resulted in first the development of a falling stage systems tract (FSST) bounded by a steep erosion surface (SB) and then followed by the LST stage. The LST developed to a lesser progradational extent because of the shorter time interval of the lowstand, but aggraded to a shallower depth because of the shallower lowstand depth (Fig. 3.5). Consequently, the accommodation space was reduced, which resulted in the development of a thinner TST wedge. Reducing the thickness of the TST, which could also be achieved by suppressing the sediment supply during the transgression, is important as the base-case simulation models a TST wedge that is much thicker (70 m)

than the suggested correlative with Hill's (1996) transparent interval (~17 m). By limiting the thickness of the TST wedge, the modeled HST wedge becomes thicker and ends up matching better with the modern delta thickness (~75 m).

The second factor contributing to shallowing the lower wedge surface is by extending the second period during which high sediment load is supplied (Fig. 3.6b). In this case, the TST_1 progradational wedge prograded over much of the underlying LST wedge. By doing so, TST_1 could easily appear as belonging to the LST wedge, which would contribute to shallowing the lower wedge. It is notable that the timing of the TST_1 corresponds closely to the period during which outburst floods may have contributed significant amount of sediments to the trough (Teller et al. 2002; Murton et al. 2010). The impacts of such events on the stratigraphy are to prograde and aggrade the LST wedge (Fig. 3.6c).

In any case, the progradation of the modeled HST is not as extensive as the modern profile. Using this setting, the only factor responsible for inducing more progradation is the sediment supply. This suggests that using the modern sediment load estimate from Carson et al. (1998) over the Holocene period is an underestimate. During the Holocene, many authors suggest the presence of a Holocene thermal maximum in the Arctic (Miller et al. 2010; Kaufman et al. 2004). A spike in temperature and humidity would have induced more precipitation, therefore larger discharges into the Mackenzie basin, which in return could have contributed to increasing the sediment supply for that period.

These model simulations also suggest that first, in order to reproduce the existing sediment volume; the total sediment supply over the period of the simulation was underestimated. Based on the initial trough geometry defined by the modern seafloor

profile and the basal seismic reflector (Fig. 3.3a), the total volume necessary to fill the trough is at least 1.817 X 10^{12} m^3, which assuming an averaged saturated grain density of 1800 kg/ m^3 represents at least 3.27 X 10^6 Mt. This total load represents an average annual load in the order of 224 Mt or 1.8 times Carson et al. annual budget of 128 Mt, which is higher than the average 1.5 times used in the base-case scenario. These calculations do not consider the irregularities in the dimensions of the trough basement nor the impact of compaction, which could limit or increase the volume of sediment needed. Secondly, these models suggest that the total load was most likely not distributed evenly across the entire run, but shared across epochs to reflect the physical and environmental variability. The results presented in Figure 3.6b suggest that the lower wedge was built from a higher sediment supply than the modern supply. This is not surprising as deglacial systems are known to supply more sediments (Hallet et al., 1996).

The modern delta front shows a much shallower slope than modeled in the simulations. In addition to sea ice coverage and ice scour action on the seafloor, storm and currents are assumed to be the processes responsible for this shallow slope (Hill et al., 2001). Although not demonstrated in the present study, Overeem et al. (2005) demonstrated that storms and currents clearly impacted the evolution of the shelf, by moving the depocentre of the delta seaward and thus to deeper water.

OTHER INFLUENTIAL PROCESSES TO CONSIDERED

Floodplain retention and subaerial deposition

Subaerial deposition as outwash plains during glacial periods or retention of sediment in delta floodplains are processes that should be considered when evaluating stratigraphy. The base-case scenarios and other simulations discussed above have however not considered this aspect. According to Carson et al. (1999)’s modern sediment budget, an

estimated 33 % of the total load is retained in the present floodplain. Figure 3.6d presents the results of running this budget estimate on the base-case scenario. In this simulation, a floodplain facies develops at the base of the trough during most of the simulation and above the LST wedge during the RSL falling stage. During the deglacial period, which mainly formed the LST wedge, it is likely that subaerial deposition was enhanced by higher sediment supply and the formation of a glacial outwash plain (Hallet et al., 1996). As the rates of sea-level rise were reduced late in the Holocene, supporting the progradation of the HST offshore, the floodplain area was enlarged and the ratio between the sediment retained in the floodplain and delivered offshore most likely increased (Syvitski and Saito, 2007). In contrast, the transgressive period in between the deglaciation and the late Holocene most likely reported a reduction in floodplain retention due to the rapidly shrinking floodplain area. Therefore, since this simulation used throughout a bed load and a ratio referring to the modern conditions, i.e. large floodplain area, the thick wedge of subearial deposits accumulated in the first 60 km of the profile during transgression is likely overestimated. Evidence of outwash deposits in the groundtruth data is limited, but both Inuvik and Unipkat boreholes record coarser sediment at their bases (Fig. 3.3a).

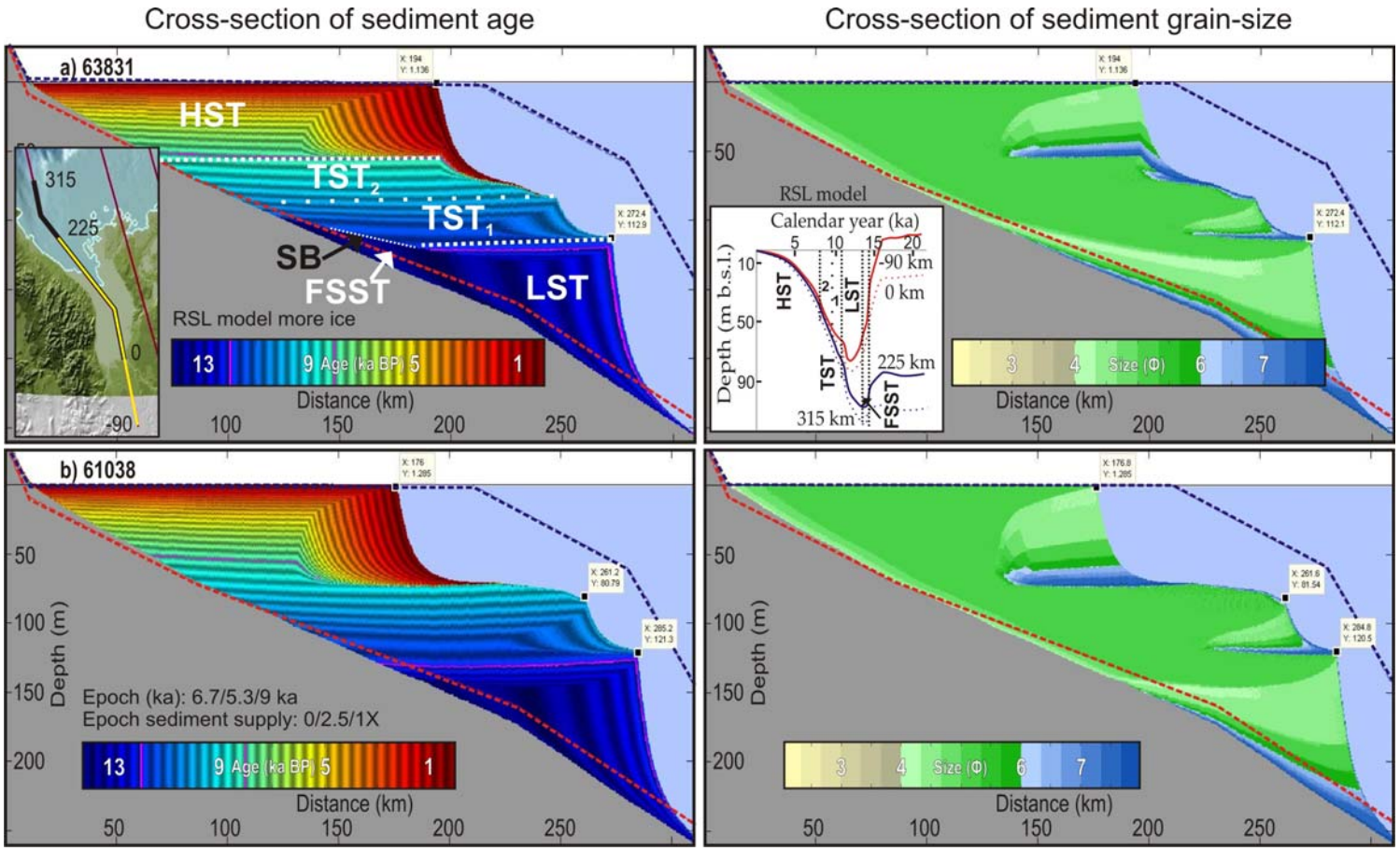

Figure 3.6: Factors contributing to a better stratigraphic match. a) RSL model data simulating more extensive ice, extracted from -90 to 225 km (inset). b) Higher sediment supply for longer period (combines epoch 2 and 3 from the base-case simulation). Cross-sections of the sediment age (left); cross-sections of grain-size (right). Seismic basal reflector (Fig. 3.3a; red dotted line); modern seafloor profile (blue dotted line). LST = Lowstand systems tract, TST = Transgressive systems tract, HST = Highstand systems tract, FSST = Falling systems tract, MFS = Maximum flooding surface, FS= Flooding surface, SB = Sequence boundary

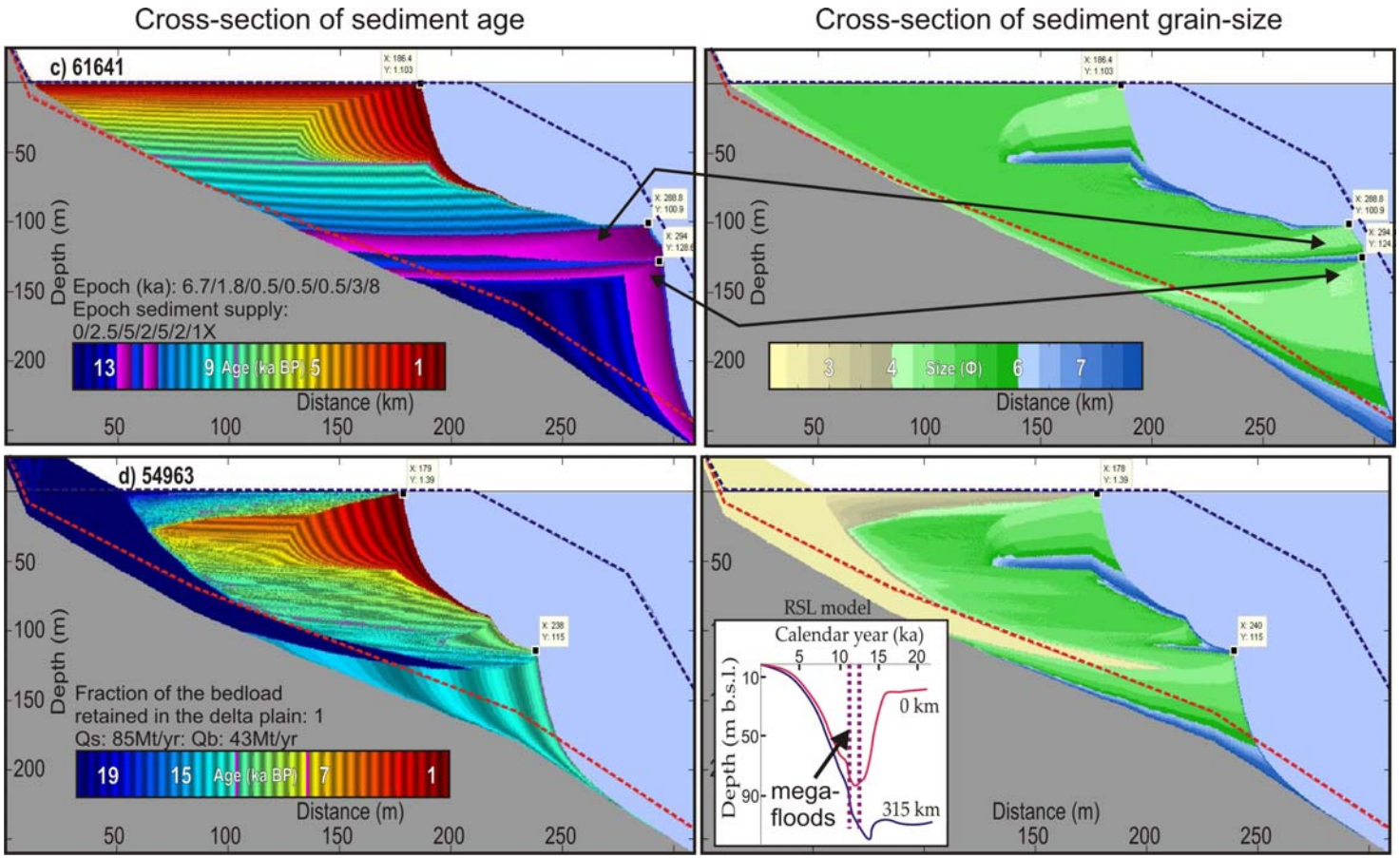

Figure 3.6 (next): c) Two short outburst events occurring between the 2nd and the 3rd epochs of the base-case scenario. d) Sediment retention in the floodplain using the Fraction of bedload retained in the delta plain. This simulation uses Carson et al. (1999) sediment budget, i.e. 33% of the total load is retained in the floodplain.

PROPOSED TIMING OF EVENTS

Due to the lack of dates available for the Mackenzie delta, pinpointing the timing of the various structures interpreted in the Mackenzie Trough is difficult. The model results confirm or propose other options to the timing presented by Hill (1996). Note that all dates are given in calendar years. Pollen data analysed in the MTW01 borehole suggest that the entire core is likely younger than 14 ka BP (Fig. 3.3a). The model shows that the stratigraphy of the Mackenzie Trough can be mostly explained by having the onset of sedimentation at 14.3 ka BP. Where the timing differs between the interpretations is for the hinge line of lower wedge and the MFS. The model interpretation suggests that the lower wedge is younger than Hill's, < 12 ka BP vs 14-15 ka BP respectively (Hill, 1996; Moran et al. 1989). By including the modeled TST_1, the surface may be as young as 10 ka BP. The MFS has not been clearly dated in the offshore, but the clay unit dated to 7.7 ka BP within the Inuvik borehole may suggest a potential timing for the MFS (Johnson and Brown, 1965), which correlates well with the MFS modeled in most simulations. This timing is also compatible with the start of modern delta progradation as most of the GIA effect has disappeared by then, leaving only a eustatic sea-level signal. This period also corresponds to the worldwide initiation of most modern world deltas (Stanley and Warne 1994).

IMPORTANCE OF GIA

It was suggested that GIA considerably impacted the RSL of the region with large along and cross-shelf variations. This suggested that one single RSL curve to represent an area as extensive as the Eastern Beaufort Shelf may be biased. To evaluate this statement the stratigraphy resulting from using the RSL model was compared with the stratigraphy

resulting from using one RSL curve, which was extracted from a single point along the transect (Fig. 3.7b). In order to evaluate the validity of the RSL model against a known standard, the RSL model stratigraphic results were first compared against the results derived from using the eustatic sea-level curve (Fig. 3.7a).

At first glance, using the dimensions and the depth of the progradational wedges, the model results using the eustatic sea-level curve (Fig. 3.7a) appear to correlate well with the original interpretation (Fig. 3.3a).This is not surprising as Hill's interpretation was based on a RSL curve (Hill et al., 1985, 1993), for which the timing post 15 ka BP is relatively similar to the eustatic curve. The differences found between the stratigraphy formed using the RSL model versus the eustatic curve can therefore be explained using similar arguments to the ones listed in the base-case scenario.

Since the stratigraphy derived from the RSL model better explained some of the details of the seismo- and lithostratigraphy collected in the area, it was necessary to evaluate to what extent a dynamic RSL model compared to a single RSL curve also using a glacio-isostatic component modified the stratigraphy (Fig. 3.7b). By using a single curve, it is thus assumed that GIA does not vary much over a large area. The results show modifications in the systems built during the first half of the simulation (Fig. 3.7b). The TST_1 progrades over the LST wedge, making the lower wedge larger and shallower, and thus more similar to the seismic profile (Fig. 3.3a). These changes will however likely differ depending on the location picked to extract the curve. For example, the simulation presented uses a RSL curve representative of an area largely influenced by isostatic displacement as it is extracted from the origin of the profile, which is under thicker ice (Fig. 3.7b inset, RSL curve at 0 km). Because of the rapidly falling RSL applied to the

entire profile, a falling stage systems tract (FSST) forms on the offshore portion of the profile, which does not happen using the dynamic RSL model (Fig. 3.5). In reality, the rapid RSL fall should only apply to the inshore portion where isostatic rebound is more pronounced than the offshore section. Because sediment supply is activated when RSL is generally lower, deposition first occurs in the offshore region. Therefore, by applying a rapidly rebounding surface to this region instead of relatively stable lowstand conditions, a FSST builds in lieu of a LST. Using a dynamic RSL model thus takes care of applying these spatial-temporal variations more appropriately along the profile.

The results of this simulation also emphasized that in order to more closely match the model results with the existing trough stratigraphy (Hill, 1996), a more extensive ice margin should be considered. Using this strongly influenced isostatic RSL curve, which may represent the half point of a RSL model profile more influenced by ice load, increases the similarity with the seismic data (Fig. 3.3a); the lower wedge includes a FS, its hinge line is shallower because of the inclusion of TST_1, and the TST wedge is thinner.

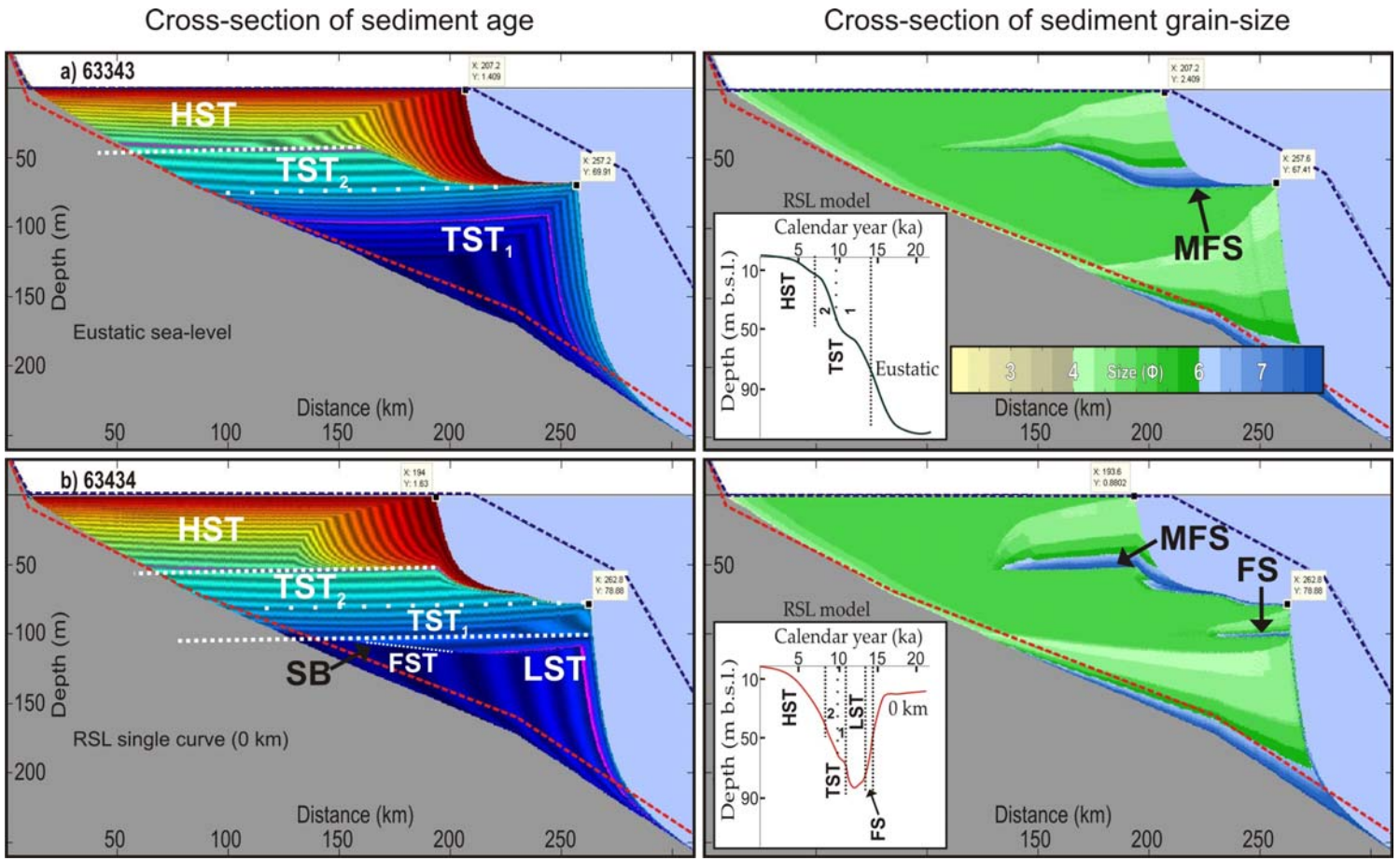

Figure 3.7: Sensitivity tests on sea-level curves a) Eustatic curve (inset 56333). b) Single curve (0 km) extracted from the RSL model. General parameters are defined in Tables 3.1 and 3.2. As a reference the base-case scenario (56333) uses four epochs (6.7/2.3/4/8 ka). cross-sections of the sediment age (left); cross-sections of grain-size (right). seismic basal reflector (Fig. 3.3; red dotted line); modern seafloor profile (blue dotted line). LST = Lowstand systems tract, TST = Transgressive systems tract, HST = Highstand systems tract, MFS = Maximum flooding surface, FS= Flooding surface.

3.5 Eastern Beaufort Shelf

3.5.1 Quaternary geology of the region

The present Eastern Beaufort Shelf offshore stratigraphic model used for geothermal model studies and others is based on a simple layer-cake approach derived from a limited amount of data including few reliable dates (Blasco et al. 1990; Blasco and Lewis, 1991; Murton, 2009). These dates come from two samples taken from the industry boreholes, Uviluk and Tarsuit, which were also used to constrain the RSL curve of Hill et al. (1985; 1993) for the region. The lithostratigraphic description of the Uviluk borehole shows three main units; a sand unit (1), showing traces of organic clay, underlying a 44 m thick mud unit (2), which is capped by a 40 m sand unit (3) (Hill et al., 1985; Fig. 3.8). This top sand unit does not contain organic material and the top of it, between 30 and 40 m, contains rounded gravel interbedded with sand beds, possibly coarsening upward. Datable material was collected at the base of the mud unit at an uncertain depth (± 20 m) amongst a peat unit. The peat sample reported an age of 25 950 ± 800 calendar year BP and indicated, from palynological assemblages, a near-shore environment mostly fluvial with periodic influxes of marine water (Hill et al., 1985).

Based on this information and additional correlations made from the lithostratigraphic units described on land (Murton, 2009), five seismostratigraphic units defined the offshore model (Blasco & Lewis 1991) (Fig. 3.9). The older unit (E) represents a thick sand layer tentatively correlated to Kendall Sediments and interpreted as glaciofluvial outwash or alternating subaerial delta plain with nearshore marine deposits. Overlaying unit E is an interbedded mud unit (D) correlated with the Hooper Clay and interpreted as delta margin deposited in an inner-shelf marine environment. The third unit (C) is sub-

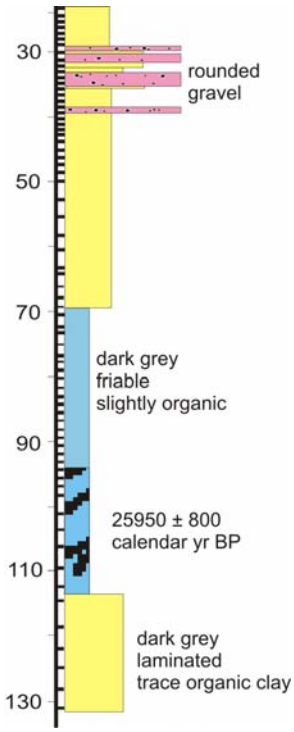

Figure 3.8: Uviluk borehole lithostratigraphic description. Pink = gravel, yellow = sand, blue = mud, blue with patterns = dated peat.

divided into three sub-facies: two sandy sub-facies (C_1 and C_2) and a diamicton sub-facies (C_3) capped by a regional unconformity correlated to a gravel lag onland. Unit C is interpreted as glacial outwash deposits overlain by aeolian, and till deposits. The seismic unconformity and the gravel lag found onshore have been correlated to an erosive surface left by glacial outburst floods (Murton et al., 2010). Finally, the youngest units (B and A) are respectively interpreted as a nearshore, high-energy marine transgressive sand, silt and clayey unit, and a marine mud, both derived mainly from the Mackenzie River sediment load.

According to the stratigraphic model (Fig. 3.9), the mud unit described in the Uviluk borehole lithostratigraphy (Fig. 3.8) would correlate with unit D, the upper sand unit with unit C, and the gravel unit with the erosional unconformity.

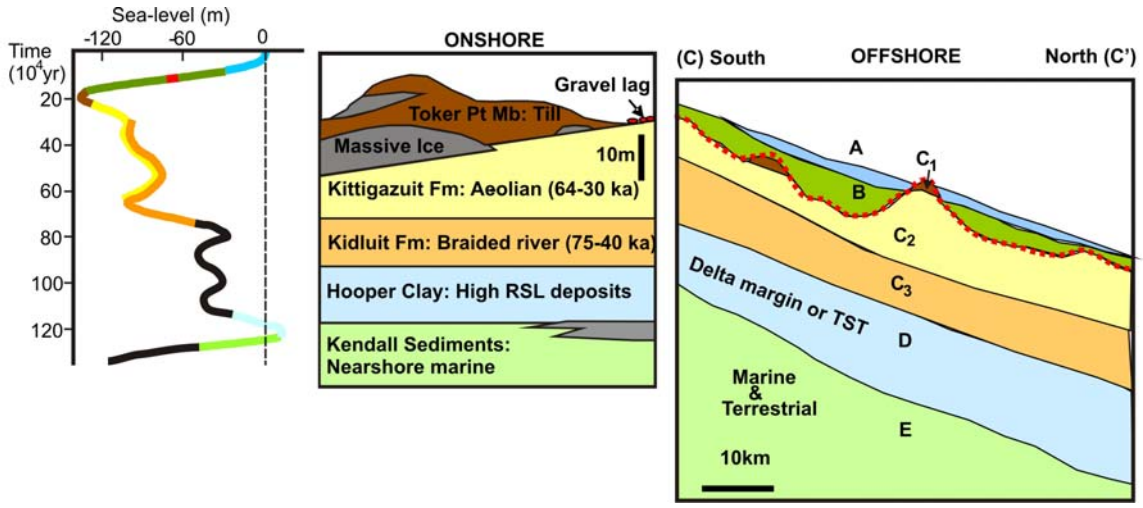

Figure 3.9: Layer cake stratigraphic model based on a lithostratigraphic section (middle) correlated to an offshore seismostratigraphic cross-section (right) north of Richard Island. Both sections are color coded and associated to their interpreted sea-level period (left). The locations of both sections are shown in Figure 3.1. The circle identifies the lithostratigraphic section whereas the line A-B identifies the seismic section. Modified from Blasco et *al.*, 1990, TAMSL, 1993, Martinson, 1987, and Murton et al., 2009.

3.5.2 Method

BOUNDARY CONDITIONS

Initial settings

Modelling the stratigraphy of the Eastern Beaufort Shelf was mostly driven by the information learned from the Mackenzie Trough experiment and the records from the Uviluk borehole. The boundary conditions (Table 3.3) were based on the age, the depth, and the environment in which the Uviluk dated sample was deposited (Fig. 3.8). The simulation was thus set over 25 ka and the initial profile was set so that the initial deposits would favour the sample depth and environment (Hill et al. 1985).

Table 3.3: Boundary conditions and sediment file for the Eastern Beaufort Shelf simulations

Model resolution	Simulation from figure 3.10	Simulation from figure 3.12
INITIATION FILE		
d_x = horizontal grid cell size (m)	100	400
d_y = vertical grid cell size (m)	0.5	1
W = basin width	60000	60000
Bathymetry file	based on Uviluk borehole dated unit	based on present seafloor bathymetry
T = Duration of simulation (yr)	21000	21000
d_t = time step	10 days	100 years
b_0 = river width (m)	2000	2000
h = river depth (m)	8	8
μ = flow velocity (m/s)	0.7	0.7
Number of grain-size	5	5
SEDIMENT FILE		
D = grain size (μm)	1200, 300, 150, 60, 5	1200, 300, 150, 60, 5
ρ_{grain} = grain density (kg/m^3)	2650	2650
$\rho_{saturated}$ = satured density (kg/m^3)	2115, 2094, 1955, 1795, 1504	2115, 2094, 1955, 1795, 1504
ρ_{grain} = water density (kg/m^3)	1030	1030
λ = removel rate (1/day)	40, 35, 20, 12, 5	40, 35, 20, 12, 5
c = compaction coefficient (1* 10^{-8})	3.6, 5, 7, 10, 36	3.6, 5, 7, 10, 36
φ_0 = minimum void ratio (-)	0.3, 0.25, 0.15, 0.1, 0.05	0.3, 0.25, 0.15, 0.1, 0.05

The sediment supply was varied throughout the simulation so as to characterise best the different stages of the past glaciation (Table 3.4) while keeping water discharge constant. Seven time periods were established (Table 3.4). The first period, 25 to 18 ka BP, represented the LGM conditions, with sediment supply intermediate between the low supply of the Holocene period and the very high supply of the deglacial period. The bedload supply was also set higher and did not follow the Mackenzie ratio, as it was considered that glacial outwash plain would be the dominant supply. The second period represented the deglacial period and since deglacial periods are known to deliver higher sediment supply, it was assigned the highest sediment supply (Hallet et al, 1996). According to Dyke et al. (2003), the onset of the ice sheet retreat from the shelf began around 18 ka BP. By 15 ka BP the LIS front was located hundreds of kilometres south and thus was probably not influencing the sedimentation on the shelf. From 15 ka BP onward (epoch 3), it was assumed that most of the sediments were being delivered through the Mackenzie drainage and therefore, only a small portion would have fed the

Eastern Beaufort Shelf. Two one year periods, epochs 4 and 6, were introduced to represent the two possible outburst floods (Murton et al. 2010; Teller et al., 2002). Their timing was averaged based on Murton et al.'s age range estimate. The sediment supply for both floods was calculated based on the water drainage estimated by Murton et al. (0.35 Sv), the ratio of water volume between the 2 outburst floods given by Teller et al., and the sediment concentration estimates (100-200 g/l) for the Missoula floods given by Denlinger and O'Connell (2010). The concentrations were adjusted because it was not possible to change the water discharge throughout the simulation. The last epoch, 7, follows the last outburst flood and represents the Holocene period where very little sediment delivered through the Mackenzie Trough fed the shelf. This epoch was assigned half the load of epochs 3 and 5.

In addition to the simulation using the standard RSL model (Chapter 2), a second simulation modeled a more extensive ice sheet (Table 3.4). Two additional simulations were carried out to compare the shelf stratigraphy resulting from low and high floodplain retention, which better represented the influence of glacial outwash. These simulations were also intended to evaluate the general stratigraphy reported for the Eastern Beaufort Shelf (Fig. 3.9). Both simulations used the present bathymetric profile crossing the Uviluk site and simulated three glacial/ interglacial sea-level cycles of 120 ka given by the RSL model.

Table 3.4: Epoch parameterization for Last Glacial Maximum simulation of the Eastern Beaufort Shelf

	25 - 18 ka BP (LGM)	18 - 15 ka BP (Deglacial)	15 - 12.5 ka BP (Mackenzie Q)	12.5 - 12.499 ka BP (1st outburst)	12.499 - 11.5ka BP (Mackenzie Q)	11.5 - 11.499 ka BP (2nd outburst)	11.499 ka BP present (Holocene)
	1	2	3	4	5	6	7
Q = Discharge (m^3/s)	11200	11200	11200	11200	11200	11200	11200
Q_{tot} = total sediment load (X 128Mt/yr)	0.5	3	0.1	60	0.1	20	0.05
Q_s = suspended sediment load (kg/m^3)							
300 µm	0.0625	0.375	0.0125	90	0.0125	60	0
150 µm	0.0375	0.225	0.0075	45	0.0075	30	0.0025
60 µm	0.0125	0.075	0.0025	22.5	0.0025	15	0.00625
5 µm	0.0125	0.075	0.0025	22.5	0.0025	15	0.00375
Q_b = bed load (kg/s)							
1200 µm	600	3000	200	280000	20	190000	5
Fraction of bedload retained in floodplain	0.8	0.8	0.8	0.5	0	0.5	0
L = bedload dumping zone (m)	5000	5000	5000	5000	5000	5000	5000

For simplification, only four time periods were specified per cycle in this simulation (Table 3.5). The first period, 0 to 80 ka, characterised the interglacial until the onset of glaciation. The second period, 80 to 100 ka, simulates the glacial period where larger sediment load than the modern load is supplied. The third period, 100 to 105 ka, characterised the deglacial

Table 3.5: Epoch parameterization for Last Glacial Interglacial simulations of the EBS

	0 - 80 ka (Interglacial)	80 - 100 ka (Growth of ice sheet)	100 - 105 ka (Deglacial)	105 - 120 ka (Post-glacial)
	1	2	3	4
Q = Discharge (m^3/s)	11200	11200	11200	11200
Q_{tot} = total sediment load (X 128Mt/yr)	0.05	0.25	1	0.05
Q_s = suspended sediment load (kg/m^3)				
150 µm	0.001756	0.00878	0.03512	0.001756
60 µm	0.0105	0.0526	0.2104	0.0105
5 µm	0.005206	0.0263	0.1052	0.005206
Q_b = bed load (kg/s)				
300 µm	5	600	3000	5
Fraction of bedload retained in floodplain	0	0/0.8	0/0.8	0
L = bedload dumping zone (m)	5000	5000	5000	5000

period with higher sediment supply and finally the fourth period (105 to 120 ka BP) represented the return to modern conditions. The difference between the third (Fig. 3.12a; low floodplain retention) and the fourth (Fig. 3.12b; high floodplain retention) simulation is in the bed load and the fraction of bedload retained in the floodplain, which simulated glacial outwash.

3.5.3 Results and discussion

BASE-CASE SCENARIO VS. THE EBS STRATIGRAPHY

The top 85 m stratigraphy of the Uviluk borehole was modeled by considering that the shelf profile depth at the start of the simulation was slightly deeper than today and the shelf break located inshore of the present (Fig. 3.10; red vs blue dashed profile respectively). Figure 3.10 presents the results of two simulations differentiated by the use of two different RSL model outputs. Simulation ‘a’ used the RSL model specific to the Uviluk transect (Fig. 3.1), whereas simulation ‘b’ simulated more extensive ice by using the RSL model data extracted from the first 185 kilometres of the Mackenzie Trough transect.

For both simulations, a finer–grained progradational wedge thickening seaward and coarsening upward developed first (Fig. 3.10, blue unit). Contributing to 40 m of shelf aggradation at 85 km (Uviluk site) and 55 m at the shelf break, this progradational wedge is deposited under marine conditions. Reflecting the onset of the deglacial period, the rate of deposition increases mid-shelf (110 km) and is represented by more spaced downlapping reflectors.

Capping this wedge is an erosional unconformity overlain by a coarser sand unit thinning seaward (Fig. 3.10, yellow unit). This unit contributes to 25 m of aggradation at the start of the profile, 15 m at 85 km (Uviluk site), and practically none at the shelf

break. As sea-level progressively falls until 15 ka BP, subaerial erosion and deposition progress seaward, respectively capping and overlaying the marine unit. This subaerial unit corresponds to a glacial outwash built over the glacial and deglacial period.

After 15 ka BP (epoch 3), RSL falls dramatically, creating a forced regression and thus considerable erosion of the shelf break (Fig. 3.11). This timing also corresponds to the end of the deglacial period, for which the associated sediment supply is considerably reduced. This results in thin forced regression deposits that contribute minimally to the overall progradation of the shelf (Fig. 3.11).

The main difference between these two simulations resides in the location of the two younger progradational units, best represented as a pink (older) and purple (younger) units in the cross-sections of sediment age (Fig. 3.10). In simulation ‘a’, the older unit (pink) is deposited onto the continental slope. The deposit is characterized by a maximum thickness of 130 m immediately following the shelf break and contributes to 2 km of progradation. The youngest unit (purple) is deposited mid-shelf and overlays the subaerial unit. The mid-shelf deposit extends over 60 km, and aggrades the shelf in this area to a maximum of 15 m at 140 km.

In simulation ‘b’, the older unit (pink) is deposited beyond the shelf break, similarly to simulation ‘a’. The deposit reaches 130 m thick immediately pass the shelf break and contributes to 2 km of shelf progradation. The younger unit (purple) however, differs from the previous simulation as it is deposited beyond the shelf break and contributes to another kilometre of shelf progradation. Its maximum thickness reaches 90 m.
In both cases, these two marine progradational deposits correspond to the two glacial outburst floods events identified by Murton et al. (2010; epoch 4 and 6) and are the main

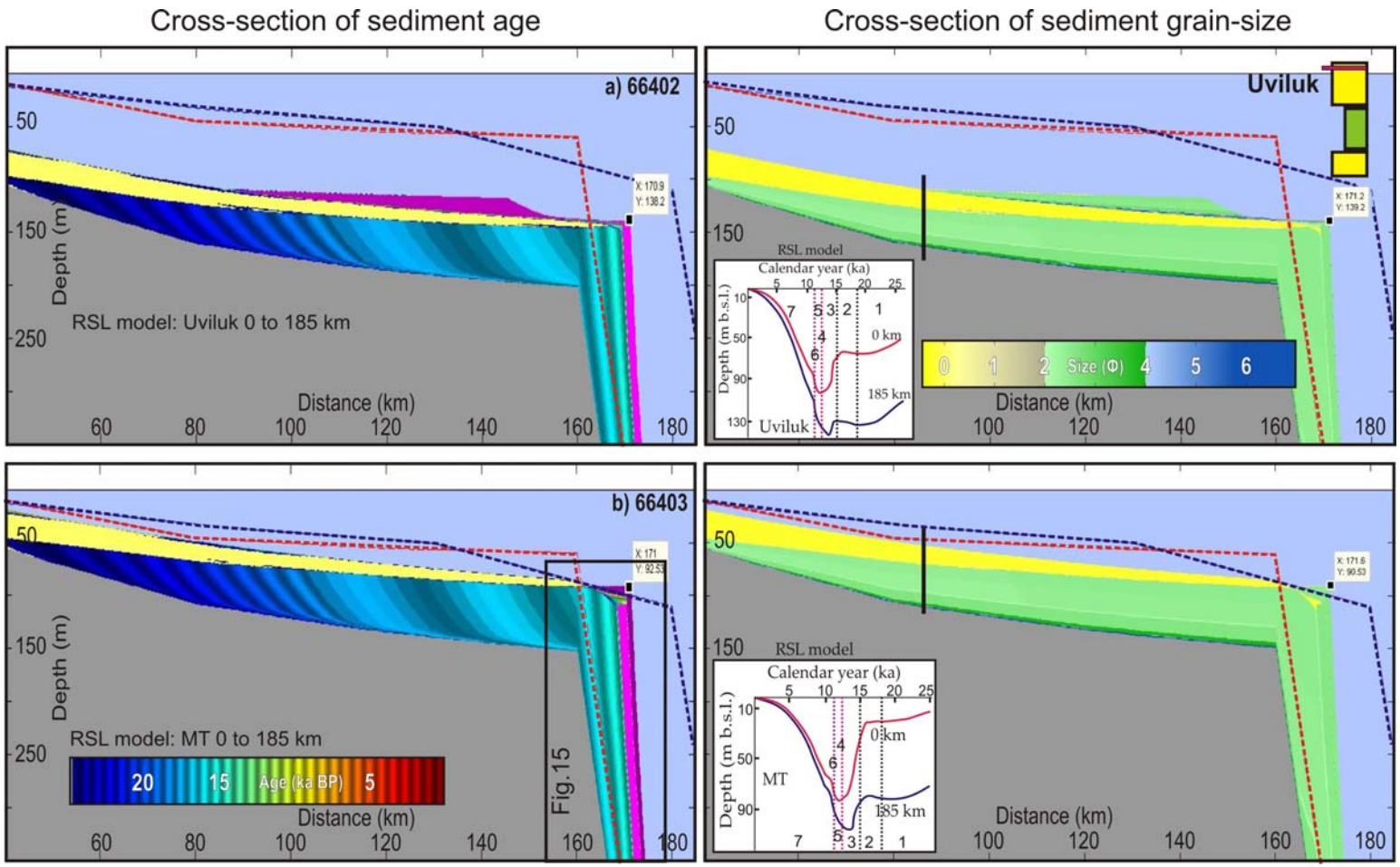

Figure 3.10: Eastern Beaufort Shelf a) RSL model data extracted for the Uviluk transect shown on Fig. 3.1. b) RSL profile simulating more extensive ice margins The RSL data was extracted from the first 185 km of the Mackenzie Trough transect. Parameters are defined in Tables 3.3 and 3.4.). Cross-sections of the sediment age (left); cross-sections of grain-size (right). seismic basal reflector (Fig. 3.3; red dotted line); modern seafloor profile (blue dotted line).

contributing stratigraphic events following 15 ka BP. The marine deposits are accompanied by correlative thin subaerial deposits representing about 40 cm of aggradation per event. These deposits are difficult to observe on the figure because of their thicknesses, but also because the expression of subaerial material on the plots is limited to yellow.

The modeled stratigraphy correlates well with the generalised seismic interpretation (Fig. 3.9) and the Uviluk borehole lithostratigraphy described above the dated sample (top 95 m; Fig. 3.8 and 3.10). The simulations generate similar thicknesses for the lower mud unit (40 vs. 44 m, respectively), which corresponds to unit D of the seismostratigraphic interpretation; having a similar seaward thickening trend (Fig. 3.10; Blasco et al., 1990). The overlying sand unit thickness is however underestimated compared to the borehole (17 vs. 40 m, respectively). This may indicate that higher sediment supply to the floodplain occurred during the glacial and deglacial period than was used in the model.

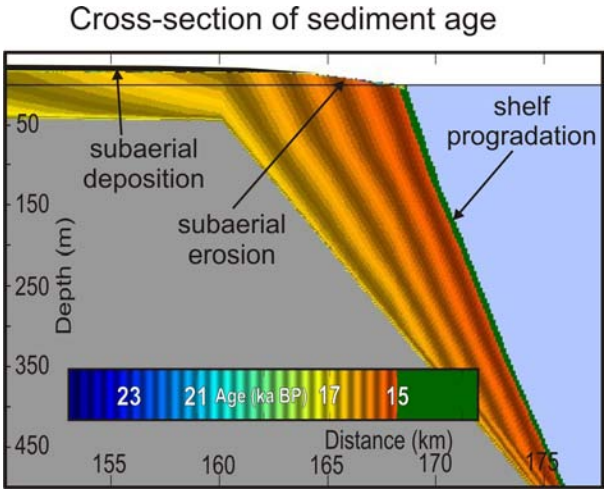

Figure 3.11: Shelf edge at 12.5 ka BP from simulation 66403 presented in Figure 3.10b. Marine shelf deposits deposited after 15 ka BP are colored green. Subaerial deposits are colored in black.

Compared to the seismic model, this sand unit would correspond to unit C. Blasco et al. also suggest a seaward thickening trend for this unit, which is not observed in the simulation results. Considering the limited extent of the seismic interpretation across the shelf (Fig. 3.1), this trend may only be local or the result of more glacial erosion landward.

The interbedded sand and gravel unit at the top of the sand deposit in the Uviluk borehole may represent the subaerial deposits of the modeled outburst flood. Above the borehole gravel interval, only sand is described and no fine-grained material. This observation corresponds well to the model, which simulates very little modern sediment deposition offshore of the 40 km mark.

The main problem of this correlation between the model and the Uviluk borehole description resides in the fact that in order to simulate 40 m of marine progradational mud in a 25 ka simulation, the bottom of the unit had to be set to around 40 m water depth. Therefore if the dated sample at the base of the mud unit was an indicator of RSL, then the simulation results are incompatible with the dated sample. The description of the sample in Hill et al. (1985) suggested that the sample was deposited in a fluvial environment with periodic influx of marine water. Such conditions are commonly found at 40 m depth in many modern delta settings, such as the Fraser River Delta (Hart and Barrie, 1995). This suggests that the dated sample should not be considered a good sea-level indicator.

INFLUENCING FACTORS OFFERING A BETTER STRATIGRAPHIC MATCH

More extensive ice

Similarly to the Mackenzie Trough simulation, a better fit between the model simulation and the stratigraphic data (Uviluk lithostratigraphy and overall transect

bathymetry) is achieved by using a RSL model transect influenced by more extensive ice (Fig. 3.10b). Because of the large net increase in RSL between the start and the end of the simulation presented in Fig. 3.10a, the stratigraphy ends up lying too deep compared to present. However, by using a RSL model isostatically more influenced, as seen in Fig. 3.10b, the net increase in RSL is lessened and so is the overall depth of the stratigraphy.

Another point supporting a more isostatically influenced RSL, which indirectly justifies the more extensive ice, is the actual depth of the shelf break. The latter occurs around the 80 m isobath, which is much shallower than the typical 120 m shelf break of most non-glaciated shelves (Jouet et al. 2006; Ridente and Trincardi 2002).

Outburst flood deposits

The deposits of two large outburst floods lasting one year were described earlier (Fig. 3.10b). The results suggest that outburst flood material were transported beyond the shelf edge and contributed to its progradation. As also suggested by the results, shelf aggradation due to floodplain deposition would have occurred. The closest evidence for such deposits is found onshore as a pebbly-boulder gravel lag (Murton et al., 2010) and as mentioned in the previous section, offshore as a seven meter thick layer of sand with pebble size material followed by another 6 m of sandy sediments in the Uviluk borehole stratigraphy (Fig. 3.8). This is conceivable considering that the best modern analog to these types of floods are the joklhlaups recorded in Iceland. These are known to contribute a large amount of sediment into the sandur as well as the Icelandic shelf. One single event contribution was estimated to 150 Mt, which represents about the same as the modern annual contribution of the Mackenzie River to the delta (Bjornsson, 1992). This amount translated in an average thickness of 4 m aggradation of the Icelandic sandur.

LAST GLACIAL/INTERGLACIAL (LGIT) SIMULATIONS

The cyclic nature of sea-level during glacial/interglacial cycles creates similar repetitive effect on a shelf stratigraphy (Syvitski et al., 2009), Figure 3.12 presents the results of two simulations where three full 120 ka RSL cycles extracted from the RSL model for the Uviluk transect were run (Table 3.5). The goal of these simulations were to better understand the influence of floodplain retention/glacial outwash on glaciated shelves and possibly extract more information to help explain the stratigraphy of the EBS.

Low vs. high floodplain retention glaciated shelves

The simulations presented in Figure 3.12 introduce two scenarios: a) the floodplain retention is null, and b) the floodplain retention represents 80 % of the bedload discharge during glacial and deglacial periods (epoch 2 and 3; Table 3.5) to simulate glacial outwash formation.

In the **low floodplain retention** simulation (Fig. 3.12a), because of the positive net aggradation (aggradation minus isostatic sediment loading), which limits the accommodation space available during the sea-level Highstand, the clinoforms are prograding seaward. Controlled by the depth of the sea-level lowstand, the hinge point however stays at a more or less constant depth. Due the substantial break in slope of the initial bathymetric profile at 120 km, more accommodation space is created before the shelf break (170 km). The prograding HST wedge thus first fills this space, downlapping onto the basement. As RSL falls, an erosion surface builds, which becomes the sequence boundary (SB) and the subsequent falling stage systems tract (FSST) finishes filling the accommodation space until it reaches the shelf edge. Since the RSL rate increases soon after, a forced regression leads the sediment supply beyond the shelf edge. The

depositional hiatus on the shelf lasts until the later transgression (105 ka), which culminates with the formation of the next HST. The rapid transgression leaves thin TST followed by the MFS represented by a thin layer of fine marine deposits. As cycles progresses the stratigraphic sequences build towards an equilibrium profile, which in this case is more progradational.

In this simulation, sand deposits accumulate mainly over the central to outer part of the shelf (Fig. 3.12a). These deposits are nearshore deposits, resulting from offshore bedload deposition within 5 km of the shoreline. The sandy deposits first accumulate mid-shelf during the first phase of sea-level fall, i.e. between 15 and 55 ka, while sea-level fluctuated between 35 and 50 m b.s.l.. During this period, because RSL was falling faster offshore, the shelf profile levelled up, and concentrated the area of nearshore deposition. After this long period of semi stable RSL conditions, short transgressive periods (70, 90, and 105 ka) occurring during the mainly falling RSL trend permitted the accumulation of shelf edge sand deposits. Because of their close relation with RSL, these small nearshore sand deposits are thus located 60 and 90 m water depth. Progradational wedges develop during the Highstand (HST), but mainly as a FSST after the first inflection point in the shelf profile (120 km) and beyond the shelf break as an LST wedge. These wedges are made of finer grain-size and are strongly eroded due to subaerial exposure during the lowstand.

In the **high floodplain retention** simulation, the most striking difference is the subaerial deposits, which contribute largely to aggrading the shelf (Fig. 3.12b). These sand deposits converge updip. The mud units are very thin and wedge out progressively further downdip. The aggradation of the floodplain deposit through time induces a

regression of the shoreline because sediment loading does not keep up with the loss of accommodation space. Since the shoreline progressively regresses and that the shelf muds are deposited mainly during highstand, every glacial-interglacial cycle, these deposits are deposited farther offshore. The regression is likely emphasized in the model since the latter does not take into account glacial erosion. Erosion would contribute to reducing the total aggradation onland and thus, limit shoreline regression. Sequence boundaries or subaerial erosion surfaces occur near the base of each sand deposit (Fig. 3.12b). Only a small portion at the base of the shelf sand deposits has been deposited in a nearshore marine environment. During the first cycle, these nearshore sand deposits are identical to the low floodplain retention simulation (Fig. 3.12a). However, during the following cycles, these deposits are developed as sharp-based sand body, which are associated with forced regression (Plint, 1988). These deposits occur more frequently as the shelf progrades and its slope is flattened by accumulation and subaerial erosion of previous cycle floodplain deposits.

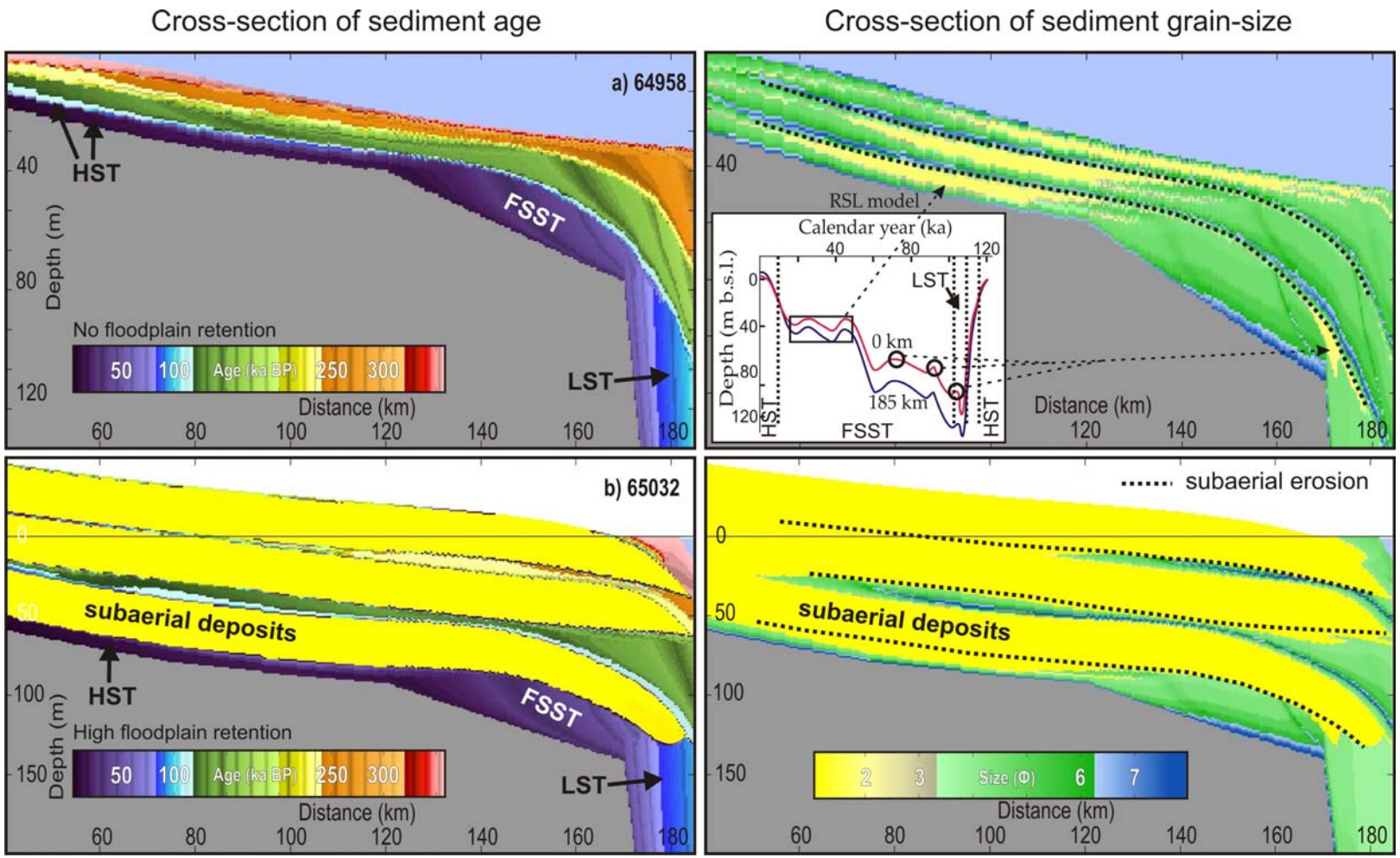

Figure 3.12: 3 glacial/interglacial cycles at the Uviluk transect using the modern bathymetry. a) No floodplain retention during the glacial period b) High floodplain retention during the glacial period. The RSL model data used was extracted from the Uviluk transect. Parameters are defined in Tables 3.3 and 3.5.

Can these long-term simulations help understand the stratigraphy of the EBS?

The present correlation between the onshore and offshore units presented as a layer-cake model shows alternating sand and mud units (Murton 2009; Fig. 3.9). The oldest units, Kendall sediments and Hooper Clay, which are correlated to the seismostratigraphic units E and D (Blasco and Lewis 1991) do not show any major hiatus between them. Their onshore lithostratigraphic composition, sandy to shelly silty clay units respectively, suggests that these deposits were deposited in a shallow marine environment. The Kendall sediments are thus interpreted as nearshore marine deposits and the Hooper Clay as highstand sea-level deposits (Murton, 2009). At present, the age of these units has yet to be determined (Murton, 2009). Overlying these units is a thick sand unit, whose origin has been interpreted as subaerial, i.e. glacio-fluvial, aeolian, and glacial. These have been correlated to three sub-facies found in unit C of the seismostratigraphic interpretation. The top seismostratigraphic units, A and B, are found only in the marine environment, representing the Holocene deposition during transgression (B) and the present Highstand (A).

The correlation between the unit descriptions and the interpretation given by Murton (2009) is supported by the high floodplain retention simulation (Fig. 3.12b). The modeled shelf mud deposits are deposited during the highstand conditions, characteristic to the interglacial periods. The mud unit, as seen between cycle 1 and 2 is made first of a marine transgressive fine-grained unit, followed by a highstand progradational fine-grained unit. Based on the RSL cycle of 120 ka presented in these last simulations, this period corresponds to about 15 ka, i.e. 5 ka prior to the Highstand for the first transgressive deposits until about 10 ka after, which is responsible for depositing the second deposits. These two contiguous depositional periods are thus correlating

respectively well with the Kendall sediments / unit E and Hooper Clay/ unit D. Overlying these modeled shelf units is the thick subaerial sand deposit, which corresponds well with the subaerial sand / unit C deposit dated between 75 and 30 ka BP (Murton, 2009). Although the contact between units D and C is poorly defined on the seismic reflection profiles (Blasco and Lewis 1991), the transition from marine to subaerial environment, as suggested in the simulation, is most likely to have created an erosional unconformity. In this simulation, the accumulation of sand, fluvial or aeolian, occurs progressively from onshore to offshore as sea-level falls during the rest of the cycle, i.e. from about 10 ka until 115 ka.

The presence of more extensive ice has been suggested throughout this study; however no long-term simulation was carried out to see the effects on the development of the shelf. More glacial isostatic displacement contributes to a larger fall in RSL post-LGM, but a shallower lowstand. It is thus expected that a lesser fall in RSL over a 120 ka cycle would contribute to maintaining a marine depositional environment for a longer period and contribute to thickening the progradational marine unit on the shelf (unit D). In addition, it would contribute to assigning a younger age to the subaerial erosional unconformity on the shelf (contact between D and C) than the approximate age interval of 115 to 60 ka BP given in Fig. 3.12. Such hypothetical simulation would thus better correlate with the Uviluk description and timing of the stratigraphy (Fig. 3.8).

3.6 Conclusions

One of the primary objectives of this study was to evaluate the impact of glacial isostatic adjustment on the stratigraphic development of glaciated environments. This was achieved using the Mackenzie Trough simulation. GIA proves to be influential in

producing a differential timing in the RSL behaviour across the shelf, resulting in the generation of more progradational rather than more retrogradational stratigraphic features.

The second objective was to better understand the stratigraphic evolution of the Mackenzie Trough. Several conclusions can be drawn on this aspect:

1) It is likely that the Trough stratigraphy above the basal hummocky reflector was entirely built over the past 14 ka BP.

2) The timing of events, especially for the pre-Holocene stratigraphy, is different from that suggested by Hill (1996) as a result of the new RSL model. The lower progradational wedge corresponds to a LST wedge and possibly part of a TST wedge.

3) If outburst flood deposits were funnelled through the Mackenzie Trough, they are probably found within the LST/TST wedge.

4) The onset of modern delta progradation began around 7.5 ka BP, which corresponds to the age of the sample dated above the sand unit in the Inuvik borehole, correlating with the MFS.

5) The modern sediment supply estimated by Carson et al. (1998) is too small to explain its total progradation. This may be explained by higher supply during the early Holocene possibly associated with the Holocene thermal maximum.

The last objectives were specific to glaciated shelves and more specifically the Eastern Beaufort Shelf. Several conclusions can be drawn on this aspect:

1) The attempts to simulate the Uviluk borehole stratigraphy concluded that the stratigraphy could be reproduced if the dated sample was not considered a sea-

level indicator. It was most likely deposited in a delta front environment at approximately 40 m water depths.

2) The sand unit overlying the sampled mud unit is likely comprised of marine and subaerial sands, amongst which the gravel found at the top may correlate with some glacial outburst flood deposits. Outburst flood deposits likely bypassed the shelf and contributed to its progradation. However, it is likely that part of the bedload carried in the floods is retained and deposited on the shelf as glacial outwash.
3) In order to reproduce more closely the stratigraphy, the ice sheet must have been more extensive.
4) Finally, the stratigraphic interpretation of the EBS by Murton (2009) is supported by the high floodplain retention simulation.

CHAPTER 4 - Conclusion

This research shows that glacial isostatic adjustment has strongly influenced the relative sea-level in the Mackenzie-Beaufort region since the LGM. Large cross-shelf and along-shelf variations in the order of 100 and 30 m respectively have been modeled. The timing and the depth of the lowstand, depending on the location, is modeled between 14 and 12 ka BP and reach between 85 and 140 m below present sea-level. These model results are important as they open new ways of thinking about stratigraphic problems related to the Canadian Beaufort Shelf and glaciated shelves in general.

Constraining RSL histories in the Arctic is important because of its implications in understanding the stratigraphic evolution of the shelf and the potential geohazards that may impede the economic development of the region. GIA proves to be influential in producing a differential timing in the RSL behaviour across the shelf, resulting in the generation of more progradational rather than more retrogradational stratigraphic features.

In the Mackenzie Trough, this results in more progradational instead of retrogradational stratigraphic patterns and therefore presents a new post-LGM geological framework. This framework suggests a different timing of events and additional information explaining the more detailed stratigraphy. For the Eastern Beaufort Shelf, this new insight into the RSL dynamics suggests that the only age constraint found for the area is not, as first interpreted, a sea-level indicator. This new interpretation thus permits the stratigraphy to be modeled.

Finally, outburst flood deposits are likely to have bypassed the shelf and contributed to its progradation. Bedload material carried by these mega-floods should be present in

the subaerially deposited units as it is likely that part of the load was retained and deposited on the shelf. This study also supports the argument that more extensive ice margins existed because such a scenario seems to improve the match between simulations and observations

In conclusion, this research highlights three key themes to consider for future research in the Beaufort area. First, RSL has varied considerably in the region because of the existing influence of GIA. Second, the geological framework of both the Mackenzie Trough and the Beaufort Shelf present a timing and pattern that strongly reflects these RSL variations, which are also likely to be more accentuated because of more extensive ice margins. Third, the shelf break is an area that underwent substantial stratigraphic changes since the LGM, which should be considered in the analysis of geohazards in the area.

Bibliography

Alvey, A., Gaina, N.J. Kusznir, and T.H. Torsvik. 2008. Integrated Crustal Thickness Mapping and Plate Reconstructions for the High Arctic. Earth and Planetary Science Letters 274 (3-4): 310–321.

Barnhardt, W. A., W. R. Gehrels, and J. T. Kelley. 1995. Late Quaternary Relative Sea-level Change in the Western Gulf of Maine: Evidence for a Migrating Glacial Forebulge. Geology 23 (4): 317 –320

Bjornsson, H. 1992. Jokulhlaups in Iceland: Predictions, Characteristics and Simulation. Annals of Glaciology. Annals of Glaciology 16: 95 –106.

Blasco, S. M., G. Fortin, P. R. Hill, M. J. O'Connor, and J. Brigham-Grette. 1990. The Late Neogene and Quaternary stratigraphy of the Canadian Beaufort continental shelf. *In* The Arctic Ocean region, ed. A. Grantz, L. Johnson, and J. F. Sweeney, 50:491–502. The Geology of North America. Geological Society of America.

Blasco, S. M., and J. F. Lewis. 1991. Offshore geology. *In* Geological, geotechnical and geophysical studies along an onshore-offshore transect of the Beaufort Shelf, 26 - 31. Dallimore SR. Open file 2408. Ottawa: Geological Survey of Canada.

Blasco, S; Bennett, R; MacKillop, K; Campbell, P; Carr, E; Hughes-Clarke. 2011. Deep water seabed geohazard investigations in the Beaufort Sea related to offshore hydrocarbon development. 39th Annual Yellowknife Geoscience Forum, abstracts of talks and posters. Edited by Fischer, B J; Watson, D M; Northwest Territories Geoscience Office, Yellowknife Geoscience Forum Abstracts Volume 2011.

Bott, M.H.P. 1992. "Modelling the Loading Stresses Associated with Active Continental Rift Systems." Tectonophysics 215 (1–2): 99–115.

Burn, C. R., and S. V. Kokelj. 2009. The environment and permafrost of the Mackenzie Delta area. Permafrost and Periglacial Processes 20 (2): 83-105.

Carson, M. A, F. Malcolm Conly, and J. N Jasper. 1999. Riverine Sediment Balance of the Mackenzie Delta, Northwest Territories, Canada. Hydrological Processes 13 (16): 2499–2518.

Carson, M. A., J. N. Jasper, and F. M. Conly. 1998. Magnitude and Sources of Sediment Input to the Mackenzie Delta, Northwest Territories, 1974-94. Arctic 51 (2): 116–124.

Coulthard, R. D., M. F.A. Furze, A. J. Pieńkowski, F. Chantel Nixon, and John H. England. 2010. New marine ΔR values for Arctic Canada. Quaternary Geochronology 5 (4) (August): 419-434.

Dallimore, S. R., S. A. Wolfe, and S. M. Solomon. 1996. Influence of ground ice and permafrost on coastal evolution, Richards Island, Beaufort Sea coast, NWT. Canadian Journal of Earth Sciences 33 (5): 664-675.

Davis, J.L., and J.X. Mitrovica, 1996. Glacial Isostatic Adjustment and the Anomalous Tide Gauge Record From Eastern North America. Nature, 379: 331-333.

Davis, J. L., M. E. Tamisiea, P. Elósegui, J. X. Mitrovica, and E. M. Hill (2008). A statistical filtering approach for Gravity Recovery and Climate Experiment (GRACE) gravity data. Journal Geophysical Research, 113, B04410, 14 pp.

Denlinger, R. P., and D. R. H. O'Connell. 2010. Simulations of Cataclysmic Outburst Floods from Pleistocene Glacial Lake Missoula. Geological Society of America Bulletin 122 (5-6): 678–689.

Dixon, J., and J. R. Dietrich. 1990. Canadian Beaufort Sea and adjacent land areas. *In* The Arctic Ocean region, ed. A. Grantz, L. Johnson, and J. F. Sweeney, 50:239–256. Har/Map. The Geology of North America. Geological Society of America.

Duk-Rodkin, A., and O. L. Hughes. 1994. "Tertiary-quaternary Drainage of the Pre-glacial Mackenzie Basin." *Quaternary International* 22-23: 221–241.

Dyke, A. S., A. Moore, and L. Robertson. 2003. Deglaciation of North America. Geological Survey of Canada Open file 1574, 2 sheets

Dyke, A. S., J.T. Andrews, P.U. Clark, J.H. England, G.H. Miller, J. Shaw, and J.J. Veillette. 2002. The Laurentide and Innuitian ice sheets during the Last Glacial Maximum. Quaternary Science Reviews 21 (1-3): 9-31.

Dyke, A. S. 2004. An outline of North American deglaciation with emphasis on central and northern Canada. *In* Quaternary Glaciations-Extent and Chronology - Part II: North America, Volume 2, Part 2:373-424.

England, J. H., M. F.A. Furze, and J. P. Doupé. 2009. Revision of the NW Laurentide Ice Sheet: Implications for Paleoclimate, the Northeast Extremity of Beringia, and Arctic Ocean Sedimentation. Quaternary Science Reviews 28 (17–18): 1573–1596.

Fairbanks, Richard G. 1989. A 17,000-year Glacio-eustatic Sea Level Record: Influence of Glacial Melting Rates on the Younger Dryas Event and Deep-ocean Circulation. Nature 342 (6250): 637–642.

Fairbanks, R. G., R. A. Mortlock, T-C. Chiu, L. Cao, A. Kaplan, T. P. Guilderson, T. W. Fairbanks, A. L. Bloom, P. M. Grootes, and M-J. Nadeau. 2005. Radiocarbon calibration curve spanning 0 to 50,000 years BP based on paired 230Th/234U/238U and ^{14}C dates on pristine corals. Quaternary Science Reviews 24 (16-17): 1781-1796.

Fjeldskaar, W. 1991. Geoidal-eustatic Changes Induced by the Deglaciation of Fennoscandia. Quaternary International 9 (0): 1–6.

Gomez, N., J. X. Mitrovica, P. Huybers, and P. U. Clark. 2010. Sea Level as a Stabilizing Factor for Marine-ice-sheet Grounding Lines. Nature Geosciences 3 (12): 850–853

Hager, B. H., and M. A. Richards. 1989. Long-Wavelength Variations in Earth's Geoid: Physical Models and Dynamical Implications. Philosophical Transactions of the Royal Society of London. Series A, Mathematical and Physical Sciences 328 (1599): 309–327.

Hallet, B., L. Hunter, and J. Bogen. 1996. Rates of Erosion and Sediment Evacuation by Glaciers: A Review of Field Data and Their Implications. Global and Planetary Change 12 (1-4): 213–235.

Hart, Bruce S., and J. Vaughn Barrie. 1995. "Environmental Geology of the Fraser Delta, Vancouver." *Geoscience Canada* 22 (4): 172-183.

Hill, P. R. 1996. Late quaternary sequence stratigraphy of the Mackenzie Delta. Canadian Journal of Earth Sciences 33 (7): 1064-1074.

Hill, P. R., K. M. Moran, and S. M. Blasco. 1982. Creep deformation of slope sediments in the Canadian Beaufort Sea. Geo-Marine Letters 2 (3-4): 163-170.

Hill, P. R., P. J. Mudie, and K. Moran. 1985. A sea-level curve for the Canadian Beaufort shelf. Canadian Journal of Earth Sciences 22 (10): 1383–1393.

Hill, P. R., S. M. Blasco, J. R. Harper, and D. B. Fissel. 1991. Sedimentation on the Canadian Beaufort Shelf. Continental Shelf Research 11 (8-10): 821-842.

Hill, P. R., A. Héquette, and M.-H. Ruz. 1993. "Holocene Sea-level History of the Canadian Beaufort Shelf." *Canadian Journal of Earth Sciences* 30 (1): 103-108.

Hill, P. R., C. P. Lewis, S. Desmarais, V. Kauppaymuthoo, and H. Rais. 2001. The Mackenzie Delta: Sedimentary Processes and Facies of a High-latitude, Fine-grained Delta. Sedimentology 48 (5): 1047–1078.

Hutton, E. W. H., and J. P. M. Syvitski. 2004. Advances in the numerical modeling of sediment failure during the development of a continental margin. Marine Geology 203 (3-4) : 367–380.

Hutton, E.W.H., and J.P.M. Syvitski. 2008. Sedflux 2.0: An advanced process-response model that generates three-dimensional stratigraphy. Computers & Geosciences 34 (10): 1319-1337.

Ivins, E. R., R. K. Dokka, and R. G. Blom. 2007. Post-glacial sediment load and subsidence in coastal Louisiana. Geophysical Research Letters 34: 5 PP.

James, T., E. J. Gowan, I. Hutchinson, J. J. Clague, J. V. Barrie, and K. W. Conway. 2009. Sea-level Change and Paleogeographic Reconstructions, Southern Vancouver Island, British Columbia, Canada. Quaternary Science Reviews 28 (13–14): 1200–1216

Johnston, G. H, and R. J. E Brown. 1965. Stratigraphy of the Mackenzie River Delta. Northwest Territories, Canada. Geological Society of America Bulletin 76 (1): 103–112.

Jouet, G., S. Berné, M. Rabineau, M.A. Bassetti, P. Bernier, B. Dennielou, F.J. Sierro, J.A. Flores, and M. Taviani. 2006. Shoreface Migrations at the Shelf Edge and Sea-level Changes Around the Last Glacial Maximum (Gulf of Lions, NW Mediterranean). Marine Geology 234 (1-4): 21–42.

Jouet, G., E. W. H. Hutton, J. P. M. Syvitski, and S. Berné. 2008. Response of the Rhône Deltaic Margin to Loading and Subsidence During the Last Climatic Cycle. Computers & Geosciences 34 (10): 1338–1357.

Judge, A.S., B.R. Pelletier, and I. Norquay. 1987. Permafrost base and distribution of gas hydrates. In Marine science atlas of the Beaufort Sea: Geology and geophysics, ed. B.R. Pelletier, Miscellaneous Report:39. Geological Survey of Canada.

Kaufmann, G., 2004. Program package ICEAGE, Version 2004. Manuscript, Institut fur Geofysil der Universitat Gottingen, 40 p.

Kaufmann, G., P. Wu, and G. Li. 2000. Glacial Isostatic Adjustment in Fennoscandia for a Laterally Heterogeneous Earth. Geophysical Journal International 143 (1): 262–273

Kaufman, D.S, T.A Ager, N.J Anderson, P.M Anderson, J.T Andrews, P.J Bartlein, L.B Brubaker. 2004. Holocene Thermal Maximum in the Western Arctic (0–180°W). Quaternary Science Reviews 23 (5–6): 529–560.

Kendall, R. A, J. X Mitrovica, and G. A Milne. 2005. On Post-glacial Sea Level – II. Numerical Formulation and Comparative Results on Spherically Symmetric Models. Geophysical Journal International 161 (3): 679–706

Kirby, J. F., and C. J. Swain. 2009. A Reassessment of Spectral Te Estimation in Continental Interiors: The Case of North America. Journal of Geophysical Research 114: 36 p.p.

Kubo, Y., J. P. M. Syvitski, E. W. H. Hutton, and A. J. Kettner. 2006. Inverse Modeling of Post Last Glacial Maximum Transgressive Sedimentation Using 2D-SedFlux: Application to the Northern Adriatic Sea. Marine Geology 234 (1-4): 233–243.

Kubo, Y., J.P.M. Syvitski, E.W.H. Hutton, and C. Paola. 2005. Advance and Application of the Stratigraphic Simulation Model 2D-SedFlux: From Tank Experiment to Geological Scale Simulation. Sedimentary Geology 178 (3-4): 187–195.

Martinson, D. G., N. G. Pisias, J. D. Hays, J. Imbrie, T. C. Moore, and N. J. Shackleton. 1987. “Age Dating and the Orbital Theory of the Ice Ages: Development of a High-resolution 0 to 300,000-year Chronostratigraphy.” Quaternary Research 27 (1): 1–29.

Meckel, T. A., U. S. ten Brink, and S. Jeffress Williams. 2006. Current subsidence rates due to compaction of Holocene sediments in southern Louisiana. Geophysical Research Letters 33: 5 PP.

Milliman, J. D., and K. L. Farnsworth. 2011. River Discharge to the Coastal Ocean: A Global Synthesis. Cambridge University Press. 394 p.

Miller, G. H., J. Brigham-Grette, R. B. Alley, L. Anderson, H. A. Bauch, M. S. V. Douglas, M. E. Edwards, et al. 2010. Temperature and Precipitation History of the Arctic. Quaternary Science Reviews 29 (15-16): 1679–1715.

Mitrovica, J. X., and G. A. Milne. 2003. On Post-glacial Sea Level: I. General Theory. Geophysical Journal International 154 (2): 253–267

Mountain, G. S., R. L. Burger, H. Delius, C. S. Fulthorpe, J. A. Austin, D. S. Goldberg, M. S. Steckler, et al. 2009. The Long-Term Stratigraphic Record on Continental Margins. *In* Continental Margin Sedimentation: From Sediment Transport to Sequence Stratigraphy. Special Publication of International Association of Sedimentologists 37. pp. Blackwell Publishing Ltd, pp. 381-458

Moran, K., P. R. Hill, and S. M. Blasco. 1989. Interpretation of piezocone penetrometer profiles in sediment from the Mackenzie Trough, Canadian Beaufort Sea. Journal of Sedimentary Research 59 (1): 88-97.

Murton, J. B. 2009. Stratigraphy and Palaeoenvironments of Richards Island and the Eastern Beaufort Continental Shelf During the Last Glacial-interglacial Cycle. Permafrost and Periglacial Processes 20 (2): 107–125.

Murton, J. B., M. D. Bateman, S. R. Dallimore, J. T. Teller, and Z. Yang. 2010. Identification of Younger Dryas outburst flood path from Lake Agassiz to the Arctic Ocean. Nature 464 (7289): 740-743.

Nguyen, T.-N., C. R. Burn, D. J. King, and S. L. Smith. 2009. Estimating the Extent of Near-surface Permafrost Using Remote Sensing, Mackenzie Delta, Northwest Territories. Permafrost and Periglacial Processes 20 (2): 141–153.

Overeem, I., J. P. M. Syvitski, E. W. H. Hutton, and A. J. Kettner. 2005. Stratigraphic Variability Due to Uncertainty in Model Boundary Conditions: A Case-study of the New Jersey Shelf over the Last 40,000 Years. Marine Geology 224 (1-4): 23–41.

Overeem, I., and J. P. M. Syvitski. 2010. Experimental Exploration of the Stratigraphy of Fjords Fed by Glaciofluvial Systems. Geological Society, London, Special Publications 344 (1): 125–142.

Paull, C. K., W. Ussler, S. R. Dallimore, S. M. Blasco, T. D. Lorenson, H. Melling, B. E. Medioli, F. M. Nixon, and F. A. McLaughlin. 2007. Origin of pingo-like features on the Beaufort Sea shelf and their possible relationship to decomposing methane gas hydrates. Geophysical Research Letters 34 (1)

Peltier, W.R. 2004. Global glacial isostasy and the surface of the ice age earth: The ICE-5G (VM2) Model and GRACE. Annual Review of Earth and Planetary Sciences 32 (1): 111–149.

Pizzuto, J. E., and A. E. Schwendt. 1997. Mathematical modeling of autocompaction of a Holocene transgressive valley-fill deposit, Wolfe Glade, Delaware. Geology 25 (1): 57 -60.

Plint, A.G. 1988. Sharp-based Shoreface Sequences and Offshore Bars in the Cardium Formation of Alberta; Their Relationship to Relative Changes in Sea Level. In Sea Level Changes—An Integrated Approach, ed. C.K. Wilgus, B.S. Hastings, C.G. Kendall, H.W. Posamentier, C.A. Ross, and J.C. Van Wagoner, 42:357–370. SEPM Special Publication. SEPM.

Rampton, V. N. 1988. Quaternary Geology of the Tuktoyaktuk Coastlands, N.W.T. Memoir. Ottawa: Geological Survey of Canada.

Reynolds, D.J., M. S. Steckler, and B. J. Coakley. 1991. The Role of the Sediment Load in Sequence Stratigraphy: The Influence of Flexural Isostasy and Compaction. Journal of Geophysical Research 96 (B4): PP. 6931-6949.

Ridente, D., and F. Trincardi. 2002. Eustatic and Tectonic Control on Deposition and Lateral Variability of Quaternary Regressive Sequences in the Adriatic Basin (Italy). Marine Geology 184 (3-4): 273–293.

Schell, T. M., D. B. Scott, A. Rochon, and S. M. Blasco. 2008. "Late Quaternary Paleoceanography and Paleo-sea Ice Conditions in the Mackenzie Trough and Canyon, Beaufort Sea." *Canadian Journal of Earth Sciences* 45 (11): 1399–1415.

Stanley, D.J., and A. G. Warne. 1994. Worldwide Initiation of Holocene Marine Deltas by Deceleration of Sea-Level Rise. Science 265 (5169): 228 –231.

Stea, R. R., G. B. J. Fader, D. B. Scott, and P.Wu. 2001. Glaciation and Relative Sea-Level Change in Maritime Canada. Geological Society of America Special Papers 351: 35–49

Steffen, H., and P.Wu. 2011. Glacial Isostatic Adjustment in Fennoscandia - A Review of Data and Modeling. Journal of Geodynamics 52 (3-4):169–204

Stokes, C R, C D Clark, and R. Storrar. 2009. Major changes in ice stream dynamics during deglaciation of the north-western margin of the Laurentide ice sheet. Quaternary Science Reviews 28 (7-8): 721-738.

Syvitski, J.M.P., J. N. Smith, E. A. Calabrese, and B. P. Boudreau. 1988. Basin Sedimentation and the Growth of Prograding Deltas. Journal of Geophysical Research 93 (C6): PP. 6895–6908.

Syvitski, J.P.M., and E.W.H. Hutton. 2001. 2D SEDFLUX 1.0C: An Advanced Process-response Numerical Model for the Fill of Marine Sedimentary Basins. Computers & Geosciences 27 (6): 731–753.

Syvitski, J. P. M., and E. W. H. Hutton. 2003. Failure of Marine Deposits and Their Redistribution by Sediment Gravity Flows. Pure and Applied Geophysics 160 (10): 2053–2069.

Syvitski, J. P.M., and Y. Saito. 2007. Morphodynamics of Deltas under the Influence of Humans. Global and Planetary Change 57 (3-4): 261–282.

Syvitski, J.P.M., L.F. Pratson, P.L. Wiberg, M.S. Steckler, M.H. García, W.R. Geyer, C.K. Harris, et al. 2009. "Prediction of Margin Stratigraphy." *In* Continental Margin Sedimentation: From Sediment Transport to Sequence Stratigraphy. Special Publication of International Association of Sedimentologists 37. pp. Blackwell Publishing Ltd, pp. 459-529.

Tarasov, L., and W.R. Peltier. 2004. "A Geophysically Constrained Large Ensemble Analysis of the Deglacial History of the North American Ice-sheet Complex." Quaternary Science Reviews 23 (3–4): 359–388.

Tarasov, L., and W. R. Peltier. 2006. "A Calibrated Deglacial Drainage Chronology for the North American Continent: Evidence of an Arctic Trigger for the Younger Dryas." Quaternary Science Reviews 25 (7-8): 659–688.

Taylor, A. E., M. J. O'Connor, S. M. Blasco, and S. I. Outcalt. 1993. Thermal analysis of acoustic permafrost features, Canadian Beaufort Shelf. In Expanded abstracts, 1993 Technical Program, 1298-1301. Washington D.C.

Taylor, A.E. 1991. Marine transgression, shoreline emergence-evidence in seabed and terrestrial ground temperatures of changing sea levels, Arctic, Canada. Journal of geophysical Research - Solid Earth and Planets 96 (B4): 6893-6909.

Taylor, A.E., S.R. Dallimore, and A.S. Judge. 1996a. Late quaternary history of the Mackenzie-Beaufort region, Arctic Canada, from modelling of permafrost temperatures .2. The Mackenzie Delta-Toktoyaktuk Coastlands. Canadian Journal of Earth Sciences 33 (1): 62-71.

Taylor, A.E., S.R. Dallimore, and S.I. Outcalt. 1996b. Late quaternary history of the Mackenzie-Beaufort region, Arctic Canada, from modelling of permafrost temperatures .1. The onshore offshore transition. Canadian Journal of Earth Sciences 33 (1): 52-61.

Teller, J. T., D. W. Leverington, and J. D. Mann. 2002. Freshwater outbursts to the oceans from glacial Lake Agassiz and their role in climate change during the last deglaciation. Quaternary Science Reviews 21 (8-9): 879-887.

Terrain Analysis & Mapping Services Limited (TAMSL). 1993. Potential granular resources and their geological constraints, Northern Richards Island. Report for the Department of Indian and Northern Affairs.

Tsuji, L. J. S., N. Gomez, J. X. Mitrovica, and R. Kendall. 2009. "Post-Glacial Isostatic Adjustment and Global Warming in Subarctic Canada: Implications for Islands of the James Bay Region." Arctic 62 (4): 458–467.

Tushingham, A. M., and W. R. Peltier. 1991. "Ice-3G: A New Global Model Of Late Pleistocene Deglaciation Based Upon Geophysical Predictions of Post-Glacial Relative Sea Level Change." Journal of Geophysical Research 96 (B3): PP. 4497–4523.

Waelbroeck, C., L. Labeyrie, E. Michel, J.C. Duplessy, J.F. McManus, K. Lambeck, E. Balbon, and M. Labracherie. 2002. Sea-level and deep water temperature changes derived from benthic foraminifera isotopic records. Quaternary Science Reviews 21 (1-3): 295-305.

Watts, A.B, and D.A. Ryan. 1976. "Flexure of the Lithosphere and Continental Margin Basins." Tectonophysics 36: 25–44.

Winsborrow, M. 2004. Ice Streams of the Laurentide Ice Sheet. Géographie physique et Quaternaire 58 (2): 269-280.

Yuill, B., D. Lavoie, and D. J. Reed. 2009. Understanding Subsidence Processes in Coastal Louisiana. Journal of Coastal Research 10054: 23-36.

Appendix A – Sensitivity tests

Sensitivity tests are an essential part of understanding a model. For this study, a suite of sensitivity simulations were carried out to analyse and weigh the impacts of the many modules and parameters available in the stratigraphic simulation model SedFlux. The primary objective was to identify the most influencing parameters controlling the stratigraphic development of the Mackenzie Trough. Doing such extensive examination of SedFlux also revealed model bugs needing further attention.

This appendix is divided per sensitivity test. Each test is accompanied by a Figure, a parameter table, and a brief result and discussion section. The appendix is organised such that the most influencing parameters are displayed first.

Table A1: Boundary conditions and process parameters common to all sensitivity tests presented in this appendix

Process parametres		Process parametres		Process parametres	
INITIATION FILE		**[bbl]**		**[debris flow]**	
margin name	Beaufort	active	yes	repeat interval (years):	250y
vertical resolution	0.75	algorithm (none|muds)	none	yield strength (Pa):	100
x resolution	60000	external sediment source file	none	kinematic viscosity:	0.083
y resolution	400	**[erosion]**		artificial viscosity:	0.5
number	1	active	yes	time step (s):	0.02
duration	21001y	reach of highest order stream (m)	10000	maximum run time (min):	240
time step	10d	relief of highest order stream (m)	1	**[turbidity current]**	
[compaction]		method (diffusion|slope)	diffusion	repeat interval (years):	1y
repeat interval	25y	**[hypopycnal plume]**		sua (Pa/m):	400
[isostasy]		active	YES	sub (Pa):	0
effective elastic thickness (m)	65000	background ocean concentration	0	entrainment constant, ea (-):	0.00153
Youngs modulus (Pa)	7.00E+10	velocity of coastal current (m/s)	0	entrainment constant, eb (-):	0.00204
relaxation time (years)	2500	maximum plume width (km)	15	drag coefficient (-):	0.004
[avulsion]		number of grid nodes in cross-shore	11	internal friction angle (deg):	20
standard deviation (deg)	0	number of grid nodes in river mouth	3	width of channel (m):	1000
minimum angle (deg)	0	**[Failure]**		length of channel (km):	10
maximum angle (deg)	180	repeat interval (years):	250y	algorithm (inflow|sakura):	inflow
hinge point	50,0	coefficient of consolidation (m^2/s):	1.00E-08		
fraction of sediment remaining in plane	1	cohesion of sediments (Pa):	1000		
seed for random number generator	1973	apparent coulomb friction angle (deg):	30		
river can branch?	no	fraction of clay for debris flow:	0.1		

Sediment supply (Fig. A1)

As mentioned in the first annex, sediment supply is based on Carson et al. (1998; 1999) studies. In the 1998 study, the authors estimated an annual sediment flux of 128 Mt/yr for the Mackenzie Delta system. In 1999, the authors suggested a sediment budget dividing the total flux into a ratio of 1:2 between the subaerial floodplain retention (43 Mt/yr) and the offshore delivery (85 Mt/yr). Sedflux requires that a flux be assigned for the bedload and the suspended load, even if the value is nul. Therefore, the total yearly sediment supplied between the bedload and the suspended load equated 128 Mt/yr. Because the simulations were done for the last 21 thousand years, periods which are assumed to have had a larger sediment supply than the modern supply were assigned a factor of the 128 Mt/yr total load.

In this first test, the two estimates of Carson et al. were tested. Scenario 56130 tested the Carson et al. (1999) budget, where 85 Mt/yr was assigned to the offshore suspended load, 4 Mt/yr assigned to the bed load, and the remaining 39 Mt/yr were assigned to the floodplain using the “ratio of floodplain to bedload rate parameter” in the bedload dumping module. Scenario 56333 tested the entire load of 124 Mt/yr assigned to the suspended load with 4 Mt/yr still assigned as the bedload discharge. For both simulations, four time periods were assigned with different magnitudes of sediment supply (see annex 1, Fig. A2 and 3). The magnitudes were of 0, 2.5, 2, and 1 time the modern sediment load.

Based only on the initial trough geometry defined by the modern seafloor profile and the seismic reflector used to calculate the initial bathymetric profile, the total volume necessary to fill the trough is at least 1.817 X 10^{12} m^3. In terms of load, this volume represents 3.27 X 10^6 Mt assuming an averaged saturated grain density of 1800 kg/ m^3. Based on the epochs and the annual discharges assigned to both loads for the simulations 56130 and 56333, the total load of sediment supplied to the trough over the 21 ka was 1.936 X 10^6 and 2.784 X 10^6 respectively. The two simulations clearly show that more sediment is needed and according to the total volume estimate, the average annual load should be in the order of 224 Mt or 1.8 times Carson et al. total budget of 128 Mt/yr. This estimate is based on a supply onset of 14.3 ka BP. As mentioned previously, the load is not distributed evenly across the entire run, but shared across periods reflecting physical and environmental changes known to have occurred over the course of the simulation.

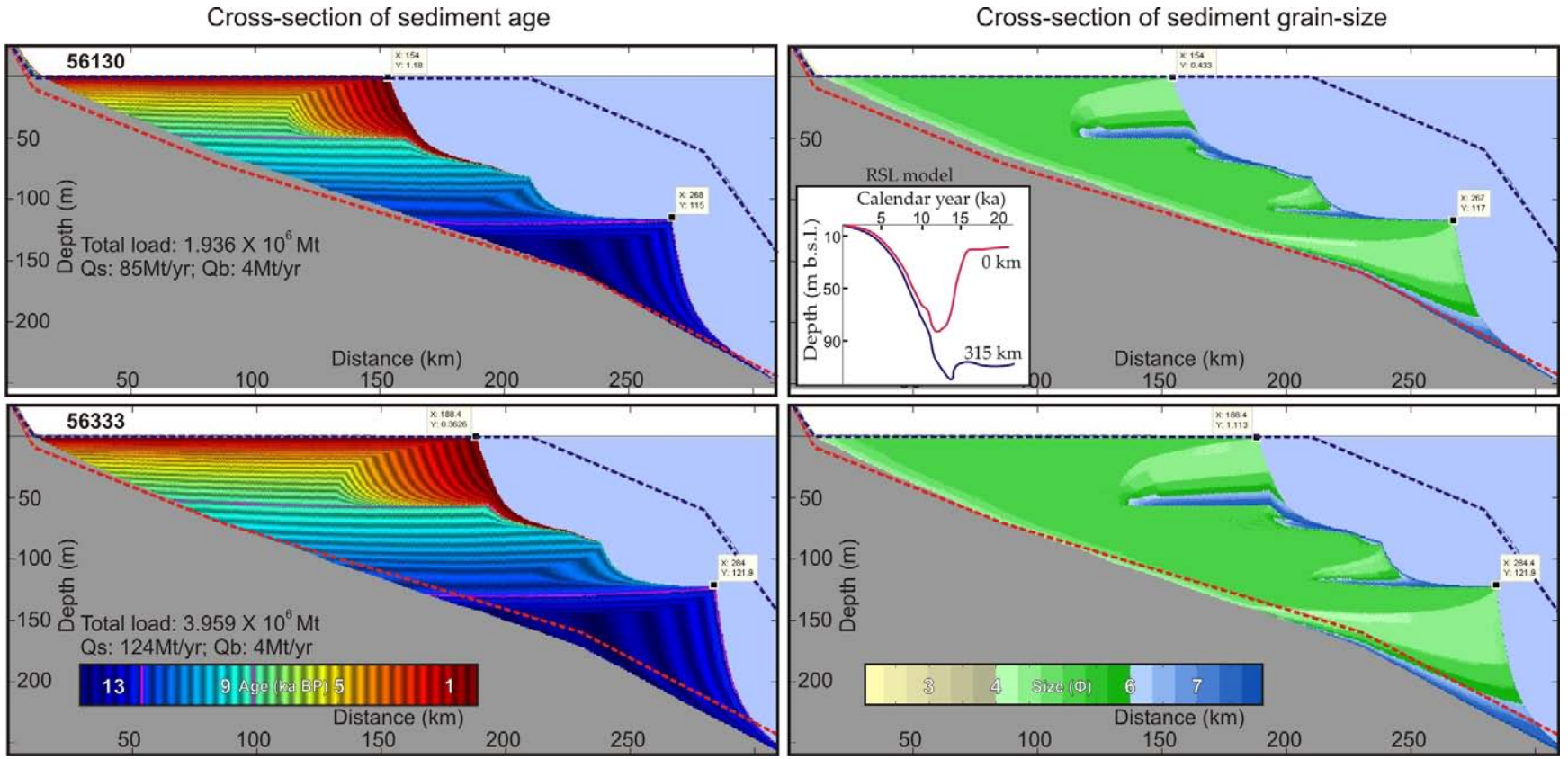

Figure A1: Sediment supply sensitivity test. Scenario 56130 is based on the sediment supply estimated by Carson et al. (1999) for the present Mackenzie River system. In this scenario, the total sediment load is divided following a ratio of 1:2 between subaerial delta plain and the offshore delivery. Scenario 56333 considered the total load being delivered to the offshore. The locations of the seismic basal reflector from which the initial profile was derived (Hill et al., 2001; red dotted line) and the modern seafloor profile (blue dotted line) are displayed. As a reference, the RSL graph presents the RSL curves corresponding to each extremity of the transect.

Table A2: Sediment supply

Files	56130	56333
Summary of processes	**Qs: 85Mt/yr; Qb: 4Mt/yr (Carson et al. 1999); Epoch length: 6.7/2.3/4/8ka; Epoch sediment supply: 0/2.5/2/1X**	**Qs: 124Mt/yr; Qb: 4Mt/yr (Carson et al. 1998); Epoch length: 6.7/2.3/7/5ka; Epoch sediment supply: 0/2.5/2/1X**
INITIATION FILE		
bathymetry file	(compensated) beaufort_bathy.csv	(compensated) beaufort_bathy.csv
PROCESS FILE		
[sea level]		
active	no	no
sea level file	beaufort_sea_level.csv	beaufort_sea_level.csv
[Subsidence]		
active:	yes	yes
Subsidence file	rates_sedflux_MT21000.dat	rates_sedflux_MT21000.dat
[compaction]		
active	no	no
[isostasy]		
active	yes	yes
enable water loading	no	no
[river 0]		
active	0y->6700y	0y->6700y
river file	beaufort_river.kvf	beaufort_river.kvf
[bedload dumping]		
active	0y->6700y	0y->6700y
distance to dump bedload (m)	5000	5000
ratio of flood plain to bedload rate	0.22	0
fraction of bedload retained in the delta plain	0	0
[river 1]		
active	6700yr -> 9000yr	6700yr -> 9000yr
river file	beaufort_river2.kvf	beaufort_river2.kvf
[bedload dumping]		
active	6700yr -> 9000yr	6700yr -> 9000yr
distance to dump bedload (m)	5000	5000
ratio of flood plain to bedload rate	0.22	0
fraction of bedload retained in the delta plain	0	0
[river 2]		
active	9000yr -> 13000y	9000yr -> 13000y
river file	beaufort_river3.kvf	beaufort_river3.kvf
[bedload dumping]		
active	9000yr -> 13000y	9000yr -> 13000y
distance to dump bedload (m)	5000	5000
ratio of flood plain to bedload rate	0.22	0
fraction of bedload retained in the delta plain	0	0
[river 3]		
active	13000y -> 21000y	13000y -> 21000y
river file	beaufort_river4.kvf	beaufort_river4.kvf

[bedload dumping]		
active	13000y -> 21000y	13000y -> 21000y
distance to dump bedload (m)	5000	5000
ratio of flood plain to bedload rate	0.22	0
fraction of bedload retained in the delta plain	0	0
[plume]		
active	YES	YES
hyperpycnal plume model	<none>	<none>
hypopycnal plume model	'hypopycnal plume'	'hypopycnal plume'
[Failure]		
active:	no	no
[debris flow]		
active:	no	no
[turbidity current]		
active:	no	no
RIVER FILES		
River0		
['Season 1']		
Duration (y)	1y	1y
Bedload (kg/s)	0	0
Suspended load concentration (kg/m^3)	0	0
velocity (m/s)	0.7	0.7
Width (m)	2000	2000
Depth (m)	8	8
River1		
['Season 1']		
Duration (y)	1y	1y
Bedload (kg/s)	325	500
Suspended load concentration (kg/m^3)	0.06018, 0.361, 0.1805	0.0878, 0.526, 0.263
velocity (m/s)	0.7	0.7
Width (m)	2000	2000
Depth (m)	8	8
River2		
['Season 1']		
Duration (y)	1y	1y
Bedload (kg/s)	260	400
Suspended load concentration (kg/m^3)	0.04814, 0.2888, 0.1444	0.07024, 0.4208, 0.2104
velocity (m/s)	0.7	0.7
Width (m)	2000	2000
Depth (m)	8	8
River3		
['Season 1']		
Duration (y)	1y	1y
Bedload (kg/s)	130	200
Suspended load concentration (kg/m^3)	0.02407, 0.1444, 0.0722	0.03512, 0.2104, 0.1052
velocity (m/s)	0.7	0.7

Width (m)	2000	2000
Depth (m)	8	8
SEDIMENT FILE		
[Grain 1 (bedload)]		
grain size (microns)	200	200
grain density (kg/m^3)	2650	2650
saturated density (kg/m^3)	2000	2000
minimum void ratio (-)	0.17	0.17
diffusion coefficient (-)	0.25	0.25
removal rate (1/day)	25	25
consolidation coefficient (m^2/yr)	100000	100000
compaction coefficient (-)	0.000000062	0.000000062
[Grain 2 (suspended)]		
grain size (microns)	150	150
grain density (kg/m^3)	2650	2650
saturated density (kg/m^3)	1955	1955
minimum void ratio (-)	0.15	0.15
diffusion coefficient (-)	0.25	0.25
removal rate (1/day)	20	20
consolidation coefficient (m^2/yr)	100000	100000
compaction coefficient (-)	0.00000007	0.000000007
[Grain 3 (suspended)]		
grain size (microns)	60	60
grain density (kg/m^3)	2650	2650
saturated density (kg/m^3)	1795	1795
minimum void ratio (-)	0.1	0.1
diffusion coefficient (-)	0.25	0.25
removal rate (1/day)	12	12
consolidation coefficient (m^2/yr)	100000	100000
compaction coefficient (-)	0.00000001	0.00000001
[Grain 4 (suspended)]		
grain size (microns)	5	5
grain density (kg/m^3)	2650	2650
saturated density (kg/m^3)	1504	1504
minimum void ratio (-)	0.05	0.05
diffusion coefficient (-)	0.25	0.25
removal rate (1/day)	3.2	3.2
consolidation coefficient (m^2/yr)	100000	100000
compaction coefficient (-)	0.00000036	0.00000036

Epochs (Fig. A2 and A3)

This sensitivity test looks into the timing of sediment supply and how best to share the load of sediment over the entire simulation. This test thus uses defined periods called epochs that are assigned varying sediment supply. Because of the functionality of epochs, sediment supply is represented as a step-function. This test is presented over two Figures.

Figure A2 presents a case between turning on sediment supply from the beginning of the run (55228) , i.e. 21 ka BP, or wait until 14.3 ka BP when the ice as retreated from the area (60997). Even though these two examples present different sediment supply, i.e. a constant 128 Mt/yr for 55228 or 320 Mt/yr (2.5 X) for 60997, the stratigraphic effects of changing the start of the supply is evident. Scenario 55228 shows the development of a Falling stage systems track (FSST) during lowering of RSL between 21 and 14 ka BP. The FSST steepness, seen better in the age cross-section, is caused by the rapid RSL fall observed landward compared to the offshore. This may be better explained using isostatic motion. In the first 6000 years of the simulation, the land is rebouding much faster landward then offshore, steepening the initial profile, and thus creating a rapid relative sea-level lowering. Because of the large sediment supply, a progradational wedge is accumulating, but is strongly defined by an erosive surface (SB). In scenario 60997, the FSST is non-existent as sediment supply is only activated after 6700 years. Instead, the stratigraphy starts with the development of the Lowstand Systems Track (LST). The same LST is apparent in the 55228 simulation, but to a smaller extent because of the smaller sediment supply.

The last point to be made on this Figure refers to the sediment supply. In the previous section, it was mentioned that based on the geometry of the modeled trough, an average of at least 224 Mt/yr (1.8 times the modern supply) was necessary to fill the trough in 14.3 ka. In the 60997 scenario, 320 Mt/yr was used as the annual supply. Considering that this amount created an extra volume to fill due to loading (between the red profile and basement), the results support the last statement and suggest that the average supply should be between 1.8 and 2.5 X the modern supply.

Figure A3 complements the previous Figure as it shows the effect of manipulating the timing of the various epochs. Compare to the base-case scenario 56333, which is discussed in length in the stratigraphic paper, simulation 61501 tests an earlier onset to sediment supply, i.e. 15.5 ka BP. The reason for starting the sediment supply earlier in the first scenario is to consider that even though it is assumed that the onset of sediment supply to the trough should start when the ice has totally retreated from the Mackenzie Trough, i.e. 14.3 ka (56333), infilling of the offshore trough by glacio-fluvial systems probably started earlier. Dyke (2002) reconstruction of the LIS suggests that following thousands of years of LGM conditions, the retreat of the Mackenzie ice lobe began around 16.3 ka BP, and entirely freed up the trough by 14.1 ka BP. Thus, using the average between these two dates, the start of the supply was set to 15.5 ka BP and tested in simulation 61501.

Scenario 56333 represents the base-case scenario and is discussed in length in the stratigraphic paper. The stratigraphic effect of starting sediment supply earlier result in the partial development of the FSST explained in the previous Figure. The development of a

FSST prism occupies some accommodation space and thus pushes the progradation of the LST prism farther offshore. Since the hinge point is dictated by the RSL and similar amount of sediment loading is applied, the hinge point lies around the same depth.

Finally, scenario 61038 compares the effect of higher sediment supply from the onset until the Late Holocene. This is simulated by combining the second and third epoch of the base-case scenario together and assigning 2,5 times the modern sediment supply. The effects are to build a more prominent transgressive systems track (TST) wedge, which progrades over much of the LST wedge. The four original epochs used in the base-case scenario and referred to in the method section of the stratigraphic paper (21 to 14.3 ka BP, 14.3 to 12 ka BP, 12 to 8 ka BP, and 8 ka BP to present) were determined based on the availability of material in the system. The third epoch was considered to be the waning phase of the glacial sediment availability before the modern conditions were established. Setting four epochs resulted in basically 3 main wedges associated with systems tracks: LST, TST (during transgression), and a Highstand systems track (HST) wedge. By lengthening the second period and assigning it the larger amount of sediment supply, the second prism prograded over most of the LST prism. The hinge point of the second prism thus reaches farther offshore and reaches shallower water depth (80 m b.s.l.). As mentioned in the stratigraphic paper, it is thus possible that in the case where the TST would develop to cover the entire length of the underlying LST, the lower wedge identified in the seismic interpretation of Hill (1996) could have potentially miss the two prisms and interpret them as one.

The last observation made from this last simulation is that using the modern sediment supply for the Holocene period (fourth period) is not enough to fill the rest of the trough to match the High Systems Track (HST) identified by Hill et al. (2001).

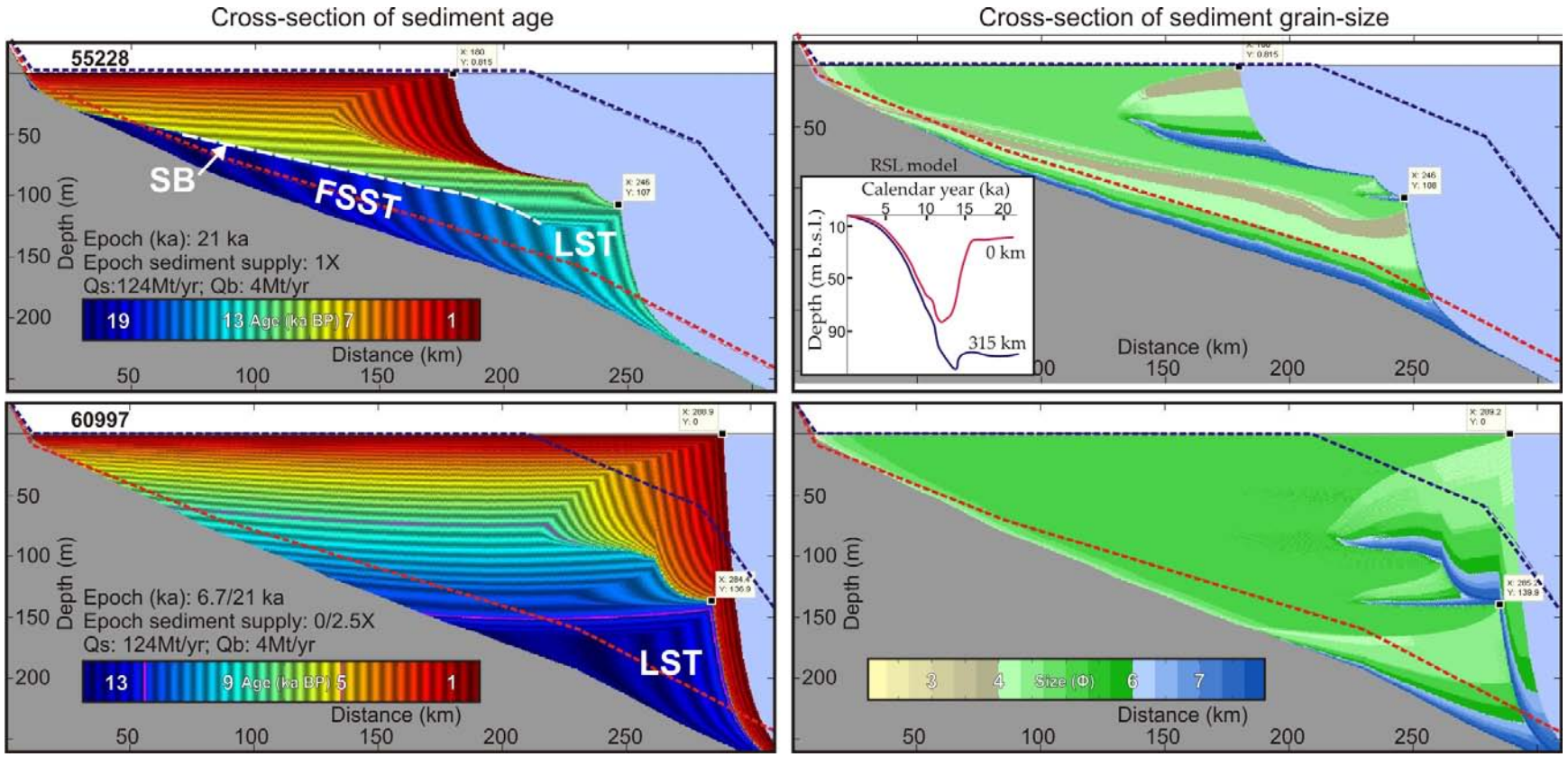

Figure A2: Epoch sensitivity test. Scenario 55228 presents a constant sediment supply over 21 ka epoch. Scenario 60997 presents two epochs: 0 - 6.7 ka with no sediment supply and 6.7 to 21 ka with constant supply. The initial bathymetric profile for both simulations was not adjusted to accommodate for sediment loading. The locations of the seismic basal reflector from which the initial profile was derived (Hill et al., 2001; red dotted line) and the modern seafloor profile (blue dotted line) are displayed. As a reference, the RSL graph presents the RSL curves corresponding to each extremity of the transect.

Table A3: Sediment supply timing

Files	**55228**	**60997**
Summary of processes	**Epoch length: 21ka; Epoch sediment supply: 1X Qs: 124Mt/yr; Qb: 4Mt/yr (Carson et al. 1998);**	**Epoch length: 6.7/21 ka Epoch sediment supply: 0/2.5X; Qs: 124Mt/yr; Qb: 4Mt/yr (Carson et al. 1998);**
INITIATION FILE		
bathymetry file	(non-compensated) beaufort_bathy.csv	(non-compensated) beaufort_bathy.csv
PROCESS FILE		
[sea level]		
active	no	no
sea level file	beaufort_sea_level.csv	beaufort_sea_level.csv
[Subsidence]		
active:	yes	yes
Subsidence file	rates_sedflux_MT21000_combined.dat	rates_sedflux_MT21000.dat
[compaction]		
active	no	no
[isostasy]		
active	yes	yes
enable water loading	no	no
[river 0]		
active	yes	yes
river file	beaufort_river.kvf	beaufort_river.kvf
[bedload dumping]		
active	yes	0y->6700y
distance to dump bedload (m)	5000	5000
ratio of flood plain to bedload rate	6.5	0.22
fraction of bedload retained in the delta plain	0	0
[river 1]		
active		6700yr -> 21000yr
river file		beaufort_river2.kvf
[bedload dumping]		
active		6700yr -> 21000yr
distance to dump bedload (m)		5000
ratio of flood plain to bedload rate		0.22
fraction of bedload retained in the delta plain		0
[plume]		
active	yes	yes
hyperpycnal plume model	<none>	<none>
hypopycnal plume model	'hypopycnal plume'	'hypopycnal plume'
[Failure]		
active:	no	no
[debris flow]		
active:	no	no
[turbidity current]		
active:	no	no
RIVER FILES		
River0		
['Season 1']		

Duration (y)			1y			1y
Bedload (kg/s)			200			0
Suspended load concentration (kg/m^3)	0.1054,	0.1473,	0.0982			0
velocity (m/s)			0.7			0.7
Width (m)			2000			2000
Depth (m)			8			8
River1						
['Season 1']						
Duration (y)						1y
Bedload (kg/s)						520
Suspended load concentration (kg/m^3)				0.09628,	0.5776,	0.2888
velocity (m/s)						0.7
Width (m)						2000
Depth (m)						8
SEDIMENT FILE						
[Grain 1 (bedload)]						
grain size (microns)			300			200
grain density (kg/m^3)			2650			2650
saturated density (kg/m^3)			2094			2000
minimum void ratio (-)			0.2			0.17
diffusion coefficient (-)			0.25			0.25
removal rate (1/day)			35			25
consolidation coefficient (m^2/yr)			100000			100000
compaction coefficient (-)			0.00000005			0.000000062
[Grain 2 (suspended)]						
grain size (microns)			200			150
grain density (kg/m^3)			2650			2650
saturated density (kg/m^3)			2000			1955
minimum void ratio (-)			0.17			0.15
diffusion coefficient (-)			0.25			0.25
removal rate (1/day)			25			20
consolidation coefficient (m^2/yr)			100000			100000
compaction coefficient (-)			0.000000062			0.00000007
[Grain 3 (suspended)]						
grain size (microns)			60			60
grain density (kg/m^3)			2650			2650
saturated density (kg/m^3)			1795			1795
minimum void ratio (-)			0.1			0.1
diffusion coefficient (-)			0.25			0.25
removal rate (1/day)			12			12
consolidation coefficient (m^2/yr)			100000			100000
compaction coefficient (-)			0.00000008			0.00000008
[Grain 4 (suspended)]						
grain size (microns)			5			5
grain density (kg/m^3)			2650			2650
saturated density (kg/m^3)			1504			1504
minimum void ratio (-)			0.05			0.05
diffusion coefficient (-)			0.25			0.25
removal rate (1/day)			3.2			3.2

consolidation coefficient (m^2/yr)	100000	100000
compaction coefficient (-)	0.00000036	0.00000036

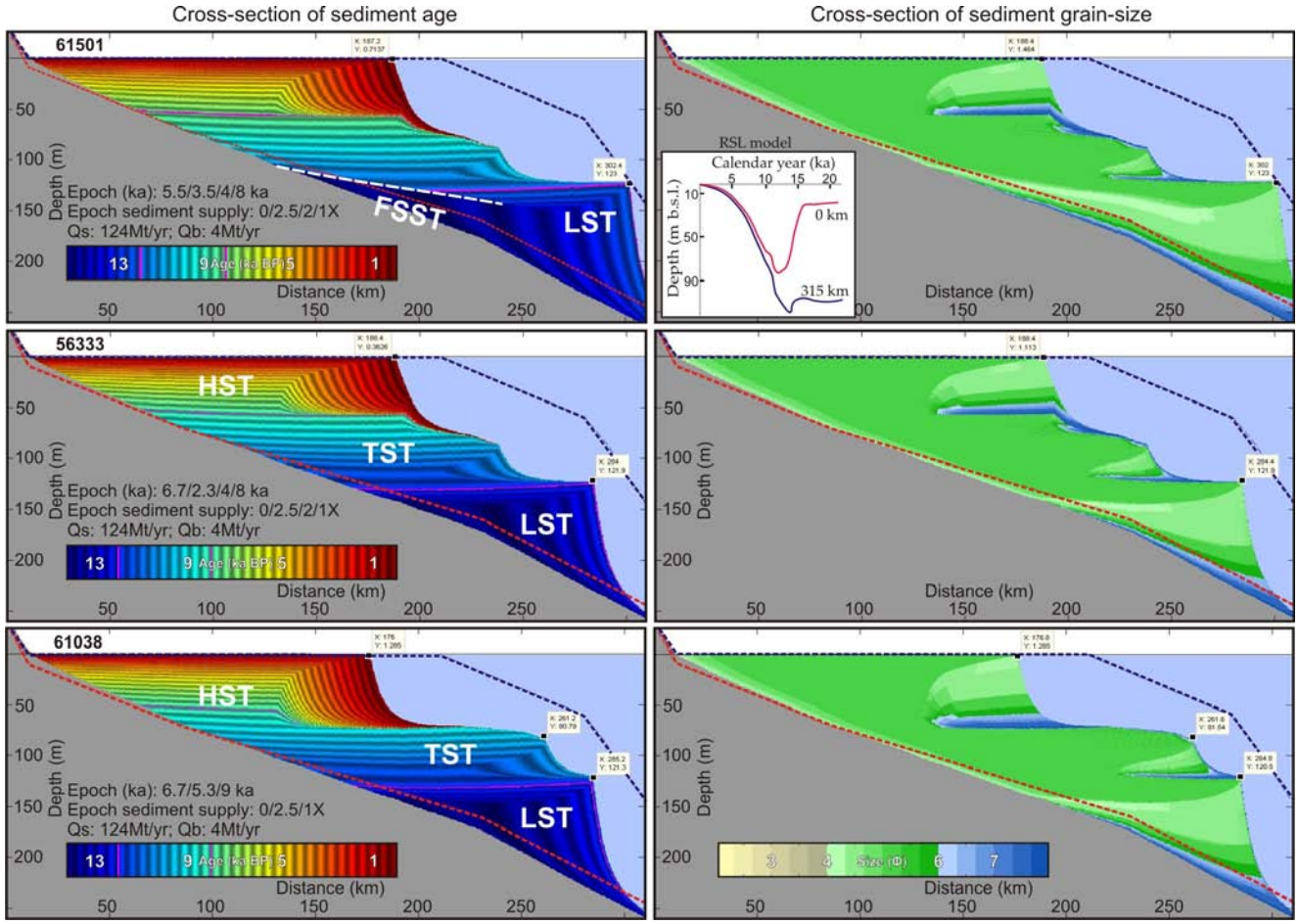

Figure A3: Epoch sensitivity test. Simulation 61501 used 4 epochs with supply starting after 5.5 ka. Simulation 56333 represents the base-case simulation and presents 4 epochs with a variable sediment supply starting at 6.7 ka. Simulation 61038 presents 3 epochs, in which epoch 2 and 3 of the base-case screnario are combined. The locations of the seismic basal reflector from which the initial profile was derived (Hill et al., 2001; red dotted line) and the modern seafloor profile (blue dotted line) are displayed. As a reference, the RSL graph presents the RSL curves corresponding to each extremity of the transect.

Table A4: Sediment supply timing (suite)

Files	61038	56333	61501
Summary of processes	**Epoch length: 6.7/5.3/9ka; Epoch sediment supply: 0/2.5/1X; Qs: 124Mt/yr; Qb: 4Mt/yr (Carson et al. 1998);**	**Epoch length: 6.7/2.3/4/8ka; Epoch sediment supply: 0/2.5/2/1X; Qs: 124Mt/yr; Qb: 4Mt/yr (Carson et al. 1998);**	**Epoch length: 5.5/4.5/4/8ka; Epoch sediment supply: 0/2.5/2/1X; Qs: 124Mt/yr; Qb: 4Mt/yr (Carson et al. 1998);**
INITIATION FILE			
bathymetry file	(compensated) beaufort_bathy.csv	(compensated) beaufort_bathy.csv	(compensated) beaufort_bathy.csv
PROCESS FILE			
[sea level]			
active	no	no	no
sea level file	beaufort_sea_level.csv	beaufort_sea_level.csv	beaufort_sea_level.csv
[Subsidence]			
active:	yes	yes	yes
Subsidence file	rates_sedflux_MT21000.dat	rates_sedflux_MT21000.dat	rates_sedflux_MT21000.dat
[compaction]			
active	no	no	no
[isostasy]			
active	yes	yes	yes
enable water loading	no	no	
[river 0]			
active	0y->6700y	0y->6700y	0y->6700y
river file	beaufort_river.kvf	beaufort_river.kvf	beaufort_river.kvf
[bedload dumping]			
active	0y->6700y	0y->6700y	0y->5500y
distance to dump bedload (m)	5000	5000	5000
ratio of flood plain to bedload rate	0	0	0
fraction of bedload retained in the delta plain	0	0	0
[river 1]			
active	6700yr -> 12000yr	6700yr -> 9000yr	5500yr -> 9000yr
river file	beaufort_river2.kvf	beaufort_river2.kvf	beaufort_river2.kvf
[bedload dumping]			
active	6700yr -> 12000yr	6700yr -> 9000yr	5500yr -> 9000yr
distance to dump bedload (m)	5000	5000	5000
ratio of flood plain to bedload rate	0	0	0
fraction of bedload retained in the delta plain	0	0	0
[river 2]			
active	12000yr -> 21000y	9000yr -> 13000y	9000yr -> 13000y
river file	beaufort_river3.kvf	beaufort_river3.kvf	beaufort_river3.kvf
[bedload dumping]			
active	12000yr -> 21000y	9000yr -> 13000y	9000yr -> 13000y
distance to dump	5000	5000	5000

bedload (m)			
ratio of flood plain to bedload rate	0	0	0
fraction of bedload retained in the delta plain	0	0	0
[river 3]			
active		13000y -> 21000y	13000y -> 21000y
river values		season	season
river file		beaufort_river4.kvf	beaufort_river4.kvf
[bedload dumping]			
active		13000y -> 21000y	13000y -> 21000y
distance to dump bedload (m)		5000	5000
ratio of flood plain to bedload rate		0	0
fraction of bedload retained in the delta plain		0	0
[plume]			
active	yes	yes	YES
hyperpycnal plume model	<none>	<none>	<none>
hypopycnal plume model	'hypopycnal plume'	'hypopycnal plume'	'hypopycnal plume'
[Failure]			
active:	no	no	no
[debris flow]			
active:	no	no	no
[turbidity current]			
active:	no	no	no
RIVER FILES			
River0			
['Season 1']			
Duration (y)	1y	1y	1y
Bedload (kg/s)	0	0	0
Suspended load concentration (kg/m^3)	0	0	0
velocity (m/s)	0.7	0.7	0.7
Width (m)	2000	2000	2000
Depth (m)	8	8	8
River1			
['Season 1']			
Duration (y)	1y	1y	1y
Bedload (kg/s)	500	500	500
Suspended load concentration (kg/m^3)	0.0878, 0.526, 0.263	0.0878, 0.526, 0.263	0.0878, 0.526, 0.263
velocity (m/s)	0.7	0.7	0.7
Width (m)	2000	2000	2000
Depth (m)	8	8	8
River2			
['Season 1']			
Duration (y)	1y	1y	1y
Bedload (kg/s)	200	400	400

Suspended load concentration (kg/m^3)	0.03512, 0.2104, 0.1052	0.07024, 0.4208, 0.2104	0.07024, 0.4208, 0.2104
velocity (m/s)	0.7	0.7	0.7
Width (m)	2000	2000	2000
Depth (m)	8	8	8
River3			
['Season 1']			
Duration (y)	1y	1y	1y
Bedload (kg/s)	200	200	200
Suspended load concentration (kg/m^3)	0.03512, 0.2104, 0.1052	0.03512, 0.2104, 0.1052	0.03512, 0.2104, 0.1052
velocity (m/s)	0.7	0.7	0.7
Width (m)	2000	2000	2000
Depth (m)	8	8	8
SEDIMENT FILE			
[Grain 1 (bedload)]			
grain size (microns)	200	200	200
grain density (kg/m^3)	2650	2650	2650
saturated density (kg/m^3)	2000	2000	2000
minimum void ratio (-)	0.17	0.17	0.17
diffusion coefficient (-)	0.25	0.25	0.25
removal rate (1/day)	25	25	25
consolidation coefficient (m^2/yr)	100000	100000	100000
compaction coefficient (-)	0.000000062	0.000000062	0.000000062
[Grain 2 (suspended)]			
grain size (microns)	150	150	150
grain density (kg/m^3)	2650	2650	2650
saturated density (kg/m^3)	1955	1955	1955
minimum void ratio (-)	0.15	0.15	0.15
diffusion coefficient (-)	0.25	0.25	0.25
removal rate (1/day)	20	20	20
consolidation coefficient (m^2/yr)	100000	100000	100000
compaction coefficient (-)	0.00000007	0.00000007	0.000000007
[Grain 3 (suspended)]			
grain size (microns)	60	60	60
grain density (kg/m^3)	2650	2650	2650
saturated density (kg/m^3)	1795	1795	1795
minimum void ratio (-)	0.1	0.1	0.1
diffusion coefficient (-)	0.25	0.25	0.25
removal rate (1/day)	12	12	12
consolidation coefficient (m^2/yr)	100000	100000	100000
compaction coefficient (-)	0.00000008	0.00000008	0.00000008
[Grain 4 (suspended)]			
grain size (microns)	5	5	5
grain density (kg/m^3)	2650	2650	2650

saturated density (kg/m^3)	1504	1504	1504
minimum void ratio (-)	0.05	0.05	0.05
diffusion coefficient (-)	0.25	0.25	0.25
removal rate (1/day)	3.2	3.2	3.2
consolidation coefficient (m^2/yr)	100000	100000	100000
compaction coefficient (-)	0.00000036	0.00000036	0.00000036

Sea-level model (Fig. A4, A5, and A6)

The following test evaluates the outcomes of using different sea-level curves. It is a valuable test it assisted in evaluating the stratigraphic importance of using a complex RSL model representative of regions influenced by glacio-isostatic adjustments in comparison to other single sea-level curves.

Eustatic (Fig. A4)

Figure A4 presents the difference in stratigraphy between using the RSL model and the eustatic curve. The results of this comparison are described in length in the stratigraphic paper. As a summary, the most obvious difference with the base-case simulation resides in the internal structure of the stratigraphy and its timing. In comparison with the base-case simulation, only two progradational wedges were formed. The lower wedge developed over two thousand additional years (4.3 ka) and is thus capped by a younger top surface (9.7 ka BP) lying in shallower waters (-70 m). The hinge point of the LST does not reach as far offshore and contrary to the timing of the base-case simulation, the lower wedge corresponds to a TST. Its progradational pattern was possible due to the sediment supply keeping up with the expanding rate of accommodation. The structure however shows clearly the retrogradational pattern associated with sea-level transgression. Post-Holocene, the rapidly rising sea-level combined with the reduction in sediment supply results in the formation of the TST (9.7 and 7.5 ka BP). The top of the deposit is identified in the grain-size cross-section by the sharp transition in grain-sizes located around 45 metres water depth. This transition corresponds to the MFS.

Finally, because the sediment deposited earlier aggraded to shallower water depths, the accommodation space made available for the HST was lessened, and thus supported more progradation of the HST wedge.

21 ka eustatic (Fig. A5)

The simulations presented in Figure A5 shows the different stratigraphy built after 21 ka of sediment supply between using the eustatic curve (63365) over the RSL model (55228). The stratigraphy using the eustatic curve is somewhat more similar to the base-case simulation (56333, Fig. A4), only stretched over a longer time period. This can be explained by the fact that the eustatic curve shape from 21 ka BP is similar to the shape of the offshore RSL curve (315 km) from 14.3 ka BP. This thus confirms that the shape of the sea-level curve is very important in establishing the stratigraphy. In simulation 55228, the rapidly falling stage develops a strong FSST wedge, whereas for the same time period, the eustatic is a lowstand, which develops a LST wedge.

Dynamic RSL or single RSL curve (Fig. A6)

The results of this simulation are not discussed here as they are explained in length in the stratigraphic paper.

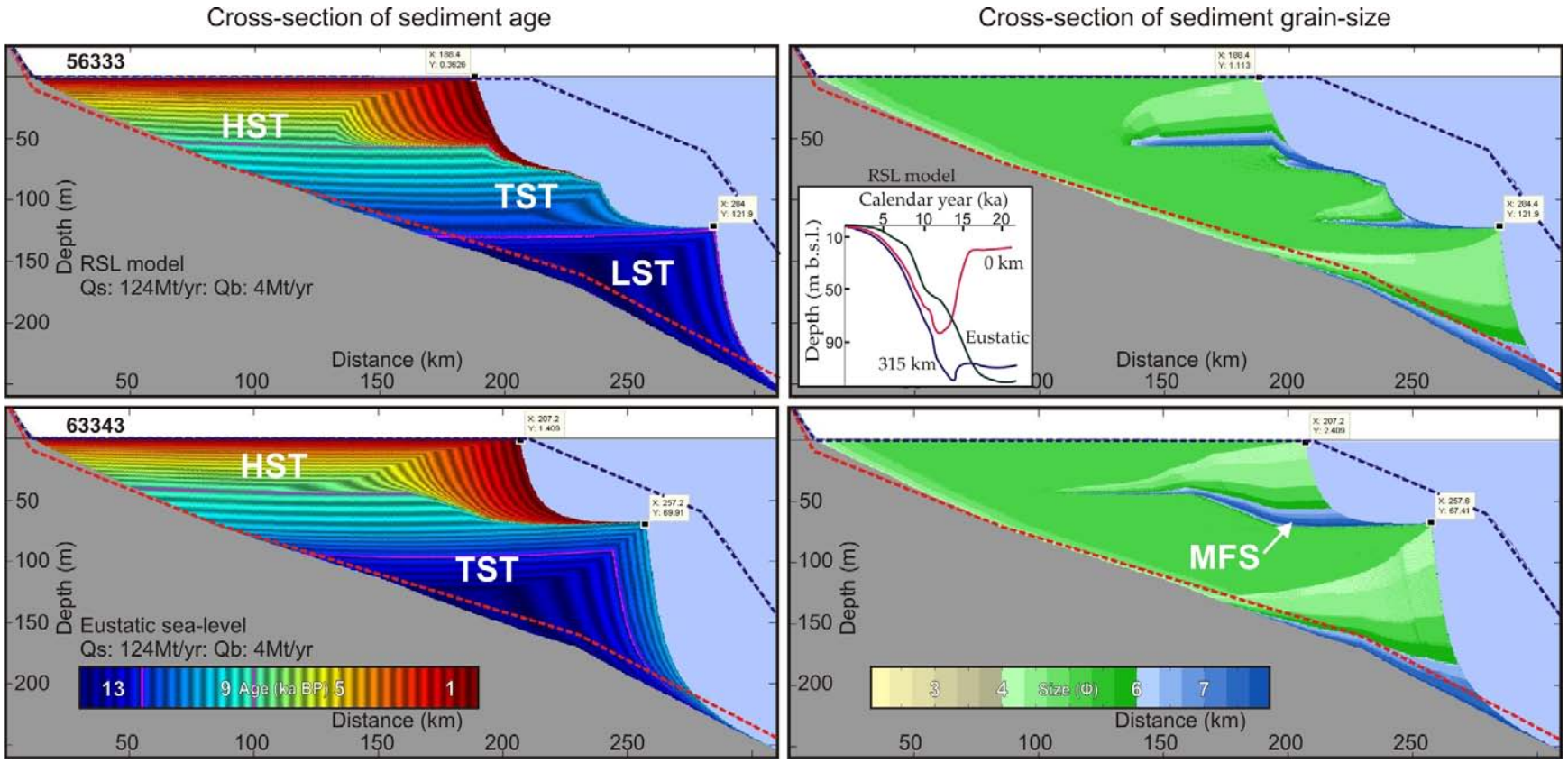

Figure A4: Sensitivity test on sea-level. Simulation 56333 uses the RSL model. Simulation 63343 uses the eustatic sea-level curve of Waelbroech et al. (2002). Both simulations integrated the sea-level data via the 'subsidence' module. The locations of the seismic basal reflector from which the initial profile was derived (Hill et al., 2001; red dotted line) and the modern seafloor profile (blue dotted line) are displayed. As a reference, the RSL graph presents the RSL curves corresponding to each extremity of the transect.

Table A5: Eustatic sea-level curve vs RSL model

Files	**56333**	**63343**
Summary of processes	**RSL model; Qs: 124Mt/yr; Qb: 4Mt/yr (Carson et al. 1998);**	**Eustatic; Qs: 85Mt/yr; Qb: 4Mt/yr (Carson et al. 1999);**
INITIATION FILE		
[global]		
bathymetry file	(compensated) beaufort_bathy.csv	(compensated) beaufort_bathy.csv
PROCESS FILE		
[sea level]		
active	no	no
sea level file	beaufort_sea_level.csv	beaufort_sea_level.csv
[Subsidence]		
active:	yes	yes
Subsidence file	rates_sedflux_MT21000.dat	rates_sedflux_MT21000_eustatic_long.dat
[compaction]		
active	no	no
[isostasy]		
active	yes	yes
enable water loading	no	no
[river 0]		
active	yes	yes
river file	beaufort_river.kvf	beaufort_river.kvf
[bedload dumping]		
active	0y->6700y	0y->6700y
distance to dump bedload (m)	5000	5000
ratio of flood plain to bedload rate	0	1
fraction of bedload retained in the delta plain	0	0
[river 1]		
active	6700yr -> 9000yr	6700yr -> 9000yr
river file	beaufort_river2.kvf	beaufort_river2.kvf
[bedload dumping]		
active	6700yr -> 9000yr	6700yr -> 9000yr
distance to dump bedload (m)	5000	5000
ratio of flood plain to bedload rate	0	1
fraction of bedload retained in the delta plain	0	0
[river 2]		
active	9000yr -> 13000y	9000yr -> 13000y
river file	beaufort_river3.kvf	beaufort_river3.kvf
[bedload dumping]		
active	9000yr -> 13000y	9000yr -> 13000y
distance to dump bedload (m)	5000	5000
ratio of flood plain to bedload rate	0	1
fraction of bedload retained in the delta plain	0	0
[river 3]		
active	13000y -> 21000y	13000y -> 21000y

river file	beaufort_river4.kvf	beaufort_river4.kvf
[bedload dumping]		
active	13000y -> 21000y	13000y -> 21000y
distance to dump bedload (m)	5000	5000
ratio of flood plain to bedload rate	0	1
fraction of bedload retained in the delta plain	0	0
[plume]		
active	yes	yes
hyperpycnal plume model	<none>	<none>
hypopycnal plume model	'hypopycnal plume'	'hypopycnal plume'
[Failure]		
active:	no	no
[debris flow]		
active:	no	no
[turbidity current]		
active:	no	no
RIVER FILES		
River0		
['Season 1']		
Duration (y)	1y	1y
Bedload (kg/s)	0	0
Suspended load concentration (kg/m^3)	0	0
velocity (m/s)	0.7	0.7
Width (m)	2000	2000
Depth (m)	8	8
River1		
['Season 1']		
Duration (y)	1y	1y
Bedload (kg/s)	500	500
Suspended load concentration (kg/m^3)	0.0878, 0.526, 0.263	0.0878, 0.526, 0.263
velocity (m/s)	0.7	0.7
Width (m)	2000	2000
Depth (m)	8	8
River2		
['Season 1']		
Duration (y)	1y	1y
Bedload (kg/s)	400	400
Suspended load concentration (kg/m^3)	0.07024, 0.4208, 0.2104	0.07024, 0.4208, 0.2104
velocity (m/s)	0.7	0.7
Width (m)	2000	2000
Depth (m)	8	8
River3		
['Season 1']		
Duration (y)	1y	1y
Bedload (kg/s)	200	200
Suspended load concentration (kg/m^3)	0.03512, 0.2104, 0.1052	0.03512, 0.2104, 0.1052

velocity (m/s)	0.7	0.7
Width (m)	2000	2000
Depth (m)	8	8
SEDIMENT FILE		
[Grain 1 (bedload)]		
grain size (microns)	200	300
grain density (kg/m^3)	2650	2650
saturated density (kg/m^3)	2000	2094
minimum void ratio (-)	0.17	0.2
diffusion coefficient (-)	0.25	0.25
removal rate (1/day)	25	35
consolidation coefficient (m^2/yr)	100000	100000
compaction coefficient (-)	0.000000062	0.00000005
[Grain 2 (suspended)]		
grain size (microns)	150	150
grain density (kg/m^3)	2650	2650
saturated density (kg/m^3)	1955	1955
minimum void ratio (-)	0.15	0.15
diffusion coefficient (-)	0.25	0.25
removal rate (1/day)	20	20
consolidation coefficient (m^2/yr)	100000	100000
compaction coefficient (-)	0.00000007	0.00000007
[Grain 3 (suspended)]		
grain size (microns)	60	60
grain density (kg/m^3)	2650	2650
saturated density (kg/m^3)	1795	1795
minimum void ratio (-)	0.1	0.1
diffusion coefficient (-)	0.25	0.25
removal rate (1/day)	12	12
consolidation coefficient (m^2/yr)	100000	100000
compaction coefficient (-)	0.00000008	0.00000008
[Grain 4 (suspended)]		
grain size (microns)	5	5
grain density (kg/m^3)	2650	2650
saturated density (kg/m^3)	1504	1504
minimum void ratio (-)	0.05	0.05
diffusion coefficient (-)	0.25	0.25
removal rate (1/day)	3.2	3.2
consolidation coefficient (m^2/yr)	100000	100000
compaction coefficient (-)	0.00000036	0.00000036

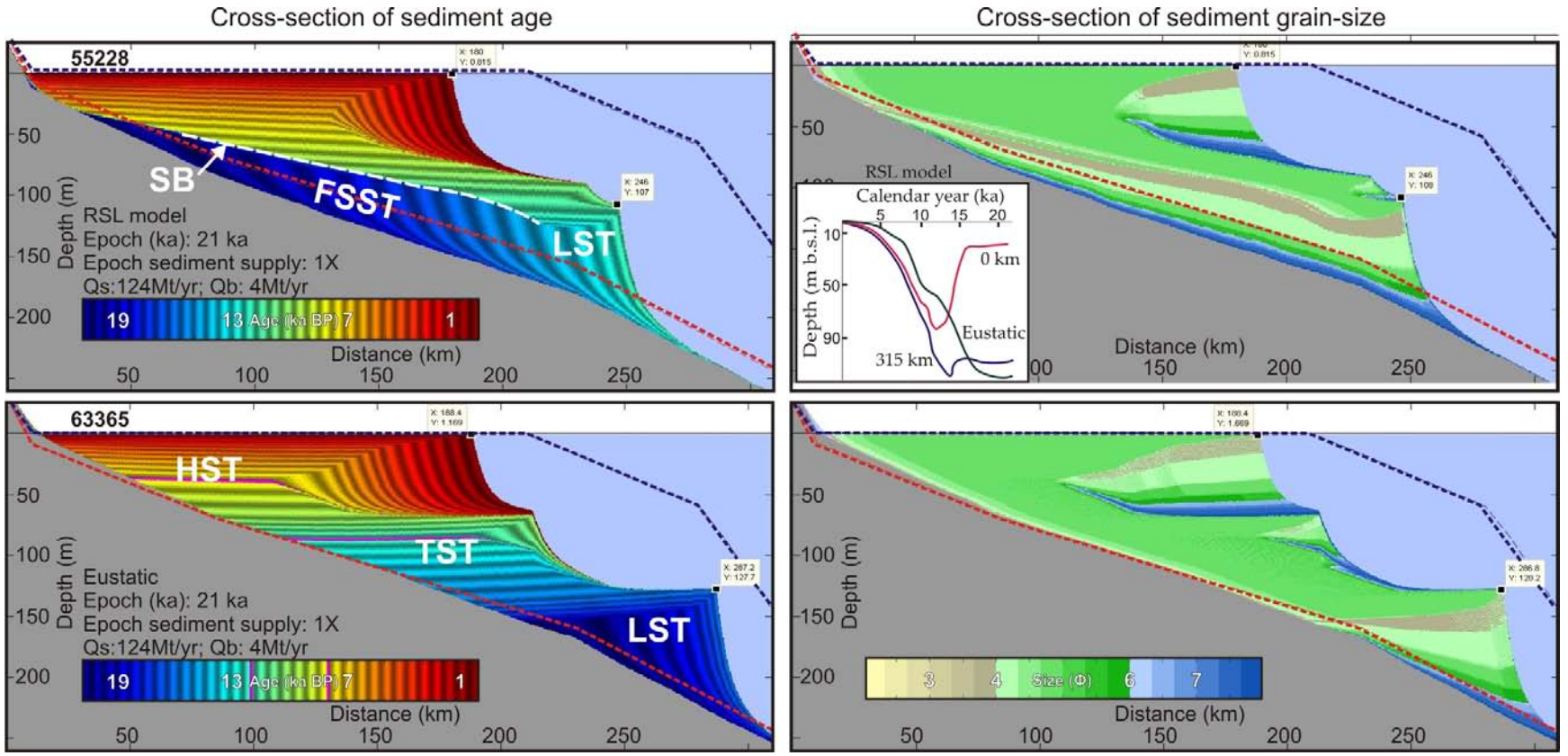

Figure A5: 21 ka eustatic vs RSL model sensitivity test. Simulation 55228 presents a constant sediment supply over 21 ka epoch using the RSL model. Simulation 63365 presents a constant sediment supply over 21 ka epoch using the eustatic sea-level. The locations of the seismic basal reflector from which the initial profile was derived (Hill et al., 2001; red dotted line) and the modern seafloor profile (blue dotted line) are displayed. As a reference, the RSL graph presents the RSL curves corresponding to each extremity of the transect.

Table A6: 21 ka sediment supply on eustatic sea-level and RSL model

Files	**55228**	**63365**
Summary of processes	**RSL model; Epoch length: 21ka; Epoch sediment supply: 1X Qs: 124Mt/yr; Qb: 4Mt/yr (Carson et al. 1998);**	**Eustatic; Epoch length: 21ka; Epoch sediment supply: 1X Qs: 124Mt/yr; Qb: 4Mt/yr (Carson et al. 1998);**
INITIATION FILE		
bathymetry file	(compensated) beaufort_bathy.csv	(compensated) beaufort_bathy.csv
PROCESS FILE		
[sea level]		
active	no	no
sea level file	beaufort_sea_level.csv	beaufort_sea_level.csv
[Subsidence]		
active:	yes	yes
Subsidence file	rates_sedflux_MT21000_combined.dat	rates_sedflux_MT21000_eustatic_long.dat
[compaction]		
active	no	no
[isostasy]		
active	yes	yes
enable water loading		
[bbl]		
active	yes	yes
algorithm (none|muds)	none	none
external sediment source file	none	none
[river 0]		
active	yes	yes
river file	beaufort_river.kvf	beaufort_river.kvf
[bedload dumping]		
active	yes	yes
distance to dump bedload (m)	5000	5000
ratio of flood plain to bedload rate	6.5	6.5
fraction of bedload retained in the delta plain	0	0
[plume]		
active	yes	yes
hyperpycnal plume model	<none>	<none>
hypopycnal plume model	'hypopycnal plume'	'hypopycnal plume'
[hypopycnal plume]		
active	yes	yes
[Failure]		
active:	no	no
[debris flow]		
active:	no	no
[turbidity current]		
active:	no	no
RIVER FILES		
River0		

['Season 1']		
Duration (y)	1y	1y
Bedload (kg/s)	200	200
Suspended load concentration (kg/m^3)	0.1054, 0.1473, 0.0982	0.1054, 0.1473, 0.0982
velocity (m/s)	0.7	0.7
Width (m)	2000	2000
Depth (m)	8	8
SEDIMENT FILE		
[Grain 1 (bedload)]		
grain size (microns)	300	300
grain density (kg/m^3)	2650	2650
saturated density (kg/m^3)	2094	2094
minimum void ratio (-)	0.2	0.2
diffusion coefficient (-)	0.25	0.25
removal rate (1/day)	35	35
consolidation coefficient (m^2/yr)	100000	100000
compaction coefficient (-)	0.00000005	0.00000005
[Grain 2 (suspended)]		
grain size (microns)	200	200
grain density (kg/m^3)	2650	2650
saturated density (kg/m^3)	2000	2000
minimum void ratio (-)	0.17	0.17
diffusion coefficient (-)	0.25	0.25
removal rate (1/day)	25	25
consolidation coefficient (m^2/yr)	100000	100000
compaction coefficient (-)	0.000000062	0.000000062
[Grain 3 (suspended)]		
grain size (microns)	60	60
grain density (kg/m^3)	2650	2650
saturated density (kg/m^3)	1795	1795
minimum void ratio (-)	0.1	0.1
diffusion coefficient (-)	0.25	0.25
removal rate (1/day)	12	12
consolidation coefficient (m^2/yr)	100000	100000
compaction coefficient (-)	0.00000008	0.00000008
[Grain 4 (suspended)]		
grain size (microns)	5	5
grain density (kg/m^3)	2650	2650
saturated density (kg/m^3)	1504	1504
minimum void ratio (-)	0.05	0.05
diffusion coefficient (-)	0.25	0.25
removal rate (1/day)	3.2	3.2
consolidation coefficient (m^2/yr)	100000	100000
compaction coefficient (-)	0.00000036	0.00000036

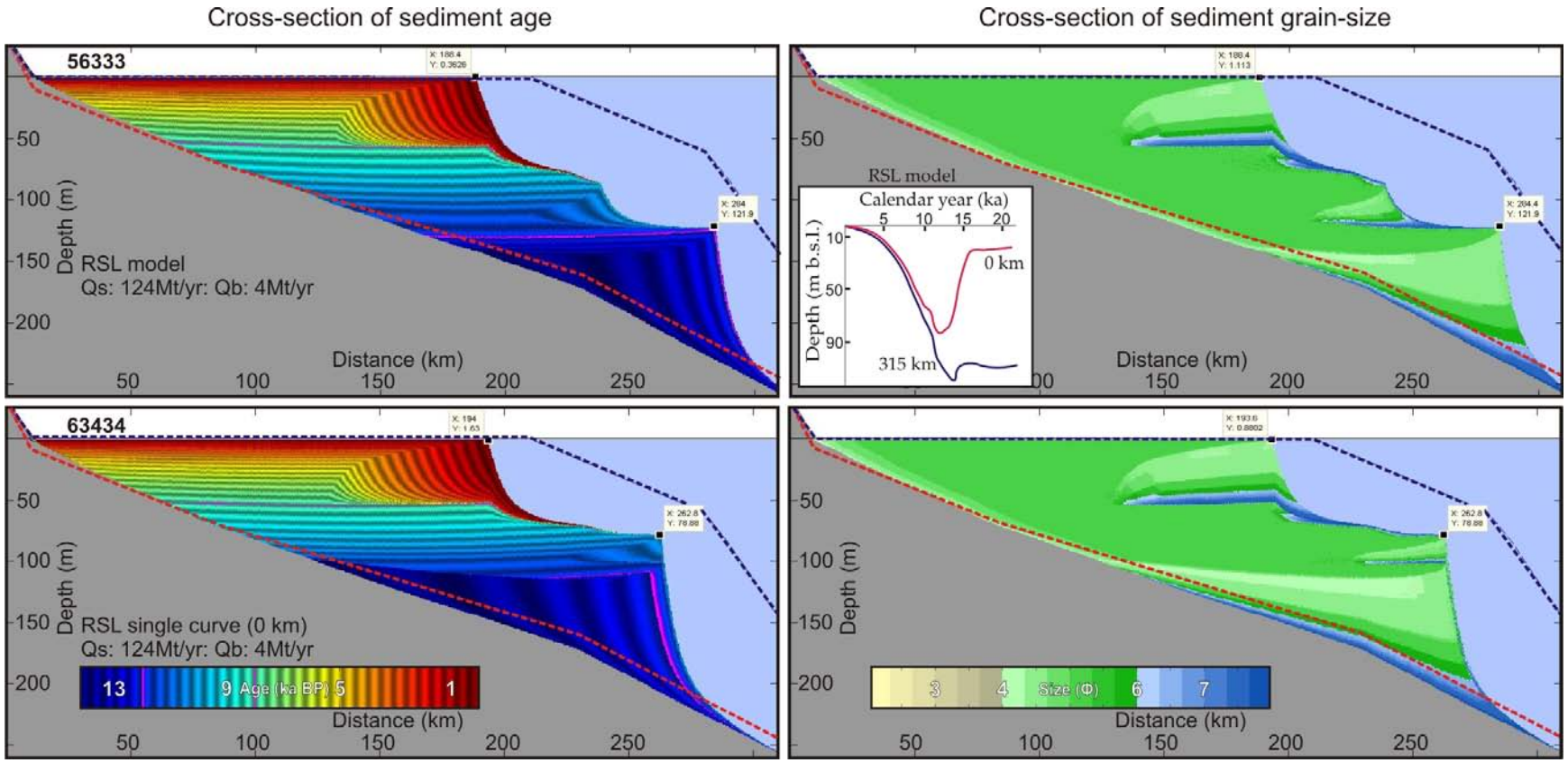

Figure A6: Sensitivity test on RSL model. Simulation 56333 uses the RSL model. Simulation 63434 uses only the RSL curve from 0 km location. The locations of the seismic basal reflector from which the initial profile was derived (Hill et al., 2001; red dotted line) and the modern seafloor profile (blue dotted line) are displayed. As a reference, the RSL graph presents the RSL curves corresponding to each extremity of the transect.

Table A7: RSL model vs RSL single curve

Files	56333	63434
Summary of processes	**RSL model; Qs: 124Mt/yr; Qb: 4Mt/yr (Carson et al. 1998);**	**RSL model single curve at 0km; Qs: 85Mt/yr; Qb: 4Mt/yr (Carson et al. 1999);**
INITIATION FILE		
bathymetry file	(compensated) beaufort_bathy.csv	(compensated) beaufort_bathy.csv
PROCESS FILE		
[sea level]		
active	no	no
sea level file	beaufort_sea_level.csv	beaufort_sea_level.csv
[Subsidence]		
active:	yes	yes
Subsidence file	rates_sedflux_MT21000.dat	rates_sedflux_MT21000_0km.dat
[compaction]		
active	no	no
[isostasy]		
active	yes	yes
enable water loading	no	no
[river 0]		
active	yes	yes
river file	beaufort_river.kvf	beaufort_river.kvf
[bedload dumping]		
active	0y->6700y	0y->6700y
distance to dump bedload (m)	5000	5000
ratio of flood plain to bedload rate	0	1
fraction of bedload retained in the delta plain	0	0
[river 1]		
active	6700yr -> 9000yr	6700yr -> 9000yr
river file	beaufort_river2.kvf	beaufort_river2.kvf
[bedload dumping]		
active	6700yr -> 9000yr	6700yr -> 9000yr
distance to dump bedload (m)	5000	5000
ratio of flood plain to bedload rate	0	1
fraction of bedload retained in the delta plain	0	0
[river 2]		
active	9000yr -> 13000y	9000yr -> 13000y
river file	beaufort_river3.kvf	beaufort_river3.kvf
[bedload dumping]		
active	9000yr -> 13000y	9000yr -> 13000y
distance to dump bedload (m)	5000	5000
ratio of flood plain to bedload rate	0	1
fraction of bedload retained in the delta plain	0	0
[river 3]		
active	13000y -> 21000y	13000y -> 21000y
river file	beaufort_river4.kvf	beaufort_river4.kvf
[bedload dumping]		

active	13000y -> 21000y	13000y -> 21000y
distance to dump bedload (m)	5000	5000
ratio of flood plain to bedload rate	0	1
fraction of bedload retained in the delta plain	0	0
[plume]		
active	yes	yes
hyperpycnal plume model	<none>	<none>
hypopycnal plume model	'hypopycnal plume'	'hypopycnal plume'
[Failure]		
active:	no	no
[debris flow]		
active:	no	no
[turbidity current]		
active:	no	no
RIVER FILES		
River0		
['Season 1']		
Duration (y)	1y	1y
Bedload (kg/s)	0	0
Suspended load concentration (kg/m^3)	0	0
velocity (m/s)	0.7	0.7
Width (m)	2000	2000
Depth (m)	8	8
River1		
['Season 1']		
Duration (y)	1y	1y
Bedload (kg/s)	500	500
Suspended load concentration (kg/m^3)	0.0878, 0.526, 0.263	0.0878, 0.526, 0.263
velocity (m/s)	0.7	0.7
Width (m)	2000	2000
Depth (m)	8	8
River2		
['Season 1']		
Duration (y)	1y	1y
Bedload (kg/s)	400	400
Suspended load concentration (kg/m^3)	0.07024, 0.4208, 0.2104	0.07024, 0.4208, 0.2104
velocity (m/s)	0.7	0.7
Width (m)	2000	2000
Depth (m)	8	8
River3		
['Season 1']		
Duration (y)	1y	1y
Bedload (kg/s)	200	200
Suspended load concentration (kg/m^3)	0.03512, 0.2104, 0.1052	0.03512, 0.2104, 0.1052
velocity (m/s)	0.7	0.7
Width (m)	2000	2000
Depth (m)	8	8

SEDIMENT FILE		
[Grain 1 (bedload)]		
grain size (microns)	200	300
grain density (kg/m^3)	2650	2650
saturated density (kg/m^3)	2000	2094
minimum void ratio (-)	0.17	0.2
diffusion coefficient (-)	0.25	0.25
removal rate (1/day)	25	35
consolidation coefficient (m^2/yr)	100000	100000
compaction coefficient (-)	0.000000062	0.00000005
[Grain 2 (suspended)]		
grain size (microns)	150	150
grain density (kg/m^3)	2650	2650
saturated density (kg/m^3)	1955	1955
minimum void ratio (-)	0.15	0.15
diffusion coefficient (-)	0.25	0.25
removal rate (1/day)	20	20
consolidation coefficient (m^2/yr)	100000	100000
compaction coefficient (-)	0.00000007	0.00000007
[Grain 3 (suspended)]		
grain size (microns)	60	60
grain density (kg/m^3)	2650	2650
saturated density (kg/m^3)	1795	1795
minimum void ratio (-)	0.1	0.1
diffusion coefficient (-)	0.25	0.25
removal rate (1/day)	12	12
consolidation coefficient (m^2/yr)	100000	100000
compaction coefficient (-)	0.00000008	0.00000008
[Grain 4 (suspended)]		
grain size (microns)	5	5
grain density (kg/m^3)	2650	2650
saturated density (kg/m^3)	1504	1504
minimum void ratio (-)	0.05	0.05
diffusion coefficient (-)	0.25	0.25
removal rate (1/day)	3.2	3.2
consolidation coefficient (m^2/yr)	100000	100000
compaction coefficient (-)	0.00000036	0.00000036

Sea-level via subsidence module or sea-level module (Fig. A7)

In Sedflux, modeling RSL changes can be done using two methods: 1) Sea-level is raised or lowered according to a static bathymetric profile (standard method) or 2) sea-level is held static, but the bathymetric profile becomes dynamic (subsidence method). The first simulation is best used for a simple curve such as the eustatic where a falling sea-level will be simulated using negatively increasing sea-level values. The second simulation however, simulates best a basement uplifting or subsiding differentially based on its position along the profile. For the study presented herein, the integration of the RSL model described by Picard and Wickert (in prep) necessitated using of the second simulation. Because the RSL model application was limited to using the subsidence simulation, there were some uncertainties about how reliable the comparisons would be with simulations using the sea-level module, such as in the eustatic simulation. Therefore, this sensitivity test was carried out using the eustatic sea-level curve to establish what differences it made to apply the curve using the different modules (Fig. A7).

In the simulation where sea-level is applied using the subsidence module (63274), the progradation of the lower wedge is reduced, mainly because shoreline transgression occurs earlier. In the sea-level module simulation (56139), shoreline transgression occurs around 10 ka BP, whereas in the subsidence simulation (63274) it happens around 11.5 ka BP. The eustatic sea-level curve (inset) show that the sea-level rising rate is slowed down between 12 and 10 ka BP, which considering enough sediment supply, should allow for progradation to happen. In the subsidence simulation however, this does not occurs because of the way the subsidence module applies its data points. It linearly interpolates between the data point, therefore if the data entry are far apart in time the change in rate

may not happened at the right time (see bottom inset). Figure A8 describe in length the impact of using a subsidence file with more closely separated data points.

The subsidence file used in simulation 63274 used 2000 years between each rate entries, therefore a slower rate was assigned at 12 ka BP and a faster rate re-applied at 10 ka BP. The effects were that because of the linear interpolation, the rates did not slow down fast enough at 12 ka BP to allow progradation to happen. Instead, the progradation was delayed to the next time step between 10 and 8 ka BP because the slowest rates were reached only by 10 ka BP and did not pick up again until 8 ka BP. Considering a better application of the rates and thus notwithstanding the artefacts created in this simulation, integrating a sea-level curve via the subsidence or the sea-level module creates similar stratigraphy.

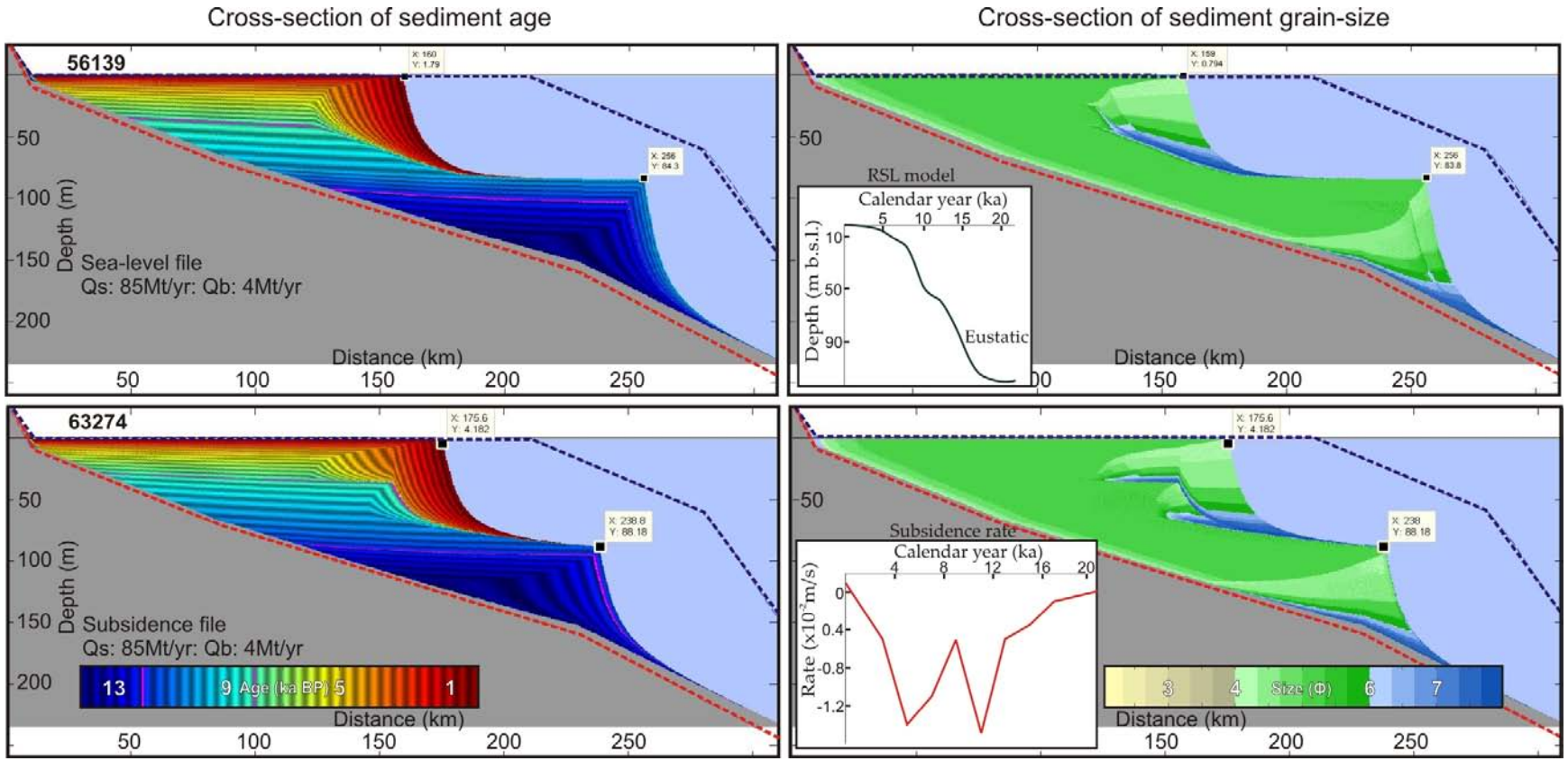

Figure A7: Sensitivity test on using sea-level via a sea-level curve or through the subsidence file. Simulation 56139 integrates sea-level using the sea-level module. Simulation 63274 integrates sea-level via the subsidence module. The subsidence rates are set for every 2000 years and linearly interpolated in between (see Fig. A8 for more info on the effect of linear interpolation). Both simulations used the eustatic sea-level curve of Waelbroech et al. (2002), which is presented in the inset. The locations of the seismic basal reflector from which the initial profile was derived (Hill et al., 2001; red dotted line) and the modern seafloor profile (blue dotted line) are displayed.

Table A8: Sea-level curve vs subsidence rates

Files	56139	63274
Summary of processes	**Eustatic curve via sea-level file; Qs: 85Mt/yr; Qb: 4Mt/yr (Carson et al. 1999);**	**Eustatic curve via Subsidence file; Qs: 85Mt/yr; Qb: 4Mt/yr (Carson et al. 1999);**
INITIATION FILE		
bathymetry file	(compensated) beaufort_bathy.csv	(compensated) beaufort_bathy.csv
PROCESS FILE		
[sea level]		
active	no	no
sea level file	beaufort_sea_level.csv	beaufort_sea_level.csv
[Subsidence]		
active:	yes	yes
Subsidence file	rates_sedflux_MT21000.dat	rates_sedflux_MT21000_eustatic_short.dat
[compaction]		
active	no	no
[isostasy]		
active	yes	yes
enable water loading		
[river 0]		
active	yes	yes
river file	beaufort_river.kvf	beaufort_river.kvf
[bedload dumping]		
active	0y->6700y	0y->6700y
distance to dump bedload (m)	5000	5000
ratio of flood plain to bedload rate	1	1
fraction of bedload retained in the delta plain	0	0
[river 1]		
active	6700yr -> 9000yr	6700yr -> 9000yr
river file	beaufort_river2.kvf	beaufort_river2.kvf
[bedload dumping]		
active	6700yr -> 9000yr	6700yr -> 9000yr
distance to dump bedload (m)	5000	5000
ratio of flood plain to bedload rate	1	1
fraction of bedload retained in the delta plain	0	0
[river 2]		
active	9000yr -> 13000y	9000yr -> 13000y
river file	beaufort_river3.kvf	beaufort_river3.kvf
[bedload dumping]		
active	9000yr -> 13000y	9000yr -> 13000y
distance to dump bedload (m)	5000	5000
ratio of flood plain to bedload rate	1	1
fraction of bedload retained in the delta plain	0	0
[river 3]		
active	13000y -> 21000y	13000y -> 21000y
river file	beaufort_river4.kvf	beaufort_river4.kvf

[bedload dumping]		
active	13000y -> 21000y	13000y -> 21000y
distance to dump bedload (m)	5000	5000
ratio of flood plain to bedload rate	1	1
fraction of bedload retained in the delta plain	0	0
[plume]		
active	yes	yes
hyperpycnal plume model	<none>	<none>
hypopycnal plume model	'hypopycnal plume'	'hypopycnal plume'
[Failure]		
active:	no	no
[debris flow]		
active:	no	no
[turbidity current]		
active:	no	no
RIVER FILES		
River0		
['Season 1']		
Duration (y)	1y	1y
Bedload (kg/s)	0	0
Suspended load concentration (kg/m^3)	0	0
velocity (m/s)	0.7	0.7
Width (m)	2000	2000
Depth (m)	8	8
River1		
['Season 1']		
Duration (y)	1y	1y
Bedload (kg/s)	325	325
Suspended load concentration (kg/m^3)	0.06018, 0.361, 0.1805	0.06018, 0.361, 0.1805
velocity (m/s)	0.7	0.7
Width (m)	2000	2000
Depth (m)	8	8
River2		
['Season 1']		
Duration (y)	1y	1y
Bedload (kg/s)	260	260
Suspended load concentration (kg/m^3)	0.04814, 0.2888, 0.1444	0.04814, 0.2888, 0.1444
velocity (m/s)	0.7	0.7
Width (m)	2000	2000
Depth (m)	8	8
River3		
['Season 1']		
Duration (y)	1y	1y
Bedload (kg/s)	130	130
Suspended load concentration (kg/m^3)	0.02407, 0.1444, 0.0722	0.02407, 0.1444, 0.0722
velocity (m/s)	0.7	0.7
Width (m)	2000	2000

Depth (m)	8	8
SEDIMENT FILE		
[Grain 1 (bedload)]		
grain size (microns)	300	300
grain density (kg/m^3)	2650	2650
saturated density (kg/m^3)	2094	2094
minimum void ratio (-)	0.2	0.2
diffusion coefficient (-)	0.25	0.25
removal rate (1/day)	35	35
consolidation coefficient (m^2/yr)	100000	100000
compaction coefficient (-)	0.00000005	0.00000005
[Grain 2 (suspended)]		
grain size (microns)	150	150
grain density (kg/m^3)	2650	2650
saturated density (kg/m^3)	1955	1955
minimum void ratio (-)	0.15	0.15
diffusion coefficient (-)	0.25	0.25
removal rate (1/day)	20	20
consolidation coefficient (m^2/yr)	100000	100000
compaction coefficient (-)	0.00000007	0.00000007
[Grain 3 (suspended)]		
grain size (microns)	60	60
grain density (kg/m^3)	2650	2650
saturated density (kg/m^3)	1795	1795
minimum void ratio (-)	0.1	0.1
diffusion coefficient (-)	0.25	0.25
removal rate (1/day)	12	12
consolidation coefficient (m^2/yr)	100000	100000
compaction coefficient (-)	0.00000008	0.00000008
[Grain 4 (suspended)]		
grain size (microns)	5	5
grain density (kg/m^3)	2650	2650
saturated density (kg/m^3)	1504	1504
minimum void ratio (-)	0.05	0.05
diffusion coefficient (-)	0.25	0.25
removal rate (1/day)	3.2	3.2
consolidation coefficient (m^2/yr)	100000	100000
compaction coefficient (-)	0.00000036	0.00000036

Subsidence rate interpolation (Fig. A8)

This sensitivity test provides more visual details about the way the subsidence module is applied. The three simulations presented here use the eustatic sea-level curve integrated in subsidence files that have progressively more entry points. The rates in the subsidence file from simulation 63288 are applied every 2000 years, in simulation 63289 every 1000 years, and in 63307 every 500 years. In fact, the last simulation tries to minimise the time before the actual rate should be reached. To do so, when a change of rate needed to be applied, the transition towards that rate was only a 500 years period. At that point the rate was maintained constant until the next change.

The difference between the first simulation (63288) and the last simulation (63307) is what was concluded in the previous test, i.e. by increasing the number of rate entries, the lower wedge should be prograding for a longer period and the overall stratigraphy should become more similar to the one using the sea-level module. Simulation 63307 can not be directly compared with simulation 56138 from Figure A7 because its initial bathymetric profile was not adjusted to compensate for the isostatic loading.

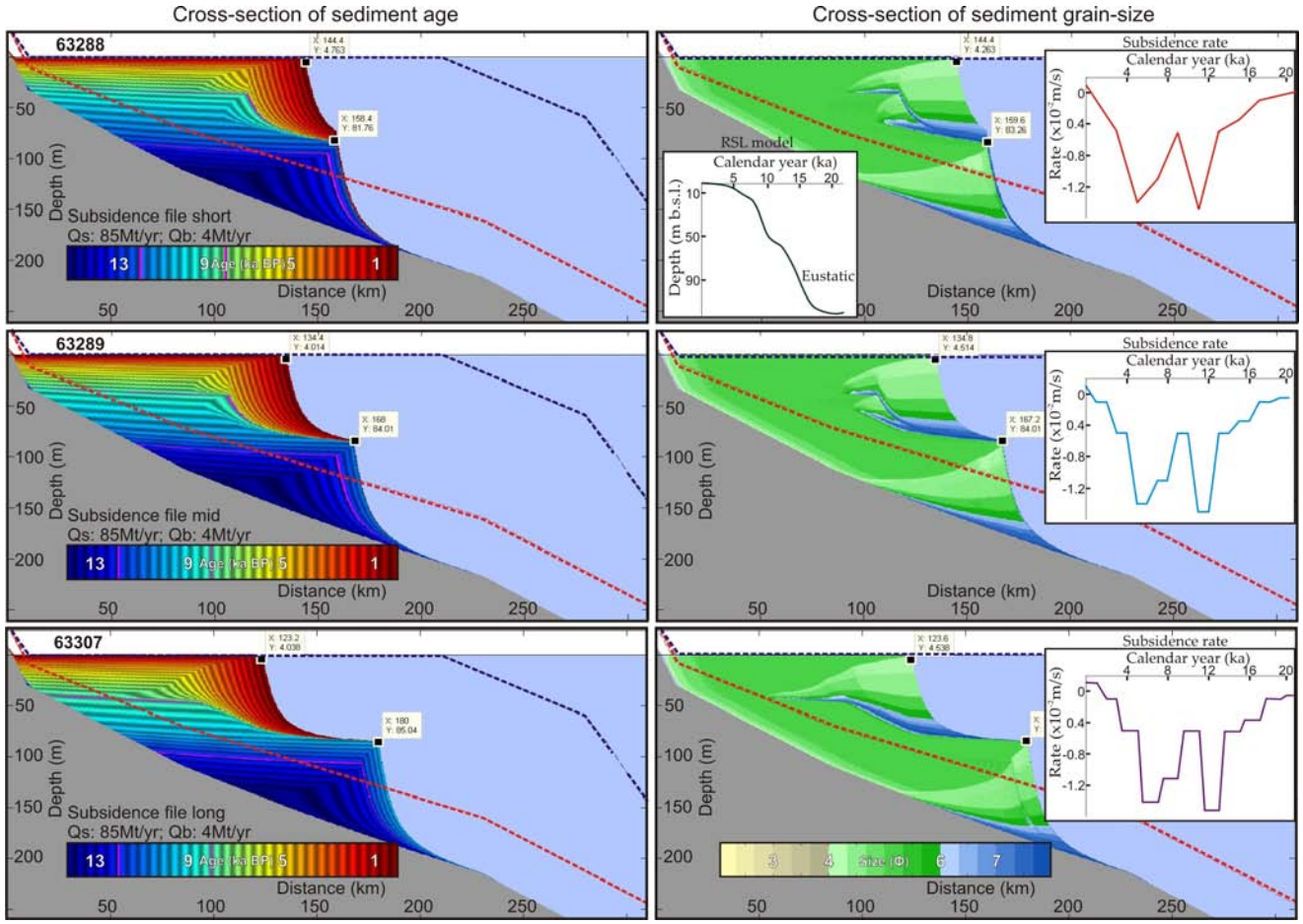

Figure A8: Sensitivity test on the number of time steps included in subsidence file. The subsidence file is defined with subsidence rates per time step. In between two consecutive time steps, SedFlux linearly interpolates the rates. Simulation 63288 is assigned a rate per 2000 years. Simulation 63289 is assigned a rate for every 1000 years. Simulation 63307 is assigned a rate for every 500 years. The insets presented in the cross-sections of sediment grain-size show the interpolation between the given subsidence rate throughout the simulations. The simulations used the eustatic sea-level curve of Waelbroech et al. (2002).

Table A9:Subsidence file interpolation

Files	**63288**	**63289**	**63307**
Summary of processes	**Subsidence file short; Bathy non-adjusted for loading; Qs: 85Mt/yr; Qb: 4Mt/yr (Carson et al. 1999);**	**Subsidence file mid; Bathy non-adjusted for loading; Qs: 85Mt/yr; Qb: 4Mt/yr (Carson et al. 1999);**	**Subsidence file long; Bathy non-adjusted for loading; Qs: 85Mt/yr; Qb: 4Mt/yr (Carson et al. 1999);**
INITIATION FILE bathymetry file	(non-compensated) beaufort_bathy.csv	(non-compensated) beaufort_bathy.csv	(non-compensated) beaufort_bathy.csv
PROCESS FILE [sea level]			
active	no	no	no
sea level file	beaufort_sea_level.csv	beaufort_sea_level.csv	beaufort_sea_level.csv
[Subsidence]			
active:	yes	yes	yes
Subsidence file	rates_sedflux_MT21000_short.dat	rates_sedflux_MT21000_eustatic_mid.dat	rates_sedflux_MT21000_eustatic_long.dat
[compaction]			
active	no	no	no
[isostasy]			
active	yes	yes	yes
enable water loading			
[river 0]			
active	yes	yes	yes
river file	beaufort_river.kvf	beaufort_river.kvf	beaufort_river.kvf
[bedload dumping]			
active	0y->6700y	0y->6700y	0y->6700y
distance to dump bedload (m)	5000	5000	5000
ratio of flood plain to bedload rate	0.22	1	1
fraction of bedload retained in the delta plain	0	0	0
[river 1]			
active	6700yr -> 9000yr	6700yr -> 9000yr	6700yr -> 9000yr
river file	beaufort_river2.kvf	beaufort_river2.kvf	beaufort_river2.kvf
[bedload dumping]			
active	6700yr -> 9000yr	6700yr -> 9000yr	6700yr -> 9000yr
distance to dump	5000	5000	5000

bedload (m)			
ratio of flood plain to bedload rate	0.22	1	1
fraction of bedload retained in the delta plain	0	0	0
[river 2]			
active	9000yr -> 13000y	9000yr -> 13000y	9000yr -> 13000y
river file	beaufort_river3.kvf	beaufort_river3.kvf	beaufort_river3.kvf
[bedload dumping]			
active	9000yr -> 13000y	9000yr -> 13000y	9000yr -> 13000y
distance to dump bedload (m)	5000	5000	5000
ratio of flood plain to bedload rate	0.22	1	1
fraction of bedload retained in the delta plain	0	0	0
[river 3]			
active	13000y -> 21000y	13000y -> 21000y	13000y -> 21000y
river file	beaufort_river4.kvf	beaufort_river4.kvf	beaufort_river4.kvf
[bedload dumping]			
active	13000y -> 21000y	13000y -> 21000y	13000y -> 21000y
distance to dump bedload (m)	5000	5000	5000
ratio of flood plain to bedload rate	0.22	1	1
fraction of bedload retained in the delta plain	0	0	0
[plume]			
active	yes	yes	yes
hyperpycnal plume model	<none>	<none>	<none>
hypopycnal plume model	'hypopycnal plume'	'hypopycnal plume'	'hypopycnal plume'
[Failure]			
active:	no	no	no
[debris flow]			
active:	no	no	no
[turbidity current]			

active:	no	no	no
RIVER FILES			
River0 ['Season 1']			
Duration (y)	1y	1y	1y
Bedload (kg/s)	0	0	0
Suspended load concentration (kg/m^3)	0	0	0
velocity (m/s)	0.7	0.7	0.7
Width (m)	2000	2000	2000
Depth (m)	8	8	8
River1 ['Season 1']			
Duration (y)	1y	1y	1y
Bedload (kg/s)	325	325	325
Suspended load concentration (kg/m^3)	0.06018, 0.361, 0.1805	0.06018, 0.361, 0.1805	0.06018, 0.361, 0.1805
velocity (m/s)	0.7	0.7	0.7
Width (m)	2000	2000	2000
Depth (m)	8	8	8
River2 ['Season 1']			
Duration (y)	1y	1y	1y
Bedload (kg/s)	260	260	260
Suspended load concentration (kg/m^3)	0.04814, 0.2888, 0.1444	0.04814, 0.2888, 0.1444	0.04814, 0.2888, 0.1444
velocity (m/s)	0.7	0.7	0.7
Width (m)	2000	2000	2000
Depth (m)	8	8	8
River3 ['Season 1']			
Duration (y)	1y	1y	1y
Bedload (kg/s)	130	130	130
Suspended load concentration (kg/m^3)	0.02407, 0.1444, 0.0722	0.02407, 0.1444, 0.0722	0.02407, 0.1444, 0.0722
velocity	0.7	0.7	0.7

(m/s)			
Width (m)	2000	2000	2000
Depth (m)	8	8	8
SEDIMENT FILE			
[Grain 1 (bedload)]			
grain size (microns)	200	300	300
grain density (kg/m^3)	2650	2650	2650
saturated density (kg/m^3)	2000	2094	2094
minimum void ratio (-)	0.17	0.2	0.2
diffusion coefficient (-)	0.25	0.25	0.25
removal rate (1/day)	25	35	35
consolidation coefficient (m^2/yr)	100000	100000	100000
compaction coefficient (-)	0.000000062	0.00000005	0.00000005
[Grain 2 (suspended)]			
grain size (microns)	150	150	150
grain density (kg/m^3)	2650	2650	2650
saturated density (kg/m^3)	1955	1955	1955
minimum void ratio (-)	0.15	0.15	0.15
diffusion coefficient (-)	0.25	0.25	0.25
removal rate (1/day)	20	20	20
consolidation coefficient (m^2/yr)	100000	100000	100000
compaction coefficient (-)	0.00000007	0.00000007	0.00000007
[Grain 3 (suspended)]			
grain size (microns)	60	60	60
grain density (kg/m^3)	2650	2650	2650
saturated density (kg/m^3)	1795	1795	1795

minimum void ratio (-)	0.1	0.1	0.1
diffusion coefficient (-)	0.25	0.25	0.25
removal rate (1/day)	12	12	12
consolidation coefficient (m^2/yr)	100000	100000	100000
compaction coefficient (-)	0.00000008	0.00000008	0.00000008
[Grain 4 (suspended)]			
grain size (microns)	5	5	5
grain density (kg/m^3)	2650	2650	2650
saturated density (kg/m^3)	1504	1504	1504
minimum void ratio (-)	0.05	0.05	0.05
diffusion coefficient (-)	0.25	0.25	0.25
removal rate (1/day)	3.2	3.2	3.2
consolidation coefficient (m^2/yr)	100000	100000	100000
compaction coefficient (-)	0.00000036	0.00000036	0.00000036

SedFlux "no water loading" parameter (Fig. A9)

The objective of this sensitivity test was to evaluate a new parameter added to suppress the water loading component included in the isostasy module of SedFlux (Fig. A9). The original module calculated concurrently the isostatic loading created by water and sediment accumulation. However since the RSL model already accounted for water loading, it was necessary to add a parameter turning off water loading.

To assess the functionality of the parameter, two simulations using the RSL model data were carried out. In the first simulation (56333), the isostatic module was applied as usual, i.e. it calculated the contribution of both water and sediment loading. In the second simulation (63845), the same parameters were used with the exception that the water loading component was turned off.

This sensitivity test shows that the new parameter disabling water loading is functional and that the water loading contribution to the base-case simulation would be about 20 m at 250 km if applied. The contribution of water to loading is noticeable in areas where water occupies a greater percentage of the accommodation space. The loading occurring in these areas is reflected as far under the areas where sediment is occupying the entire column because of the visco-elastic properties of the earth.

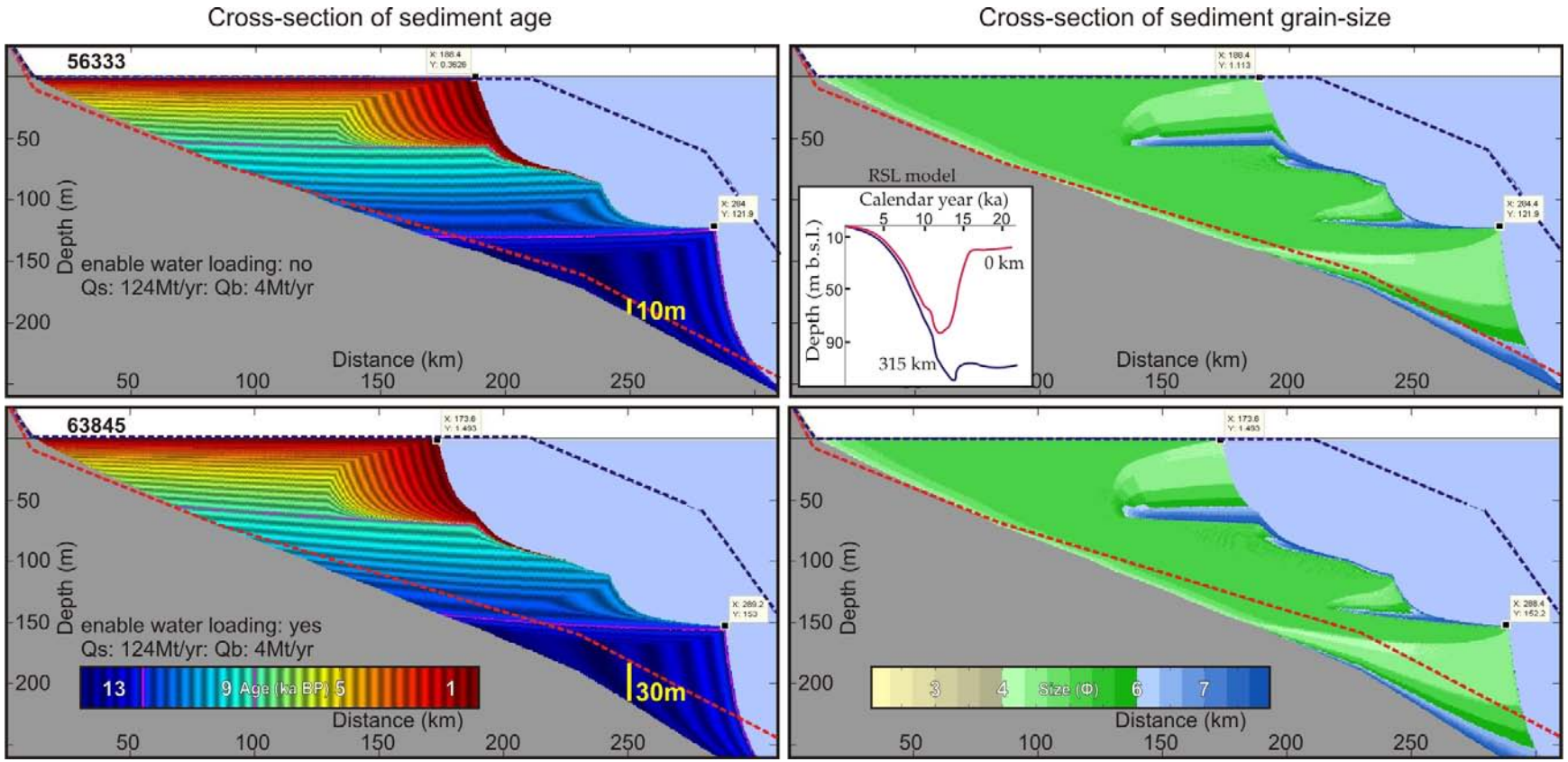

Figure A9: Sensitivity test on the newly added water loading parameter of Sedflux. This sensitivity test evaluates if the 'no water loading' parameter added to Sedflux functions properly. Simulation 56333 uses the isostasy module prior to modifications. Simulation 63845 uses the new parameter 'no water loading' added to Sedflux. Both simulations uses a bathymetric profile compensated for sediment loading, therefore the value marked in yellow on the graphs help in calculating the additional contribution due to water loading. The locations of the seismic basal reflector from which the initial profile was derived (Hill et al., 2001; red dotted line) and the modern seafloor profile (blue dotted line) are displayed. As a reference, the RSL graph presents the RSL curves corresponding to each extremity of the transect.

Table A10: No water loading parameter

Files	56333	63845
Summary of processes	**no water loading; Qs: 124Mt/yr; Qb: 4Mt/yr (Carson et al. 1998);**	**water loading on; Qs: 85Mt/yr; Qb: 4Mt/yr (Carson et al. 1999);**
INITIATION FILE		
bathymetry file	(compensated) beaufort_bathy.csv	(compensated) beaufort_bathy.csv
PROCESS FILE		
[sea level]		
active	no	no
sea level file	beaufort_sea_level.csv	beaufort_sea_level.csv
[Subsidence]		
active:	yes	yes
Subsidence file	rates_sedflux_MT21000.dat	rates_sedflux_MT21000.dat
[compaction]		
active	no	no
[isostasy]		
active	yes	yes
enable water loading	no	no
[river 0]		
active	yes	yes
river file	beaufort_river.kvf	beaufort_river.kvf
[bedload dumping]		
active	0y->6700y	0y->6700y
distance to dump bedload (m)	5000	5000
ratio of flood plain to bedload rate	0	1
fraction of bedload retained in the delta plain	0	0
[river 1]		
active	6700yr -> 9000yr	6700yr -> 9000yr
river file	beaufort_river2.kvf	beaufort_river2.kvf
[bedload dumping]		
active	6700yr -> 9000yr	6700yr -> 9000yr
distance to dump bedload (m)	5000	5000
ratio of flood plain to bedload rate	0	1
fraction of bedload retained in the delta plain	0	0
[river 2]		
active	9000yr -> 13000y	9000yr -> 13000y
river file	beaufort_river3.kvf	beaufort_river3.kvf
[bedload dumping]		
active	9000yr -> 13000y	9000yr -> 13000y
distance to dump bedload (m)	5000	5000
ratio of flood plain to bedload rate	0	1
fraction of bedload retained in the delta plain	0	0
[river 3]		
active	13000y -> 21000y	13000y -> 21000y
river file	beaufort_river4.kvf	beaufort_river4.kvf

[bedload dumping]		
active	13000y -> 21000y	13000y -> 21000y
distance to dump bedload (m)	5000	5000
ratio of flood plain to bedload rate	0	1
fraction of bedload retained in the delta plain	0	0
[plume]		
active	yes	yes
hyperpycnal plume model	<none>	<none>
hypopycnal plume model	'hypopycnal plume'	'hypopycnal plume'
[Failure]		
active:	no	no
[debris flow]		
active:	no	no
[turbidity current]		
active:	no	no
RIVER FILES		
River0		
['Season 1']		
Duration (y)	1y	1y
Bedload (kg/s)	0	0
Suspended load concentration (kg/m^3)	0	0
velocity (m/s)	0.7	0.7
Width (m)	2000	2000
Depth (m)	8	8
River1		
['Season 1']		
Duration (y)	1y	1y
Bedload (kg/s)	500	500
Suspended load concentration (kg/m^3)	0.0878, 0.526, 0.263	0.0878, 0.526, 0.263
velocity (m/s)	0.7	0.7
Width (m)	2000	2000
Depth (m)	8	8
River2		
['Season 1']		
Duration (y)	1y	1y
Bedload (kg/s)	400	400
Suspended load concentration (kg/m^3)	0.07024, 0.4208, 0.2104	0.07024, 0.4208, 0.2104
velocity (m/s)	0.7	0.7
Width (m)	2000	2000
Depth (m)	8	8
River3		
['Season 1']		
Duration (y)	1y	1y
Bedload (kg/s)	200	200
Suspended load concentration (kg/m^3)	0.03512, 0.2104, 0.1052	0.03512, 0.2104, 0.1052
velocity (m/s)	0.7	0.7
Width (m)	2000	2000

Depth (m)	8	8
SEDIMENT FILE		
[Grain 1 (bedload)]		
grain size (microns)	200	300
grain density (kg/m^3)	2650	2650
saturated density (kg/m^3)	2000	2094
minimum void ratio (-)	0.17	0.2
diffusion coefficient (-)	0.25	0.25
removal rate (1/day)	25	35
consolidation coefficient (m^2/yr)	100000	100000
compaction coefficient (-)	0.000000062	0.00000005
[Grain 2 (suspended)]		
grain size (microns)	150	150
grain density (kg/m^3)	2650	2650
saturated density (kg/m^3)	1955	1955
minimum void ratio (-)	0.15	0.15
diffusion coefficient (-)	0.25	0.25
removal rate (1/day)	20	20
consolidation coefficient (m^2/yr)	100000	100000
compaction coefficient (-)	0.00000007	0.00000007
[Grain 3 (suspended)]		
grain size (microns)	60	60
grain density (kg/m^3)	2650	2650
saturated density (kg/m^3)	1795	1795
minimum void ratio (-)	0.1	0.1
diffusion coefficient (-)	0.25	0.25
removal rate (1/day)	12	12
consolidation coefficient (m^2/yr)	100000	100000
compaction coefficient (-)	0.00000008	0.00000008
[Grain 4 (suspended)]		
grain size (microns)	5	5
grain density (kg/m^3)	2650	2650
saturated density (kg/m^3)	1504	1504
minimum void ratio (-)	0.05	0.05
diffusion coefficient (-)	0.25	0.25
removal rate (1/day)	3.2	3.2
consolidation coefficient (m^2/yr)	100000	100000
compaction coefficient (-)	0.00000036	0.00000036

Sediment loading (Fig. A10)

Isostatic loading derived from sediment accumulation on the lithosphere is an essential process to account for when modelling long term stratigraphic development. A sensitivity test was thus pursued to estimate the amount of loading created under specific conditions and to evaluate the impacts on stratigraphy once integrated into the modeling.

Three simulations, displayed in Figure A10, were set to address these objectives. Simulation 50763 did not use the sediment loading module. Simulation 54996 added the loading component to the first simulation. The third simulation, 56333, presents a simulation where the initial bathymetric profile has been adjusted accordingly to the loading information measured in simulation 54996. The aim of this adjustment is so that the resulting basement surface (grey block) ends up aligned with the present location of the seismic basal reflector (see method section from the stratigraphy paper).

Sediment loading, based on the boundary conditions set for this simulation resulted in a maximum negative displacement of the basement of 32 m at 150 km. At the hinge point of the lower wedge, which is located farther away from the main sediment mass, about 22 m of loading occurred. The impact of loading was thus to create additional accommodation space, which resulted in a reduction of the progradation and a basement surface that did not match with the expected present profile. By modifying the SedFlux initial bathymetric profile by the amount of loading that was created during the simulation 54996, the overall stratigraphy becomes stretched laterally compared to having no loading (50763). This change in lateral geometry is caused by the effect of changing the initial profile, which is described in the next Figure (A11). Therefore, by accommodating for sediment loading, the effect is not to

vertically translate the stratigraphic structures upward, but to spread it laterally, keeping the main features at the same depths. For a particular samples however, if it is dated with a specific date, it will be affected vertically by loading, but it might belong to a different stratigraphic structure than first thought.

The latter may be an artefact of the method used to integrate the RSL model data i.e. via the subsidence module, which simulates RSL fluctuations by moving vertically the starting profile. Since deposition occurs at the shoreline, i.e. where the profile crosses the x-axis, the locus of deposition is thus moved seaward when the starting profile is raised, with the final depth of a structure unchanged since it is guided by the sea-level only. Rising the initial profile was however essential in this modeling experiment if the assumption was to line up the model basement with the basal reflector. It is possible that decoupling the eustatic sea-level signal from the GIA signal in the RSL outputs to then integrate them into their respective modules, i.e. sea-level and subsidence, would get rid of this problem. This was partly tested in a simulation not presented here, that concluded with similar results. This suggest that more intuitive results may come from a more complex solution, which does not involve taken into consideration sediment loading from the start of the run with the initiation profile.

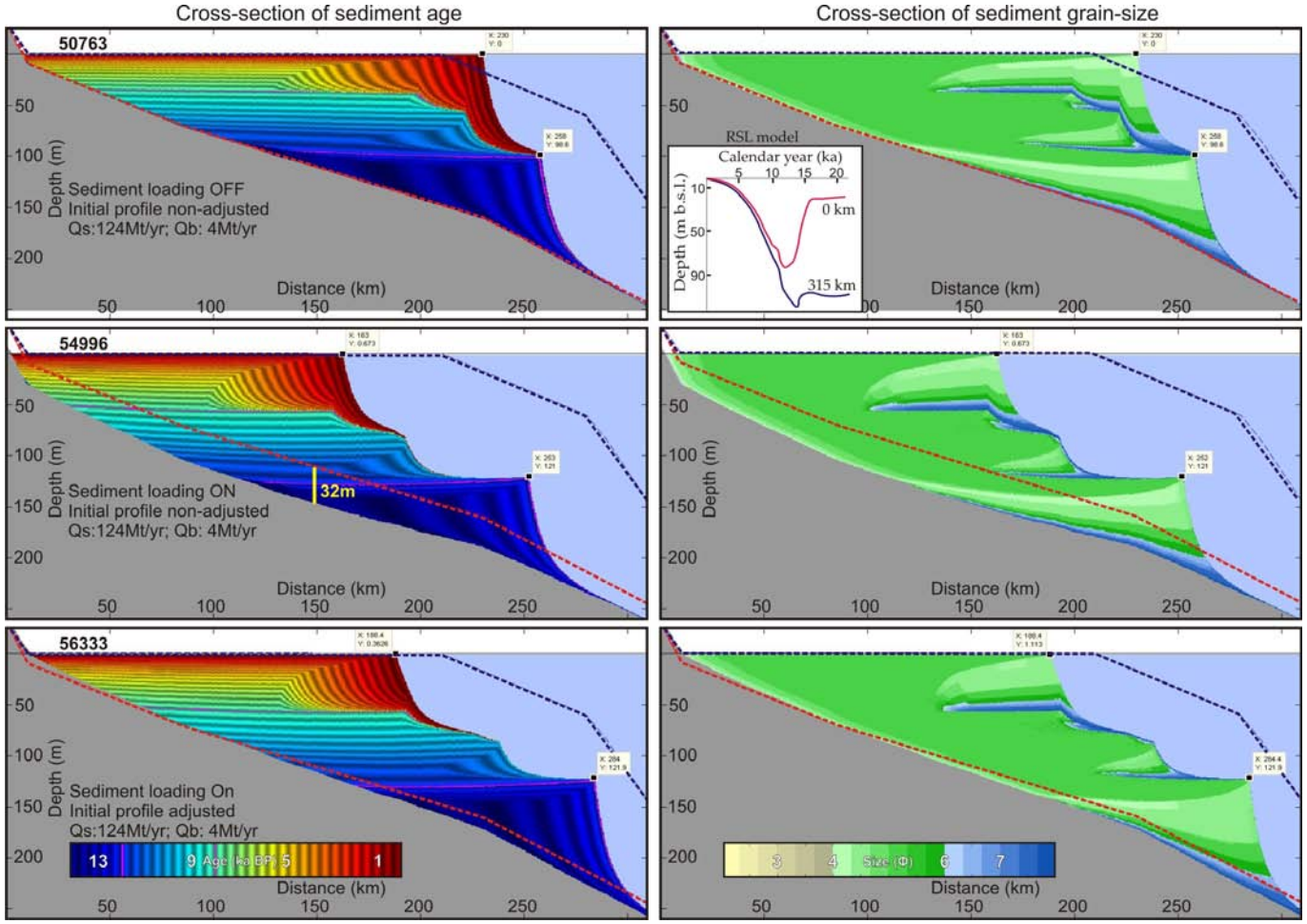

Figure A10: Sensitivity test on sediment loading. Simulation 50763 presents no sediment loading and uses an initial profile not compensated for loading. Simulation 54996 presents sediment loading and uses an initial profile not compensated for loading. Simulation 56333 presents sediment loading and uses an initial profile compensated for loading.

Table A11: Sediment loading

Files	50763	54996	56333
Summary of processes	**No sediment loading; Initial profile non-adjusted for loading; Qs: 124Mt/yr; Qb: 4Mt/yr (Carson et al. 1998)**	**Sediment loading; Initial profile non-adjusted for loading; Qs: 124Mt/yr; Qb: 4Mt/yr (Carson et al. 1998)**	**Sediment loading; Initial profile adjusted for loading; Qs: 124Mt/yr; Qb: 4Mt/yr (Carson et al. 1998)**
INITIATION FILE			
bathymetry file	(non-compensated) beaufort_bathy.csv	(non-compensated) beaufort_bathy.csv	(compensated) beaufort_bathy.csv
PROCESS FILE			
[sea level]			
active	no	no	no
sea level file	beaufort_sea_level.csv	beaufort_sea_level.csv	beaufort_sea_level.csv
[Subsidence]			
active:	yes	yes	yes
Subsidence file	rates_sedflux_MT21000.dat	rates_sedflux_MT21000.dat	rates_sedflux_MT21000.dat
[compaction]			
active	no	no	no
[isostasy]			
active	no	yes	yes
enable water loading		no	no
[river 0]			
active	yes	yes	yes
river file	beaufort_river.kvf	beaufort_river.kvf	beaufort_river.kvf
[bedload dumping]			
active	0y->6700y	0y->6700y	0y->6700y
distance to dump bedload (m)	5000	5000	5000
ratio of flood plain to bedload rate	0	0	0
fraction of bedload retained in the delta plain	0	0	0
[river 1]			
active	6700yr -> 9000yr	6700yr -> 9000yr	6700yr -> 9000yr
river file	beaufort_river2.kvf	beaufort_river2.kvf	beaufort_river2.kvf
[bedload dumping]			
active	6700yr -> 9000yr	6700yr -> 9000yr	6700yr -> 9000yr
distance to dump bedload (m)	10000	5000	5000
ratio of flood plain to bedload rate	1	0	0
fraction of bedload retained in the delta plain	diffusion	0	0
[river 2]			
active	9000yr -> 13000y	9000yr -> 13000y	9000yr -> 13000y
river file	beaufort_river3.kvf	beaufort_river3.kvf	beaufort_river3.kvf
[bedload dumping]			
active	9000yr -> 13000y	9000yr -> 13000y	9000yr -> 13000y
distance to dump bedload (m)	10000	5000	5000

ratio of flood plain to bedload rate	1	0	0
fraction of bedload retained in the delta plain	diffusion	0	0
[river 3]			
active	13000y -> 21000y	13000y -> 21000y	13000y -> 21000y
river file	beaufort_river4.kvf	beaufort_river4.kvf	beaufort_river4.kvf
[bedload dumping]			
active	13000y -> 21000y	13000y -> 21000y	13000y -> 21000y
distance to dump bedload (m)	10000	5000	5000
ratio of flood plain to bedload rate	1	0	0
fraction of bedload retained in the delta plain	diffusion	0	0
[plume]			
active	yes	yes	yes
hyperpycnal plume model	<none>	<none>	<none>
hypopycnal plume model	'hypopycnal plume'	'hypopycnal plume'	'hypopycnal plume'
[Failure]			
active:	no	no	no
[debris flow]			
active:	no	no	no
[turbidity current]			
active:	no	no	no
RIVER FILES			
River0			
['Season 1']			
Duration (y)	1y	1y	1y
Bedload (kg/s)	0	0	0
Suspended load concentration (kg/m^3)	0	0	0
velocity (m/s)	0.7	0.7	0.7
Width (m)	2000	2000	2000
Depth (m)	8	8	8
River1			
['Season 1']			
Duration (y)	1y	1y	1y
Bedload (kg/s)	500	500	500
Suspended load concentration (kg/m^3)	0.0878, 0.526, 0.263	0.0878, 0.526, 0.263	0.0878, 0.526, 0.263
velocity (m/s)	0.7	0.7	0.7
Width (m)	2000	2000	2000
Depth (m)	8	8	8
River2			
['Season 1']			
Duration (y)	1y	1y	1y
Bedload (kg/s)	400	400	400
Suspended load concentration (kg/m^3)	0.07024, 0.4208, 0.2104	0.07024, 0.4208, 0.2104	0.07024, 0.4208, 0.2104
velocity (m/s)	0.7	0.7	0.7
Width (m)	2000	2000	2000
Depth (m)	8	8	8

River3			
['Season 1']			
Duration (y)	1y	1y	1y
Bedload (kg/s)	200	200	200
Suspended load concentration (kg/m^3)	0.03512, 0.2104, 0.1052	0.03512, 0.2104, 0.1052	0.03512, 0.2104, 0.1052
velocity (m/s)	0.7	0.7	0.7
Width (m)	2000	2000	2000
Depth (m)	8	8	8
SEDIMENT FILE			
[Grain 1 (bedload)]			
grain size (microns)	300	300	200
grain density (kg/m^3)	2650	2650	2650
saturated density (kg/m^3)	2094	2094	2000
minimum void ratio (-)	0.2	0.2	0.17
diffusion coefficient (-)	0.25	0.25	0.25
removal rate (1/day)	35	35	25
consolidation coefficient (m^2/yr)	100000	100000	100000
compaction coefficient (-)	0.00000005	0.00000005	0.000000062
[Grain 2 (suspended)]			
grain size (microns)	150	150	150
grain density (kg/m^3)	2650	2650	2650
saturated density (kg/m^3)	1955	1955	1955
minimum void ratio (-)	0.15	0.15	0.15
diffusion coefficient (-)	0.25	0.25	0.25
removal rate (1/day)	20	20	20
consolidation coefficient (m^2/yr)	100000	100000	100000
compaction coefficient (-)	0.00000007	0.00000007	0.00000007
[Grain 3 (suspended)]			
grain size (microns)	60	60	60
grain density (kg/m^3)	2650	2650	2650
saturated density (kg/m^3)	1795	1795	1795
minimum void ratio (-)	0.1	0.1	0.1
diffusion coefficient (-)	0.25	0.25	0.25
removal rate (1/day)	12	12	12
consolidation coefficient (m^2/yr)	100000	100000	100000
compaction coefficient (-)	0.00000008	0.00000008	0.00000008
[Grain 4 (suspended)]			
grain size (microns)	5	5	5
grain density (kg/m^3)	2650	2650	2650
saturated density (kg/m^3)	1504	1504	1504
minimum void ratio (-)	0.05	0.05	0.05
diffusion coefficient (-)	0.25	0.25	0.25
removal rate (1/day)	3.2	3.2	3.2
consolidation coefficient (m^2/yr)	100000	100000	100000
compaction coefficient (-)	0.00000036	0.00000036	0.00000036

Initial bathymetric profile (Fig. A11)

Overeem et al. (2005) highlighted the importance of the initial profile on the stratigraphic development. The additional information learned from the previous figure is that in the simulations when sediment loading is compensated for by raising the initial profile, it results in laterally translating and stretching the sediment deposits (56130). Rising the initial profile is however essential in this modeling exercise since the assumption is to line up the model basement with the basal reflector (red line, see method and Fig. 3.4 from Chapter 3). This translation happens because deposition occurs at the shoreline, i.e. where the profile crosses the x-axis, and thus when the initial profile is moved upward, so is the shoreline. Accounting for sediment load therefore does not change the final depth of a structure as it is guided by the sea-level only (Fig. A11).

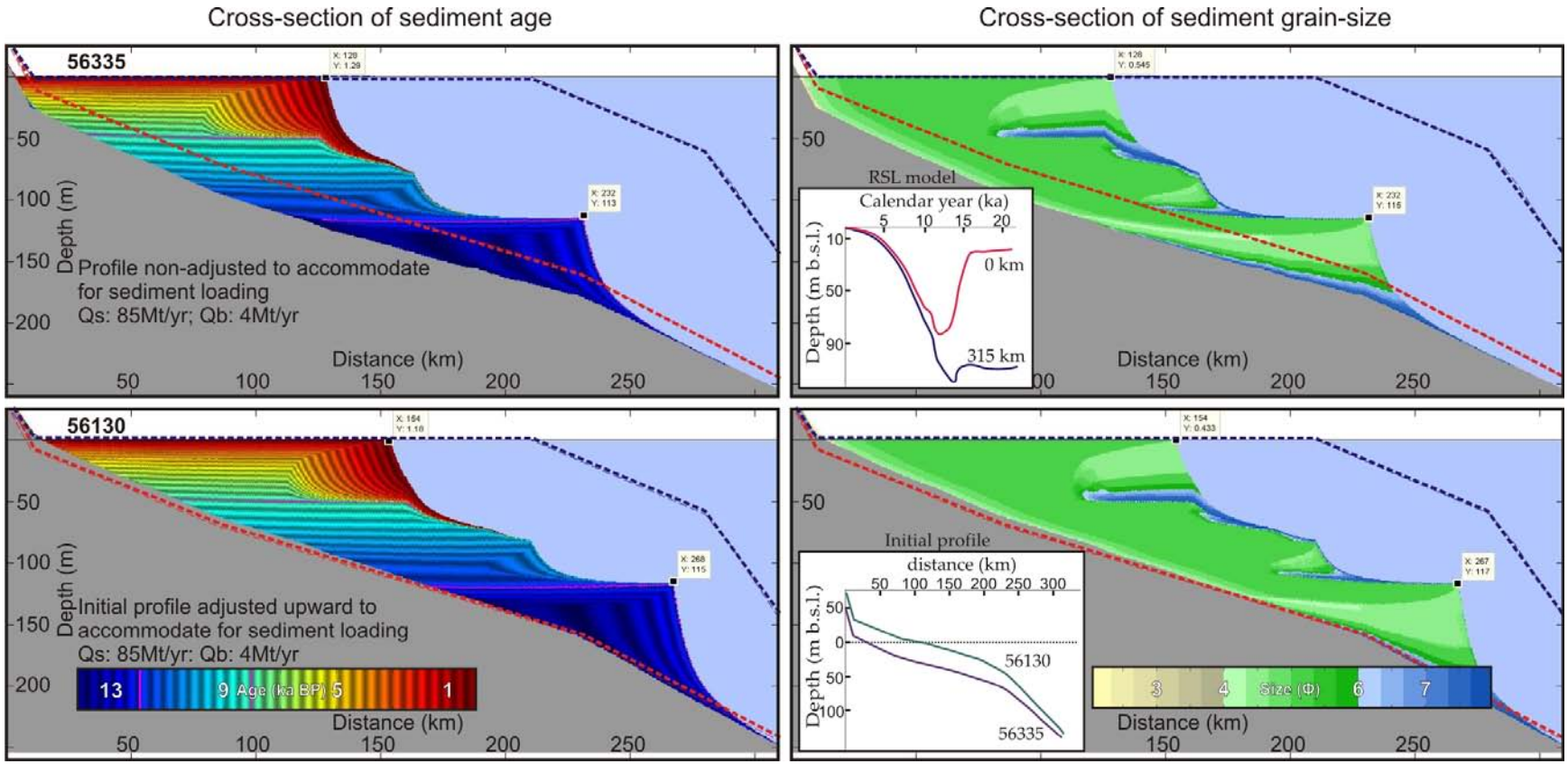

Figure A11: Sensitivity test on the initial bathymetric profile. Simulation 56335 presents the results from an initial bathymetric profile that is not adjusted to accommodate for sediment loading. In this case, the deposition starts where the profile crosses the o m depth line, i.e. around 25 km from the start of the profile. Simulation 56130 presents the results from an initial bathymetric profile that as been adjusted upward to accommodate for sediment loading during the model run. In this case, the profile crosses to 0m line farther offshore (100 km). The profiles shown in the inset reflect the starting profiles at 21 ka BP, but the sediment supply is only turned on after 6.7 ka or 14.3 ka BP. At this time, RSL as fallen or the land as risen, which means that deposition for both simulations starts farther offshore. The location can be observed on the cross-sections of sediment age by the upper limit of the darkest blue unit.

Table A12: Initial bathymetric profile

Files	56130	56335
Summary of processes	**Profile compensated upward to accommodate sediment loading Qs: 85Mt/yr; Qb: 4Mt/yr (Carson et al. 1999);**	**Profile non-compensated to accommodate sediment loading Qs: 85Mt/yr; Qb: 4Mt/yr (Carson et al. 1999);**
INITIATION FILE		
bathymetry file	(compensated) beaufort_bathy.csv	(non-compensated) beaufort_bathy.csv
PROCESS FILE		
[sea level]		
active	no	no
sea level file	beaufort_sea_level.csv	beaufort_sea_level.csv
[Subsidence]		
active:	yes	yes
Subsidence file	rates_sedflux_MT21000.dat	rates_sedflux_MT21000.dat
[compaction]		
active	no	no
[isostasy]		
active	yes	yes
enable water loading	no	no
[river 0]		
active	yes	yes
river file	beaufort_river.kvf	beaufort_river.kvf
[bedload dumping]		
active	0y->6700y	0y->6700y
distance to dump bedload (m)	5000	5000
ratio of flood plain to bedload rate	0.22	0.22
fraction of bedload retained in the delta plain	0	0
[river 1]		
active	6700yr -> 9000yr	6700yr -> 9000yr
river file	beaufort_river2.kvf	beaufort_river2.kvf
[bedload dumping]		
active	6700yr -> 9000yr	6700yr -> 9000yr
distance to dump bedload (m)	5000	5000
ratio of flood plain to bedload rate	0.22	0.22
fraction of bedload retained in the delta plain	0	0
[river 2]		
active	9000yr -> 13000y	9000yr -> 13000y
river file	beaufort_river3.kvf	beaufort_river3.kvf
[bedload dumping]		
active	9000yr -> 13000y	9000yr -> 13000y
distance to dump bedload (m)	5000	5000
ratio of flood plain to bedload rate	0.22	0.22
fraction of bedload retained in the delta plain	0	0
[river 3]		
active	13000y -> 21000y	13000y -> 21000y

river file	beaufort_river4.kvf	beaufort_river4.kvf
[bedload dumping]		
active	13000y -> 21000y	13000y -> 21000y
distance to dump bedload (m)	5000	5000
ratio of flood plain to bedload rate	0.22	0.22
fraction of bedload retained in the delta plain	0	0
[plume]		
active	yes	yes
hyperpycnal plume model	<none>	<none>
hypopycnal plume model	'hypopycnal plume'	'hypopycnal plume'
[Failure]		
active:	no	no
[debris flow]		
active:	no	no
[turbidity current]		
active:	no	no
RIVER FILES		
River0		
['Season 1']		
Duration (y)	1y	1y
Bedload (kg/s)	0	0
Suspended load concentration (kg/m^3)	0	0
velocity (m/s)	0.7	0.7
Width (m)	2000	2000
Depth (m)	8	8
River1		
['Season 1']		
Duration (y)	1y	1y
Bedload (kg/s)	325	325
Suspended load concentration (kg/m^3)	0.06018, 0.361, 0.1805	0.06018, 0.361, 0.1805
velocity (m/s)	0.7	0.7
Width (m)	2000	2000
Depth (m)	8	8
River2		
['Season 1']		
Duration (y)	1y	1y
Bedload (kg/s)	260	260
Suspended load concentration (kg/m^3)	0.04814, 0.2888, 0.1444	0.04814, 0.2888, 0.1444
velocity (m/s)	0.7	0.7
Width (m)	2000	2000
Depth (m)	8	8
River3		
['Season 1']		
Duration (y)	1y	1y
Bedload (kg/s)	130	130

Suspended load concentration (kg/m^3)	0.02407, 0.1444, 0.0722	0.02407, 0.1444, 0.0722
velocity (m/s)	0.7	0.7
Width (m)	2000	2000
Depth (m)	8	8
SEDIMENT FILE		
[Grain 1 (bedload)]		
grain size (microns)	200	200
grain density (kg/m^3)	2650	2650
saturated density (kg/m^3)	2000	2000
minimum void ratio (-)	0.17	0.17
diffusion coefficient (-)	0.25	0.25
removal rate (1/day)	25	25
consolidation coefficient (m^2/yr)	100000	100000
compaction coefficient (-)	0.000000062	0.000000062
[Grain 2 (suspended)]		
grain size (microns)	150	150
grain density (kg/m^3)	2650	2650
saturated density (kg/m^3)	1955	1955
minimum void ratio (-)	0.15	0.15
diffusion coefficient (-)	0.25	0.25
removal rate (1/day)	20	20
consolidation coefficient (m^2/yr)	100000	100000
compaction coefficient (-)	0.00000007	0.000000007
[Grain 3 (suspended)]		
grain size (microns)	60	60
grain density (kg/m^3)	2650	2650
saturated density (kg/m^3)	1795	1795
minimum void ratio (-)	0.1	0.1
diffusion coefficient (-)	0.25	0.25
removal rate (1/day)	12	12
consolidation coefficient (m^2/yr)	100000	100000
compaction coefficient (-)	0.00000008	0.00000008
[Grain 4 (suspended)]		
grain size (microns)	5	5
grain density (kg/m^3)	2650	2650
saturated density (kg/m^3)	1504	1504
minimum void ratio (-)	0.05	0.05
diffusion coefficient (-)	0.25	0.25
removal rate (1/day)	3.2	3.2
consolidation coefficient (m^2/yr)	100000	100000
compaction coefficient (-)	0.00000036	0.00000036

Fraction of bedload retained in the delta plain vs Ratio of floodplain to bedload rate (Fig. A12)

This sensitivity test compares the two possible parameters available in the bedload dumping module to simulate subaerial deposition. Their functionality was explained in detailed in the method section. Because both parameters use the bedload discharge to calculate the subaerial deposition, a large proportion of the total load was assigned to the bedload.

In the first simulation, 55236, the ratio of floodplain to bedload rate parameter is tested and assigned a value of 2 in favour of the flooplain rate. According to the dimensions assigned on the bedload dumping module, the sedimentation rate of bedload offshore was about 5 cm/yr. With a ratio of 2, this meant that the floodplain rates would be 10 cm/yr over the entire available subaerial plain. It is difficult to estimate the effect of such rate in the model results, but assuming that from the start of the sediment delivery at 14.3 ka BP to the lowstand around 12.5 ka BP, the subaerial area is at its widest (> 100km). It is thus suspected that all areas between the 0 and 100 km are under subaerial conditions for about 2000 years. At the sedimentation rate listed, 200 m should have been deposited. This is obviously not the case, which led to further exploration of the ratio parameter. The results are displayed in Figure A13.

The second simulation (54963) tests the “fraction of the bedload retained in the delta plain” parameter under the same conditions as listed for simulation 55236. A fraction of 1 was assigned, meaning that all of the bedload discharge was to be retained and distributed evenly over the floodplain area. Assuming modern conditions combined to the model dimensions, 43 Mt/yr spread over the entire floodplain (210 X 60 km), should result in an approximate sedimentation rate of 1.228 mm/yr or 1.228 m/ka. Because the bedload discharge set for each epoch is constant over that epoch, but the floodplain area varies with the RSL, the sedimentation rate

increase with the RSL rising. This explains the sandy wedge growing upward (grain-size cross-section). In the age cross-section, the floodplain deposition is not assigned an age and thus is displayed in marine blue. When SedFlux averages the age of the cells that have submarine and subaerial deposition, the coloring becomes very spotted and not true to the scale anymore. Even though, this representation is most likely resulting from a bug in SedFlux, it is still possible to understand and interpret the stratigraphic results. These suggests that due to the reduction in floodplain area during sea-level transgression, the sedimentation rates becomes too high and thus should be adjusted consequently using smaller bedload discharge during this period (Fig. A14).

By comparing the two simulations, it is evident that floodplain retention changes the geometry of the strata, especially the lower progradational wedge. The limited progradation clearly results from having only two third of the total sediment load being deposited offshore (54963).

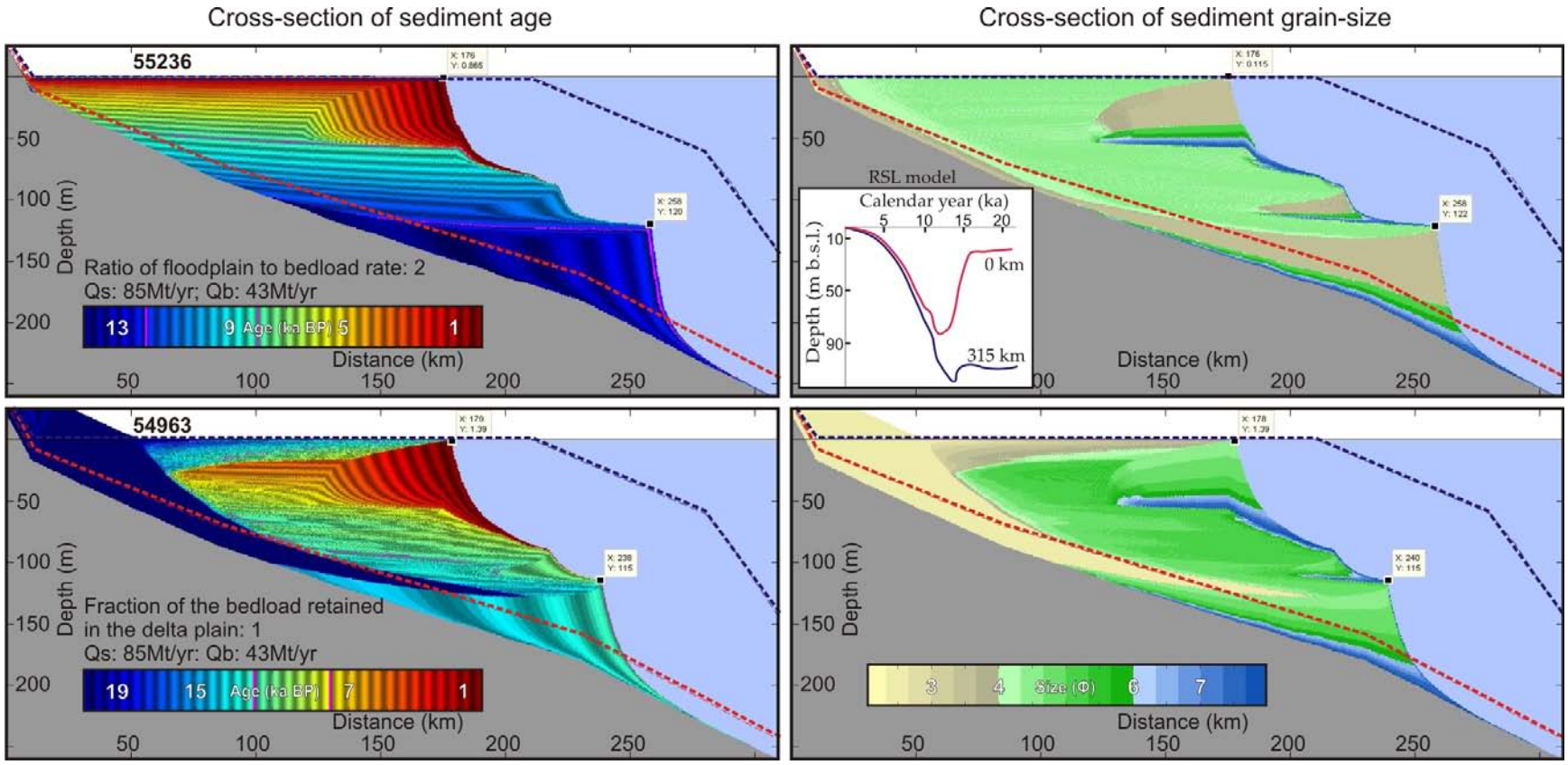

Figure A122: Sensitivity test on the two floodplain retention methods. Simulation 55236 presents the "Ratio of floodplain to bedload rate" method.. Simulation 54963 presents the "Fraction of bedload retained in the delta plain". This method uses a fraction of the bedload and distributes it over the available floodplain area; therefore, the larger the floodplain, the smaller the sedimentation rate. The location can be observed on the cross-sections of sediment age by the upper limit of the darkest blue unit. The location can be observed on the cross-sections of sediment age by the upper limit of the darkest blue unit.The locations of the seismic basal reflector from which the initial profile was derived (Hill et al., 2001; red dotted line) and the modern seafloor profile (blue dotted line) are displayed. As a reference, the RSL graph presents the RSL curves corresponding to each extremity of the transect

Table A13:Fraction of bedload retained in the floodplain

Files	54963	55236
Summary of processes	**Fraction of bedload retained in the delta plain: 1; Qs: 85Mt/yr; Qb: 43Mt/yr (Carson et al. 1999)**	**Ratio of floodplain to bedload rate: 2; Qs: 85Mt/yr; Qb: 43Mt/yr (Carson et al. 1999)**
INITIATION FILE		
bathymetry file	(non-compensated) beaufort_bathy.csv	(non-compensated) beaufort_bathy.csv
PROCESS FILE		
[sea level]		
active	no	no
sea level file	beaufort_sea_level.csv	beaufort_sea_level.csv
[Subsidence]		
active:	yes	yes
Subsidence file	rates_sedflux_MT21000_combined.dat	rates_sedflux_MT21000_combined.dat
[compaction]		
active	no	no
[isostasy]		
active	yes	yes
enable water loading		
[river 0]		
active	yes	yes
river file	beaufort_river.kvf	beaufort_river.kvf
[bedload dumping]		
active	0y->6700y	0y->6700y
distance to dump bedload (m)	5000	5000
ratio of flood plain to bedload rate	0	2
fraction of bedload retained in the delta plain	1	0
[river 1]		
active	6700yr -> 9000yr	6700yr -> 9000yr
river file	beaufort_river2.kvf	beaufort_river2.kvf
[bedload dumping]		
active	6700yr -> 9000yr	6700yr -> 9000yr
distance to dump bedload (m)	5000	5000
ratio of flood plain to bedload rate	0	2
fraction of bedload retained in the delta plain	1	0
[river 2]		
active	9000yr -> 13000y	9000yr -> 13000y
river file	beaufort_river3.kvf	beaufort_river3.kvf
[bedload dumping]		
active	9000yr -> 13000y	9000yr -> 13000y
distance to dump bedload (m)	5000	5000
ratio of flood plain to bedload rate	0	2
fraction of bedload retained in the delta plain	1	0
[river 3]		
active	13000y -> 21000y	13000y -> 21000y
river file	beaufort_river4.kvf	beaufort_river4.kvf

[bedload dumping]		
active	13000y -> 21000y	13000y -> 21000y
distance to dump bedload (m)	5000	5000
ratio of flood plain to bedload rate	0	2
fraction of bedload retained in the delta plain	1	0
[plume]		
active	yes	yes
hyperpycnal plume model	<none>	<none>
hypopycnal plume model	'hypopycnal plume'	'hypopycnal plume'
[Failure]		
active:	no	no
[debris flow]		
active:	no	no
[turbidity current]		
active:	no	no
RIVER FILES		
River0		
['Season 1']		
Duration (y)	1y	1y
Bedload (kg/s)	0	0
Suspended load concentration (kg/m^3)	0	0
velocity (m/s)	0.7	0.7
Width (m)	2000	2000
Depth (m)	8	8
River1		
['Season 1']		
Duration (y)	1y	1y
Bedload (kg/s)	3250	3250
Suspended load concentration (kg/m^3)	0.0585, 0.351075, 0.175525	0.0585, 0.351075, 0.175525
velocity (m/s)	0.7	0.7
Width (m)	2000	2000
Depth (m)	8	8
River2		
['Season 1']		
Duration (y)	1y	1y
Bedload (kg/s)	2600	2600
Suspended load concentration (kg/m^3)	0.04680, 0.28086, 0.14042	0.04680, 0.28086, 0.14042
velocity (m/s)	0.7	0.7
Width (m)	2000	2000
Depth (m)	8	8
River3		
['Season 1']		
Duration (y)	1y	1y
Bedload (kg/s)	1300	1300
Suspended load concentration (kg/m^3)	0.02340, 0.14043, 0.07021	0.02340, 0.14043, 0.07021
velocity (m/s)	0.7	0.7
Width (m)	2000	2000

Depth (m)	8	8
SEDIMENT FILE		
[Grain 1 (bedload)]		
grain size (microns)	200	200
grain density (kg/m^3)	2650	2650
saturated density (kg/m^3)	2000	2000
minimum void ratio (-)	0.17	0.17
diffusion coefficient (-)	0.25	0.25
removal rate (1/day)	25	25
consolidation coefficient (m^2/yr)	100000	100000
compaction coefficient (-)	0.000000062	0.000000062
[Grain 2 (suspended)]		
grain size (microns)	150	150
grain density (kg/m^3)	2650	2650
saturated density (kg/m^3)	1955	1955
minimum void ratio (-)	0.15	0.15
diffusion coefficient (-)	0.25	0.25
removal rate (1/day)	20	20
consolidation coefficient (m^2/yr)	100000	100000
compaction coefficient (-)	0.00000007	0.000000007
[Grain 3 (suspended)]		
grain size (microns)	60	60
grain density (kg/m^3)	2650	2650
saturated density (kg/m^3)	1795	1795
minimum void ratio (-)	0.1	0.1
diffusion coefficient (-)	0.25	0.25
removal rate (1/day)	12	12
consolidation coefficient (m^2/yr)	100000	100000
compaction coefficient (-)	0.00000008	0.00000008
[Grain 4 (suspended)]		
grain size (microns)	5	5
grain density (kg/m^3)	2650	2650
saturated density (kg/m^3)	1504	1504
minimum void ratio (-)	0.05	0.05
diffusion coefficient (-)	0.25	0.25
removal rate (1/day)	3.2	3.2
consolidation coefficient (m^2/yr)	100000	100000
compaction coefficient (-)	0.00000036	0.00000036

Ratio of floodplain to bedload rate (Fig. A13)

Following the previous test, it was suggested that the ratio parameter did not work as expected. This sensitivity test confirms this statement as it failed to simulate the amount of floodplain retention expressed by Carson et al. (1998). As explained in the method section of the stratigraphy paper, the ratio of floodplain to bedload rate uses a ratio to determine the rate of sedimentation that will be applied to the floodplain. It was determined from modern experiments that a ratio of 0.22 or 1:5 existed between the floodplain and the bedload rate. Thus, this ratio was tested over a full length simulation. Considering a bedload discharge of 4 Mt/yr and a ratio of 0.22, the total load retained in the floodplain according to modern parameters would be about 43 Mt/yr. The suspended load was then assigned 85 Mt/yr.

This comparative simulation resulted in identical stratigraphy without any evidence of floodplain deposition (56337 vs 56140). The conclusion of this test suggested that even though the ratio parameter was the preferred option to simulate floodplain deposition, the “fraction of bedload” parameter would have to be used to simulate floodplain deposition.

It is also worth mentioning that these simulations used a higher ratio of sediment for all epochs, which resulted in a total sediment delivery of 3.12×10^6 Mt. As expected, this amount was not enough to fill the trough. These runs were also set to have a longer third epoch, i.e. instead of 12 to 8 ka BP, the epoch lasted until the mid-Holocene at 5 ka BP. This resulted in further progradation of the early HST, followed by retrogradation due to the sudden change of sediment supply from 3 to 1 time during a still rapidly rising RSL.

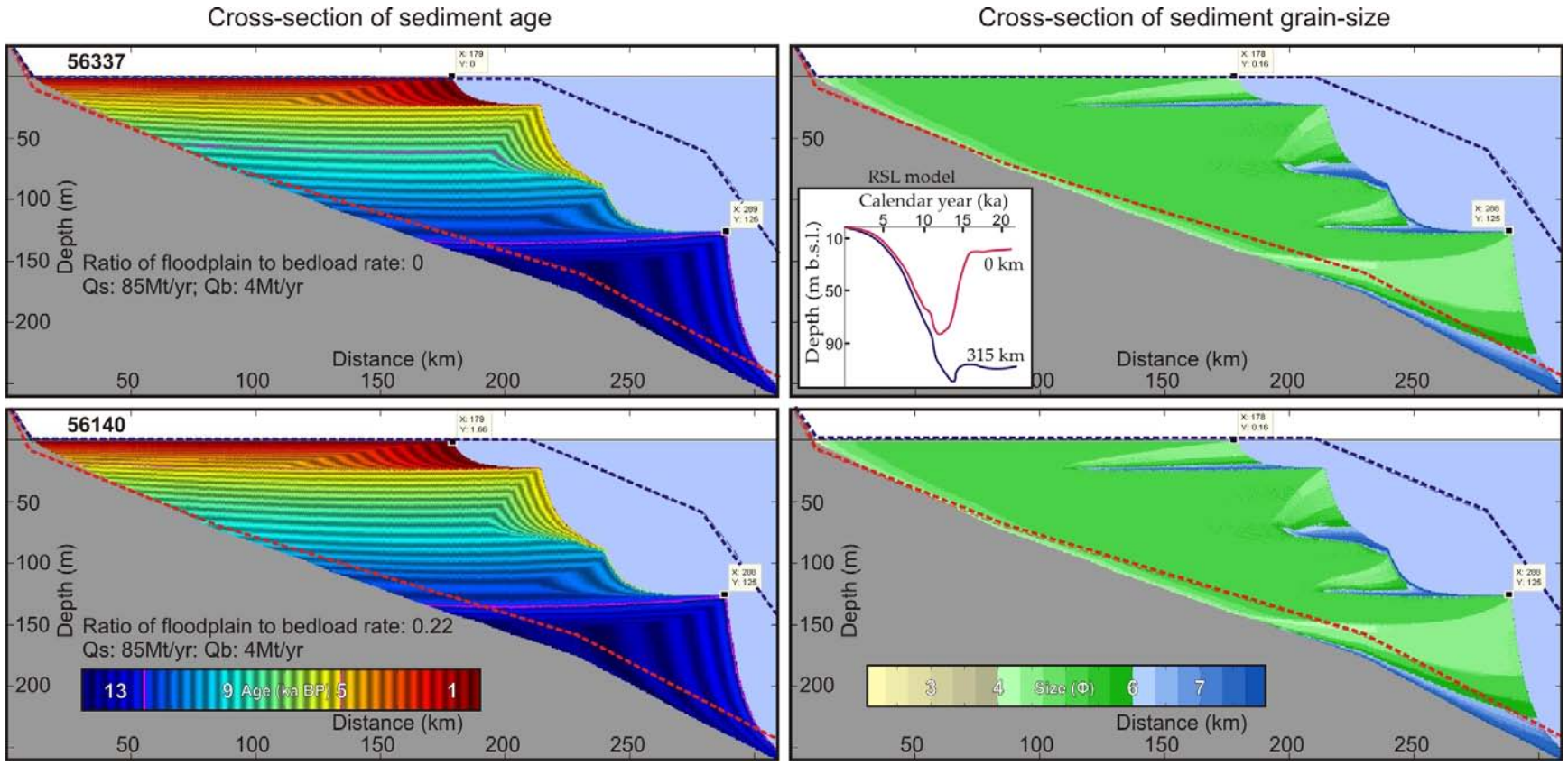

Figure A13: Sensitivity test on the floodplain sedimentation using the "Ratio" parameter. Simulation 56337 presents a case where the ratio is null, thus no sedimentation on the floodplain. Simulation 56140 considers a ratio of 0.22, which was established after calculating the expected modern floodplain sedimentation rate based on the sediment flux budget estimated by Carson et al. (1999). This ratio suggests that modern sedimentation rate offshore is approximately five times the floodplain rate. This is to be expected since the floodplain area is so large compared to the offshore deposition area for bedload. The location can be observed on the cross-sections of sediment age by the upper limit of the darkest blue unit. The locations of the seismic basal reflector from which the initial profile was derived (Hill et al., 2001; red dotted line) and the modern seafloor profile (blue dotted line) are displayed. As a reference, the RSL graph presents the RSL curves corresponding to each extremity of the transect.

Table A14: Ration of floodplain to bedload rate

Files	56140	56337
Summary of processes	**Qs: 85Mt/yr; Qb: 4Mt/yr (Carson et al. 1999); Ratio of floodplain to bedload rate: 0.22**	**Qs: 85Mt/yr; Qb: 4Mt/yr (Carson et al. 1999); Ratio of floodplain to bedload rate: 0**
INITIATION FILE		
bathymetry file	(compensated) beaufort_bathy.csv	(compensated) beaufort_bathy.csv
PROCESS FILE		
[sea level]		
active	no	no
sea level file	beaufort_sea_level.csv	beaufort_sea_level.csv
[Subsidence]		
active:	yes	yes
Subsidence file	rates_sedflux_MT21000.dat	rates_sedflux_MT21000.dat
[compaction]		
active	no	no
[isostasy]		
active	yes	yes
enable water loading	no	no
[river 0]		
active	yes	yes
river file	beaufort_river.kvf	beaufort_river.kvf
[bedload dumping]		
active	0y->6700y	0y->6700y
distance to dump bedload (m)	5000	5000
ratio of flood plain to bedload rate	0.22	0
fraction of bedload retained in the delta plain	0	0
[river 1]		
active	6700yr -> 9000yr	6700yr -> 9000yr
river file	beaufort_river2.kvf	beaufort_river2.kvf
[bedload dumping]		
active	6700yr -> 9000yr	6700yr -> 9000yr
distance to dump bedload (m)	5000	5000
ratio of flood plain to bedload rate	0.22	0
fraction of bedload retained in the delta plain	0	0
[river 2]		
active	9000yr -> 16000y	9000yr -> 16000y
river file	beaufort_river3.kvf	beaufort_river3.kvf
[bedload dumping]		
active	9000yr -> 16000y	9000yr -> 16000y
distance to dump bedload (m)	5000	5000
ratio of flood plain to bedload rate	0.22	0
fraction of bedload retained in the delta plain	0	0
[river 3]		
active	16000y -> 21000y	16000y -> 21000y
river file	beaufort_river4.kvf	beaufort_river4.kvf
[bedload dumping]		

active	16000y -> 21000y	16000y -> 21000y
distance to dump bedload (m)	5000	5000
ratio of flood plain to bedload rate	0.22	0
fraction of bedload retained in the delta plain	0	0
[plume]		
active	yes	yes
hyperpycnal plume model	<none>	<none>
hypopycnal plume model	'hypopycnal plume'	'hypopycnal plume'
[Failure]		
active:	no	no
[debris flow]		
active:	no	no
[turbidity current]		
active:	no	no
RIVER FILES		
River0		
['Season 1']		
Duration (y)	1y	1y
Bedload (kg/s)	0	0
Suspended load concentration (kg/m^3)	0	0
velocity (m/s)	0.7	0.7
Width (m)	2000	2000
Depth (m)	8	8
River1		
['Season 1']		
Duration (y)	1y	1y
Bedload (kg/s)	520	520
Suspended load concentration (kg/m^3)	0.09628, 0.5776, 0.2888	0.09628, 0.5776, 0.2888
velocity (m/s)	0.7	0.7
Width (m)	2000	2000
Depth (m)	8	8
River2		
['Season 1']		
Duration (y)	1y	1y
Bedload (kg/s)	390	390
Suspended load concentration (kg/m^3)	0.07221, 0.4332, 0.2166	0.07221, 0.4332, 0.2166
velocity (m/s)	0.7	0.7
Width (m)	2000	2000
Depth (m)	8	8
River3		
['Season 1']		
Duration (y)	1y	1y
Bedload (kg/s)	130	130
Suspended load concentration (kg/m^3)	0.02407, 0.1444, 0.0722	0.02407, 0.1444, 0.0722
velocity (m/s)	0.7	0.7
Width (m)	2000	2000
Depth (m)	8	8

SEDIMENT FILE		
[Grain 1 (bedload)]		
grain size (microns)	200	200
grain density (kg/m^3)	2650	2650
saturated density (kg/m^3)	2000	2000
minimum void ratio (-)	0.17	0.17
diffusion coefficient (-)	0.25	0.25
removal rate (1/day)	25	25
consolidation coefficient (m^2/yr)	100000	100000
compaction coefficient (-)	0.000000062	0.000000062
[Grain 2 (suspended)]		
grain size (microns)	150	150
grain density (kg/m^3)	2650	2650
saturated density (kg/m^3)	1955	1955
minimum void ratio (-)	0.15	0.15
diffusion coefficient (-)	0.25	0.25
removal rate (1/day)	20	20
consolidation coefficient (m^2/yr)	100000	100000
compaction coefficient (-)	0.00000007	0.000000007
[Grain 3 (suspended)]		
grain size (microns)	60	60
grain density (kg/m^3)	2650	2650
saturated density (kg/m^3)	1795	1795
minimum void ratio (-)	0.1	0.1
diffusion coefficient (-)	0.25	0.25
removal rate (1/day)	12	12
consolidation coefficient (m^2/yr)	100000	100000
compaction coefficient (-)	0.00000008	0.00000008
[Grain 4 (suspended)]		
grain size (microns)	5	5
grain density (kg/m^3)	2650	2650
saturated density (kg/m^3)	1504	1504
minimum void ratio (-)	0.05	0.05
diffusion coefficient (-)	0.25	0.25
removal rate (1/day)	3.2	3.2
consolidation coefficient (m^2/yr)	100000	100000
compaction coefficient (-)	0.00000036	0.00000036

Fraction of bedload retained in the floodplain (Fig. A14)

Figure A14 presents the results using smaller bedload with the “fraction” parameter, which were as expected. The fraction of bedload should therefore be higher at the beginning of the simulation, and then progressively reduced as the subaerial plain area reduces, i.e. as the run progresses in this case. This way the bedload is progressively transferred back to the bedload module and gets distributed in the offshore region. This suggestion is somewhat interfering with the reality as it is expected that the larger the floodplain the more sediment get retained. Therefore, it may be a better idea to forget about the sediment build up “artefact” created by the model at the beginning of the profile (0-50km) and consider this parameter appropriate.

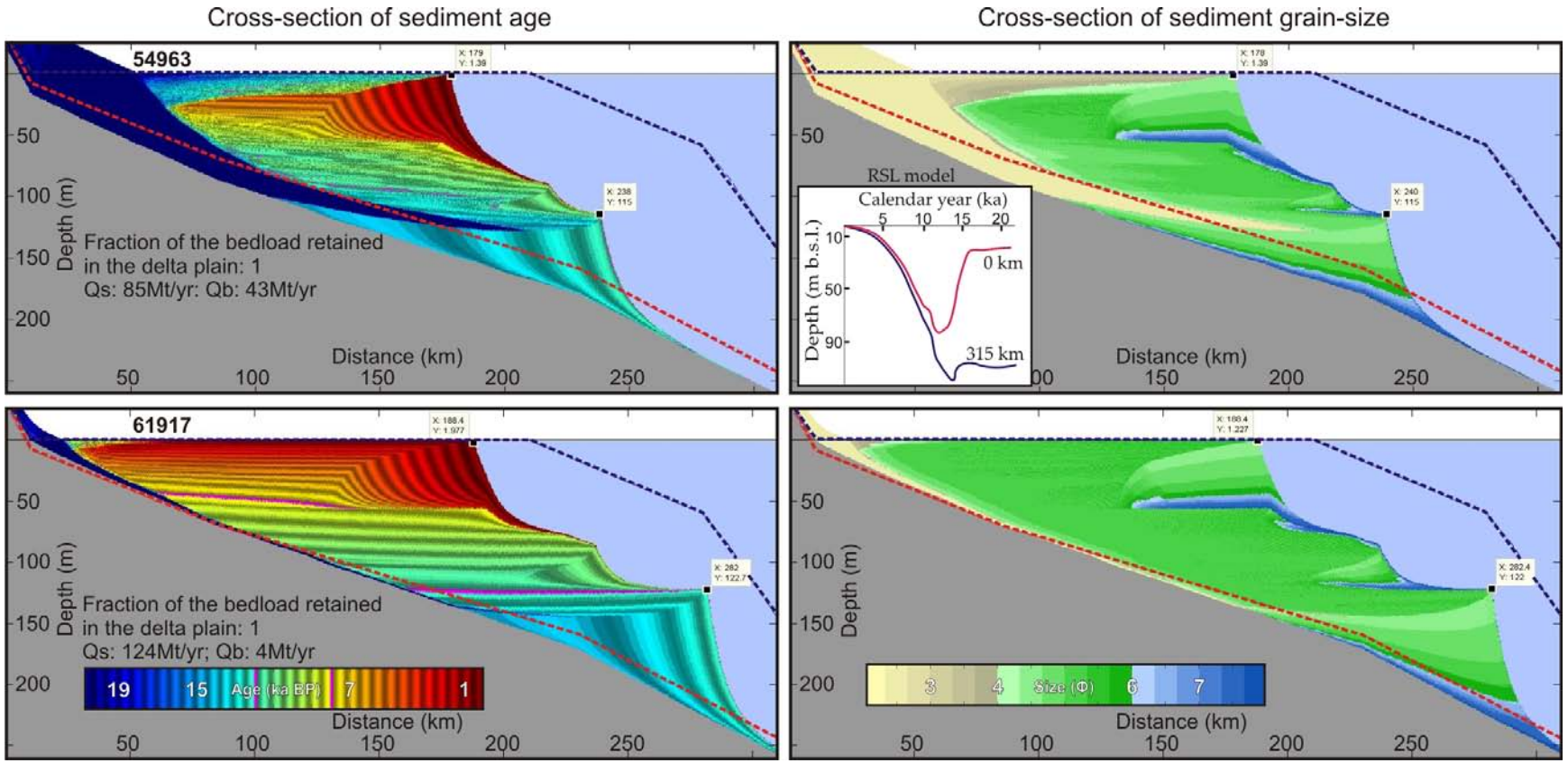

Figure A14: Sensitivity test on the amount of bedload discharge to be retained in the floodplain via the fraction parameter. Simulation 54963 uses 43 Mt/yr fully retained in the floodplain. The sediment budget is based on Carson et al. (1999). Simulation 61917 uses a low bedload discharge of 4 Mt/yr. The sediment budget is based on Carson et al. (1998). The locations of the seismic basal reflector from which the initial profile was derived (Hill et al., 2001; red dotted line) and the modern seafloor profile (blue dotted line) are displayed. As a reference, the RSL graph presents the RSL curves corresponding to each extremity of the transect.

Table A15: High vs low Qb using fraction of bedload retained in the delta plain

Files	54963	55236
Summary of processes	**Large Qb; Qs: 85Mt/yr; Qb: 43Mt/yr (Carson et al. 1999)**	**Small Qb; Qs: 124Mt/yr; Qb: 4Mt/yr (Carson et al. 1998)**
INITIATION FILE		
bathymetry file	(compensated) beaufort_bathy.csv	(compensated) beaufort_bathy.csv
PROCESS FILE		
[sea level]		
active	no	no
sea level file	beaufort_sea_level.csv	beaufort_sea_level.csv
[Subsidence]		
active:	yes	yes
Subsidence file	rates_sedflux_MT21000_combined.dat	rates_sedflux_MT21000_combined.dat
[compaction]		
active	no	no
[isostasy]		
active	yes	yes
enable water loading		
[river 0]		
active	yes	yes
river file	beaufort_river.kvf	beaufort_river.kvf
[bedload dumping]		
active	0y->6700y	0y->6700y
distance to dump bedload (m)	5000	5000
ratio of flood plain to bedload rate	0	2
fraction of bedload retained in the delta plain	1	0
[river 1]		
active	6700yr -> 9000yr	6700yr -> 9000yr
river file	beaufort_river2.kvf	beaufort_river2.kvf
[bedload dumping]		
active	6700yr -> 9000yr	6700yr -> 9000yr
distance to dump bedload (m)	5000	5000
ratio of flood plain to bedload rate	0	2
fraction of bedload retained in the delta plain	1	0
[river 2]		
active	9000yr -> 13000y	9000yr -> 13000y
river file	beaufort_river3.kvf	beaufort_river3.kvf
[bedload dumping]		
active	9000yr -> 13000y	9000yr -> 13000y
distance to dump bedload (m)	5000	5000
ratio of flood plain to bedload rate	0	2
fraction of bedload retained in the delta plain	1	0
[river 3]		
active	13000y -> 21000y	13000y -> 21000y
river file	beaufort_river4.kvf	beaufort_river4.kvf
[bedload dumping]		

active	13000y -> 21000y	13000y -> 21000y
distance to dump bedload (m)	5000	5000
ratio of flood plain to bedload rate	0	2
fraction of bedload retained in the delta plain	1	0
[plume]		
active	yes	yes
hyperpycnal plume model	<none>	<none>
hypopycnal plume model	'hypopycnal plume'	'hypopycnal plume'
[Failure]		
active:	no	no
[debris flow]		
active:	no	no
[turbidity current]		
active:	no	no
RIVER FILES		
River0		
['Season 1']		
Duration (y)	1y	1y
Bedload (kg/s)	0	0
Suspended load concentration (kg/m^3)	0	0
velocity (m/s)	0.7	0.7
Width (m)	2000	2000
Depth (m)	8	8
River1		
['Season 1']		
Duration (y)	1y	1y
Bedload (kg/s)	3250	3250
Suspended load concentration (kg/m^3)	0.0585, 0.351075, 0.175525	0.0585, 0.351075, 0.175525
velocity (m/s)	0.7	0.7
Width (m)	2000	2000
Depth (m)	8	8
River2		
['Season 1']		
Duration (y)	1y	1y
Bedload (kg/s)	2600	2600
Suspended load concentration (kg/m^3)	0.04680, 0.28086, 0.14042	0.04680, 0.28086, 0.14042
velocity (m/s)	0.7	0.7
Width (m)	2000	2000
Depth (m)	8	8
River3		
['Season 1']		
Duration (y)	1y	1y
Bedload (kg/s)	1300	1300
Suspended load concentration (kg/m^3)	0.02340, 0.14043, 0.07021	0.02340, 0.14043, 0.07021
velocity (m/s)	0.7	0.7
Width (m)	2000	2000
Depth (m)	8	8

SEDIMENT FILE		
[Grain 1 (bedload)]		
grain size (microns)	200	200
grain density (kg/m^3)	2650	2650
saturated density (kg/m^3)	2000	2000
minimum void ratio (-)	0.17	0.17
diffusion coefficient (-)	0.25	0.25
removal rate (1/day)	25	25
consolidation coefficient (m^2/yr)	100000	100000
compaction coefficient (-)	0.000000062	0.000000062
[Grain 2 (suspended)]		
grain size (microns)	150	150
grain density (kg/m^3)	2650	2650
saturated density (kg/m^3)	1955	1955
minimum void ratio (-)	0.15	0.15
diffusion coefficient (-)	0.25	0.25
removal rate (1/day)	20	20
consolidation coefficient (m^2/yr)	100000	100000
compaction coefficient (-)	0.00000007	0.000000007
[Grain 3 (suspended)]		
grain size (microns)	60	60
grain density (kg/m^3)	2650	2650
saturated density (kg/m^3)	1795	1795
minimum void ratio (-)	0.1	0.1
diffusion coefficient (-)	0.25	0.25
removal rate (1/day)	12	12
consolidation coefficient (m^2/yr)	100000	100000
compaction coefficient (-)	0.00000008	0.00000008
[Grain 4 (suspended)]		
grain size (microns)	5	5
grain density (kg/m^3)	2650	2650
saturated density (kg/m^3)	1504	1504
minimum void ratio (-)	0.05	0.05
diffusion coefficient (-)	0.25	0.25
removal rate (1/day)	3.2	3.2
consolidation coefficient (m^2/yr)	100000	100000
compaction coefficient (-)	0.00000036	0.00000036

Grain-size (Fig. A15)

This sensitivity test aimed at evaluating the stratigraphic impacts of supplying coarser grains. The present Mackenzie Delta supply is composed of fine grains only, but the supply was most likely to be coarser during glacial periods. In SedFlux it is however, not possible to change the composition of the grains between epoch, mainly because the bedload size is a set value. Therefore, this test became useful in determining what would be the impacts of changing the grain-size composition if SedFlux was to allow variability between epochs.

Simulation 56333 used a grain-size composition following the modern composition. The composition ranged from fine sand (2.3 φ) for bedload to bordering a clay size (7.6 φ) for the smallest suspended particle size. Simulation 57157 used the same supply and parameters as 56333, but used a coarser grain-size composition. The grain-sizes ranged from very coarse sand (-0.2 φ) for the bedload to a coarse silt/ very fine sand size (4 φ) for the finest grain in the suspended load. The results showed that using coarser grain-sizes reduces the total volume occupied by the sediments. The volume lost is explained by the difference in the saturated grain density, which averaged about 1800 kg/m^3 for the fine grained base-case simulation (Fig.4) and 1950 kg/m^3 for the coarse grained simulation presented here. Hence, for a same total load (2.784×10^{15} kg), the finer grain stratigraphy occupied an additional volume equalled to approximately 120 km^3 compared to the coarser grain stratigraphy. These numbers suggests that if specific periods needed to be represented by coarser grain distribution, than the volume occupied by sediments during these periods would be lessened. This conclusion is only applicable in the case where no compaction is taken into consideration. Where compaction would be included, the

total volume lost would be smaller, because finer grain-sizes have smaller minimum void ratio and larger compaction coefficients, thus favouring tighter compaction (Table A16). No sensitivity test has however been done to confirm this affirmation.

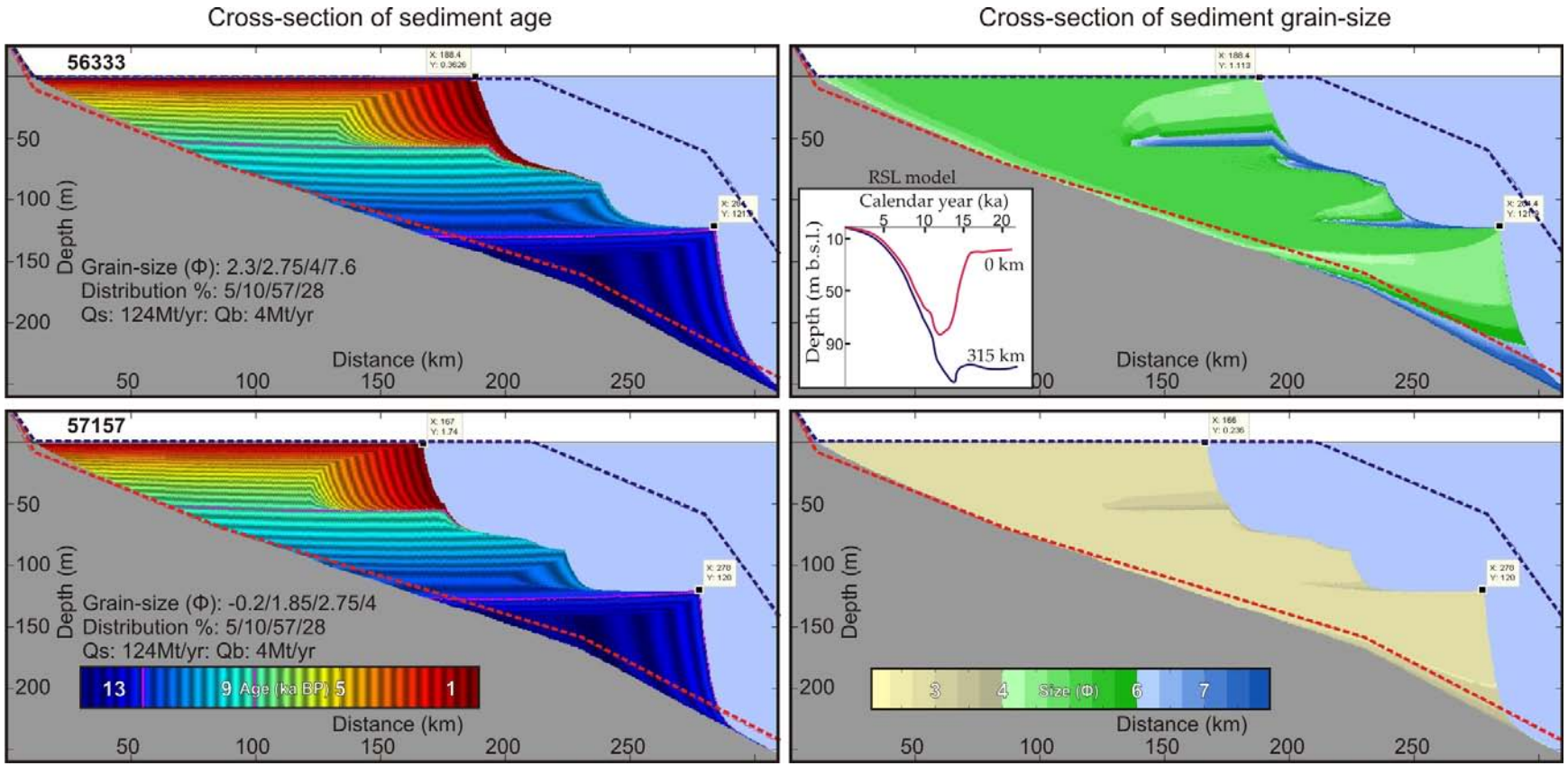

Figure A15: Sensitivity test on grain-size distribution. Simulation 56333 uses four fine grain-sizes: 2.3 Φ (200 µm) representing the bedload, and 2.75 Φ (150 µm), 4 Φ (60 µm) , and 7.6 Φ (5 µm)µ representing the suspended load. Simulation 57157 uses four coarser grain-sizes: -0.2 Φ (1200 µm) representing the bedload, and 1.85 Φ (300 µm), 2.75 Φ (150 µm), and 4 Φ (60 µm) representing the suspended load. For both simulations the grain-sizes were distributed with the following percentages: 5, 10, 57, and 28 % respectively. The locations of the seismic basal reflector from which the initial profile was derived (Hill et al., 2001; red dotted line) and the modern seafloor profile (blue dotted line) are displayed. As a reference, the RSL graph presents the RSL curves corresponding to each extremity of the transect.

Table A16: Grain-size

Files	56333	57157
Summary of processes	**Grain-size: 200/150/60/5 um Qs: 124Mt/yr; Qb: 4Mt/yr (Carson et al. 1998);**	**Grain-size: 1200/300/150/60um; Qs: 124Mt/yr; Qb: 4Mt/yr (Carson et al. 1998);**
INITIATION FILE		
bathymetry file	(compensated) beaufort_bathy.csv	(compensated) beaufort_bathy.csv
PROCESS FILE		
[sea level]		
active	no	no
sea level file	beaufort_sea_level.csv	beaufort_sea_level.csv
[Subsidence]		
active:	yes	yes
Subsidence file	rates_sedflux_MT21000.dat	rates_sedflux_MT21000.dat
[compaction]		
active	no	no
[isostasy]		
active	yes	yes
enable water loading	no	no
[river 0]		
active	yes	yes
river file	beaufort_river.kvf	beaufort_river.kvf
[bedload dumping]		
active	0y->6700y	0y->6700y
distance to dump bedload (m)	5000	5000
ratio of flood plain to bedload rate	0	0
fraction of bedload retained in the delta plain	0	0
[river 1]		
active	6700yr -> 9000yr	6700yr -> 9000yr
river file	beaufort_river2.kvf	beaufort_river2.kvf
[bedload dumping]		
active	6700yr -> 9000yr	6700yr -> 9000yr
distance to dump bedload (m)	5000	5000
ratio of flood plain to bedload rate	0	0
fraction of bedload retained in the delta plain	0	0
[river 2]		
active	9000yr -> 13000y	9000yr -> 13000y
river file	beaufort_river3.kvf	beaufort_river3.kvf
[bedload dumping]		
active	9000yr -> 13000y	9000yr -> 13000y
distance to dump bedload (m)	5000	5000
ratio of flood plain to bedload rate	0	0
fraction of bedload retained in the delta plain	0	0
[river 3]		
active	13000y -> 21000y	13000y -> 21000y
river file	beaufort_river4.kvf	beaufort_river4.kvf

[bedload dumping]		
active	13000y -> 21000y	13000y -> 21000y
distance to dump bedload (m)	5000	5000
ratio of flood plain to bedload rate	0	0
fraction of bedload retained in the delta plain	0	0
[plume]		
active	yes	yes
hyperpycnal plume model	<none>	<none>
hypopycnal plume model	'hypopycnal plume'	'hypopycnal plume'
[Failure]		
active:	no	no
[debris flow]		
active:	no	no
[turbidity current]		
active:	no	no
RIVER FILES		
River0		
['Season 1']		
Duration (y)	1y	1y
Bedload (kg/s)	0	0
Suspended load concentration (kg/m^3)	0	0
velocity (m/s)	0.7	0.7
Width (m)	2000	2000
Depth (m)	8	8
River1		
['Season 1']		
Duration (y)	1y	1y
Bedload (kg/s)	500	500
Suspended load concentration (kg/m^3)	0.0878, 0.526, 0.263	0.0878, 0.526, 0.263
velocity (m/s)	0.7	0.7
Width (m)	2000	2000
Depth (m)	8	8
River2		
['Season 1']		
Duration (y)	1y	1y
Bedload (kg/s)	400	400
Suspended load concentration (kg/m^3)	0.07024, 0.4208, 0.2104	0.07024, 0.4208, 0.2104
velocity (m/s)	0.7	0.7
Width (m)	2000	2000
Depth (m)	8	8
River3		
['Season 1']		
Duration (y)	1y	1y
Bedload (kg/s)	200	200
Suspended load concentration	0.03512, 0.2104, 0.1052	0.03512, 0.2104, 0.1052

(kg/m^3)		
velocity (m/s)	0.7	0.7
Width (m)	2000	2000
Depth (m)	8	8
SEDIMENT FILE		
[Grain 1 (bedload)]		
grain size (microns)	200	1200
grain density (kg/m^3)	2650	2700
saturated density (kg/m^3)	2000	2115
minimum void ratio (-)	0.17	0.3
diffusion coefficient (-)	0.25	0.25
removal rate (1/day)	25	50
consolidation coefficient (m^2/yr)	100000	100000
compaction coefficient (-)	0.000000062	3.68E-08
[Grain 2 (suspended)]		
grain size (microns)	150	300
grain density (kg/m^3)	2650	2718
saturated density (kg/m^3)	1955	2094
minimum void ratio (-)	0.15	0.2
diffusion coefficient (-)	0.25	0.25
removal rate (1/day)	20	35
consolidation coefficient (m^2/yr)	100000	100000
compaction coefficient (-)	0.00000007	0.00000005
[Grain 3 (suspended)]		
grain size (microns)	60	150
grain density (kg/m^3)	2650	2650
saturated density (kg/m^3)	1795	1955
minimum void ratio (-)	0.1	0.15
diffusion coefficient (-)	0.25	0.25
removal rate (1/day)	12	20
consolidation coefficient (m^2/yr)	100000	100000
compaction coefficient (-)	0.00000008	0.00000007
[Grain 4 (suspended)]		
grain size (microns)	5	60
grain density (kg/m^3)	2650	2676
saturated density (kg/m^3)	1504	1795
minimum void ratio (-)	0.05	0.1
diffusion coefficient (-)	0.25	0.25
removal rate (1/day)	3.2	12
consolidation coefficient (m^2/yr)	100000	100000
compaction coefficient (-)	0.00000036	0.00000008

Compaction (Fig. A16)

This sensitivity test was carried out to evaluate the impacts of compaction on the stratigraphy. Syvitski et al. (2001) provides an explanation on how the compaction module works in SedFlux. Compaction is dependant on the porosity of the sediment and the overlying sediment load, it does not take into consideration the pore water pressure. Maximum compaction is reached when the grains involved in the process have reached their “closest packed” arrangement.

In SedFlux, the porosity of each grain sizes is defined in the sediment file (Table A17). Simulation 56333 shows the results without compaction, whereas 63837 include compaction. The results show that compaction increased the bulk density of the sediments, contributed to the deformation of the strata, and reduced the total volume occupied by sediments. In areas where thick sediment is deposited, such as under the subaerial delta plain, up to 10 m of subsidence is created within the internal structures. This value is not out of range since up to 40 % of the sediment wedge thickness as been suggested as being the product of compaction (Reynolds, Steckler, and Coakley 1991). Based on the geometry of the deposits, the approximate total volume lost equates to about 188 km^3. In terms of mass, averaged using a saturated density of 1800 kg/m^3, this volume represents about 339 000 Mt of sediment or 2 700 additional years of sedimentation using the modern sediment supply rate. These numbers do not estimate for the additional space that would be created from the compaction process by adding this amount of sediments.

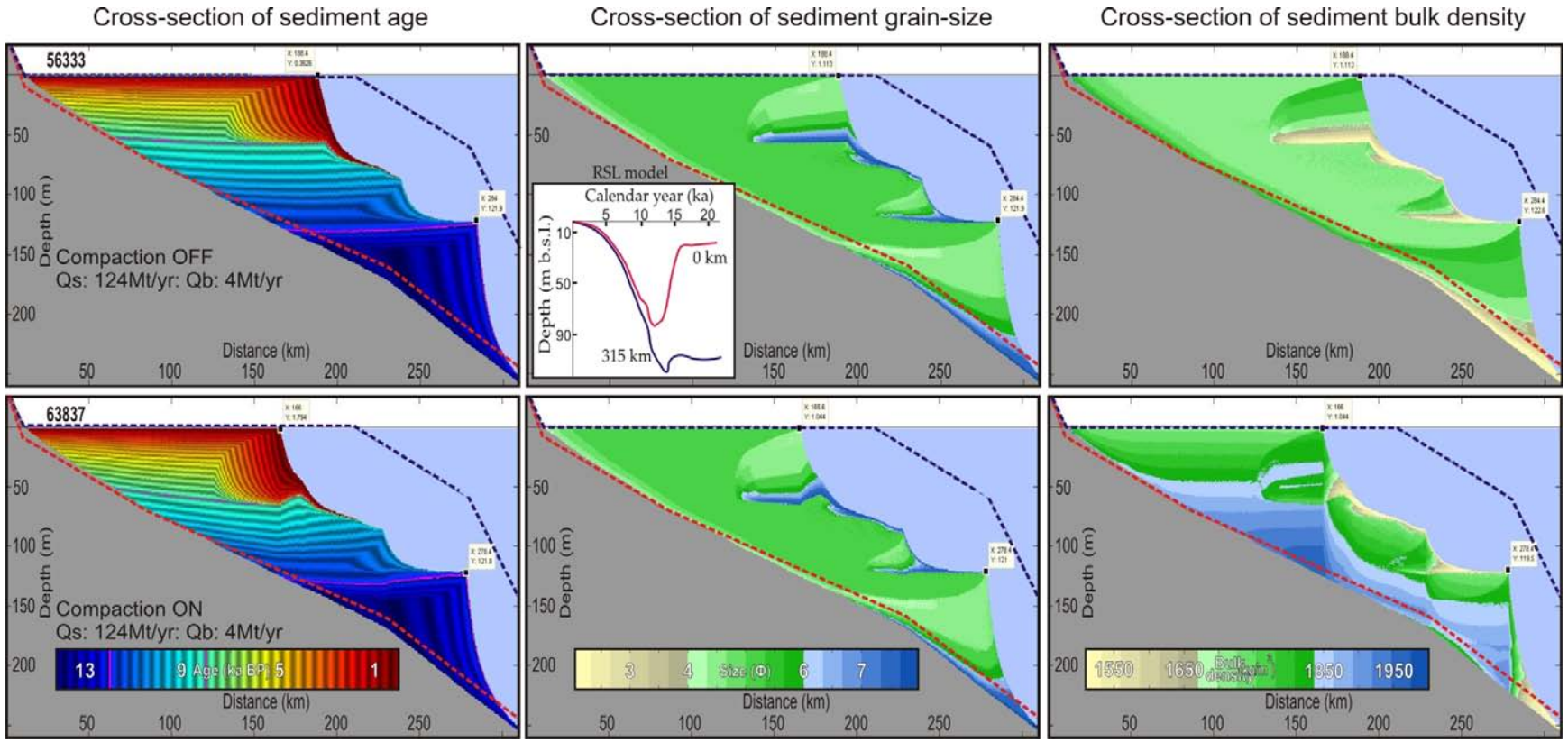

Figure A16: Sensitivity test on compaction. Simulation 56333 does not calculate the compaction. Simulation 63837 calculates the compaction. The bulk density graphs are also presented. The locations of the seismic basal reflector from which the initial profile was derived (Hill et al., 2001; red dotted line) and the modern seafloor profile (blue dotted line) are displayed. As a reference, the RSL graph presents the RSL curves corresponding to each extremity of the transect.

Table A17: Compaction

Files	56333	63837
Summary of processes	**No compaction; Qs: 124Mt/yr; Qb: 4Mt/yr (Carson et al. 1998);**	**Compaction; Qs: 124Mt/yr; Qb: 4Mt/yr (Carson et al. 1998);**
INITIATION FILE		
bathymetry file	(compensated) beaufort_bathy.csv	(compensated) beaufort_bathy.csv
PROCESS FILE		
[sea level]		
active	no	no
sea level file	beaufort_sea_level.csv	beaufort_sea_level.csv
[Subsidence]		
active:	yes	yes
Subsidence file	rates_sedflux_MT21000.dat	rates_sedflux_MT21000.dat
[compaction]		
active	no	yes
[isostasy]		
active	yes	yes
enable water loading	no	no
[river 0]		
active	yes	yes
river file	beaufort_river.kvf	beaufort_river.kvf
[bedload dumping]		
active	0y->6700y	0y->6700y
distance to dump bedload (m)	5000	5000
ratio of flood plain to bedload rate	0	0
fraction of bedload retained in the delta plain	0	0
[river 1]		
active	6700yr -> 9000yr	6700yr -> 9000yr
river file	beaufort_river2.kvf	beaufort_river2.kvf
[bedload dumping]		
active	6700yr -> 9000yr	6700yr -> 9000yr
distance to dump bedload (m)	5000	5000
ratio of flood plain to bedload rate	0	0
fraction of bedload retained in the delta plain	0	0
[river 2]		
active	9000yr -> 13000y	9000yr -> 13000y
river file	beaufort_river3.kvf	beaufort_river3.kvf
[bedload dumping]		
active	9000yr -> 13000y	9000yr -> 13000y
distance to dump bedload (m)	5000	5000
ratio of flood plain to bedload rate	0	0
fraction of bedload retained in the delta plain	0	0
[river 3]		
active	13000y -> 21000y	13000y -> 21000y
river file	beaufort_river4.kvf	beaufort_river4.kvf

[bedload dumping]		
active	13000y -> 21000y	13000y -> 21000y
distance to dump bedload (m)	5000	5000
ratio of flood plain to bedload rate	0	0
fraction of bedload retained in the delta plain	0	0
[plume]		
active	yes	yes
hyperpycnal plume model	<none>	<none>
hypopycnal plume model	'hypopycnal plume'	'hypopycnal plume'
[Failure]		
active:	no	no
[debris flow]		
active:	no	no
[turbidity current]		
active:	no	no
RIVER FILES		
River0		
['Season 1']		
Duration (y)	1y	1y
Bedload (kg/s)	0	0
Suspended load concentration (kg/m^3)	0	0
velocity (m/s)	0.7	0.7
Width (m)	2000	2000
Depth (m)	8	8
River1		
['Season 1']		
Duration (y)	1y	1y
Bedload (kg/s)	500	500
Suspended load concentration (kg/m^3)	0.0878, 0.526, 0.263	0.0878, 0.526, 0.263
velocity (m/s)	0.7	0.7
Width (m)	2000	2000
Depth (m)	8	8
River2		
['Season 1']		
Duration (y)	1y	1y
Bedload (kg/s)	400	400
Suspended load concentration (kg/m^3)	0.07024, 0.4208, 0.2104	0.07024, 0.4208, 0.2104
velocity (m/s)	0.7	0.7
Width (m)	2000	2000
Depth (m)	8	8
River3		
['Season 1']		
Duration (y)	1y	1y
Bedload (kg/s)	200	200
Suspended load concentration	0.03512, 0.2104, 0.1052	0.03512, 0.2104, 0.1052

(kg/m^3)		
velocity (m/s)	0.7	0.7
Width (m)	2000	2000
Depth (m)	8	8
SEDIMENT FILE		
[Grain 1 (bedload)]		
grain size (microns)	200	200
grain density (kg/m^3)	2650	2650
saturated density (kg/m^3)	2000	2000
minimum void ratio (-)	0.17	0.17
diffusion coefficient (-)	0.25	0.25
removal rate (1/day)	25	25
consolidation coefficient (m^2/yr)	100000	100000
compaction coefficient (-)	0.000000062	0.000000062
[Grain 2 (suspended)]		
grain size (microns)	150	150
grain density (kg/m^3)	2650	2650
saturated density (kg/m^3)	1955	1955
minimum void ratio (-)	0.15	0.15
diffusion coefficient (-)	0.25	0.25
removal rate (1/day)	20	20
consolidation coefficient (m^2/yr)	100000	100000
compaction coefficient (-)	0.00000007	0.00000007
[Grain 3 (suspended)]		
grain size (microns)	60	60
grain density (kg/m^3)	2650	2650
saturated density (kg/m^3)	1795	1795
minimum void ratio (-)	0.1	0.1
diffusion coefficient (-)	0.25	0.25
removal rate (1/day)	12	12
consolidation coefficient (m^2/yr)	100000	100000
compaction coefficient (-)	0.00000008	0.00000008
[Grain 4 (suspended)]		
grain size (microns)	5	5
grain density (kg/m^3)	2650	2650
saturated density (kg/m^3)	1504	1504
minimum void ratio (-)	0.05	0.05
diffusion coefficient (-)	0.25	0.25
removal rate (1/day)	3.2	3.2
consolidation coefficient (m^2/yr)	100000	100000
compaction coefficient (-)	0.00000036	0.00000036

More extensive ice margins/better earth structure parametization (Fig. A17 and A18)

The RSL model used in this study is derived from global models, such as ICE5G-VM2, and customisation for regional purposes is not yet possible. It was mentioned in the RSL paper (Picard et al. in prep) that certain geophysical parameters, such as elastic thickness and relaxation time of the lithosphere, may be considerably different in the region of interest than the parameters used for the global models. If global models were able to incorporate regional values for their controlling parameters, their outputs would inherently be affected and different. Considering the additional uncertainties rose on the ice sheet extent from field data (England et al. 2009), suggesting more extensive ice, it is suspected that the RSL model outputs for the region could in fact resembled the ones calculated for a location south of the present transect. A southern location would mean thicker ice, thus more loading, which could also simulate a thinner lithospheric elastic thickness. Sensitivity tests were thus carried out to simulate these possible effects and presented in length in the stratigraphy paper (Picard and Hill, in prep).

Figure A17 compares the use of RSL model data extracted for the original transect (56140) with a transect starting 90 km south (56507). Simulation 56506 presents the intermediate step between simulation 56140 and 56507, where additional loading is created by using the new transect and therefore should be accounted for in the initial bathymetric profile. This simulation shows that more than 40 m of additional loading takes place.

The results between 56140 and 56507 and the simulations presented in Figure A18 suggest little variation in the stratigraphy. The important difference however is that because RSL does not reach as low values as the original transect, the stratigraphic features reach

shallower depths. The depth difference is relatively small because by the time the sediment supply is activated (14.3 ka BP), the additional changes in RSL between the original and the more extensive ice transect are small (13 m, see inset 56506). However, for areas that would have sediment supply starting earlier, such as for the Beaufort Shelf, the difference would be much more noticeable as the additional variation in RSL is much larger for the early period.

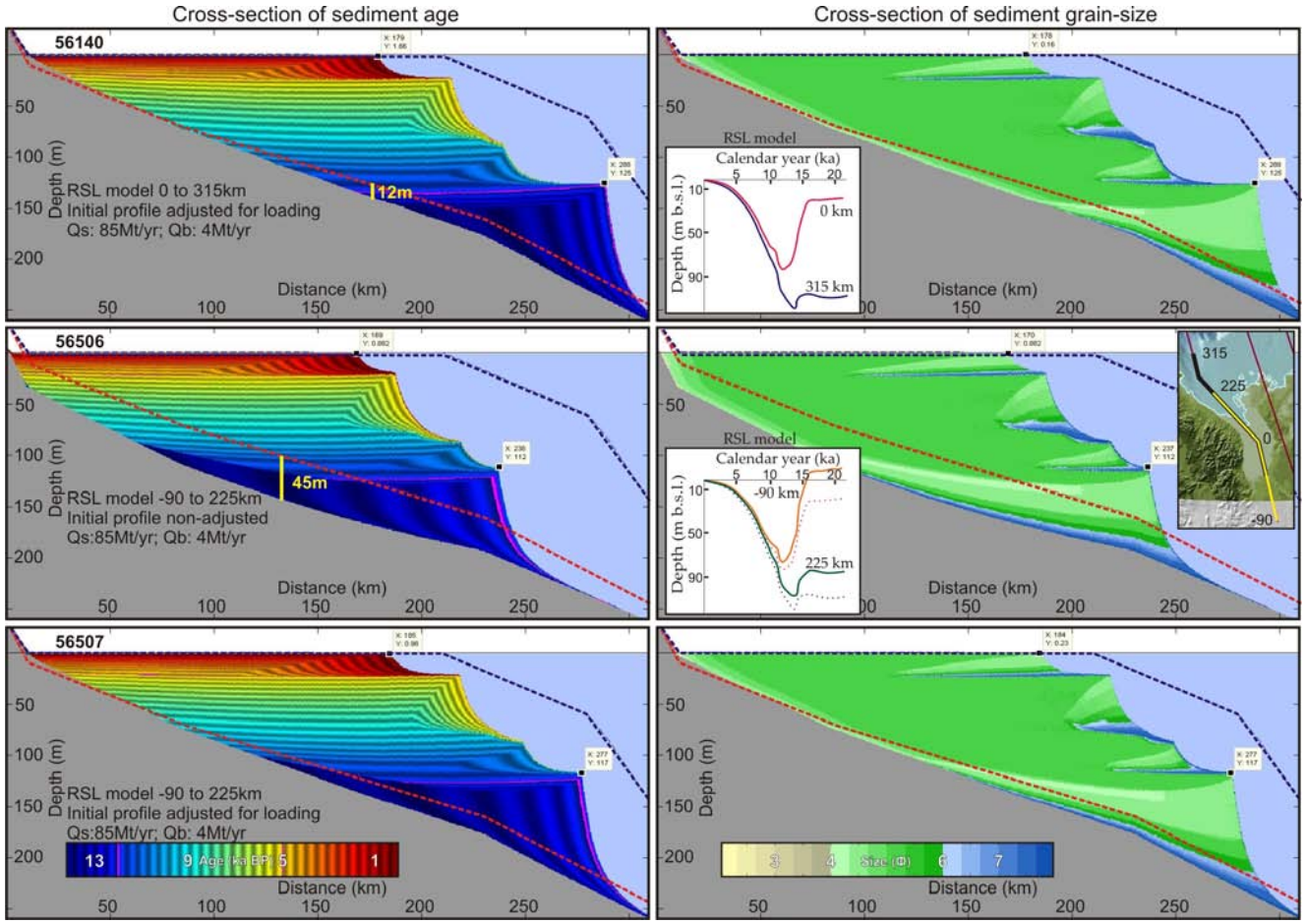

Figure A17: Sensitivity test on the RSL model transect section and associated additional loading. This test provides additional information to Figure A10 test in terms of the additional loading induced by using a different section of the RSL model. Simulation 56140 uses the original transect section of the RSL model. Simulation 56506 uses the RSL model data starting 90 km south on the initial profile of 56140. Simulation 56507 presents 56506 on a modified initial profile compensating for the additional loading. All simulations used larger sediment supply per epochs (0/4/3/1 time the Carson et al. (1999) estimate).

Table A18:More extensive ice margins and/or different parametization of earth structure with high Qs

Files	56140	56506	56507
Summary of processes	**Regular subsidence file; Initial profile compensated for loading; Qs: 85Mt/yr; Qb: 4Mt/yr (Carson et al. 1999); Epoch sediment supply: 0/4/3/1X**	**Southern subsidence file; no additional compensation for loading; Qs: 85Mt/yr; Qb: 4Mt/yr (Carson et al. 1999); Epoch sediment supply: 0/4/3/1X**	**Southern subsidence file; additional compensation for loading; Qs: 85Mt/yr; Qb: 4Mt/yr (Carson et al. 1999); Epoch sediment supply: 0/4/3/1X**
INITIATION FILE			
bathymetry file	(compensated) beaufort_bathy.csv	(compensated) beaufort_bathy.csv	(additional compensation) beaufort_bathy.csv
PROCESS FILE			
[sea level]			
active	no	no	no
sea level file	beaufort_sea_level.csv	beaufort_sea_level.csv	beaufort_sea_level.csv
[Subsidence]			
active:	yes	yes	yes
Subsidence file	rates_sedflux_MT21000.dat	rates_sedflux_MTlong21000_first315km	rates_sedflux_MTlong21000_first315km
[compaction]			
active	no	no	no
[isostasy]			
active	yes	yes	yes
enable water loading	no	no	no
[river 0]			
active	yes	yes	yes
river file	beaufort_river.kvf	beaufort_river.kvf	beaufort_river.kvf
[bedload dumping]			
active	0y->6700y	0y->6700y	0y->6700y
distance to dump bedload (m)	5000	5000	5000
ratio of flood plain to bedload rate	0.22	0.22	0.22
fraction of bedload retained in the delta plain	0	0	0
[river 1]			
active	6700yr -> 9000yr	6700yr -> 9000yr	6700yr -> 9000yr
river file	beaufort_river2.kvf	beaufort_river2.kvf	beaufort_river2.kvf
[bedload dumping]			
active	6700yr -> 9000yr	6700yr -> 9000yr	6700yr -> 9000yr
distance to dump bedload (m)	5000	5000	5000
ratio of flood plain to bedload rate	0.22	0.22	0.22
fraction of bedload retained in the delta plain	0	0	0
[river 2]			
active	9000yr -> 16000y	9000yr -> 16000y	9000yr -> 16000y
river file	beaufort_river3.kvf	beaufort_river3.kvf	beaufort_river3.kvf
[bedload dumping]			
active	9000yr -> 16000y	9000yr -> 16000y	9000yr -> 16000y

distance to dump bedload (m)	5000	5000	5000
ratio of flood plain to bedload rate	0.22	0.22	0.22
fraction of bedload retained in the delta plain	0	0	0
[river 3]			
active	16000y -> 21000y	16000y -> 21000y	16000y -> 21000y
river file	beaufort_river4.kvf	beaufort_river4.kvf	beaufort_river4.kvf
[bedload dumping]			
active	16000y -> 21000y	16000y -> 21000y	16000y -> 21000y
distance to dump bedload (m)	5000	5000	5000
ratio of flood plain to bedload rate	0.22	0.22	0.22
fraction of bedload retained in the delta plain	0	0	0
[plume]			
active	yes	yes	yes
hyperpycnal plume model	<none>	<none>	<none>
hypopycnal plume model	'hypopycnal plume'	'hypopycnal plume'	'hypopycnal plume'
[Failure]			
active:	no	no	no
[debris flow]			
active:	no	no	no
[turbidity current]			
active:	no	no	no
RIVER FILES			
River0			
['Season 1']			
Duration (y)	1y	1y	1y
Bedload (kg/s)	0	0	0
Suspended load concentration (kg/m^3)	0	0	0
velocity (m/s)	0.7	0.7	0.7
Width (m)	2000	2000	2000
Depth (m)	8	8	8
River1			
['Season 1']			
Duration (y)	1y	1y	1y
Bedload (kg/s)	520	520	520
Suspended load concentration (kg/m^3)	0.09628, 0.5776, 0.2888	0.09628, 0.5776, 0.2888	0.09628, 0.5776, 0.2888
velocity (m/s)	0.7	0.7	0.7
Width (m)	2000	2000	2000
Depth (m)	8	8	8
River2			
['Season 1']			
Duration (y)	1y	1y	1y
Bedload (kg/s)	390	390	390
Suspended load concentration (kg/m^3)	0.07221, 0.4332, 0.2166	0.07221, 0.4332, 0.2166	0.07221, 0.4332, 0.2166
velocity (m/s)	0.7	0.7	0.7
Width (m)	2000	2000	2000

Depth (m)	8	8	8
River3			
['Season 1']			
Duration (y)	1y	1y	1y
Bedload (kg/s)	130	130	130
Suspended load	0.02407, 0.1444, 0.0722	0.02407, 0.1444, 0.0722	0.02407, 0.1444, 0.0722
concentration (kg/m^3)			
velocity (m/s)	0.7	0.7	0.7
Width (m)	2000	2000	2000
Depth (m)	8	8	8
SEDIMENT FILE			
[Grain 1 (bedload)]			
grain size (microns)	200	200	200
grain density (kg/m^3)	2650	2650	2650
saturated density (kg/m^3)	2000	2000	2000
minimum void ratio (-)	0.17	0.17	0.17
diffusion coefficient (-)	0.25	0.25	0.25
removal rate (1/day)	25	25	25
consolidation coefficient (m^2/yr)	100000	100000	100000
compaction coefficient (-)	0.000000062	0.000000062	0.000000062
[Grain 2 (suspended)]			
grain size (microns)	150	150	150
grain density (kg/m^3)	2650	2650	2650
saturated density (kg/m^3)	1955	1955	1955
minimum void ratio (-)	0.15	0.15	0.15
diffusion coefficient (-)	0.25	0.25	0.25
removal rate (1/day)	20	20	20
consolidation coefficient (m^2/yr)	100000	100000	100000
compaction coefficient (-)	0.00000007	0.00000007	0.00000007
[Grain 3 (suspended)]			
grain size (microns)	60	60	60
grain density (kg/m^3)	2650	2650	2650
saturated density (kg/m^3)	1795	1795	1795
minimum void ratio (-)	0.1	0.1	0.1
diffusion coefficient (-)	0.25	0.25	0.25
removal rate (1/day)	12	12	12
consolidation coefficient (m^2/yr)	100000	100000	100000
compaction coefficient (-)	0.00000008	0.00000008	0.00000008
[Grain 4 (suspended)]			
grain size (microns)	5	5	5
grain density (kg/m^3)	2650	2650	2650
saturated density (kg/m^3)	1504	1504	1504
minimum void ratio (-)	0.05	0.05	0.05
diffusion coefficient (-)	0.25	0.25	0.25
removal rate (1/day)	3.2	3.2	3.2
consolidation coefficient (m^2/yr)	100000	100000	100000
compaction coefficient (-)	0.00000036	0.00000036	0.00000036

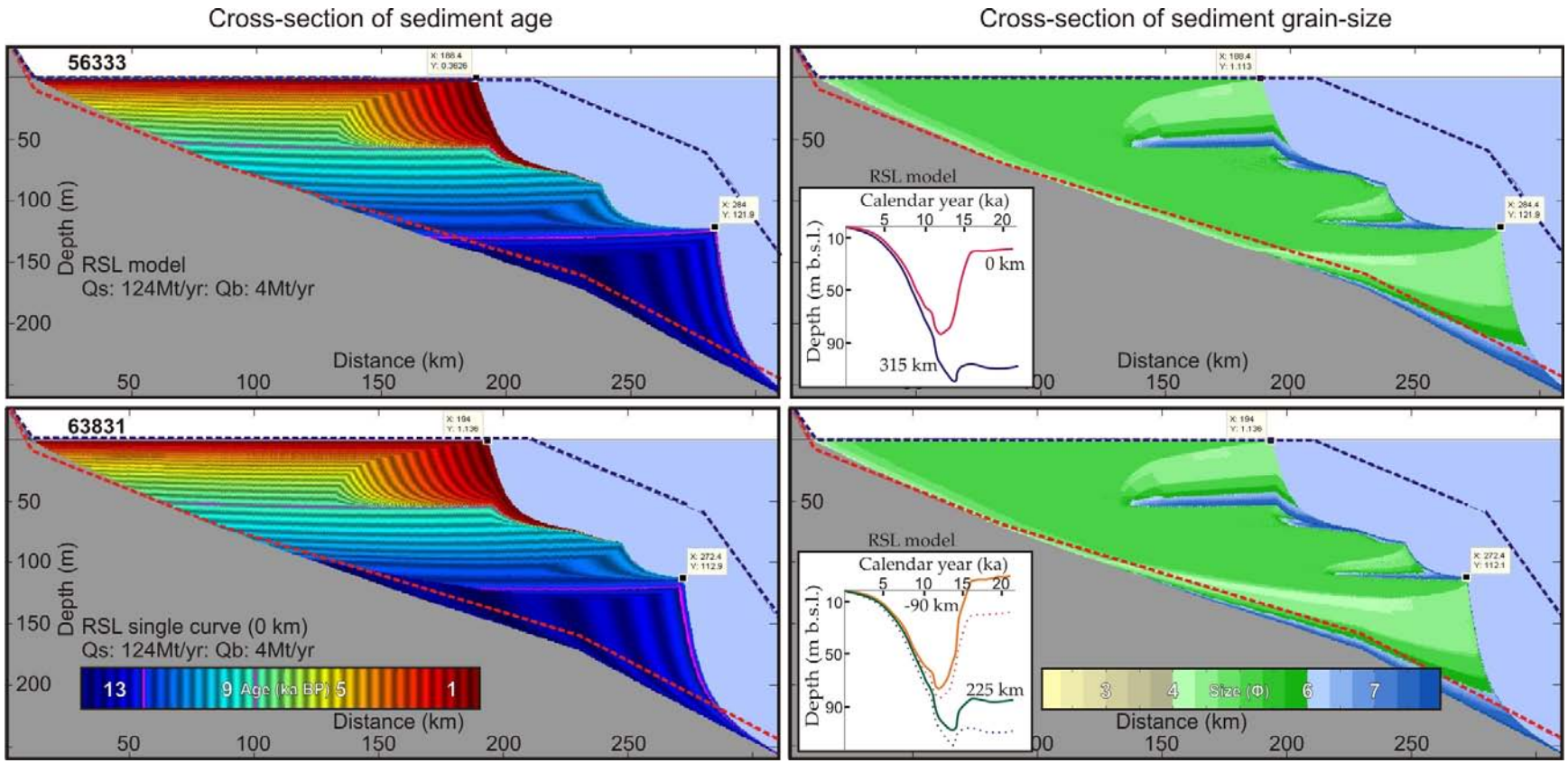

Figure A18: Sensitivity test on using a RSL model representing more extensive ice. Simulation 56333 is the base-case simulation and uses the original section of the RSL model. Simulation 63831 uses the RSL model data starting 90 km south. All simulations use the base-case simulation sediment supply epochs (0/2.5/2/1 X Carson et al. (1998)). The locations of the seismic basal reflector from which the initial profile was derived (Hill et al., 2001; red dotted line) and the modern seafloor profile (blue dotted line) are displayed. As a reference, the RSL graph presents the RSL curves corresponding to each extremity of the transect.

Table A19: More extensive ice margins and/or different parametization of earth structure with base-case simulation Qs

Files	**56333**	**63831**
Summary of processes	**Original RSL model; Qs: 124Mt/yr; Qb: 4Mt/yr (Carson et al. 1998);**	**Southern RSL model; Qs: 124Mt/yr; Qb: 4Mt/yr (Carson et al. 1998);**
INITIATION FILE bathymetry file	(compensated) beaufort_bathy.csv	(compensated) beaufort_bathy.csv
PROCESS FILE		
[sea level]		
active	no	no
sea level file	beaufort_sea_level.csv	beaufort_sea_level.csv
[Subsidence]		
active:	yes	yes
Subsidence file	rates_sedflux_MT21000.dat	rates_sedflux_MTlong21000_first315km
[compaction]		
active	no	yes
[isostasy]		
active	yes	yes
enable water loading	no	no
[river 0]		
active	yes	yes
river file	beaufort_river.kvf	beaufort_river.kvf
[bedload dumping]		
active	0y->6700y	0y->6700y
distance to dump bedload (m)	5000	5000
ratio of flood plain to bedload rate	0	0
fraction of bedload retained in the delta plain	0	0
[river 1]		
active	6700yr -> 9000yr	6700yr -> 9000yr
river file	beaufort_river2.kvf	beaufort_river2.kvf
[bedload dumping]		
active	6700yr -> 9000yr	6700yr -> 9000yr
distance to dump bedload (m)	5000	5000
ratio of flood plain to bedload rate	0	0
fraction of bedload retained in the delta plain	0	0
[river 2]		
active	9000yr -> 13000y	9000yr -> 13000y
river file	beaufort_river3.kvf	beaufort_river3.kvf
[bedload dumping]		
active	9000yr -> 13000y	9000yr -> 13000y
distance to dump bedload (m)	5000	5000
ratio of flood plain to bedload rate	0	0
fraction of bedload retained in the delta plain	0	0
[river 3]		
active	13000y -> 21000y	13000y -> 21000y
river file	beaufort_river4.kvf	beaufort_river4.kvf
[bedload dumping]		

active	13000y -> 21000y	13000y -> 21000y
distance to dump bedload (m)	5000	5000
ratio of flood plain to bedload rate	0	0
fraction of bedload retained in the delta plain	0	0
[plume]		
active	yes	yes
hyperpycnal plume model	<none>	<none>
hypopycnal plume model	'hypopycnal plume'	'hypopycnal plume'
[Failure]		
active:	no	no
[debris flow]		
active:	no	no
[turbidity current]		
active:	no	no
RIVER FILES		
River0		
['Season 1']		
Duration (y)	1y	1y
Bedload (kg/s)	0	0
Suspended load concentration (kg/m^3)	0	0
velocity (m/s)	0.7	0.7
Width (m)	2000	2000
Depth (m)	8	8
River1		
['Season 1']		
Duration (y)	1y	1y
Bedload (kg/s)	500	500
Suspended load concentration (kg/m^3)	0.0878, 0.526, 0.263	0.0878, 0.526, 0.263
velocity (m/s)	0.7	0.7
Width (m)	2000	2000
Depth (m)	8	8
River2		
['Season 1']		
Duration (y)	1y	1y
Bedload (kg/s)	400	400
Suspended load concentration (kg/m^3)	0.07024, 0.4208, 0.2104	0.07024, 0.4208, 0.2104
velocity (m/s)	0.7	0.7
Width (m)	2000	2000
Depth (m)	8	8
River3		
['Season 1']		
Duration (y)	1y	1y
Bedload (kg/s)	200	200
Suspended load concentration (kg/m^3)	0.03512, 0.2104, 0.1052	0.03512, 0.2104, 0.1052
velocity (m/s)	0.7	0.7
Width (m)	2000	2000
Depth (m)	8	8

SEDIMENT FILE		
[Grain 1 (bedload)]		
grain size (microns)	200	200
grain density (kg/m^3)	2650	2650
saturated density (kg/m^3)	2000	2000
minimum void ratio (-)	0.17	0.17
diffusion coefficient (-)	0.25	0.25
removal rate (1/day)	25	25
consolidation coefficient (m^2/yr)	100000	100000
compaction coefficient (-)	0.000000062	0.000000062
[Grain 2 (suspended)]		
grain size (microns)	150	150
grain density (kg/m^3)	2650	2650
saturated density (kg/m^3)	1955	1955
minimum void ratio (-)	0.15	0.15
diffusion coefficient (-)	0.25	0.25
removal rate (1/day)	20	20
consolidation coefficient (m^2/yr)	100000	100000
compaction coefficient (-)	0.00000007	0.00000007
[Grain 3 (suspended)]		
grain size (microns)	60	60
grain density (kg/m^3)	2650	2650
saturated density (kg/m^3)	1795	1795
minimum void ratio (-)	0.1	0.1
diffusion coefficient (-)	0.25	0.25
removal rate (1/day)	12	12
consolidation coefficient (m^2/yr)	100000	100000
compaction coefficient (-)	0.00000008	0.00000008
[Grain 4 (suspended)]		
grain size (microns)	5	5
grain density (kg/m^3)	2650	2650
saturated density (kg/m^3)	1504	1504
minimum void ratio (-)	0.05	0.05
diffusion coefficient (-)	0.25	0.25
removal rate (1/day)	3.2	3.2
consolidation coefficient (m^2/yr)	100000	100000
compaction coefficient (-)	0.00000036	0.00000036

Outburst flood periods (Fig. A19 and A20)

The effects of potential outburst floods on the stratigraphy using Figure A19 are discussed in length in the stratigraphy paper (Picard and Hill, in prep). Simulation 61641 however used a fine grain-size distribution for the outburst flood events, not considering that higher discharges have a higher power of erosion and transportation, thus are more likely to carry coarser sediments (Milliman and Farnsworth, 2011). Simulation 61642 therefore presents the results using coarser grain-size distribution than 61641 during the outburst flood events. During these two short periods, because SedFlux cannot change the composition of the grain-size, the distribution of the load was altered toward the coarser grain-size already in used. Instead of a distribution of 5, 10, 58, and 27 % for the phi sizes of 2.3, 2.75, 4, and 7.6 respectively, the load for each of these sizes was set in accordance to the following percentages: 10, 58, 27, and 5 %. As expected after interpreting the results of the grain-size test presented in Figure A15, the use of coarser distribution of material reduces the total volume occupied by the sediments.

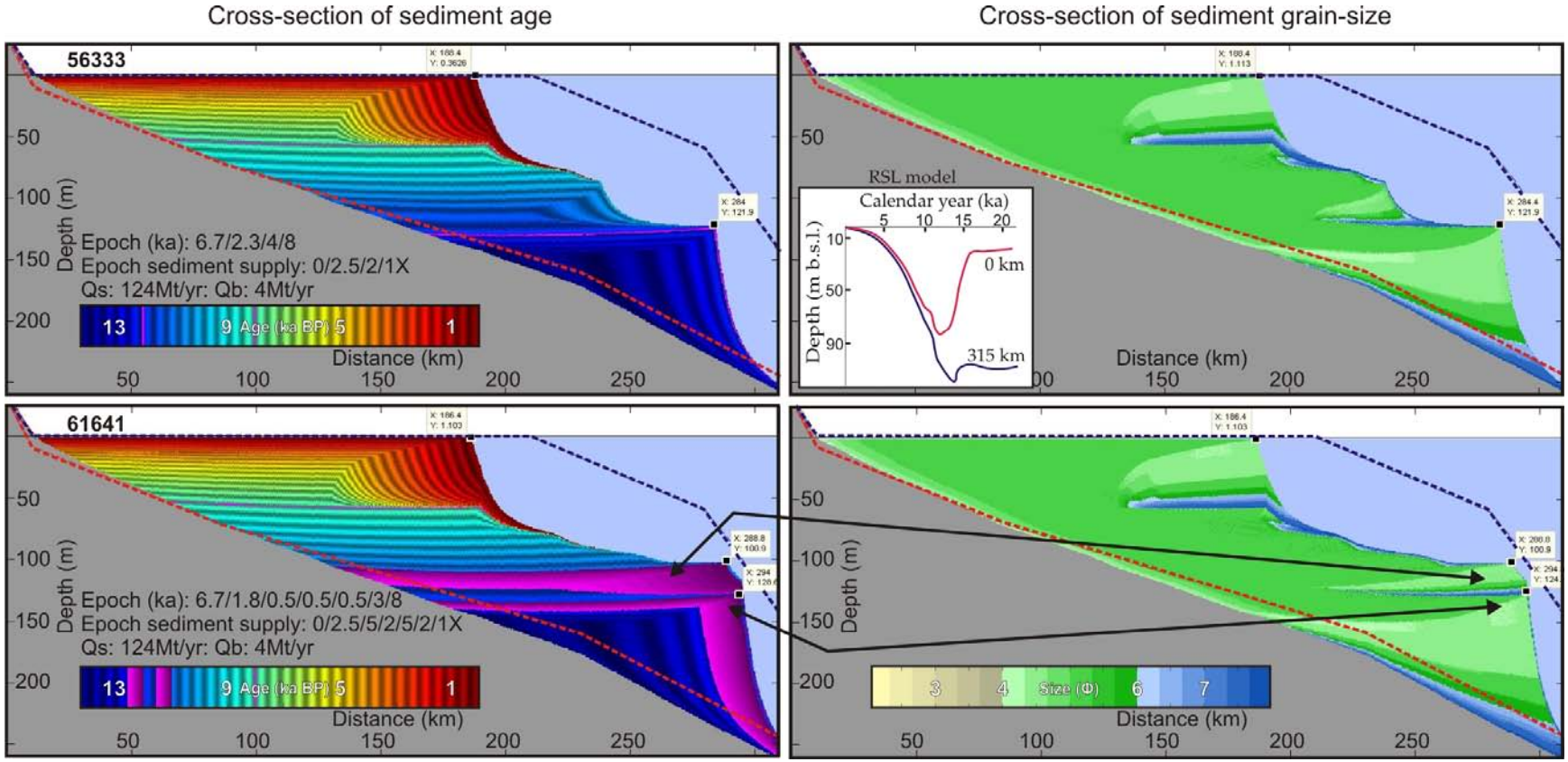

Figure A19: Sensitivity test on short high sediment supply outburst events of 500 years. Simulation 56333 represents a standard simulation with 4 epochs. The two intermediate epochs, representing periods of higher sediment supply due to the availability of large quantities of glacial material as well as the occurrence of glacial outburst floods (Murton et al., 2010). Simulation 61641 simulates specifically two short outburst events delivering higher sediment supply over a 500 year period (pink strata on the age cross-section).The locations of the seismic basal reflector from which the initial profile was derived (Hill et al., 2001; red dotted line) and the modern seafloor profile (blue dotted line) are displayed. As a reference, the RSL graph presents the RSL curves corresponding to each extremity of the transect.

Table A20: Outburst flood events

Files	56333	61641
Summary of processes	**Epoch sediment supply: 0/2.5/2/1X; Epoch length: 6.7/2.3/4/8ka; Qs: 124Mt/yr; Qb: 4Mt/yr (Carson et al. 1998);**	**Epoch sediment supply: 0/2.5/5/2/5/2/1X; Epoch length: 6.7/1.8/0.5/0.5/0.5/3/8ka; Qs: 124Mt/yr; Qb: 4Mt/yr (Carson et al. 1998);**
INITIATION FILE		
bathymetry file	(compensated) beaufort_bathy.csv	(compensated) beaufort_bathy.csv
PROCESS FILE		
[sea level]		
active	no	no
sea level file	beaufort_sea_level.csv	beaufort_sea_level.csv
[Subsidence]		
active:	yes	yes
Subsidence file	rates_sedflux_MT21000.dat	rates_sedflux_MT21000.dat
[compaction]		
active	no	no
logging	yes	yes
repeat interval	25y	25y
[isostasy]		
active	yes	yes
enable water loading	no	no
[river 0]		
active	yes	yes
river file	beaufort_river.kvf	beaufort_river.kvf
[bedload dumping]		
active	0y->6700y	0y->6700y
distance to dump bedload (m)	5000	5000
ratio of flood plain to bedload rate	0	0
fraction of bedload retained in the delta plain	0	0
[river 1]		
active	6700yr -> 9000yr	6700yr -> 8500yr
river file	beaufort_river2.kvf	beaufort_river2.kvf
[bedload dumping]		
active	6700yr -> 9000yr	6700yr -> 8500yr
distance to dump bedload (m)	5000	5000
ratio of flood plain to bedload rate	0	0
fraction of bedload retained in the delta plain	0	0
[river 2]		
active	9000yr -> 13000y	8500yr -> 9000y
river file	beaufort_river3.kvf	beaufort_river3.kvf
[bedload dumping]		
active	9000yr -> 13000y	8500yr -> 9000y
distance to dump bedload (m)	5000	5000
ratio of flood plain to bedload rate	0	2
fraction of bedload retained in the delta plain	0	0
[river 3]		
active	13000y -> 21000y	9000y -> 9500y
river file	beaufort_river4.kvf	beaufort_river4.kvf

[bedload dumping]		
active	13000y -> 21000y	9000y -> 9500y
distance to dump bedload (m)	5000	5000
ratio of flood plain to bedload rate	0	0
fraction of bedload retained in the delta plain	0	0
[river 4]		
active		9500y -> 10000y
river file		beaufort_river5.kvf
[bedload dumping]		
active		9500y -> 10000y
distance to dump bedload (m)		5000
ratio of flood plain to bedload rate		2
fraction of bedload retained in the delta plain		0
[river 5]		
active		10000y -> 13000y
river file		beaufort_river6.kvf
[bedload dumping]		
active		10000y -> 13000y
distance to dump bedload (m)		5000
ratio of flood plain to bedload rate		0
fraction of bedload retained in the delta plain		0
[river 6]		
active		13000y -> 21000y
river file		beaufort_river7.kvf
[bedload dumping]		
active		13000y -> 21000y
distance to dump bedload (m)		5000
ratio of flood plain to bedload rate		0
fraction of bedload retained in the delta plain		0
[plume]		
active	yes	yes
hyperpycnal plume model	<none>	<none>
hypopycnal plume model	'hypopycnal plume'	'hypopycnal plume'
[Failure]		
active:	no	no
[debris flow]		
active:	no	no
[turbidity current]		
active:	no	no
RIVER FILES		
River0		
['Season 1']		
Duration (y)	1y	1y
Bedload (kg/s)	0	0
Suspended load concentration (kg/m^3)	0	0
velocity (m/s)	0.7	0.7

Width (m)			2000			2000
Depth (m)			8			8
River1						
['Season 1']						
Duration (y)			1y			1y
Bedload (kg/s)			500			500
Suspended load concentration (kg/m^3)	0.0878,	0.526,	0.263	0.0878,	0.526,	0.263
velocity (m/s)			0.7			0.7
Width (m)			2000			2000
Depth (m)			8			8
River2						
['Season 1']						
Duration (y)			1y			1y
Bedload (kg/s)			400			1000
Suspended load concentration (kg/m^3)	0.07024,	0.4208,	0.2104	0.1756,	0.1052,	0.526
velocity (m/s)			0.7			0.7
Width (m)			2000			2000
Depth (m)			8			8
River3						
['Season 1']						
Duration (y)			1y			1y
Bedload (kg/s)			200			400
Suspended load concentration (kg/m^3)	0.03512,	0.2104,	0.1052	0.07024,	0.4208,	0.2104
velocity (m/s)			0.7			0.7
Width (m)			2000			2000
Depth (m)			8			8
River4						
['Season 1']						1y
Duration (y)						1000
Bedload (kg/s)				0.1756,	0.1052,	0.526
Suspended load concentration (kg/m^3)						0.7
velocity (m/s)						2000
Width (m)						8
Depth (m)						
River5						
['Season 1']						1y
Duration (y)						400
Bedload (kg/s)				0.07024,	0.4208,	0.2104
Suspended load concentration (kg/m^3)						0.7
velocity (m/s)						2000
Width (m)						8
Depth (m)						
River6						
['Season 1']						1y
Duration (y)						200
Bedload (kg/s)				0.03512,	0.2104,	0.1052
Suspended load concentration (kg/m^3)						0.7
velocity (m/s)						2000
Width (m)						8

Depth (m)		
SEDIMENT FILE		
[Grain 1 (bedload)]		
grain size (microns)	200	200
grain density (kg/m^3)	2650	2650
saturated density (kg/m^3)	2000	2000
minimum void ratio (-)	0.17	0.17
diffusion coefficient (-)	0.25	0.25
removal rate (1/day)	25	25
consolidation coefficient (m^2/yr)	100000	100000
compaction coefficient (-)	0.000000062	0.000000062
[Grain 2 (suspended)]		
grain size (microns)	150	150
grain density (kg/m^3)	2650	2650
saturated density (kg/m^3)	1955	1955
minimum void ratio (-)	0.15	0.15
diffusion coefficient (-)	0.25	0.25
removal rate (1/day)	20	20
consolidation coefficient (m^2/yr)	100000	100000
compaction coefficient (-)	0.00000007	0.00000007
[Grain 3 (suspended)]		
grain size (microns)	60	60
grain density (kg/m^3)	2650	2650
saturated density (kg/m^3)	1795	1795
minimum void ratio (-)	0.1	0.1
diffusion coefficient (-)	0.25	0.25
removal rate (1/day)	12	12
consolidation coefficient (m^2/yr)	100000	100000
compaction coefficient (-)	0.00000008	0.00000008
[Grain 4 (suspended)]		
grain size (microns)		5
grain density (kg/m^3)	2650	2650
saturated density (kg/m^3)	1504	1504
minimum void ratio (-)	0.05	0.05
diffusion coefficient (-)	0.25	0.25
removal rate (1/day)	3.2	3.2
consolidation coefficient (m^2/yr)	100000	100000
compaction coefficient (-)	0.00000036	0.00000036

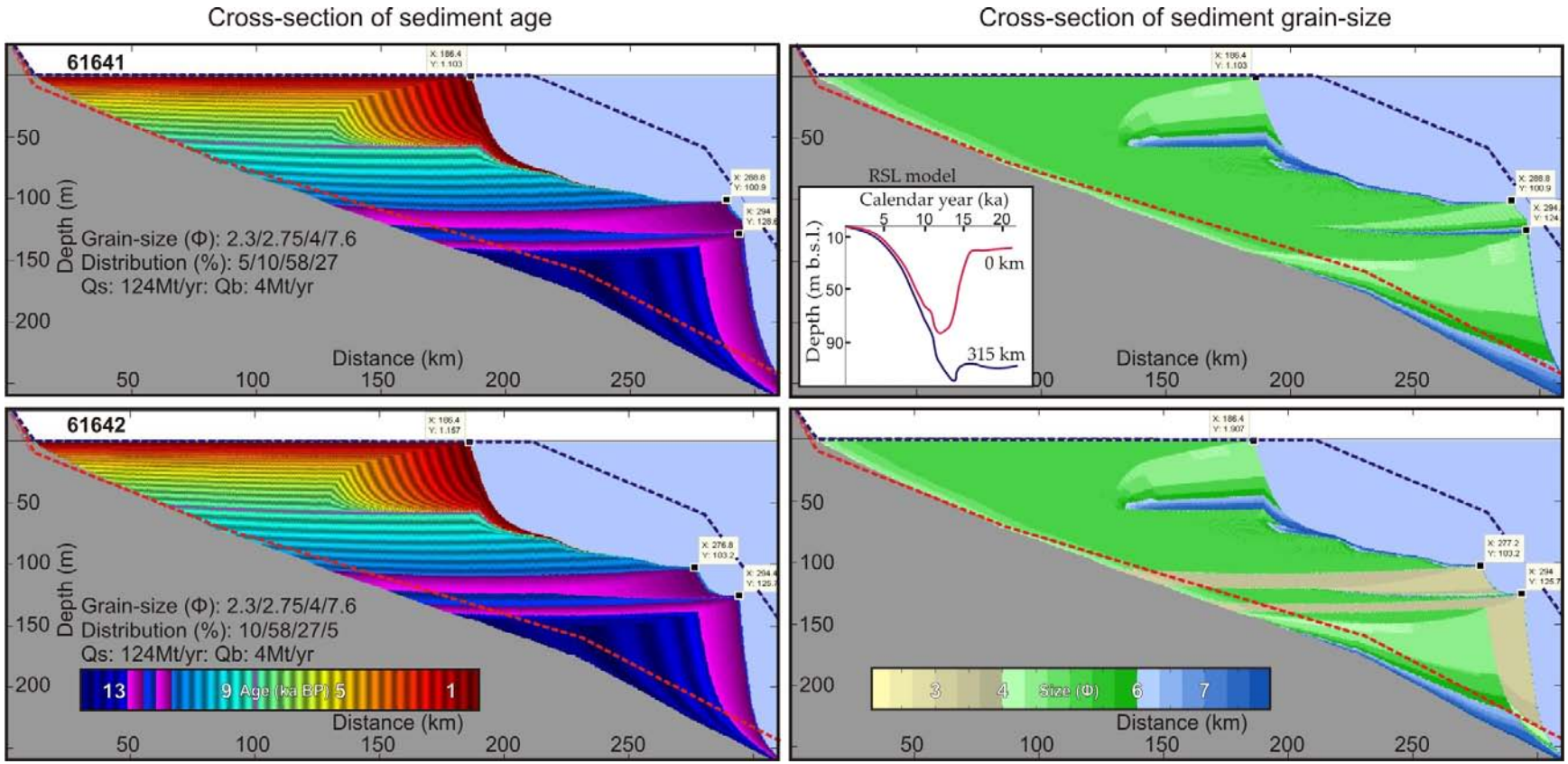

Figure A20: Sensitivity test on short outburst events with coarser grain-size. Simulation 61641 simulates two short outburst events delivering higher sediment supply, with the same fine grain-size distribution used in other simulations, over a 500 year period (pink strata on the age cross-section). Simulation 61642 simulates the two short outburst events, but with a coarser grain-size distribution. The locations of the seismic basal reflector from which the initial profile was derived (Hill et al., 2001; red dotted line) and the modern seafloor profile (blue dotted line) are displayed. As a reference, the RSL graph presents the RSL curves corresponding to each extremity of the transect.

Table A21: Outburst flood events with coarser grain-size

Files	**61641**	**61642**
Summary of processes	**Grain-size: 200/150/60/5 um; Distribution: 5/10/58/27; Qs: 124Mt/yr; Qb: 4Mt/yr (Carson et al. 1998);**	**Grain-size: 200/150/60/5 um; Distribution: 10/58/27/5; Qs: 124Mt/yr; Qb: 4Mt/yr (Carson et al. 1998);**
INITIATION FILE		
bathymetry file	(compensated) beaufort_bathy.csv	(compensated) beaufort_bathy.csv
PROCESS FILE		
[sea level]		
active	no	no
sea level file	beaufort_sea_level.csv	beaufort_sea_level.csv
[Subsidence]		
active:	yes	yes
Subsidence file	rates_sedflux_MT21000.dat	rates_sedflux_MT21000.dat
[compaction]		
active	no	no
logging	yes	yes
repeat interval	25y	25y
[isostasy]		
active	yes	yes
enable water loading	no	no
[river 0]		
active	yes	yes
river file	beaufort_river.kvf	beaufort_river.kvf
[bedload dumping]		
active	0y->6700y	0y->6700y
distance to dump bedload (m)	5000	5000
ratio of flood plain to bedload rate	0	0
fraction of bedload retained in the delta plain	0	0
[river 1]		
active	6700yr -> 8500yr	6700yr -> 8500yr
river file	beaufort_river2.kvf	beaufort_river2.kvf
[bedload dumping]		
active	6700yr -> 8500yr	6700yr -> 8500yr
distance to dump bedload (m)	5000	5000
ratio of flood plain to bedload rate	0	0
fraction of bedload retained in the delta plain	0	0
[river 2]		
active	8500yr -> 9000y	8500yr -> 9000y
river file	beaufort_river3.kvf	beaufort_river3.kvf
[bedload dumping]		
active	8500yr -> 9000y	8500yr -> 9000y
distance to dump bedload (m)	5000	5000
ratio of flood plain to bedload rate	2	2
fraction of bedload retained in the delta plain	0	0
[river 3]		
active	9000y -> 9500y	9000y -> 9500y
river file	beaufort_river4.kvf	beaufort_river4.kvf

[bedload dumping]		
active	9000y -> 9500y	9000y -> 9500y
distance to dump bedload (m)	5000	5000
ratio of flood plain to bedload rate	0	0
fraction of bedload retained in the delta plain	0	0
[river 4]		
active	9500y -> 10000y	9500y -> 10000y
river file	beaufort_river5.kvf	beaufort_river5.kvf
[bedload dumping]		
active	9500y -> 10000y	9500y -> 10000y
distance to dump bedload (m)	5000	5000
ratio of flood plain to bedload rate	2	2
fraction of bedload retained in the delta plain	0	0
[river 5]		
active	10000y -> 13000y	10000y -> 13000y
river file	beaufort_river6.kvf	beaufort_river6.kvf
[bedload dumping]		
active	10000y -> 13000y	10000y -> 13000y
distance to dump bedload (m)	5000	5000
ratio of flood plain to bedload rate	0	0
fraction of bedload retained in the delta plain	0	0
[river 6]		
active	13000y -> 21000y	13000y -> 21000y
river file	beaufort_river7.kvf	beaufort_river7.kvf
[bedload dumping]		
active	13000y -> 21000y	13000y -> 21000y
distance to dump bedload (m)	5000	5000
ratio of flood plain to bedload rate	0	0
fraction of bedload retained in the delta plain	0	0
[plume]		
active	yes	yes
hyperpycnal plume model	<none>	<none>
hypopycnal plume model	'hypopycnal plume'	'hypopycnal plume'
[Failure]		
active:	no	no
[debris flow]		
active:	no	no
[turbidity current]		
active:	no	no
RIVER FILES		
River0		
['Season 1']		
Duration (y)	1y	1y
Bedload (kg/s)	0	0
Suspended load concentration (kg/m^3)	0	0
velocity (m/s)	0.7	0.7
Width (m)	2000	2000
Depth (m)	8	8

River1		
['Season 1']		
Duration (y)	1y	1y
Bedload (kg/s)	500	500
Suspended load concentration (kg/m^3)	0.0878, 0.526, 0.263	0.0878, 0.526, 0.263
velocity (m/s)	0.7	0.7
Width (m)	2000	2000
Depth (m)	8	8
River2		
['Season 1']		
Duration (y)	1y	1y
Bedload (kg/s)	1000	2048
Suspended load concentration (kg/m^3)	0.1756, 0.1052, 0.526	1.06887, 0.49758, 0.0921445
velocity (m/s)	0.7	0.7
Width (m)	2000	2000
Depth (m)	8	8
River3		
['Season 1']		
Duration (y)	1y	1y
Bedload (kg/s)	400	400
Suspended load concentration (kg/m^3)	0.07024, 0.4208, 0.2104	0.07024, 0.4208, 0.2104
velocity (m/s)	0.7	0.7
Width (m)	2000	2000
Depth (m)	8	8
River4		
['Season 1']	1y	1y
Duration (y)	1000	2048
Bedload (kg/s)	0.1756, 0.1052, 0.526	1.06887, 0.49758, 0.0921445
Suspended load concentration (kg/m^3)	0.7	0.7
velocity (m/s)	2000	2000
Width (m)	8	8
Depth (m)		
River5		
['Season 1']	1y	1y
Duration (y)	400	400
Bedload (kg/s)	0.07024, 0.4208, 0.2104	0.07024, 0.4208, 0.2104
Suspended load concentration (kg/m^3)	0.7	0.7
velocity (m/s)	2000	2000
Width (m)	8	8
Depth (m)		
River6		
['Season 1']	1y	1y
Duration (y)	200	200
Bedload (kg/s)	0.03512, 0.2104, 0.1052	0.03512, 0.2104, 0.1052
Suspended load concentration (kg/m^3)	0.7	0.7
velocity (m/s)	2000	2000
Width (m)	8	8
Depth (m)		

SEDIMENT FILE		
[Grain 1 (bedload)]		
grain size (microns)	200	200
grain density (kg/m^3)	2650	2650
saturated density (kg/m^3)	2000	2000
minimum void ratio (-)	0.17	0.17
diffusion coefficient (-)	0.25	0.25
removal rate (1/day)	25	25
consolidation coefficient (m^2/yr)	100000	100000
compaction coefficient (-)	0.000000062	0.000000062
[Grain 2 (suspended)]		
grain size (microns)	150	150
grain density (kg/m^3)	2650	2650
saturated density (kg/m^3)	1955	1955
minimum void ratio (-)	0.15	0.15
diffusion coefficient (-)	0.25	0.25
removal rate (1/day)	20	20
consolidation coefficient (m^2/yr)	100000	100000
compaction coefficient (-)	0.00000007	0.00000007
[Grain 3 (suspended)]		
grain size (microns)	60	60
grain density (kg/m^3)	2650	2650
saturated density (kg/m^3)	1795	1795
minimum void ratio (-)	0.1	0.1
diffusion coefficient (-)	0.25	0.25
removal rate (1/day)	12	12
consolidation coefficient (m^2/yr)	100000	100000
compaction coefficient (-)	0.00000008	0.00000008
[Grain 4 (suspended)]		
grain size (microns)	5	5
grain density (kg/m^3)	2650	2650
saturated density (kg/m^3)	1504	1504
minimum void ratio (-)	0.05	0.05
diffusion coefficient (-)	0.25	0.25
removal rate (1/day)	3.2	3.2
consolidation coefficient (m^2/yr)	100000	100000
compaction coefficient (-)	0.00000036	0.00000036

Slope failure, debris flow, and turbidity currents (Fig. A21 and A22)

The objective of this sensitivity test was to evaluate if slope failures, debris flows, and or turbidity currents occurred with the boundary conditions set for the simulations. The parameters used in each module are listed in Table A22 and A23 and were set based on default values taken from the CSDMS website (http://csdms.colorado.edu/trac/sedflux/wiki/SedfluxModuleList). Hutton and Syvitski (2004; 2008) provide details and examples on the modules.

Two tests were carried out to meet the objective. The first tested the response of the modules on simulations using the eustatic sea-level curve (Figure A21), whereas the second tested on simulations using the RSL model (Figure A22).

The results of both tests concluded that no slope failure, debris flow, and or turbidity currents were triggered under the boundary conditions set throughout the simulations. Even though the delta front of most system tracts shown on the Figures appears to be overly steepened, it is an illusion caused by the scale of the Figure. For example, in simulation 60339, the slope of the LST front at its steepest location (284 to 290 km) is only 1:100 or 1 % (Fig. A22). Hutton and Syvitski (2004) showed an example where failures occurred, but in their case, the slope was approximating 4.5 %. This sensitivity test also confirmed that no hyperpycnal flows were triggered at the river mouth.

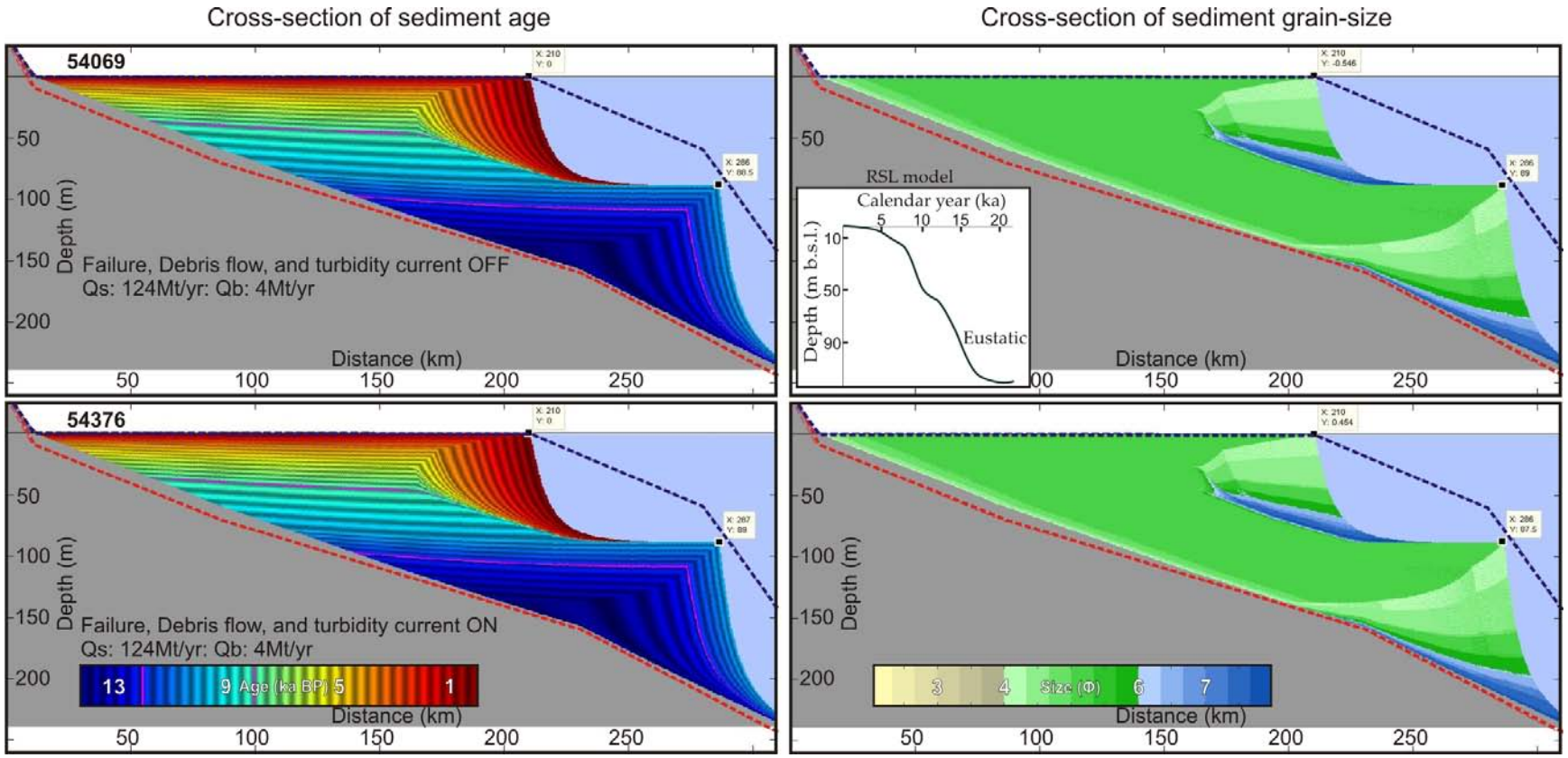

Figure A21: Sensitivity test on slope failure, debris flow and turbidity currents using the eustatic curve and variable sediment supply. Simulation 54069 does not calculate for slope failure, debris flow, or turbidity currents. Simulation 54376 calculates for slope failure, debris flow, or turbidity currents. The locations of the seismic basal reflector from which the initial profile was derived (Hill et al., 2001; red dotted line) and the modern seafloor profile (blue dotted line) are displayed. As a reference, the RSL graph presents the RSL curves corresponding to each extremity of the transect.

Table A22: Slope failures, debris flow, and turbidity currents using eustatic sea-level curve

Files	**54069**	**54376**
Summary of processes	**No Failure, debris flow, Turbidity currents; Eustatic curve; Qs: 124Mt/yr; Qb: 4Mt/yr (Carson et al. 1998);**	**Failure, debris flow, Turbidity currents; Eustatic curve; Qs: 124Mt/yr; Qb: 4Mt/yr (Carson et al. 1998);**
INITIATION FILE		
bathymetry file	(compensated) beaufort_bathy.csv	(compensated) beaufort_bathy.csv
PROCESS FILE		
[sea level]		
active	yes	yes
sea level file	beaufort_sea_level.csv	beaufort_sea_level.csv
[Subsidence]		
active:	no	no
Subsidence file	rates_sedflux_MT21000.dat	rates_sedflux_MT21000.dat
[compaction]		
active	no	no
[isostasy]		
active	yes	yes
enable water loading		
[river 0]		
active	yes	yes
river file	beaufort_river.kvf	beaufort_river.kvf
[bedload dumping]		
active	0y->6700y	0y->6700y
distance to dump bedload (m)	5000	5000
ratio of flood plain to bedload rate	0	0
fraction of bedload retained in the delta plain	0	0
[river 1]		
active	6700yr -> 9000yr	6700yr -> 9000yr
river file	beaufort_river2.kvf	beaufort_river2.kvf
[bedload dumping]		
active	6700yr -> 9000yr	6700yr -> 9000yr
distance to dump bedload (m)	10000	10000
ratio of flood plain to bedload rate	1	1
fraction of bedload retained in the delta plain	diffusion	diffusion
[river 2]		
active	9000yr -> 13000y	9000yr -> 13000y
river file	beaufort_river3.kvf	beaufort_river3.kvf
[bedload dumping]		
active	9000yr -> 13000y	9000yr -> 13000y
distance to dump bedload (m)	10000	10000
ratio of flood plain to bedload rate	1	1
fraction of bedload retained in the delta plain	diffusion	diffusion
[river 3]		
active	13000y -> 21000y	13000y -> 21000y
river file	beaufort_river4.kvf	beaufort_river4.kvf
[bedload dumping]		
active	13000y -> 21000y	13000y -> 21000y

distance to dump bedload (m)	10000	10000
ratio of flood plain to bedload rate	1	1
fraction of bedload retained in the delta plain	diffusion	diffusion
[plume]		
active	yes	yes
hyperpycnal plume model	<none>	<none>
hypopycnal plume model	'hypopycnal plume'	'hypopycnal plume'
[Failure]		
active:	no	yes
[debris flow]		
active:	no	yes
[turbidity current]		
active:	no	yes
RIVER FILES		
River0		
['Season 1']		
Duration (y)	1y	1y
Bedload (kg/s)	0	0
Suspended load concentration (kg/m^3)	0	0
velocity (m/s)	0.7	0.7
Width (m)	2000	2000
Depth (m)	8	8
River1		
['Season 1']		
Duration (y)	1y	1y
Bedload (kg/s)	500	500
Suspended load concentration (kg/m^3)	0.0878, 0.526, 0.263	0.0878, 0.526, 0.263
velocity (m/s)	0.7	0.7
Width (m)	2000	2000
Depth (m)	8	8
River2		
['Season 1']		
Duration (y)	1y	1y
Bedload (kg/s)	400	400
Suspended load concentration (kg/m^3)	0.07024, 0.4208, 0.2104	0.07024, 0.4208, 0.2104
velocity (m/s)	0.7	0.7
Width (m)	2000	2000
Depth (m)	8	8
River3		
['Season 1']		
Duration (y)	1y	1y
Bedload (kg/s)	200	200
Suspended load concentration (kg/m^3)	0.03512, 0.2104, 0.1052	0.03512, 0.2104, 0.1052
velocity (m/s)	0.7	0.7
Width (m)	2000	2000
Depth (m)	8	8

SEDIMENT FILE		
[Grain 1 (bedload)]		
grain size (microns)	300	300
grain density (kg/m^3)	2650	2650
saturated density (kg/m^3)	2094	2094
minimum void ratio (-)	0.2	0.2
diffusion coefficient (-)	0.25	0.25
removal rate (1/day)	35	35
consolidation coefficient (m^2/yr)	100000	100000
compaction coefficient (-)	0.00000005	0.00000005
[Grain 2 (suspended)]		
grain size (microns)	150	150
grain density (kg/m^3)	2650	2650
saturated density (kg/m^3)	1955	1955
minimum void ratio (-)	0.15	0.15
diffusion coefficient (-)	0.25	0.25
removal rate (1/day)	20	20
consolidation coefficient (m^2/yr)	100000	100000
compaction coefficient (-)	0.00000007	0.00000007
[Grain 3 (suspended)]		
grain size (microns)	60	60
grain density (kg/m^3)	2650	2650
saturated density (kg/m^3)	1795	1795
minimum void ratio (-)	0.1	0.1
diffusion coefficient (-)	0.25	0.25
removal rate (1/day)	12	12
consolidation coefficient (m^2/yr)	100000	100000
compaction coefficient (-)	0.00000008	0.00000008
[Grain 4 (suspended)]		
grain size (microns)	5	5
grain density (kg/m^3)	2650	2650
saturated density (kg/m^3)	1504	1504
minimum void ratio (-)	0.05	0.05
diffusion coefficient (-)	0.25	0.25
removal rate (1/day)	3.2	3.2
consolidation coefficient (m^2/yr)	100000	100000
compaction coefficient (-)	0.00000036	0.00000036

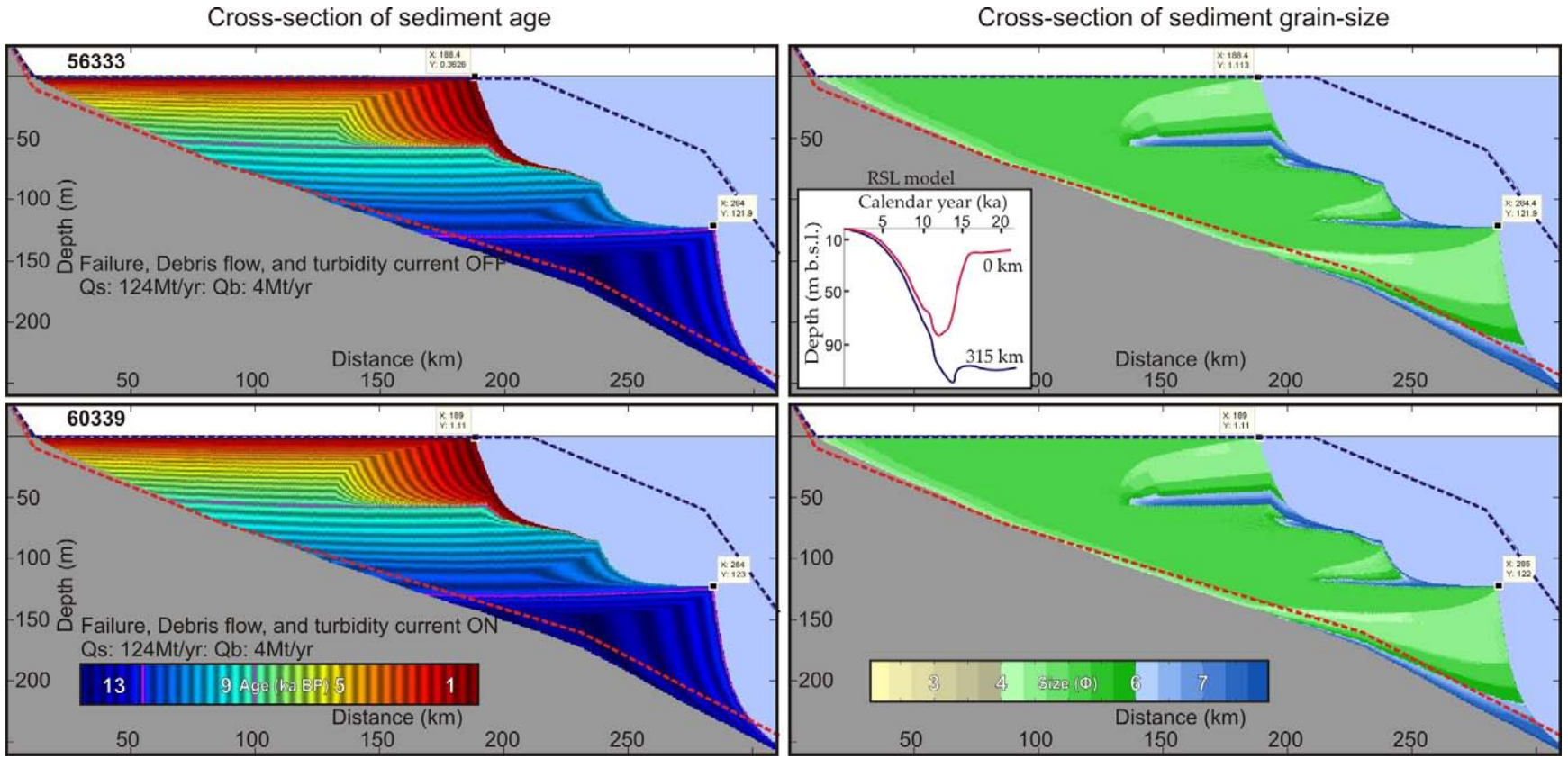

Figure A22: Sensitivity test on slope failure, debris flow and turbidity currents using the RSL model and variable sediment supply. Simulation 56333 does not calculate for slope failure, debris flow, or turbidity currents. Simulation 60339 calculates for slope failure, debris flow, or turbidity currents. Both simulations were run using the RSL model. The locations of the seismic basal reflector from which the initial profile was derived (Hill et al., 2001; red dotted line) and the modern seafloor profile (blue dotted line) are displayed. As a reference, the RSL graph presents the RSL curves corresponding to each extremity of the transect.

Table A23: Slope failure, debris flow, and turbidity currents using RSL model

Files	**56333**	**60339**
Summary of processes	**No Failure, debris flow, Turbidity currents; RSL model; Qs: 124Mt/yr; Qb: 4Mt/yr (Carson et al. 1998);**	**Failure, debris flow, Turbidity currents; RSL model; Qs: 124Mt/yr; Qb: 4Mt/yr (Carson et al. 1998);**
INITIATION FILE		
bathymetry file	(compensated) beaufort_bathy.csv	(compensated) beaufort_bathy.csv
PROCESS FILE		
[sea level]		
active	no	no
sea level file	beaufort_sea_level.csv	beaufort_sea_level.csv
[Subsidence]		
active:	yes	yes
Subsidence file	rates_sedflux_MT21000.dat	rates_sedflux_MT21000.dat
[compaction]		
active	no	no
[isostasy]		
active	yes	yes
enable water loading	no	no
[river 0]		
active	yes	yes
river file	beaufort_river.kvf	beaufort_river.kvf
[bedload dumping]		
active	0y->6700y	0y->6700y
distance to dump bedload (m)	5000	5000
ratio of flood plain to bedload rate	0	0
fraction of bedload retained in the delta plain	0	0
[river 1]		
active	6700yr -> 9000yr	6700yr -> 9000yr
river file	beaufort_river2.kvf	beaufort_river2.kvf
[bedload dumping]		
active	6700yr -> 9000yr	6700yr -> 9000yr
distance to dump bedload (m)	5000	5000
ratio of flood plain to bedload rate	0	0
fraction of bedload retained in the delta plain	0	0
[river 2]		
active	9000yr -> 13000y	9000yr -> 13000y
river file	beaufort_river3.kvf	beaufort_river3.kvf
[bedload dumping]		
active	9000yr -> 13000y	9000yr -> 13000y
distance to dump bedload (m)	5000	5000
ratio of flood plain to bedload rate	0	0
fraction of bedload retained in the delta plain	0	0
[river 3]		
active	13000y -> 21000y	13000y -> 21000y
river file	beaufort_river4.kvf	beaufort_river4.kvf
[bedload dumping]		

active	13000y -> 21000y	13000y -> 21000y
distance to dump bedload (m)	5000	5000
ratio of flood plain to bedload rate	0	0
fraction of bedload retained in the delta plain	0	0
[plume]		
active	yes	yes
hyperpycnal plume model	<none>	turbidity flow'
hypopycnal plume model	'hypopycnal plume'	'hypopycnal plume'
[Failure]		
active:	no	yes
[debris flow]		
active:	no	yes
[turbidity current]		
active:	no	yes
RIVER FILES		
River0		
['Season 1']		
Duration (y)	1y	1y
Bedload (kg/s)	0	0
Suspended load concentration (kg/m^3)	0	0
velocity (m/s)	0.7	0.7
Width (m)	2000	2000
Depth (m)	8	8
River1		
['Season 1']		
Duration (y)	1y	1y
Bedload (kg/s)	500	500
Suspended load concentration (kg/m^3)	0.0878, 0.526, 0.263	0.0878, 0.526, 0.263
velocity (m/s)	0.7	0.7
Width (m)	2000	2000
Depth (m)	8	8
River2		
['Season 1']		
Duration (y)	1y	1y
Bedload (kg/s)	400	400
Suspended load concentration (kg/m^3)	0.07024, 0.4208, 0.2104	0.07024, 0.4208, 0.2104
velocity (m/s)	0.7	0.7
Width (m)	2000	2000
Depth (m)	8	8
River3		
['Season 1']		
Duration (y)	1y	1y
Bedload (kg/s)	200	200
Suspended load concentration (kg/m^3)	0.03512, 0.2104, 0.1052	0.03512, 0.2104, 0.1052
velocity (m/s)	0.7	0.7
Width (m)	2000	2000
Depth (m)	8	8

SEDIMENT FILE		
[Grain 1 (bedload)]		
grain size (microns)	200	200
grain density (kg/m^3)	2650	2650
saturated density (kg/m^3)	2000	2000
minimum void ratio (-)	0.17	0.17
diffusion coefficient (-)	0.25	0.25
removal rate (1/day)	25	25
consolidation coefficient (m^2/yr)	100000	100000
compaction coefficient (-)	0.000000062	0.000000062
[Grain 2 (suspended)]		
grain size (microns)	150	150
grain density (kg/m^3)	2650	2650
saturated density (kg/m^3)	1955	1955
minimum void ratio (-)	0.15	0.15
diffusion coefficient (-)	0.25	0.25
removal rate (1/day)	20	20
consolidation coefficient (m^2/yr)	100000	100000
compaction coefficient (-)	0.00000007	0.00000007
[Grain 3 (suspended)]		
grain size (microns)	60	60
grain density (kg/m^3)	2650	2650
saturated density (kg/m^3)	1795	1795
minimum void ratio (-)	0.1	0.1
diffusion coefficient (-)	0.25	0.25
removal rate (1/day)	12	12
consolidation coefficient (m^2/yr)	100000	100000
compaction coefficient (-)	0.00000008	0.00000008
[Grain 4 (suspended)]		
grain size (microns)	5	5
grain density (kg/m^3)	2650	2650
saturated density (kg/m^3)	1504	1504
minimum void ratio (-)	0.05	0.05
diffusion coefficient (-)	0.25	0.25
removal rate (1/day)	3.2	3.2
consolidation coefficient (m^2/yr)	100000	100000
compaction coefficient (-)	0.00000036	0.00000036

Fluvial erosion and deposition (Fig. A23)

This sensitivity test was carried out to understand the erosion module included in SedFlux. Simulation 55236 was run with the erosion module on, while the other simulation 61056 was run without the module. The parameters of the module were set as follow: the diffusion model of Paola and al. (1992) was selected, and the reach and the relief of highest order stream were set to 10000 and 1 m respectively. A description of the module integration and impacts on stratigraphic modeling is available in part in the method section, but in details in Hutton et al. (2008).

Based on the simulation results compared in Figure A23, the erosion module does not seem to affect the stratigraphy. The reason fluvial erosion and deposition is not affecting the subaerial plain is because the slope ratio threshold of 1:10000 set in the module is at all time greater than the slope of the floodplain in these simulations. The initial profile is recording an approximate slope of 1:12000, therefore never triggers erosion. Erosion is however observed in simulation 55228 from Figure A2. The top reflector (SB) of the FSST prism formed between 21 and 14 ka BP shows an erosional unconformity. The slope of the unconformity is approximately 1:2500 and therefore was subjected to constant erosion until it was submerged. The equilibrium profile of 1:10000 set in the parameter's file was thus never obtained. Although not presented here, but supporting this statement is that at 16 ka BP the slope of the FSST at 182 km was in the order of 1:180 and was located on the delta front. Following RSL fall and exposure of the deposit around 13.5 ka BP, that same slope was reduced to a ratio of 1:7500. This therefore supports the fact that the erosion module functions properly and that the results obtained in Figure A23 were the consequence of the deposit never reaching steeper slope than 1:10000 while exposed.

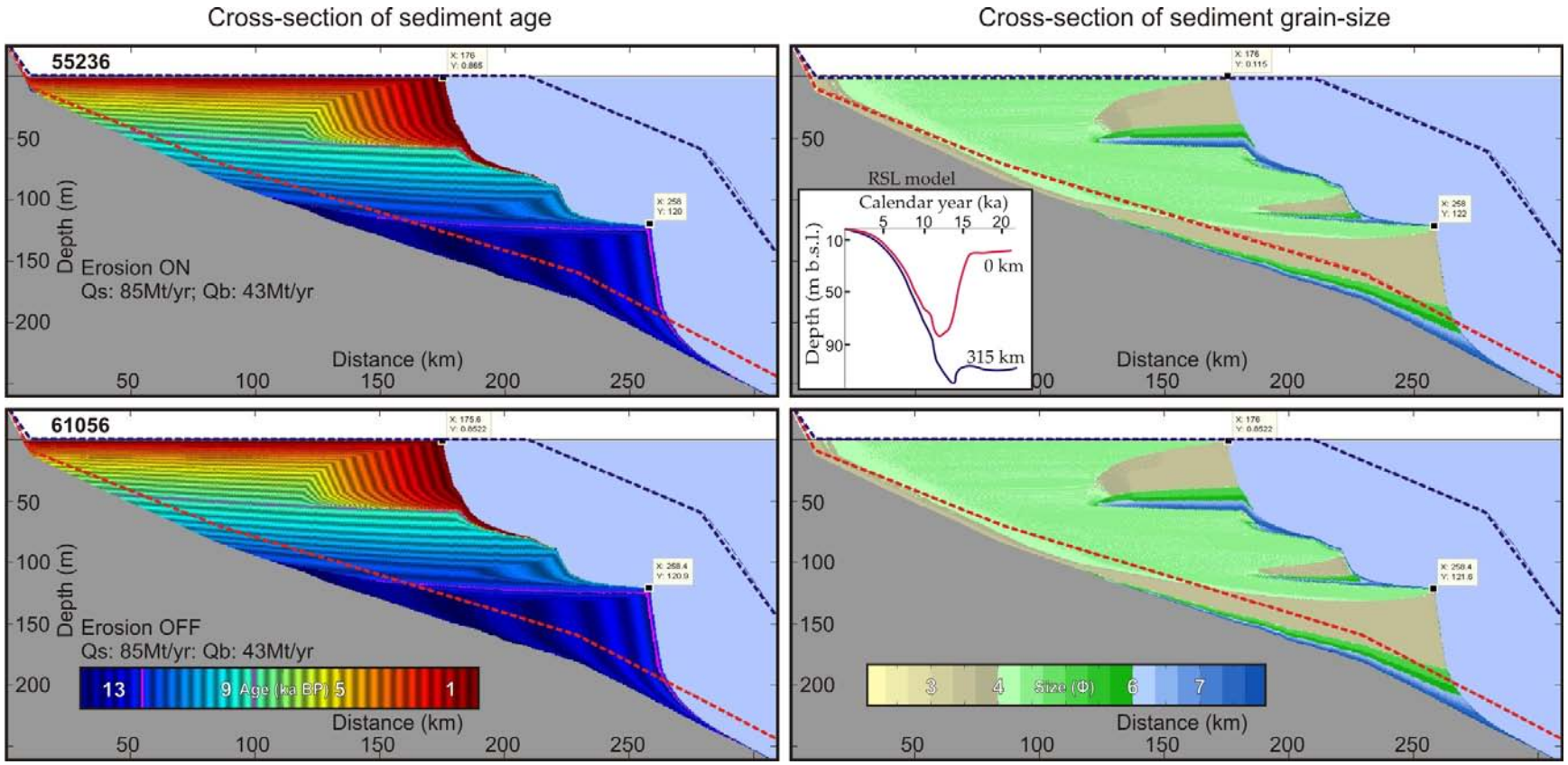

Figure A23: Sensitivity test on the erosion module. Simulation 55236 presents a simulation where the erosion module is active. Simulation 61056 presents the same simulation as 55236, but with the erosion module inactive. The locations of the seismic basal reflector from which the initial profile was derived (Hill et al., 2001; red dotted line) and the modern seafloor profile (blue dotted line) are displayed. As a reference, the RSL graph presents the RSL curves corresponding to each extremity of the transect.

Table A24:Erosion

Files	55236	61056
Summary of processes	**Erosion ON; Ratio of floodplain to bedload rate: 2; Qs: 85Mt/yr; Qb: 43Mt/yr (Carson et al. 1999);**	**Erosion OFF; Ratio of floodplain to bedload rate: 2; Qs: 85Mt/yr; Qb: 43Mt/yr (Carson et al. 1999);**
INITIATION FILE		
bathymetry file	(compensated) beaufort_bathy.csv	(compensated) beaufort_bathy.csv
PROCESS FILE		
[sea level]		
active	no	no
sea level file	beaufort_sea_level.csv	beaufort_sea_level.csv
[Subsidence]		
active:	yes	yes
Subsidence file	rates_sedflux_MT21000_combined.dat	rates_sedflux_MT21000_combined.dat
[compaction]		
active	no	NO
[isostasy]		
active	yes	yes
enable water loading		
[river 0]		
active	yes	yes
river file	beaufort_river.kvf	beaufort_river.kvf
[bedload dumping]		
active	0y->6700y	0y->6700y
distance to dump bedload (m)	5000	5000
ratio of flood plain to bedload rate	2	2
fraction of bedload retained in the delta plain	0	0
[river 1]		
active	6700yr -> 9000yr	6700yr -> 9000yr
river file	beaufort_river2.kvf	beaufort_river2.kvf
[bedload dumping]		
active	6700yr -> 9000yr	6700yr -> 9000yr
distance to dump bedload (m)	5000	5000
ratio of flood plain to bedload rate	2	2
fraction of bedload retained in the delta plain	0	0
[river 2]		
active	9000yr -> 13000y	9000yr -> 13000y
river file	beaufort_river3.kvf	beaufort_river3.kvf
[bedload dumping]		
active	9000yr -> 13000y	9000yr -> 13000y
distance to dump bedload (m)	5000	5000
ratio of flood plain to bedload rate	2	2
fraction of bedload retained in the delta plain	0	0
[river 3]		
active	13000y -> 21000y	13000y -> 21000y
river file	beaufort_river4.kvf	beaufort_river4.kvf

[bedload dumping]		
active	13000y -> 21000y	13000y -> 21000y
distance to dump bedload (m)	5000	5000
ratio of flood plain to bedload rate	2	2
fraction of bedload retained in the delta plain	0	0
[plume]		
active	yes	YES
hyperpycnal plume model	<none>	<none>
hypopycnal plume model	'hypopycnal plume'	'hypopycnal plume'
[Failure]		
active:	no	no
[debris flow]		
active:	no	no
[turbidity current]		
active:	no	no
RIVER FILES		
River0		
['Season 1']		
Duration (y)	1y	1y
Bedload (kg/s)	0	0
Suspended load concentration (kg/m^3)	0	0
velocity (m/s)	0.7	0.7
Width (m)	2000	2000
Depth (m)	8	8
River1		
['Season 1']		
Duration (y)	1y	1y
Bedload (kg/s)	3250	3250
Suspended load concentration (kg/m^3)	0.0585, 0.351075, 0.175525	0.0585, 0.351075, 0.175525
velocity (m/s)	0.7	0.7
Width (m)	2000	2000
Depth (m)	8	8
River2		
['Season 1']		
Duration (y)	1y	1y
Bedload (kg/s)	2600	2600
Suspended load concentration (kg/m^3)	0.04680, 0.28086, 0.14042	0.04680, 0.28086, 0.14042
velocity (m/s)	0.7	0.7
Width (m)	2000	2000
Depth (m)	8	8
River3		
['Season 1']		
Duration (y)	1y	1y
Bedload (kg/s)	1300	1300
Suspended load concentration (kg/m^3)	0.02340, 0.14043, 0.07021	0.02340, 0.14043, 0.07021
velocity (m/s)	0.7	0.7
Width (m)	2000	2000

Depth (m)	8	8
SEDIMENT FILE		
[Grain 1 (bedload)]		
grain size (microns)	200	200
grain density (kg/m^3)	2650	2650
saturated density (kg/m^3)	2000	2000
minimum void ratio (-)	0.17	0.17
diffusion coefficient (-)	0.25	0.25
removal rate (1/day)	25	25
consolidation coefficient (m^2/yr)	100000	100000
compaction coefficient (-)	0.000000062	0.000000062
[Grain 2 (suspended)]		
grain size (microns)	150	150
grain density (kg/m^3)	2650	2650
saturated density (kg/m^3)	1955	1955
minimum void ratio (-)	0.15	0.15
diffusion coefficient (-)	0.25	0.25
removal rate (1/day)	20	20
consolidation coefficient (m^2/yr)	100000	100000
compaction coefficient (-)	0.00000007	0.00000007
[Grain 3 (suspended)]		
grain size (microns)	60	60
grain density (kg/m^3)	2650	2650
saturated density (kg/m^3)	1795	1795
minimum void ratio (-)	0.1	0.1
diffusion coefficient (-)	0.25	0.25
removal rate (1/day)	12	12
consolidation coefficient (m^2/yr)	100000	100000
compaction coefficient (-)	0.00000008	0.00000008
[Grain 4 (suspended)]		
grain size (microns)	5	5
grain density (kg/m^3)	2650	2650
saturated density (kg/m^3)	1504	1504
minimum void ratio (-)	0.05	0.05
diffusion coefficient (-)	0.25	0.25
removal rate (1/day)	3.2	3.2
consolidation coefficient (m^2/yr)	100000	100000
compaction coefficient (-)	0.00000036	0.00000036

Sediment delivery period (Fig. A24)

Carson et al. (1998) estimated that most of the annual sediment load delivered to the Mackenzie Trough occurs during the three summer months. This statement motivated the sensitivity test presented in Figure A24. Simulation 56333 presents the results of the total load distributed and supplied evenly over the course of one full year. The second simulation 60739 supplied the entire load over only three months. The results suggest that there is no change between the two simulations, with the exception the bedload distribution located at the beginning of the profile in the seasonal simulation. A layer of coarse sediment was deposited during the entire simulation over the constantly evolving subearial area of the profile. This deposit is similar to the results of simulation 61917 presented in Figure A14 where the fraction of bedload retained in the floodplain is on. This change is difficult to explain with the present knowledge of SedFlux internal calculations. The possible reasons explaining this result is most likely associated with the bedload or the erosional modules as they are the only modules affecting the floodplain deposition. In the seasonal simulation, the bedload had to be largely concentrated compared to the annual simulation.

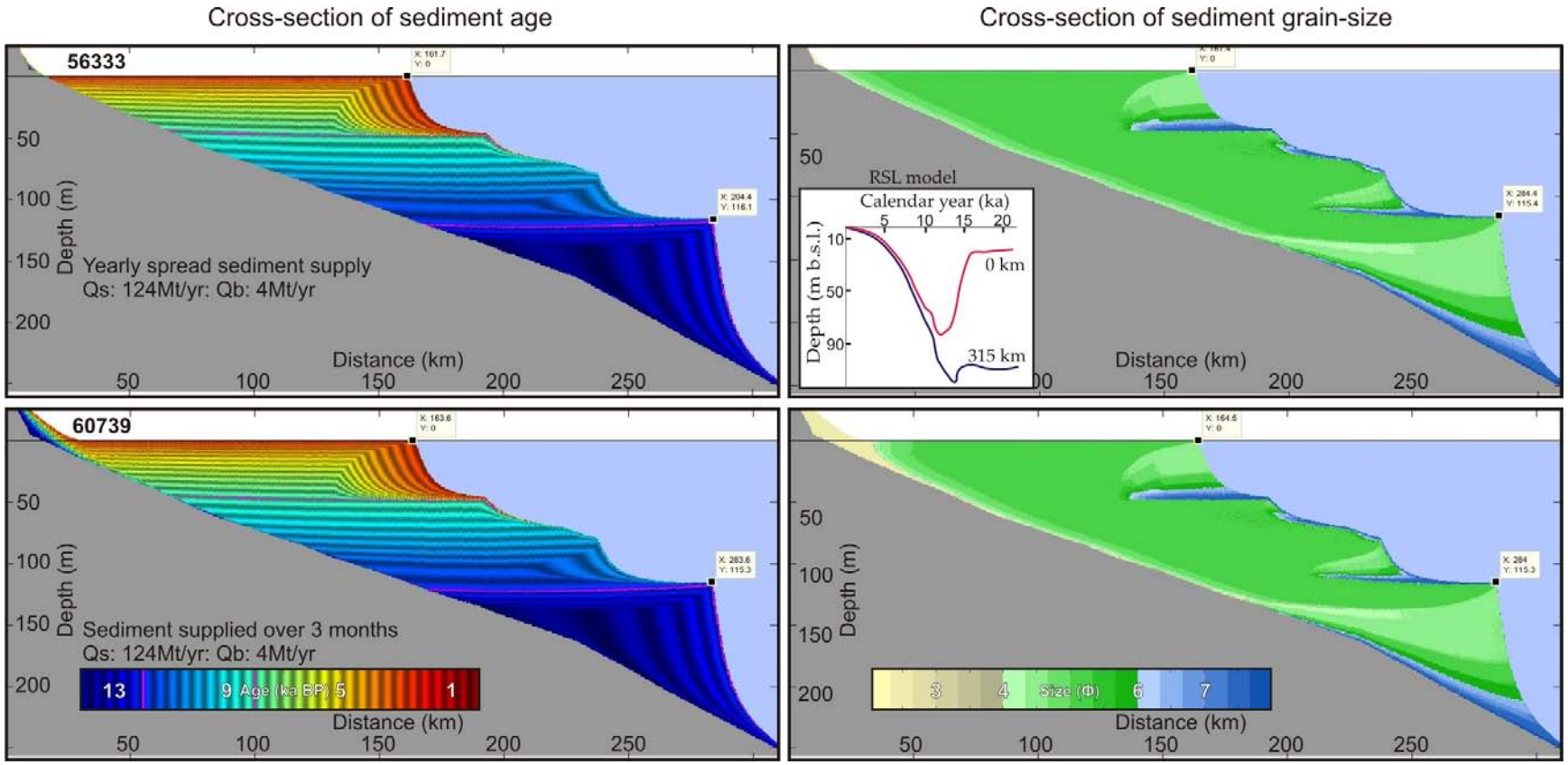

Figure A24: Sensitivity test on the sediment delivery period. Carson et al. (1998) estimate that most of the sediment supply is delivered to the Mackenzie Trough during the 3 summer months (June, July, and August). Simulation 56333 simulates the total yearly sediment supply distributed evenly over one continuous year. Simulation 60739 simulates the total sediment supply delivered to the system in 3 months. The graphs show the stratigraphy after 18.5 ka of simulation, or up until 2.5 ka BP. As a reference, the RSL graph presents the RSL curves for each extremity of the transect.

Table A25: Seasonality of sediment supply

Files	56333	60739
Summary of processes	**No season; sediment supply distributed over 1 year; Qs: 124Mt/yr; Qb: 4Mt/yr (Carson et al. 1998);**	**2 Seasons; sediment supply distributed over 3 months; Qs: 124Mt/yr; Qb: 4Mt/yr (Carson et al. 1998);**
INITIATION FILE		
bathymetry file	(compensated) beaufort_bathy.csv	(compensated) beaufort_bathy.csv
PROCESS FILE		
[sea level]		
active	no	no
sea level file	beaufort_sea_level.csv	beaufort_sea_level.csv
[Subsidence]		
active:	yes	yes
Subsidence file	rates_sedflux_MT21000.dat	rates_sedflux_MT21000.dat
[compaction]		
active	no	no
[isostasy]		
active	yes	yes
enable water loading	no	no
[river 0]		
active	yes	yes
river file	beaufort_river.kvf	beaufort_river.kvf
[bedload dumping]		
active	0y->6700y	0y->6700y
distance to dump bedload (m)	5000	5000
ratio of flood plain to bedload rate	0	0
fraction of bedload retained in the delta plain	0	0
[river 1]		
active	6700yr -> 9000yr	6700yr -> 9000yr
river file	beaufort_river2.kvf	beaufort_river2.kvf
[bedload dumping]		
active	6700yr -> 9000yr	6700yr -> 9000yr
distance to dump bedload (m)	5000	5000
ratio of flood plain to bedload rate	0	0
fraction of bedload retained in the delta plain	0	0
[river 2]		
active	9000yr -> 13000y	9000yr -> 13000y
river file	beaufort_river3.kvf	beaufort_river3.kvf
[bedload dumping]		
active	9000yr -> 13000y	9000yr -> 13000y
distance to dump bedload (m)	5000	5000
ratio of flood plain to bedload rate	0	0
fraction of bedload retained in the delta plain	0	0
[river 3]		
active	13000y -> 21000y	13000y -> 21000y
river file	beaufort_river4.kvf	beaufort_river4.kvf
[bedload dumping]		

active	13000y -> 21000y	13000y -> 21000y
distance to dump bedload (m)	5000	5000
ratio of flood plain to bedload rate	0	0
fraction of bedload retained in the delta plain	0	0
[plume]		
active	yes	yes
hyperpycnal plume model	<none>	<none>
hypopycnal plume model	'hypopycnal plume'	'hypopycnal plume'
[Failure]		
active:	no	no
[debris flow]		
active:	no	no
[turbidity current]		
active:	no	no
RIVER FILES		
River0		
['Season 1']		
Duration (y)	1y	1y
Bedload (kg/s)	0	0
Suspended load concentration (kg/m^3)	0	0
velocity (m/s)	0.7	0.7
Width (m)	2000	2000
Depth (m)	8	8
River1		
['Season 1']		
Duration (y)	1y	3m
Bedload (kg/s)	500	1925
Suspended load concentration (kg/m^3)	0.0878, 0.526, 0.263	0.35000, 2.075, 1.0395
velocity (m/s)	0.7	0.7
Width (m)	2000	2000
Depth (m)	8	8
['Season 2']		
Duration (y)		9m
Bedload (kg/s)		25
Suspended load concentration (kg/m^3)		0.0004, 0.009675, 0.004175
velocity (m/s)		0.7
Width (m)		2000
Depth (m)		8
River2		
['Season 1']		
Duration (y)	1y	3m
Bedload (kg/s)	400	1540
Suspended load concentration (kg/m^3)	0.07024, 0.4208, 0.2104	0.2800, 1.6600, 0.8316
velocity (m/s)	0.7	0.7
Width (m)	2000	2000
Depth (m)	8	8
['Season 2']		
Duration (y)		9m

Bedload (kg/s)						20
Suspended load concentration (kg/m^3)				0.00032,	0.00774,	0.00334
velocity (m/s)						0.7
Width (m)						2000
Depth (m)						8
River3						
['Season 1']						3m
Duration (y)			1y			770
Bedload (kg/s)			200	0.14000,	0.8300,	0.4158
Suspended load concentration (kg/m^3)	0.03512,	0.2104,	0.1052			0.7
velocity (m/s)			0.7			2000
Width (m)			2000			8
Depth (m)			8			
['Season 2']						
Duration (y)						9m
Bedload (kg/s)						10
Suspended load concentration (kg/m^3)				0.00016,	0.00387,	0.00167
velocity (m/s)						0.7
Width (m)						2000
Depth (m)						8
SEDIMENT FILE						
[Grain 1 (bedload)]						
grain size (microns)			200			200
grain density (kg/m^3)			2650			2650
saturated density (kg/m^3)			2000			2000
minimum void ratio (-)			0.17			0.17
diffusion coefficient (-)			0.25			0.25
removal rate (1/day)			25			25
consolidation coefficient (m^2/yr)			100000			100000
compaction coefficient (-)			0.000000062			0.000000062
[Grain 2 (suspended)]						
grain size (microns)			150			150
grain density (kg/m^3)			2650			2650
saturated density (kg/m^3)			1955			1955
minimum void ratio (-)			0.15			0.15
diffusion coefficient (-)			0.25			0.25
removal rate (1/day)			20			20
consolidation coefficient (m^2/yr)			100000			100000
compaction coefficient (-)			0.00000007			0.00000007
[Grain 3 (suspended)]						
grain size (microns)			60			60
grain density (kg/m^3)			2650			2650
saturated density (kg/m^3)			1795			1795
minimum void ratio (-)			0.1			0.1
diffusion coefficient (-)			0.25			0.25
removal rate (1/day)			12			12
consolidation coefficient (m^2/yr)			100000			100000
compaction coefficient (-)			0.00000008			0.00000008
[Grain 4 (suspended)]						

grain size (microns)	5	5
grain density (kg/m^3)	2650	2650
saturated density (kg/m^3)	1504	1504
minimum void ratio (-)	0.05	0.05

Order of processes (Fig. A25)

This sensitivity test was carried out to question the importance of the order in which SedFlux computes the various processes. SedFlux normally resolves the erosion module first, then follows with the bedload deposition module, and finally ends with the dispersion of sediments in the marine environment trough the plume module. It was suggested that this computational order might not advantage the subaerial deposition, especially in the later part of the Holocene, because erosion tends to contribute to the RSL rise, which consequently narrows the floodplain. As mentioned in Figure A12, for the same fraction of bedload, a narrow floodplain increases the subaerial sedimentation rate. For example, the modern delta floodplain extends to 210 km along the profile. If erosion is computed first, then transgression occurs and the floodplain becomes much narrower. However, if the order of processes is changed to first deposit the plume, then the bedload, and finally deals with the erosion, then the floodplain should be at its widest when subaerial deposition happens. This thought process is not intuitive, but was suggested to get around computational artefacts. The results of the test were inconclusive, since it appears that no change is seen by changing the order. Further testing may be needed to make sure that the process order is actually functioning as it should.

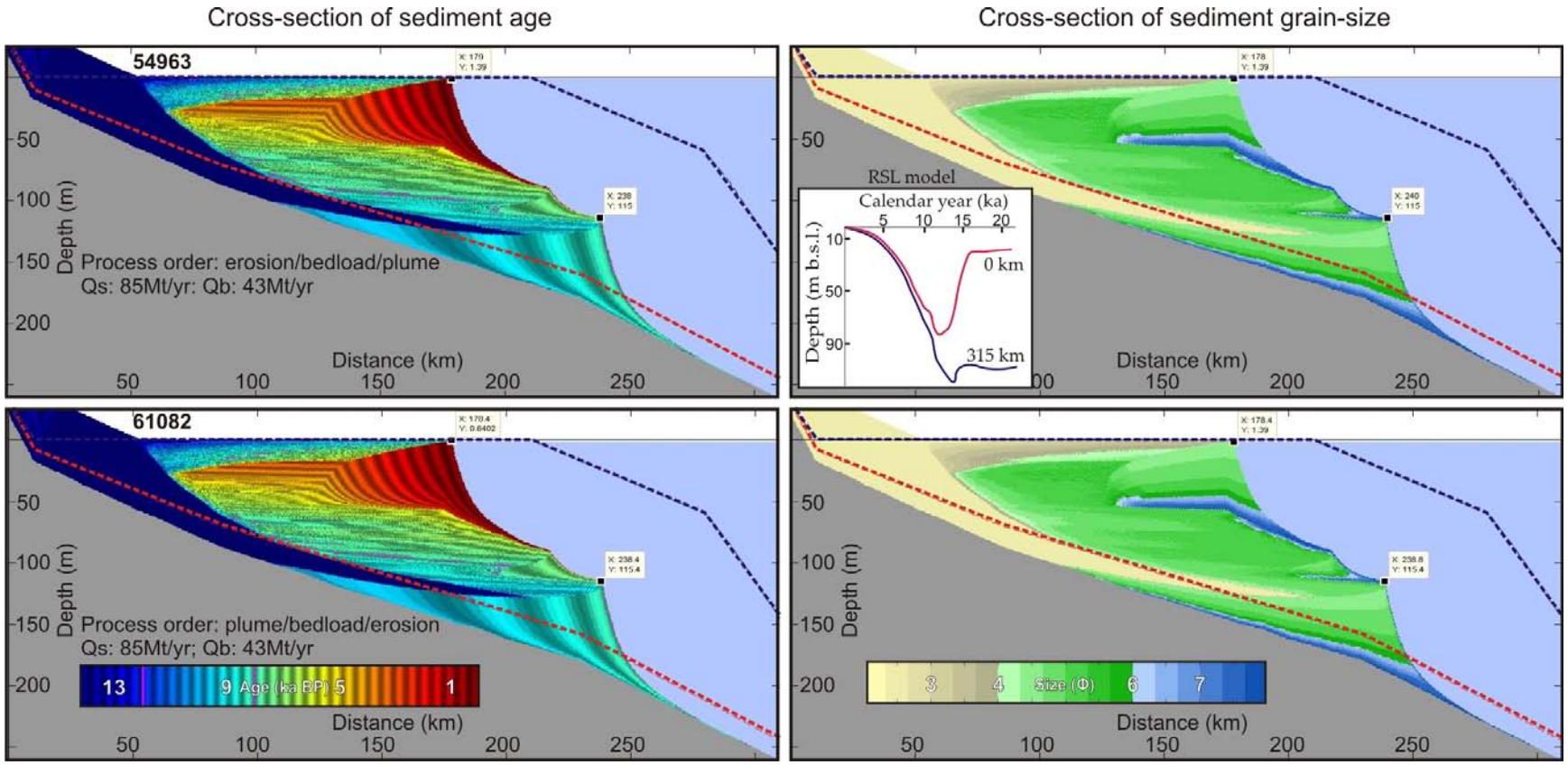

Figure A25: Sensitivity test on the order in which Sedflux resolves processes. Simulation 54963 presents the standard order, i.e. erosion/bedload/plume. Simulation 61082 presents the altenative order, i.e. plume/bedload/erosion. Both simulation were done using the "Fraction of bedload retained in the delta plain" equalling 1, which means that 100% of the bedload is distributed over the available floodplain area. The larger the floodplain, the smaller the sedimentation rate. The locations of the seismic basal reflector from which the initial profile was derived (Hill et al., 2001; red dotted line) and the modern seafloor profile (blue dotted line) are displayed. As a reference, the RSL graph presents the RSL curves corresponding to each extremity of the transect.

Table A26: Process order

Files	54963	61082
Summary of processes	**Process order : Erosion/ Bedload/ Plume; Qs: 85Mt/yr; Qb: 43Mt/yr (Carson et al. 1999); Fraction of bedload retained in the delta plain: 1**	**Process order : Plume/Bedload/Erosion; Qs: 85Mt/yr; Qb: 43Mt/yr (Carson et al. 1999); Fraction of bedload retained in the delta plain: 1**
INITIATION FILE		
bathymetry file	(compensated) beaufort_bathy.csv	(compensated) beaufort_bathy.csv
PROCESS FILE		
[sea level]		
active	no	no
sea level file	beaufort_sea_level.csv	beaufort_sea_level.csv
[Subsidence]		
active:	yes	yes
Subsidence file	rates_sedflux_MT21000_combined.dat	rates_sedflux_MT21000_combined.dat
[compaction]		
active	no	no
[isostasy]		
active	yes	yes
enable water loading		
[river 0]		
active	yes	yes
river file	beaufort_river.kvf	beaufort_river.kvf
[bedload dumping]		
active	0y->6700y	0y->6700y
distance to dump bedload (m)	5000	5000
ratio of flood plain to bedload rate	0	0
fraction of bedload retained in the delta plain	1	1
[river 1]		
active	6700yr -> 9000yr	6700yr -> 9000yr
river file	beaufort_river2.kvf	beaufort_river2.kvf
[bedload dumping]		
active	6700yr -> 9000yr	6700yr -> 9000yr
distance to dump bedload (m)	5000	5000
ratio of flood plain to bedload rate	0	0
fraction of bedload retained in the delta plain	1	1
[river 2]		
active	9000yr -> 13000y	9000yr -> 13000y
river file	beaufort_river3.kvf	beaufort_river3.kvf
[bedload dumping]		
active	9000yr -> 13000y	9000yr -> 13000y
distance to dump bedload (m)	5000	5000
ratio of flood plain to bedload rate	0	0
fraction of bedload retained in the delta plain	1	1
[river 3]		
active	13000y -> 21000y	13000y -> 21000y
river file	beaufort_river4.kvf	beaufort_river4.kvf
[bedload dumping]		
active	13000y -> 21000y	13000y -> 21000y

distance to dump bedload (m)	5000	5000
ratio of flood plain to bedload rate	0	0
fraction of bedload retained in the delta plain	1	1
[plume]		
active	yes	yes
hyperpycnal plume model	<none>	<none>
hypopycnal plume model	'hypopycnal plume'	'hypopycnal plume'
[Failure]		
active:	no	no
[debris flow]		
active:	no	no
[turbidity current]		
active:	no	no
RIVER FILES		
River0		
['Season 1']		
Duration (y)	1y	1y
Bedload (kg/s)	0	0
Suspended load concentration (kg/m^3)	0	0
velocity (m/s)	0.7	0.7
Width (m)	2000	2000
Depth (m)	8	8
River1		
['Season 1']		
Duration (y)	1y	1y
Bedload (kg/s)	3250	3250
Suspended load concentration (kg/m^3)	0.0585, 0.351075, 0.175525	0.0585, 0.351075, 0.175525
velocity (m/s)	0.7	0.7
Width (m)	2000	2000
Depth (m)	8	8
River2		
['Season 1']		
Duration (y)	1y	1y
Bedload (kg/s)	2600	2600
Suspended load concentration (kg/m^3)	0.04680, 0.28086, 0.14042	0.04680, 0.28086, 0.14042
velocity (m/s)	0.7	0.7
Width (m)	2000	2000
Depth (m)	8	8
River3		
['Season 1']		
Duration (y)	1y	1y
Bedload (kg/s)	1300	1300
Suspended load concentration (kg/m^3)	0.02340, 0.14043, 0.07021	0.02340, 0.14043, 0.07021
velocity (m/s)	0.7	0.7
Width (m)	2000	2000
Depth (m)	8	8
SEDIMENT FILE		

[Grain 1 (bedload)]		
grain size (microns)	200	200
grain density (kg/m^3)	2650	2650
saturated density (kg/m^3)	2000	2000
minimum void ratio (-)	0.17	0.17
diffusion coefficient (-)	0.25	0.25
removal rate (1/day)	25	25
consolidation coefficient (m^2/yr)	100000	100000
compaction coefficient (-)	0.000000062	0.000000062
[Grain 2 (suspended)]		
grain size (microns)	150	150
grain density (kg/m^3)	2650	2650
saturated density (kg/m^3)	1955	1955
minimum void ratio (-)	0.15	0.15
diffusion coefficient (-)	0.25	0.25
removal rate (1/day)	20	20
consolidation coefficient (m^2/yr)	100000	100000
compaction coefficient (-)	0.00000007	0.00000007
[Grain 3 (suspended)]		
grain size (microns)	60	60
grain density (kg/m^3)	2650	2650
saturated density (kg/m^3)	1795	1795
minimum void ratio (-)	0.1	0.1
diffusion coefficient (-)	0.25	0.25
removal rate (1/day)	12	12
consolidation coefficient (m^2/yr)	100000	100000
compaction coefficient (-)	0.00000008	0.00000008
[Grain 4 (suspended)]		
grain size (microns)	5	5
grain density (kg/m^3)	2650	2650
saturated density (kg/m^3)	1504	1504
minimum void ratio (-)	0.05	0.05
diffusion coefficient (-)	0.25	0.25
removal rate (1/day)	3.2	3.2
consolidation coefficient (m^2/yr)	100000	100000
compaction coefficient (-)	0.00000036	0.00000036

Bedload use as bed or suspended load (Fig. A26)

Carson et al. (1999) estimated that most of the sediment load of the Mackenzie River system belonged to the washload (< 425 um), with only 3-5% of the grain with a greater size. This portion was qualified as bedload, even though it is carried within the suspended load. The authors also declared that 33% of the load was retained within the delta plain with the remaining delivered to the offshore. These two statements thus suggest that most of the sediment retained in the subaerial plain come from the suspended load. Since there is no option to retain sediment in the floodplain using the suspended load in SedFux, the bed load module has to be used.

The objective of this sensitivity test was to simulate sediment distribution according to whether the 33% of sediment was included in the suspended load or in the bedload. Simulation 55230 included the 33% (43 Mt/yr) in the bedload and thus, was subjected to the bedload dumping module. Simulation 55228 set 30% of bedload portion as the coarsest sediment grain-size of the suspended load while 3% remained in the bedload discharge.

The results presented in Figure A26 show that while the stratigraphy stays similar in both simulations, the distribution of sediment changes, especially in the foreset area (grain-size cross-section). In simulation 55230, where a third of the total load is distributed as bedload, the foresets are mainly composed of sand. In Sedflux-2D, bedload is deposited using the bedload dumping module. This module spreads the bedload evenly across the plain and over a user-defined length set in this case to 5 km. In the simulation where the bedload size is included in the suspended load, the distribution pattern changes because the sediment ends up distributed over a larger area lengthwise and thus spread more thinly.

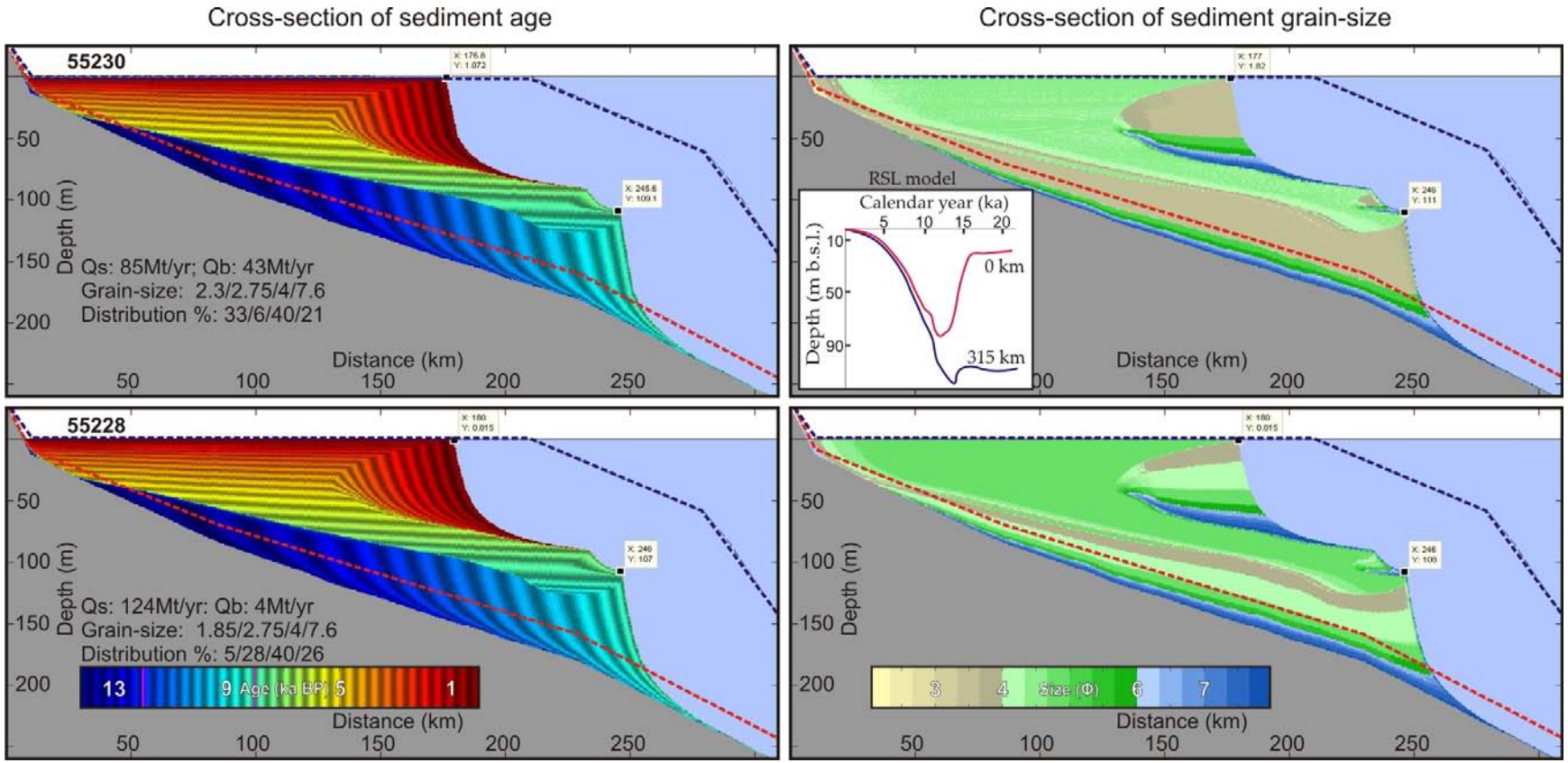

Figure A26: Sensitivity test on bedload use as bed load or within the suspended load. Carson et al. (1999) suggest that 33% of the total load of the Mackenzie River system is retained in the subaerial delta plain. The authors also state that most of the bedload is carried within the suspended load. Simulation 56230 simulates the 33% of the total load carried as bed load and thus, subject to the "bedload dumping' module. Simulation 56228 simulates Carson et al. assumption that 30% of the bed load is transported in suspension and 3% is distributed accordingly to 'bedload dumping' processes. The locations of the seismic basal reflector from which the initial profile was derived (Hill et al., 2001; red dotted line) and the modern seafloor profile (blue dotted line) are displayed. As a reference, the RSL graph presents the RSL curves corresponding to each extremity of the transect.

Table A27: Bed load discharge included in Qs or in Qb

Files	55230	55228
Summary of processes	**Qs: 85Mt/yr; Qb: 43Mt/yr (Carson et al. 1999); Epoch length: 21ka; Epoch sediment supply: 1X**	**Qs: 124Mt/yr; Qb: 4Mt/yr (Carson et al. 1998); Epoch length: 21ka; Epoch sediment supply: 1X**
INITIATION FILE		
bathymetry file	(compensated) beaufort_bathy.csv	(compensated) beaufort_bathy.csv
PROCESS FILE		
[sea level]		
active	no	no
sea level file	beaufort_sea_level.csv	beaufort_sea_level.csv
[Subsidence]		
active:	yes	yes
Subsidence file	rates_sedflux_MT21000_combined.dat	rates_sedflux_MT21000_combined.dat
[compaction]		
active	no	no
[isostasy]		
active	yes	yes
enable water loading		
[river 0]		
active	yes	yes
river file	beaufort_river.kvf	beaufort_river.kvf
[bedload dumping]		
active	yes	yes
distance to dump bedload (m)	5000	5000
ratio of flood plain to bedload rate	6.5	6.5
fraction of bedload retained in the delta plain	0	0
[plume]		
active	yes	yes
hyperpycnal plume model	<none>	<none>
hypopycnal plume model	'hypopycnal plume'	'hypopycnal plume'
[Failure]		
active:	no	no
[debris flow]		
active:	no	no
[turbidity current]		
active:	no	no
RIVER FILES		
River0		
['Season 1']		
Duration (y)	1y	1y
Bedload (kg/s)	1300	200
Suspended load concentration (kg/m^3)	0.02340, 0.14043, 0.07021	0.1054, 0.1473, 0.0982
velocity (m/s)	0.7	0.7
Width (m)	2000	2000
Depth (m)	8	8
SEDIMENT FILE		

[Grain 1 (bedload)]		
grain size (microns)	200	300
grain density (kg/m^3)	2650	2650
saturated density (kg/m^3)	2000	2094
minimum void ratio (-)	0.17	0.2
diffusion coefficient (-)	0.25	0.25
removal rate (1/day)	25	35
consolidation coefficient (m^2/yr)	100000	100000
compaction coefficient (-)	0.000000062	0.00000005
[Grain 2 (suspended)]		
grain size (microns)	150	200
grain density (kg/m^3)	2650	2650
saturated density (kg/m^3)	1955	2000
minimum void ratio (-)	0.15	0.17
diffusion coefficient (-)	0.25	0.25
removal rate (1/day)	20	25
consolidation coefficient (m^2/yr)	100000	100000
compaction coefficient (-)	0.00000007	0.000000062
[Grain 3 (suspended)]		
grain size (microns)	60	60
grain density (kg/m^3)	2650	2650
saturated density (kg/m^3)	1795	1795
minimum void ratio (-)	0.1	0.1
diffusion coefficient (-)	0.25	0.25
removal rate (1/day)	12	12
consolidation coefficient (m^2/yr)	100000	100000
compaction coefficient (-)	0.00000008	0.00000008
[Grain 4 (suspended)]		
grain size (microns)	5	5
grain density (kg/m^3)	2650	2650
saturated density (kg/m^3)	1504	1504
minimum void ratio (-)	0.05	0.05
diffusion coefficient (-)	0.25	0.25
removal rate (1/day)	3.2	3.2
consolidation coefficient (m^2/yr)	100000	100000
compaction coefficient (-)	0.00000036	0.00000036

Storms

SedFlux contains a module to calculate the impacts of storm events, which redistribute sediments via ocean-wave energy. Unfortunately, at the time this study was done, the module did not function and therefore the impact of such process could not be evaluated. The only test that can be used was done and described by Hutton and Syvitski (2008). The authors evaluated the effect of cross-shore transport create by storm of the development of the Po River delta. The results of their simulation ran without storm showed similar shoreface geometry to the ones presented in the simulations of the present study (Hutton and Syvitski, 2008; Figure A7). On the other hand, the results of their storm simulation clearly showed that storms contribute to the flattening of the delta front. The authors used average storms waves of about 3.4 m, which is a similar value to the one estimated for the Beaufort Sea area (< 4 m; Hill et al., 1991). Notwithstanding the fact that the Beaufort Sea can only be subjected to storms during ice free conditions, but considering the other basic similarities and the test results for the Po River Delta, similar effects should be expected on the geomorphology of the Mackenzie Trough deposits.

Appendix B – Method

Sedflux stratigraphic simulation model integrates a wide variety of process modules that can be activated to simulate the lithologic character of basin stratigraphy. The stratigraphy paper explains the functionality and parametization of most of them, with the exception of only few. Additional notes on the processes described in chapter 2 and details of the processes that have not been discussed are described in this appendix.

Process modules

Bottom boundary layer

The *bottom boundary layer* module was required to be activated at all time in order for sediments to be freed up from the boundary layer.

Avulsion

The process of a*vulsion* for delta building process module in the 2D version of Sedlux is not used, since the results are averaged over the width of the basin. In 3D though, this process allows to set the location of the river mouth along the shore and the standard deviation, which refers to the angle at which avulsion will occur. A minimum and maximum angle of avulsion can be set, so the river mouth does not turn back on itself. It is worth noting for future studies that a new parameter was added to SedFlux to deal with closed in environments, such as troughs and fjord. In the original version, SedFlux considers an open space environment. In this case, sediments do not get lost as the boundary box is usually set large enough to keep the plume sedimentation within the boundaries. If it is not large enough, than sediment just get lost and is assumed that it becomes part of an adjacent area. For the closed in scenarios, the new parameter (left and right boundary for delta plain) permits to define a boundary box, so that once the

sediments hit the marine environment, they stay contained within the boundary box rather than being dispersed and lost to an inexistent adjacent area.

Erosion

The erosion process takes place landward of the river mouth for each defined time-steps in the river file. It assures that both, erosion and deposition, occurs along the river bed. The user can choose between two erosion mechanisms: diffusion or slope dependent. Diffusion uses an algorithm where the river's equilibrium profile is linear along its entire length (Paola et al., 1992). Tracking the river mouth is important, especially during sea-level rise. Diffusion assures that the amount of erosion is based on the profile's current distance from equilibrium. The second method assumes linear interpolation by giving a sloping plane on which erosion will occur. The slope is given by two parameters, reach and relief of the highest order stream in metres. If reach is 5000 m and relief 50 m, than the slope would be 1%. This study used the diffusion mechanism.

Hypopycnal plume

This process module disperses the sediment in the offshore region using hypopycnal plume as indicated (Syvitski et al. 1998). Three parameters are important: 1) the maximum plume width, 2 & 3) the number of grid nodes in the cross-shore and for the river mouth area. The maximum plume width is a way to limit the run-time because the very low concentrations that fall beyond the plume width are dismissed. Otherwise, the model would keep on running until no particles are left in the water column. Therefore, if most of the sediments and representative concentrations fall within a relatively narrow plume, it is in the interest of the user to save computational time by narrowing down the number. The very low concentrations have very little impact on the averaged

stratigraphy. The second and third parameters are used to compute the plume dispersion and its resolution. These numbers affect the resolution of the plume, but also the computational time. For instance, the river and sediment characteristic will help in determining the best numbers. For a wide river, such as the modelled Mackenzie, the number of grid nodes in the river mouths should be increased. In our case, we used 7 instead of 3, which were used for a 1 metre wide river. As for the number of grid nodes detailing the cross-shore, the length of the profile should be taken into account. For a long profile like the Mackenzie setting with 315 km, the number was divided in half to 11 instead of 21. This allowed to get rid of some blockiness artefacts. For details on these parameters, refer to the original publication of the module, i.e. Syvitski et al. (1998). A fourth parameter could be turned on, the velocity of coastal current, which is only effective in the 3D version of Sedflux (Hutton and Syvitski, 2008).

Hyperpycnal plume

The algorithm used for turbidity currents are also the same when computing hyperpycnal flows. To activate the hyperpycnal plume module, specify ‘turbidity current’ in the hyperpycnal plume model of the section “plume”. In this particular setting, the modern concentrations of sediments delivered by the Mackenzie River were too low to trigger any hyperpycnal flow.

Storm and currents

Other than slope failure, currents are another way to change the geometry of the shelf or delta slope. Even though this process module has limited parameter constraints in SedFlux, it allows impact assessment of cross-shore transport due to ocean storms. During the course of this research, the module was not functioning properly. However, if

it was, the parameters would have been set as follow: The average wave height of the study area would have been 1.2m (Hill et al., 2001; Syvitski et al., 2007). The parameter “fraction of events” refers to yearly frequency of event, thus 0.1 is 10% of the year or once every 35 days. Storms in the Arctic only affect the ocean and the seabed when there are ice-free conditions, which means only 90 days of the year. The present module however does not allow constraining events to a particular season. It would have been assume though that if no sediment is being supply during the winter season, the storms do not affect much the seabed. The cross-shore parameter allows the user to enter current values. Bottom currents on the inner shelf of the region of interest (<20m) have been estimated between 0.08 to 0.16 m/s, therefore 0.1m/s would have been used. This process module allows for the selection of one grain-size to be assigned to along-shore currents, which in this study would have been the bedload.